LA-11972-PR
Progress Report

UC-000 and UC-413
Issued: December 1990

LA--11972-PR

DE91 004902

Nuclear Theory and Applications Progress Report

January 1, 1989–April 1, 1990

Compiled by
D. D. Strottman
A. D. Mutschlecner

Los Alamos National Laboratory
Los Alamos,New Mexico 87545

CONTENTS

NUCLEAR THEORY AND APPLICATIONS PROGRESS REPORT

January 1, 1989-April 1, 1990

Compiled by

D. D. Strottman and A. D. Mutschlecner

ABSTRACT

This progress report describes the activities of the Los Alamos Nuclear Theory and Applications Group for January 1, 1989 through April 1, 1990. The topical content is summarized in the Contents.

I. DATA EVALUATION AND LIBRARIES

A. Data Evaluations for Version VI of ENDF/B-VI (P. G. Young, D. Dodder, G. M. Hale, and R. E. MacFarlane)

Evaluations of neutron-induced data for the upcoming issue of Version VI of ENDF/B are complete or in progress for ^{1}H, ^{3}He, ^{6}Li, ^{7}Li, ^{10}B, ^{11}B, ^{14}N, ^{15}N, ^{16}O, ^{151}Eu, ^{153}Eu, ^{165}Ho, ^{197}Au, ^{235}U, ^{238}U, ^{237}Np, and ^{239}Pu. Additionally, proton-induced evaluated data files for ^{1}H and ^{3}He targets have been accepted for ENDF/B-VI. Over the past year, evaluations for all these materials except ^{14}N and ^{16}O were provided to the National Nuclear Data Center at Brookhaven for Version VI. The analyses for ^{14}N and ^{16}O are still in progress and are described in Secs. B and C.

The evaluations cover the incident nucleon energy range up to 20 MeV or higher and, in most cases, new ENDF/B formats that permit precise specification of energy-angle correlations in emission spectra are utilized. In addition to incorporating up-to-date assessments of the available experimental data, each evaluation includes results of theoretical analyses to complement the experimental information. In the case of light elements, R-matrix analyses have been performed; for heavier materials, Hauser-Feshbach statistical calculations with supporting coupled-channel or spherical optical model, preequilibrium, direct reaction, and fission theory (for actinides) analyses are complete. A summary of the theoretical analyses for the actinide evaluations is given in Section B.

B. Analysis and Evaluation of n + ^{14}N Nuclear Reactions for ENDF/B-VI (P. G. Young)

An evaluation of n + ^{14}N nuclear data was begun in 1989 and will be completed for the first issue of ENDF/B-VI in 1990. The evaluation is divided into two parts: (1) a coupled-channel, R-matrix analysis incorporating all available data (including polarization and p + ^{14}C data) is being performed up to the threshold for inelastic scattering (E_n = 2.5 MeV), and (2) an assessment and evaluation of all experimental data are being carried out for the incident neutron energy range E_n = 2 - 20 MeV. At present, the R-matrix analysis is still in progress, but the experimental data evaluation is essentially complete and is summarized below.

The previous evaluation of neutron-induced reactions with ^{14}N was completed in the early 1970's[1] and was part of an intensive effort by the Defense Nuclear Agency to improve calculational capabilities for transporting neutrons and γ-rays through the atmosphere. The results of that analysis have been carried over basically unchanged in ENDF/B libraries since that time.[2] The availability of new and improved experimental data and theoretical techniques, together with the identification of discrepancies between measurements and calculations involving the transport of neutrons through large distances in air, has motivated the present effort. For orientation, graphs of the total, elastic, and nonelastic scattering cross sections are given in Fig. I-1. The importance of adequately describing properties of the low-energy resonances, particularly as regards the transport of lower energy neutrons, is clear from the figure. While our R-matrix analysis will represent the resonances to 2 MeV, it is important to note that pronounced structure continues to neutron energies of 9 MeV or higher, with a major feature of the data (from the point of view of neutron transport) being the neutron total cross section minimum near 5 MeV.

Major new experiments completed since 1973 include measurements by Chardine *et al.*[3] of neutron elastic and inelastic scattering angular distributions to the lowest five excited states of ^{14}N for incident neutron energies between 7.7 and 13.5 MeV, and elastic scattering measurements by Templon *et al.*[4] at three energies between 11 and 17 MeV, by Perey and Dickens[5] between 4.3 and 8.6 MeV, by Baba *et al.*[6] at 14.2 MeV, and by Petler *et al.*[7] at 20 and 25 MeV. Important new information on neutron inelastic scattering is provided by the measurements of Nelson *et al.*,[8] Auchampaugh and Wender* and Rogers *et al.*[9] up to E_n = 20 MeV, as well as the extensive double-differential neutron emission measurements by Baba *et al.*[6] and Takahashi *et al.*[10] for $E_n \cong$ 14 MeV. A comprehensive new measurement of ^{14}N(n,p) and ^{14}N(n,α) cross sections to discrete states by Morgan[11] up to E_n = 14 MeV is useful for the experimental data evaluation as well as the R-matrix studies. Unfortunately, the only major new total cross section measurement,[12] covering the important energy range E_n = 0.97 to 5.3 MeV, is in substantial disagreement (~14%) with older, precision measurements and was not included in our evaluation.

* George Auchampaugh and Steven Wender (Los Alamos National Laboratory) supplied this information in 1986.

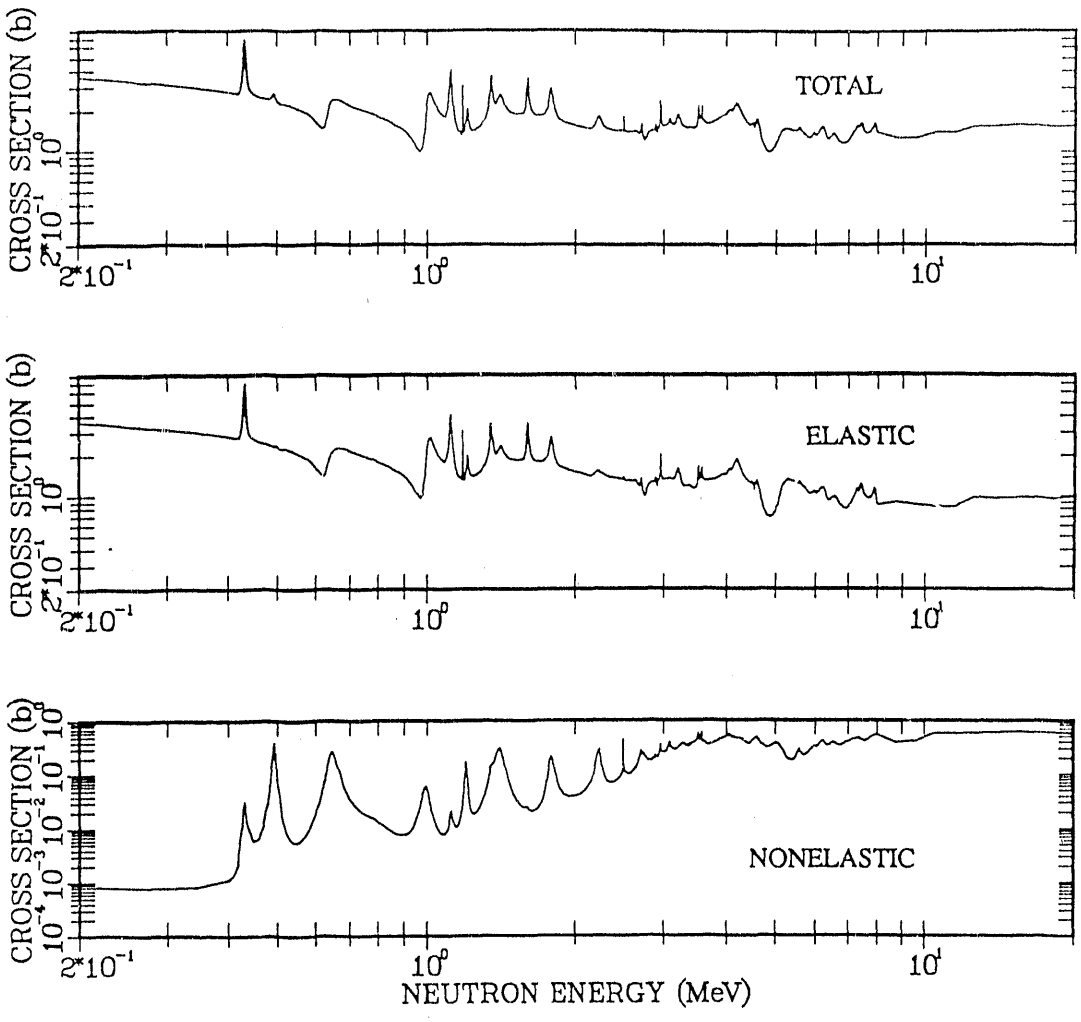

Fig. I-1. Total, elastic, and nonelastic cross sections for n + ^{14}N interactions.

The new experimental measurements resulted in considerable modification of some of the evaluated data. Comparisons of the newly evaluated ^{14}N(n,n') cross sections to the first 3 excited states with the previous ENDF/B evaluations are given in the upper halves of Figs. I-2 through I-4, also including the available experimental data. Gamma-ray production cross sections for emission of prominent γ-rays from these same states are shown in the lower halves of Figs. I-2 - I-4. To further illustrate the extent of some of the changes, new and old inelastic (E_x = 2.31 MeV) angular distributions are compared at selected energies in Figs. I-5 and I-6. Finally, a comparison of the new and previous evaluated elastic scattering cross section between 6 and 20 MeV is given in Fig. I-7. Note that the cross section has increased by some 9% at E_n = 14 MeV.

The results of the R-matrix analysis and experimental data evaluation summarized here will be included in the first issue of ENDF/B-VI.

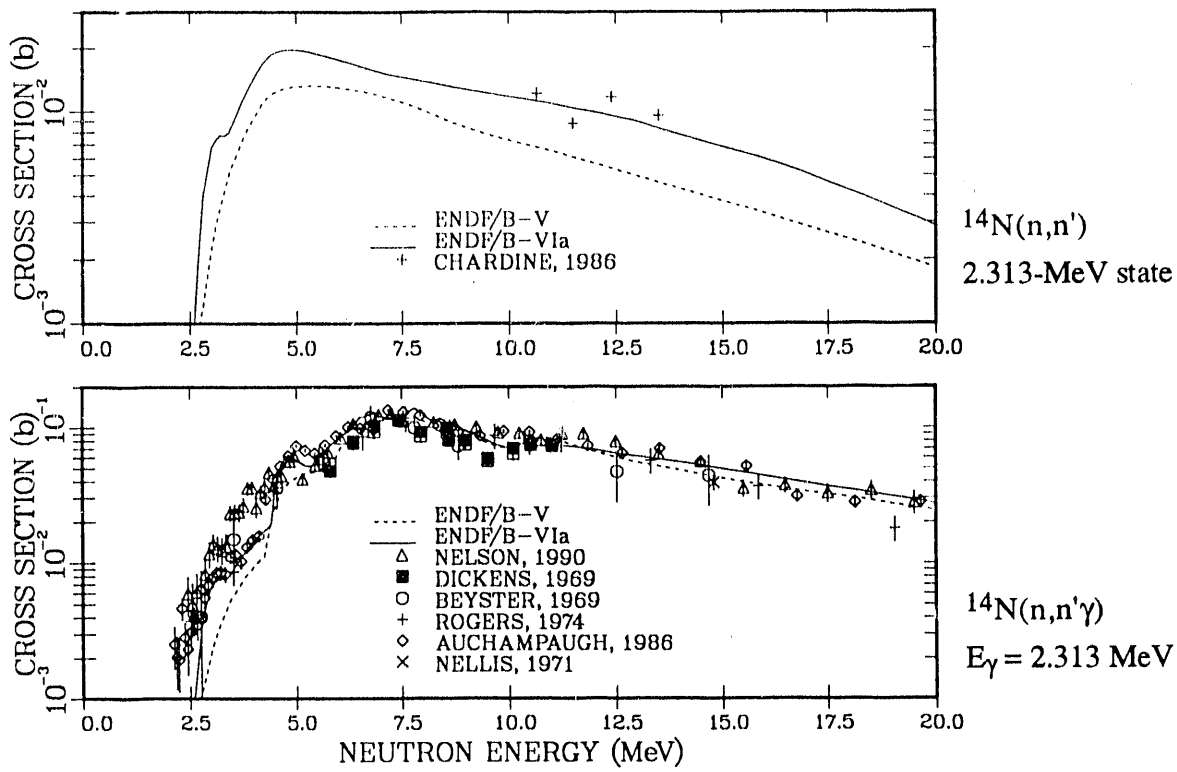

Fig. I-2. Inelastic neutron and γ-ray cross sections from ^{14}N(n,n') reactions to the first excited state (E_x = 2.313 MeV) of ^{14}N. The new evaluation (solid curve) is compared with the previous ENDF/B-V evaluation (dashed curve) and with the available experimental data.

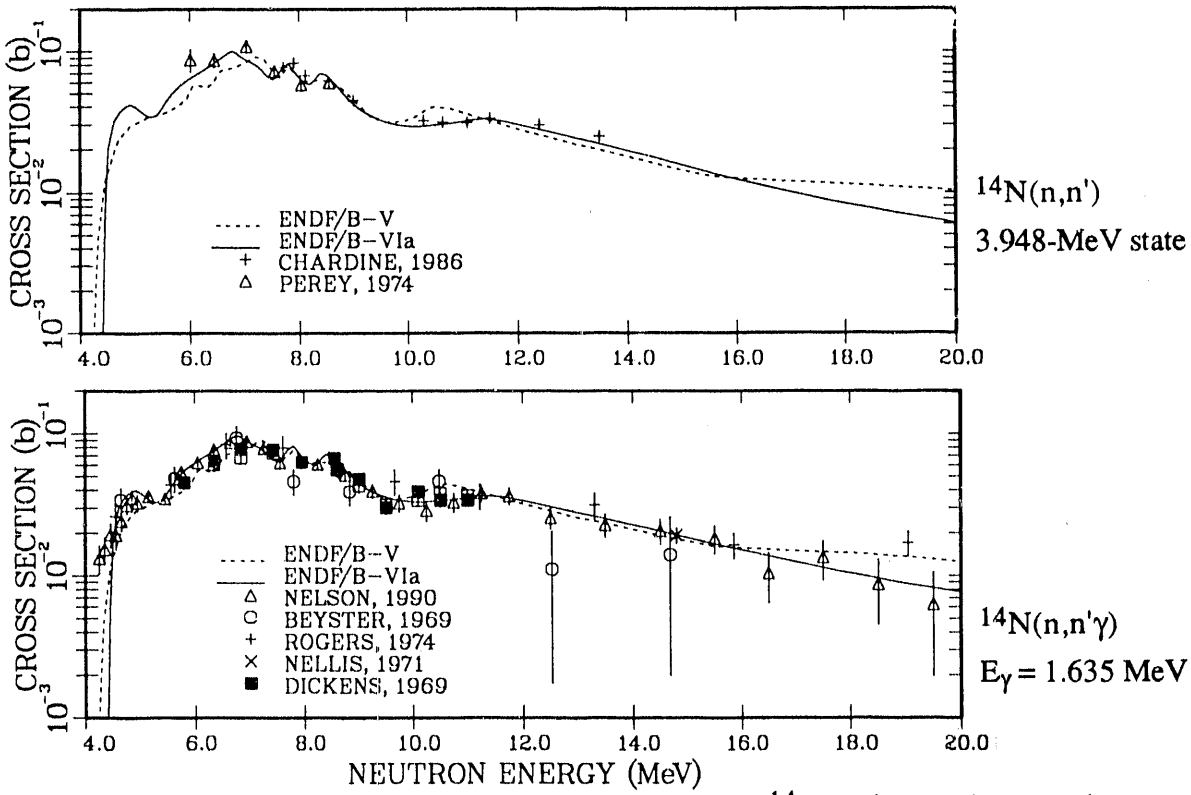

Fig. I-3. Inelastic neutron and γ-ray cross sections from ^{14}N(n,n') reactions to the second excited state (E_x = 3.948 MeV) of ^{14}N. The new evaluation (solid curve) is compared with the previous ENDF/B-V evaluation (dashed curve) and with the available experimental data.

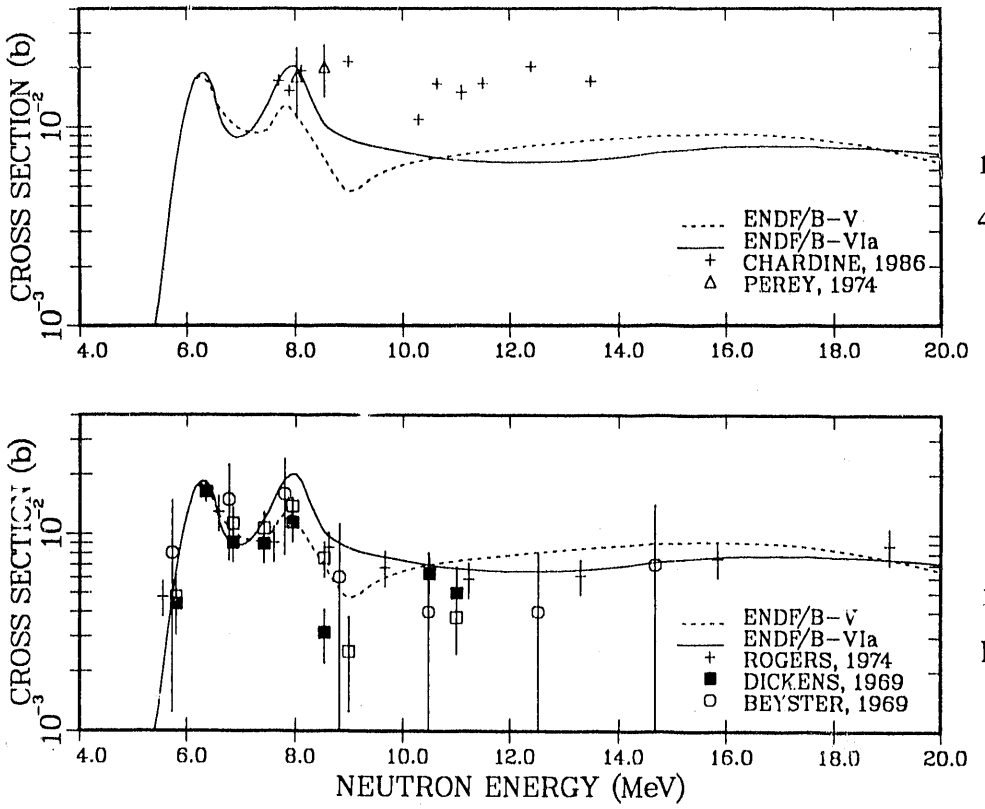

Fig. I-4. Inelastic neutron and γ-ray cross sections from $^{14}N(n,n')$ reactions to the third excited state (E_x = 4.915 MeV) of ^{14}N. The new evaluation (solid curve) is compared with the previous ENDF/B-V evaluation (dashed curve) and to the available experimental data.

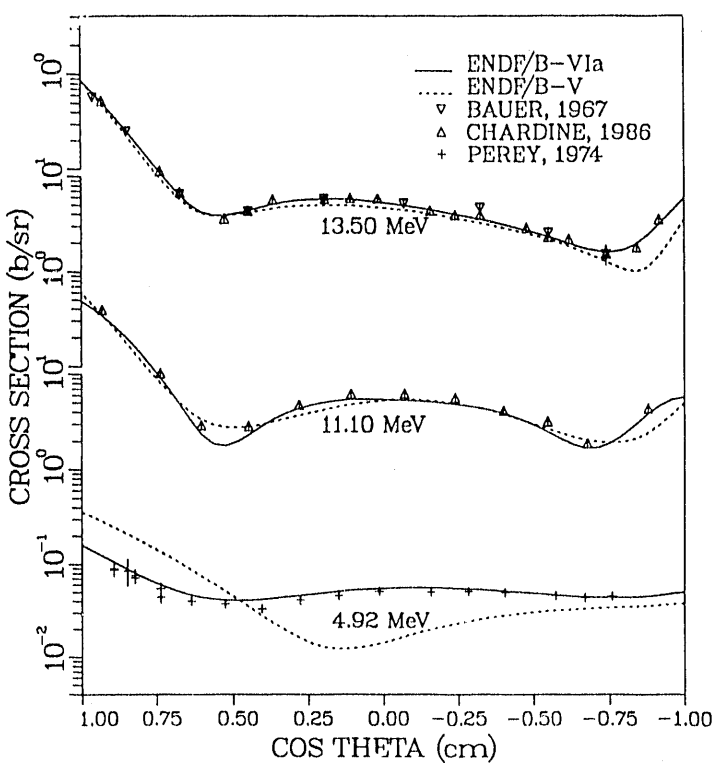

Fig. I-5. Measured and evaluated n + ^{14}N elastic scattering angular distributions. The solid curves are the present evaluation and the dashed curves are ENDF/B-V.

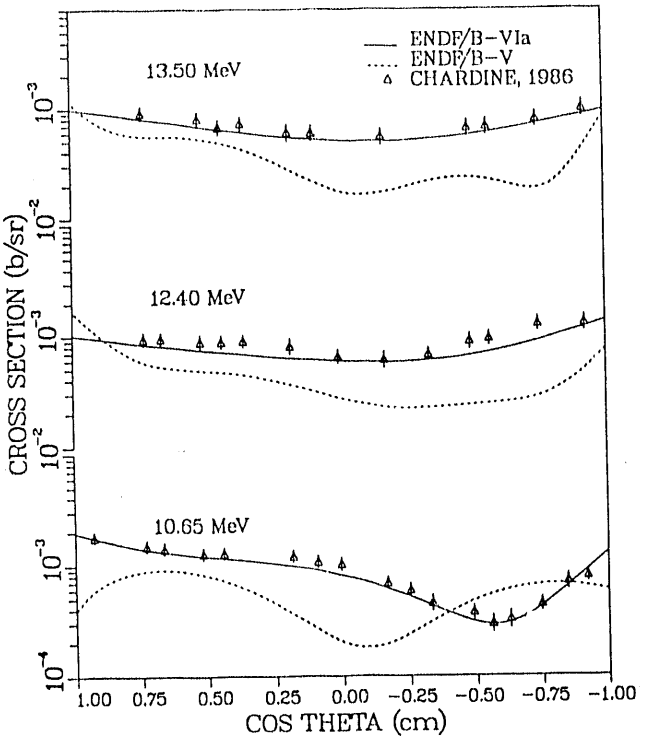

Fig. I-6. Measured and evaluated inelastic scattering angular distributions for the first excited state of ^{14}N at $E_x = 2.313$ MeV. The solid curves are the present evaluation and the dashed curves are ENDF/B-V.

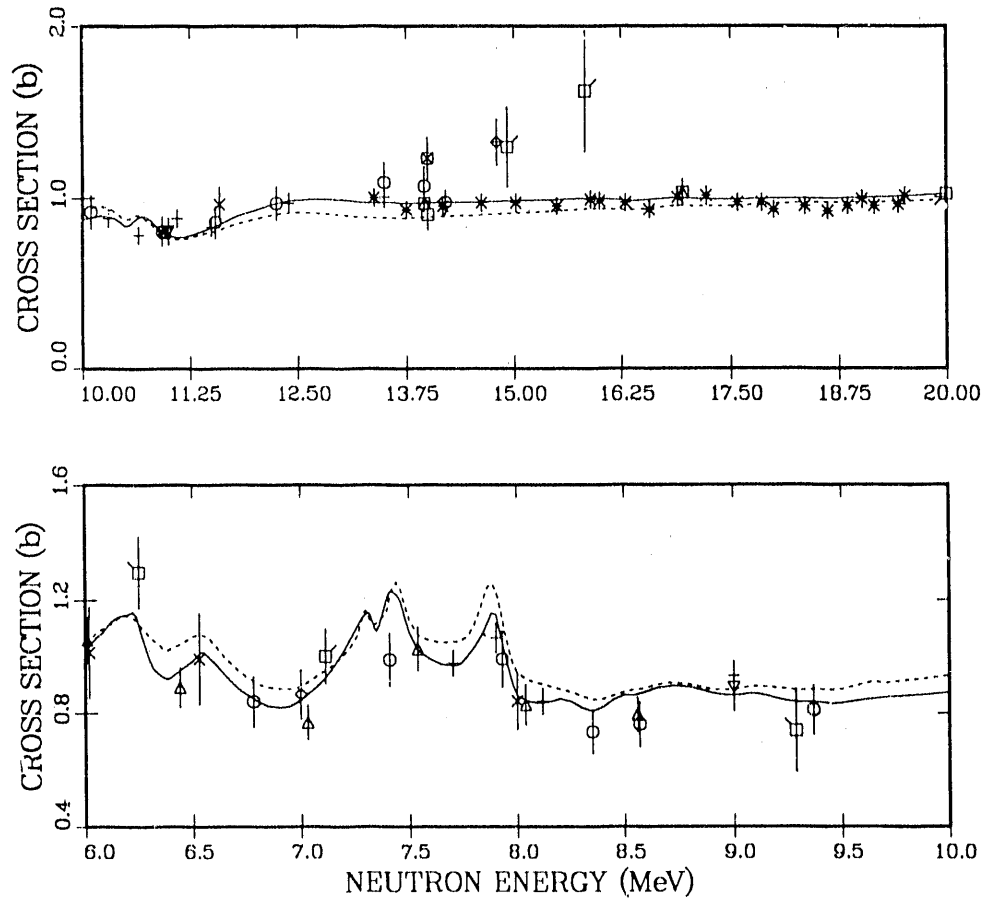

Fig. I-7. Neutron elastic scattering cross section for ^{14}N between 6 and 20 MeV. The solid curve is the present evaluation and the dashed curve is from ENDF/B-V.

C. R-Matrix Analysis of the ^{17}O System [G. M. Hale, P. G. Young, and Z. P. Chen (Beijing Univ.)]

We have updated our previous analysis[13] of the ^{17}O reactions with more recent experimental data and level structure information at excitation energies below 10 MeV. New measurements of the n+^{16}O total cross section by Larson,[14] Cierjacks *et al.*[15] and Okubo* were included at neutron energies from 1 keV to 6.5 MeV. We also included new measurements in the 2-4 MeV energy range of elastic scattering differential cross sections and polarizations by Drigo *et al.*[16]

The channel configuration and data summary for the analysis are given in Table I-I. R-matrix parameters for 45 levels were varied in order to fit the more than 3500 data points included for the three reactions considered. The level structure found agrees for the most part with the recommended data,[17] but with different parity assignments for some of the resonances and minor differences in positions and widths for the others. The resulting fit is a good representation of the data for all reactions. As an example, we show in Fig. I-8 the n+^{16}O total and reaction cross sections at energies below 6 MeV. One sees that all the details of the considerable structure in the cross sections are well described by the fit.

The neutron cross sections from this analysis are being used up to about 6 MeV in a new ENDF evaluation for ^{16}O. Revisions of the higher-energy cross sections that reflect the new measurements in that region are currently in progress. The new evaluation is scheduled to be included in version VI of the ENDF/B file.

TABLE I-I

CHANNEL CONFIGURATION AND DATA SUMMARY FOR THE ^{17}O SYSTEM R-MATRIX ANALYSIS

Channel	l_{max}	a_c (fm)
n-^{16}O	4	4.44
α-^{13}C	4	5.69

Reaction	Energy Range	Observable Types	# Data Points
$^{16}O(n,n)^{16}O$	E_n=0-6.5 MeV	σ_T, $\sigma_{nn}(\theta)$, $A(\theta)$	2421
$^{16}O(n,\alpha)^{13}C$	E_n=0-6.0 MeV	σ_{reac}, $\sigma_{n\alpha}(\theta)$, $A(\theta)$	904
$^{13}C(\alpha,\alpha)^{13}C$	E_α=0-4.6 MeV	$\sigma_{\alpha\alpha}(\theta)$	207
Totals:		7 obs.	3532

* W. Okubo (Japan Atomic Energy Research Institute) supplied this information in 1984.

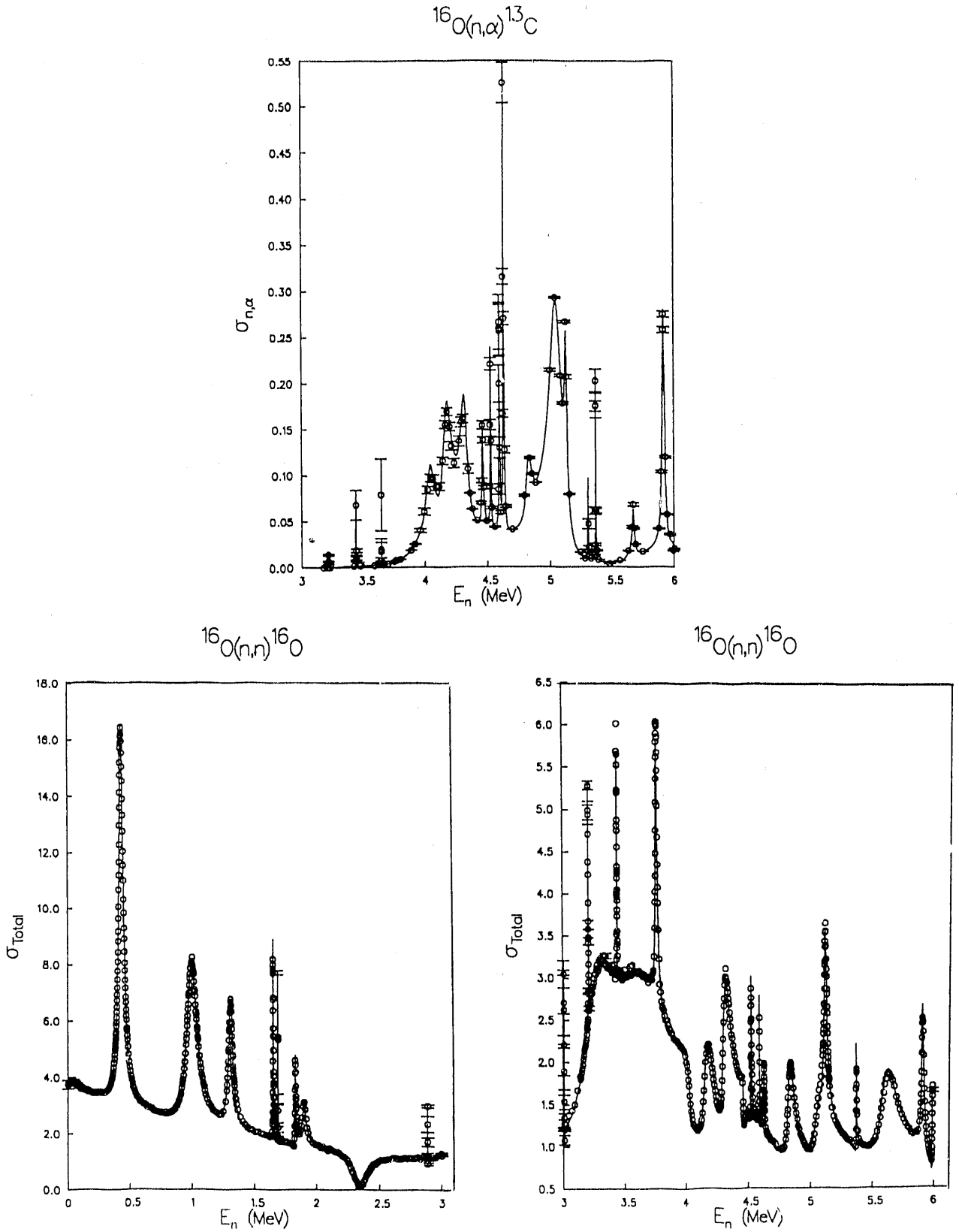

Fig. I-8. Total (bottom) and reaction (top) cross sections for n + ^{16}O at energies up to 6 MeV. The curves are the R-matrix calculation and the data are those of Refs. 14-15.

D. Theoretical Analyses of Neutron-Induced Reactions on Actinides for ENDF/B-VI: ^{235}U, ^{238}U, ^{237}Np, and ^{239}Pu (P. G. Young and E. D. Arthur)

We have performed theoretical analyses of neutron-induced reactions on ^{235}U, ^{238}U, ^{237}Np, and ^{239}Pu over the incident energy range 0.01-20 MeV in support of the ENDF/B-VI evaluation effort. The primary purpose of performing the theoretical analyses is to provide data on the reactions and energy ranges where little or no experimental data exist, especially for neutron emission reactions, with particular emphasis on the odd-A actinides. For most of these nuclei, neutron total and fission cross section measurements exist,[18] so that parameters in the calculations can be optimized to those data. Additionally, limited elastic and inelastic angular distribution data were available for the analyses of $^{235,238}U$ and ^{239}Pu.[19] In the case of n+^{237}Np, however, there were no experimental total cross section data above E_n=14 keV when this analysis was done*, virtually no elastic or inelastic scattering data, only fragmentary information on (n,γ) and (n,2n) reactions, and no experimental data on (n,3n) reactions or secondary neutron energy distributions. The only reaction that is reasonably described experimentally for ^{237}Np is fission, as new fission ratio measurements have recently been completed at WNR[20] and Argonne.[21] For all these actinides, prompt $\bar{\nu}$ measurements have been made over much of the energy range of interest,[22] but almost no data are available on neutron energy and angular distributions at energies above a few MeV. Therefore, depending on the specific nuclide involved, the main function of the theoretical analyses is to provide total, elastic, inelastic, (n,2n), and (n,3n) cross sections, and in all cases, the angular and energy distributions of secondary neutrons.

To summarize the analyses briefly, coupled-channel deformed optical model calculations were performed with the ECIS code[23] over the incident neutron energy range from approximately 0.001 to 20 MeV. The starting point for our optical model analyses were usually extensions[24] of the potentials of Lagrange,[22,25] which were then further modified for the present analysis to improve the calculations above 10 MeV. The role of the coupled-channel calculations in the present analysis is to obtain total, elastic, and ground-state rotational-band (n,n') cross sections, and to provide neutron transmission coefficients for Hauser-Feshbach statistical theory calculations. The deformed optical model potentials from the various analyses are given in Table I-II. The neutron total cross sections from the optical potentials are compared to experimental data in Fig. I-9.

* A new measurement of the ^{237}Np total cross section has subsequently been completed at WNR by Lisowski and coworkers.

TABLE I-II

OPTICAL MODEL AND DEFORMATION PARAMETERS USED IN THE COUPLED-CHANNEL CALCULATIONS*

n + ^{235}U Parameters

Potential		r_i	a_i
$V = 46.4 - 0.3E$		1.26	0.63
$W_{SD} = 3.3 + 0.4E$	$E \leq 8$ MeV	1.24	0.50
$W_{SD} = 6.5 - 0.046(E-8)$	$E > 8$ MeV	1.24	0.52
$W_V = -0.7 + 0.1E$	$E \geq 7$ MeV	1.26	0.63
$V_{SO} = 6.2$		1.12	0.47
$\beta_2 = 0.215$	$\beta_4 = 0.075$	(3 States Coupled)	

n + ^{238}U Parameters

Potential		r_i	a_i
$V = 46.2 - 0.275E$		1.26	0.63
$W_{SD} = 3.18 + 0.4E$	$E \leq 8$ MeV	1.26	0.52
$W_{SD} = 6.38 - 0.046(E-8)$	$E > 8$ MeV	1.26	0.52
$W_V = -1.4 + 0.175E$	$E \geq 8$ MeV	1.26	0.63
$V_{SO} = 6.2$		1.12	0.47
$\beta_2 = 0.198$	$\beta_4 = 0.057$	(3 States Coupled)	

n + ^{237}Np Parameters

Potential		r_i	a_i
$V = 46.2 - 0.3E$		1.26	0.63
$W_{SD} = 3.6 + 0.4E$	$E \leq 8$ MeV	1.24	0.52
$W_{SD} = 6.8 - 0.046(E-8)$	$E > 8$ MeV	1.24	0.52
$W_V = -0.7 + 0.1E$	$E \geq 7$ MeV	1.26	0.63
$V_{SO} = 6.2$		1.12	0.47
$\beta_2 = 0.214$	$\beta_4 = 0.074$	(3 States Coupled)	

n + ^{239}Pu Parameters

Potential		r_i	a_i
$V = 46.2 - 0.3E$		1.26	0.63
$W_{SD} = 3.3 + 0.45E$	$E \leq 8$ MeV	1.24	0.50
$W_{SD} = 6.9 - 0.046(E-8)$	$E > 8$ MeV	1.24	0.52
$W_V = -0.7 + 0.1E$	$E \geq 7$ MeV	1.26	0.63
$V_{SO} = 6.2$		1.12	0.47
$\beta_2 = 0.205$	$\beta_4 = 0.075$	(7 States Coupled)	

* The well depths and energies are in MeV; geometric parameters are in fermis. A Woods-Saxon form factor is used throughout.

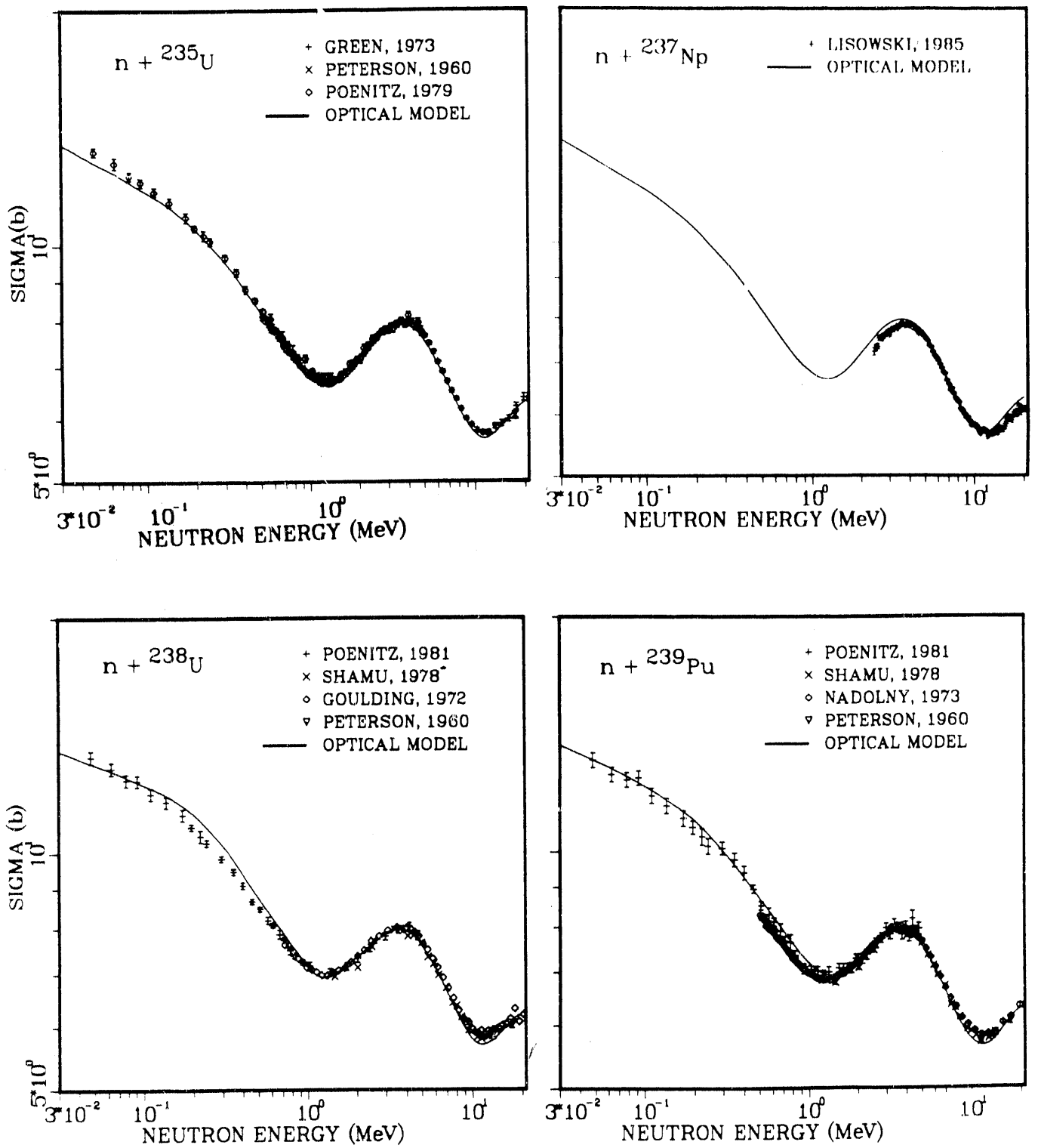

Fig. I-9. Neutron total cross sections for ^{235}U, ^{238}U, ^{237}Np, and ^{239}Pu from 30 keV to 20 MeV. The points represent experimental data[19] and the solid curves are the results of coupled-channel optical model calculations.

The Hauser-Feshbach statistical calculations were performed with the COMNUC[26] and GNASH[27] codes. Both codes include a double-humped fission barrier model, using uncoupled oscillators for the barrier representation in GNASH and coupled or uncoupled oscillators in COMNUC. The COMNUC calculations include width-fluctuation corrections, which are needed at lower energies, whereas GNASH provides the preequilibrium corrections that are required at higher energies. Accordingly, COMNUC was used in the calculations below the threshold for second chance fission (approximately 5 MeV), utilizing fairly strongly damped coupled oscillators. The GNASH code was employed at higher energies, using uncoupled oscillators for second and higher chance fission. Fission transition state spectra were calculated from inputted bandhead parameters or were constructed by taking known (or calculated) energy levels and compressing their spacing by a factor of 2. As usual, Gilbert and Cameron[28] phenomenological level density functions were used to represent continuum levels at ground-state deformations, appropriately matched to available experimental level data. Multiplicative factors were applied to the level density functions to account for enhancements in the fission transition-state densities at barriers due to increased asymmetry conditions.

The fission barrier parameters for the various compound systems are given in Table I-III. The fission cross sections calculated with these parameters are compared with experimental data in Fig. I-10. The dashed curves given in Fig. I-10 for the ^{235}U and ^{237}Np cases illustrate the contributions from first-, second-, and third-chance fission.

Although most of the direct reaction contribution to inelastic scattering is provided by the coupled-channel calculations of the ground state rotational bands (usually the first three members), additional direct contributions come from vibrational states, generally lying at higher excitation energies. Because of the close spacing of levels in ^{235}U, ^{237}Np, and ^{239}Pu, experimental information on (n,n') reactions to such vibrational states is essentially nonexistent. Therefore, to account for such contributions, we performed distorted-wave Born approximation (DWBA) calculations on nearby even-even nuclei (^{234,238}U, ^{238,240}Pu), using reduced transition probabilities B(Eℓ) from (d,d') and Coulomb excitation measurements[29] to obtain absolute (n,n') cross sections, and a weak coupling model to apply the results to states in ^{235}U, ^{237}Np, and ^{239}Pu. The strongest transitions observed in the (d,d') measurements involve population of 3^- and 2^+ vibrational states, corresponding to angular momentum transfers of ℓ=3 and ℓ=2, respectively. For ^{237}Np, the deformation parameters needed for normalizing the DWUCK calculations were estimated from systematics, that is, the required B(E2) and B(E3) values were estimated from those determined in the analyses for ^{235,238}U and ^{239}Pu, and all the ℓ=2 and ℓ=3 vibrational strength was placed into two fictitious states near E_x = 1 MeV. In the case of ^{235}U, the sum of (n,n') cross sections calculated from the dominant ℓ=3 and ℓ=2 transitions amounted to approximately 10% of the coupled-channel direct reactions at a neutron energy of 3 MeV, 30% at 8 MeV, and 23% at 20 MeV. While

these direct contributions are not large, they do lead to a hardening of the inelastic neutron spectrum that should be included in the ENDF/B-VI evaluations. All the DWBA calculations were performed with the DWUCK code.[30]

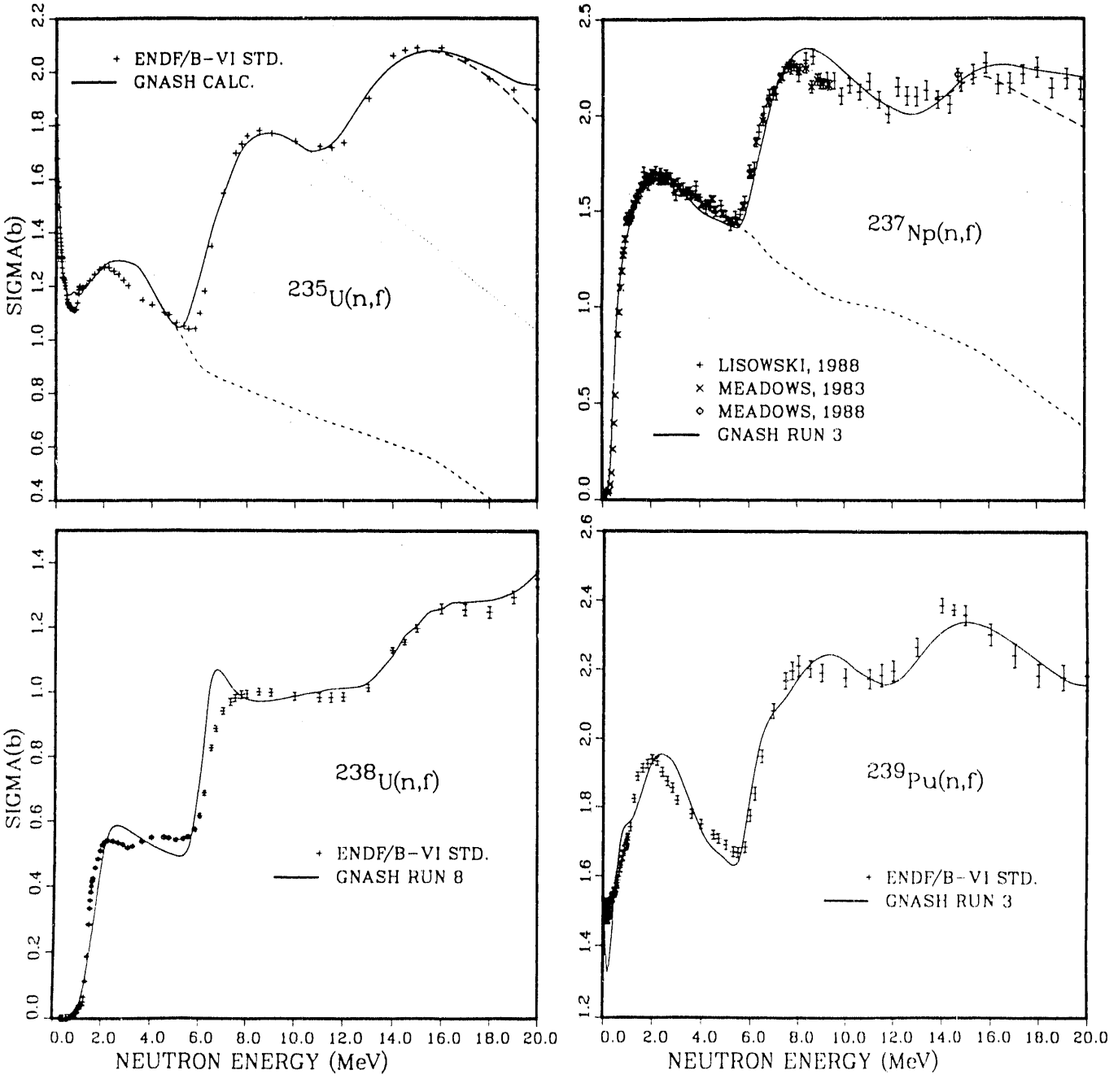

Fig. I-10. Calculated and measured neutron-induced fission cross sections for ^{235}U, ^{238}U, ^{237}Np, and ^{239}Pu from approximately 50 keV to 20 MeV. The points represent experimental data[19] and the curves are the results of our theoretical analysis. The dashed and dotted curves shown for ^{235}U and ^{237}Np represent the calculated contributions from first-, second-, and third-chance fission.

TABLE I-III

BARRIER PARAMETERS USED IN THE FISSION CALCULATIONS

	$n + {}^{235}U$ Compound Systems			
	^{236}U	^{235}U	^{234}U	^{233}U
E_A (MeV)	5.57	5.56	5.25	5.50
$\hbar\omega_A$ (MeV)	0.90	0.85	0.70	0.85
E_B (MeV)	5.49	5.46	5.15	5.30
$\hbar\omega_B$ (MeV)	0.50	0.55	0.50	0.55
Density Enhancements:				
Barrier A	2.15	2.5	1.0	5.0
Barrier B	2.15	2.0	1.0	2.0

	$n + {}^{238}U$ Compound Systems			
	^{239}U	^{238}U	^{237}U	^{236}U
E_A (MeV)	6.25	5.83	6.03	6.10
$\hbar\omega_A$ (MeV)	0.75	0.50	0.50	0.50
E_B (MeV)	6.00	5.33	5.63	5.90
$\hbar\omega_B$ (MeV)	0.50	0.50	0.50	0.50
Density Enhancements:				
Barrier A	15.	3.8	1.8	1.0
Barrier B	2.	2.0	1.8	1.0

	$n + {}^{237}Np$ Compound Systems			
	^{238}Np	^{237}Np	^{236}Np	^{235}Np
E_A (MeV)	5.87	6.20	5.70	6.40
$\hbar\omega_A$ (MeV)	0.31	0.85	0.50	0.85
E_B (MeV)	5.40	5.50	5.40	5.90
$\hbar\omega_B$ (MeV)	0.36	0.55	0.40	0.55
Density Enhancements:				
Barrier A	4.5	4.5	1.0	1.0
Barrier B	4.5	4.5	1.0	1.0

	$n + {}^{239}Pu$ Compound Systems			
	^{240}Pu	^{239}Pu	^{238}Pu	^{237}Pu
E_A (MeV)	5.78	5.75	5.65	5.65
$\hbar\omega_A$ (MeV)	0.80	0.63	0.90	1.00
E_B (MeV)	5.46	5.10	5.10	5.10
$\hbar\omega_B$ (MeV)	0.60	0.52	0.85	0.55
Density Enhancements:				
Barrier A	16.	1.1	1.0	2.5
Barrier B	2.	1.1	1.0	2.5

Very limited experimental elastic and inelastic scattering angular distribution data exist for the odd-A actinides. Comparisons between the calculations and measurements of n + ^{235}U elastic and inelastic angular distributions by Haouat *et al.*[19] are given in Fig. I-11. The dashed curves in Fig. I-12 represent the previous ENDF/B-V results, given as isotropic for all inelastic scattering. The new analyses are seen to significantly improve agreement with experiment.

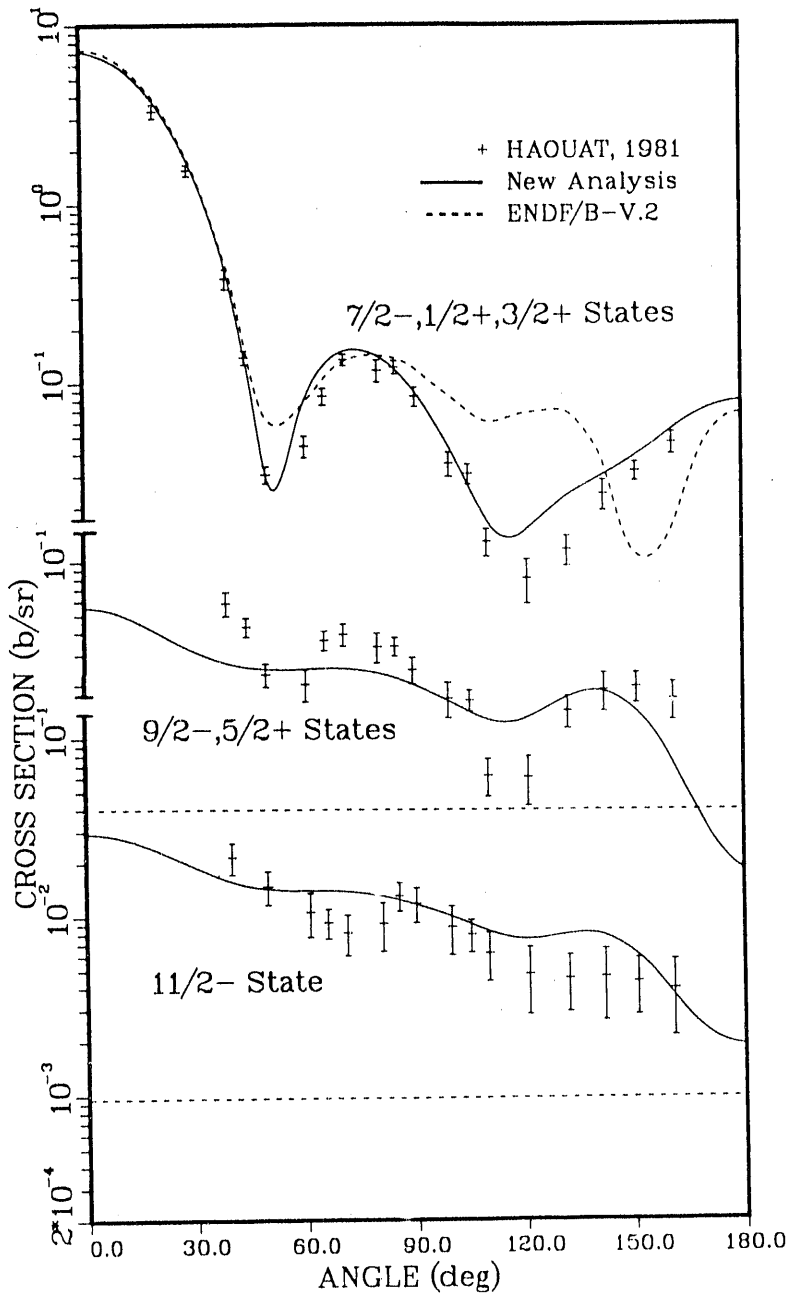

Fig. I-11. Calculated and measured neutron elastic and inelastic scattering angular distributions for 3.4-MeV neutrons on ^{235}U. Note that the measurements for several of the states (including the ground state) were not resolved, so the calculated curves have been combined appropriately.

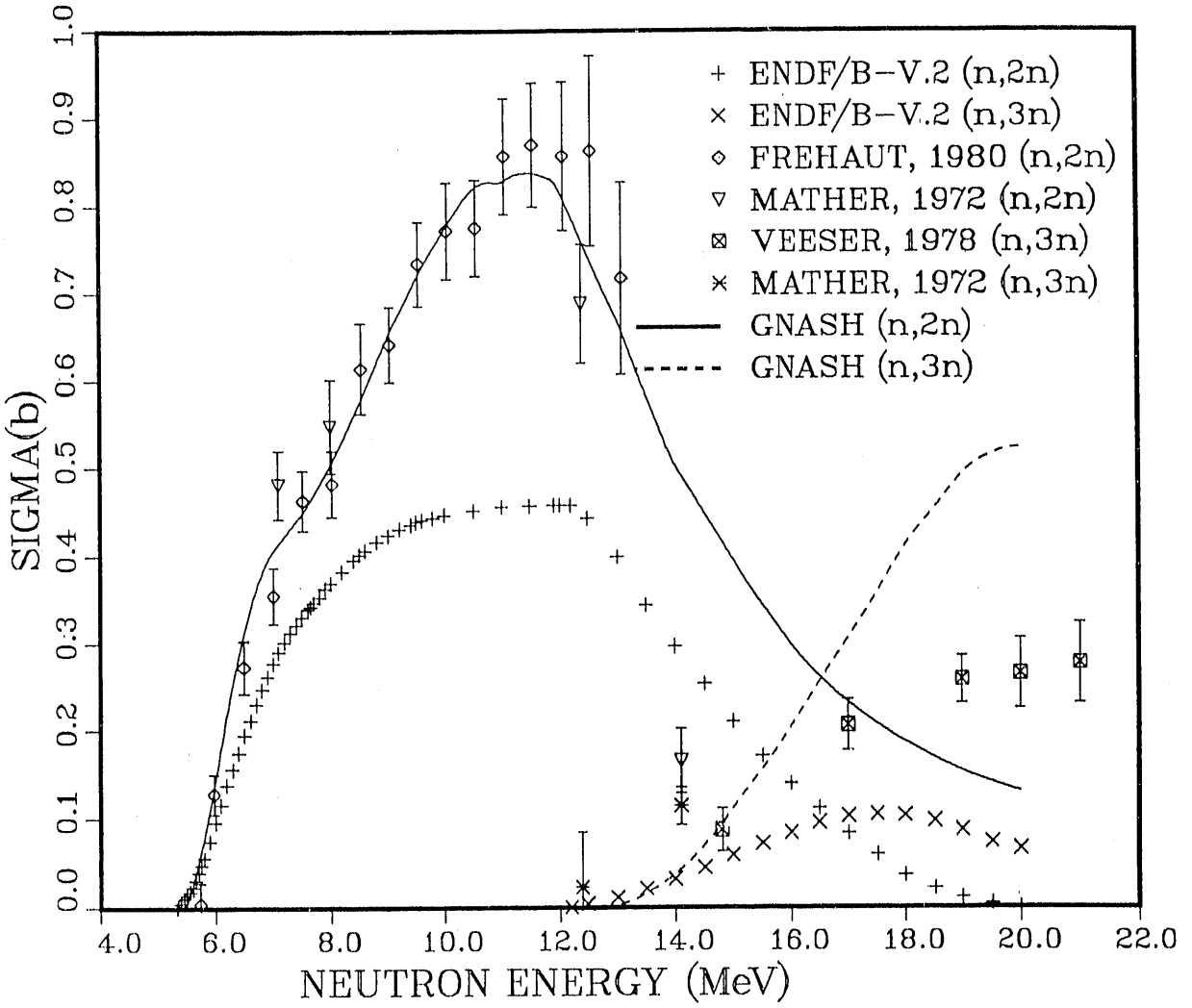

Fig. I-12. Measured and calculated ^{235}U(n,2n) and (n,3n) cross sections from threshold to 20 MeV. The curves represent the present analysis, the plus and cross symbols are the previous ENDF/B-V evaluation of the (n,2n) and (n,3n) cross sections, and the points are experimental data.[18]

Comparisons of calculated and measured ^{235}U(n,xn) cross sections are given in Fig. I-12. Note that the plus and cross symbols represent the previous ENDF/B-V evaluations of the (n,2n) and (n,3n) cross sections, which are in substantial disagreement with the measurements.

In summary, the present analyses result in substantially improved agreement with the available data for the major odd-A actinides. Except for the fission cross sections, which are accurately determined from experiments, results from the present analyses are being used in the MeV region for all major cross sections, angular and energy distributions in the ENDF/B-VI evaluations for ^{235}U, ^{237}Np, and ^{239}Pu. Because more experimental data are available for n + ^{238}U reactions, we have used covariance analyses of the experimental data as well as previous ENDF/B-V analyses of data to represent the cross sections for several of the ^{238}U reactions, mainly utilizing our theoretical results for continuum neutron energy and angular distributions.

E. Transport Data Libraries for Incident Proton and Neutron Energies to 100 MeV [P. Young, E. D. Arthur, M. Bozoian, T. R. England, G. M. Hale, R. J. LaBauve, R. C. Little (X-6), R. E. MacFarlane, D. G. Madland, R. T. Perry (N-12), and W. B. Wilson)]

A program is being carried out at Los Alamos National Laboratory to develop and implement proton, neutron, and photon transport libraries for incident energies up to 100 MeV. The project involves both the Applied Nuclear Science (T-2) and Radiation Transport (X-6) Groups. The motivation for this effort is principally the need to incorporate better nuclear physics data in applied calculations that have appreciable sensitivity to proton, neutron, and photon energies below 100 MeV. A common technique in such calculations is to utilize intranuclear-cascade/evaporation models to generate the required nuclear data. Because the physical assumptions embodied in such models are most applicable above a few hundred MeV, the use of these models below ~100 MeV is questionable. To circumvent this problem, we have extended to higher energy the range of validity of nuclear models that have been developed and tested for several tens of MeV and are constructing evaluated data libraries for proton and neutron energies to 100 MeV using these models and experimental data. The major steps involved in this effort are: (1) extension and validation of low-energy nuclear physics theoretical models for applicability up to 100 MeV; (2) development of evaluated (ENDF/B) data formats appropriate for higher energies; (3) calculation and evaluation of nuclear data in ENDF/B-VI format for appropriate materials up to 100 MeV; (4) development of processing code capabilities to handle the higher energy data; and (5) development of the appropriate interfaces and code patches for use of the data in transport codes such as MCNP.

Over the past year, new data libraries were completed and processed for incident neutron reactions on ^{9}Be, W, and ^{238}U, and for incident protons on ^{1}H, ^{9}Be, Si, Fe, W, and ^{238}U. Including earlier work, complete transport libraries are now in place and processed for proton- and neutron-induced reactions on the following nine materials: ^{1}H, ^{9}Be, ^{12}C, ^{16}O, ^{27}Al, ^{28}Si, Fe, W, and ^{238}U. A report describing this activity has been completed[31] and will be issued in 1990. In this report we emphasize the activities being carried out in the Applied Nuclear Science Group, that is, steps (1) through (4) above that involve development and processing of the transport data library. In addition to giving details of the nuclear model improvements, we include comparisons of calculated and measured data that have been used to validate the modeling. The resulting transport data libraries are described and illustrated in some detail.

F. References-Section I

1. P. G. Young and D. G. Foster, Jr., "An Evaluation of the Neutron and Gamma-Ray Production Cross Sections for Nitrogen," Los Alamos Scientific Laboratory report LA-4725 (1972).

2. P. G. Young and D. G. Foster, Jr., ENDF/B-V data file for ^{14}N (MAT 1275), described in "ENDF/B Summary Documentation," R. Kinsey, Comp., Brookhaven National Laboratory report BNL-NCS-17541 (ENDF-201), 1979 (available from the National Nuclear Data Center, Brookhaven National Laboratory, Upton, N.Y).

3. J. Chardine, G. Haouat, S. Seguin, and C. Humeau, "Diffusion Elastique et Inelastique de Neutrons sur ^{14}N Entre 7.7 et 13.5 MeV," Commissariat à l'Energie Atomique report CEA-N-2506 (1986).

4. J. A. Templon, J. H. Dave, C. R. Gould, and S. Singkarat, "Neutron Scattering Cross Sections form ^{14}N and ^{9}Be at 11, 14, and 17 MeV," Nucl. Sci. Eng. 91, 451 (1985).

5. F. G. Perey and J. K. Dickens, "Nitrogen Neutron Elastic and Inelastic Scattering Cross Sections from 4.34 to 8.56 MeV," Oak Ridge National Laboratory report ORNL-4805 (1974).

6. M. Baba, M. Ono, N. Yabuta, T. Kikuti, and N. Hirakawa, "Scattering of 14.1-MeV Neutrons from ^{10}B, ^{11}B, C, N, O, F, and Si," Proc. Int. Conf. on Nuclear Data for Basic and Applied Science, Santa Fe, New Mexico, 13-17 May 1985, v.1, p.223.

7. J. S. Petler, M. S. Isslam, R. W. Finlay, and F. S. Dietrich, "Microscopic Optical Model Analysis of Nucleon Scattering from Light Nuclei," Phys. Rev. C 32, 673 (1985).

8. R. O. Nelson, S. A. Wender, C. M. Laymon, H. A. O'Brien, R. C. Haight, G. L. Morgan, D. Drake, P. G. Young, M. Drosg, H. Vonach, A. Pavlik, D. C. Larson, P. Englert, and J. Brueckner, "Studies of Higher-Order (n,xγ) Reactions at the WNR Spallation Neutron Source," presentation at the Washington meeting of the American Physical Society, 16-19 April 1990.

9. V. C. Rogers, V. J. Orphan, C. G. Hoot, and V. V. Verbinski, "Gamma-Ray Production Cross Sections for Carbon and Nitrogen from Threshold to 20.7 MeV," Defense Nuclear Agency report DNA 3495F (1974).

10. A. Takahashi, J. Yamamoto, K. Ohshima, M. Fukazawa, Y. Yanagi, M. Ueda, J. Miyaguchi, S. Kohno, K. Yugami, H. Nonaka, E. Ichimura, H. Sugimoto, and K. Sumita, "Double-Differential Neutron Emission Cross Sections around 14 MeV," Osaka University report OKTAVIAN-87-01 (1987).

11. G. L. Morgan, "Cross Sections for the $^{14}N(n,p_0)$, (n,α_0), and (n,α_1) Reactions from 0.5 to 15 MeV," Nucl. Sci. Eng. 70, 163 (1979).

12. J. Bommer, "The Total Neutron Cross Sections of ^{14}N and ^{24}Mg," Nucl. Phys. A263, 86 (1976).

13. G. M. Hale, P. G. Young, and D. G. Foster, Jr., "R-Matrix Analysis of the ^{17}O System; ENDF/B-IV," Trans. Amer. Nucl. Soc. 18, 366 (1974).

14. D. C. Larson, "ORELA Measurements to Meet Fusion Energy Neutron Cross Section Needs", Proc. Symp. on Neutron Cross Sections from 10 to 50 MeV (BNL-NCS-51245), 277 (1980).

15. S. Cierjacks, F. Hinterberger, G. Schmalz, D. Erbe, P. Rossen, and B. Leugers, "High Precision Time-of-Flight Measurements of Neutron Resonance Energies in Carbon and Oxygen Between 3 and 30 MeV," Nucl. Inst. Meth. 169, 185 (1980).

16. L. Drigo, G. Tornielli, and G. Zannoni, "Polarization in the $^{16}O(n,n)$ Reaction," Nuov. Cim. 31, 1 (1976).

17. F. Ajzenberg-Selove, "Energy Levels of Light Nuclei A = 16-17," Nucl. Phys. A460, 77 (1986).

18. Experimental data available from the CSISRS compilation by the National Nuclear Data Center, Brookhaven National Laboratory, Upton, Long Island, New York.

19. G. Haouat, J. Lachkar, Ch. Lagrange, J. Jary, J. Sigaud, and Y. Patin, "Neutron Scattering Cross Sections for ^{232}Th, ^{233}U, ^{235}U, ^{238}U, ^{239}Pu, and ^{242}Pu Between 0.6 and 3.4 MeV," Nucl. Sci. Eng. 81, 491 (1982).

20. P. W. Lisowski, J. L. Ullmann, S. J. Balestrini, A. D. Carlson, O. A. Wasson, and N. W. Hill, "Neutron-Induced Fission Cross-Section Ratios for ^{232}Th, $^{235,238}U$, ^{237}Np, and ^{239}Pu from 1 to 400 MeV," Int. Conf. on Nucl. Data for Science and Technology, Mito, Japan, May 30 - June 3, 1988 (Ed. S. Igarasi, Saikon Publ. Co., Ltd., 1988) p. 97.

21. J. W. Meadows, "The Fission Cross Section of ^{237}Np Relative to ^{235}U from 0.1 to 9.4 MeV," Nucl. Sci. Eng. 85, 271 (1983); J. W. Meadows, "The Fission Cross Sections of ^{230}Th, ^{232}Th, ^{233}U, ^{234}U, ^{236}U, ^{238}U, ^{237}Np, ^{239}Pu and ^{242}Pu Relative to ^{235}U at 14.74 MeV Neutron Energy," Ann. Nucl. Eng. 15,421 (1988).

22. For example, see R. Gwin, R. R. Spencer, and R. W. Ingle, "Measurements of the Energy Dependence of Prompt Neutron Emission from ^{233}U, ^{235}U, and ^{239}Pu for E_n = 0.0005 to 10 MeV Relative to Emission from Spontaneous Fission of ^{252}Cf," Nucl. Sci. Eng. 94, 365 (1986); J. Fréhaut, "Coherent Evaluation of $\bar{\nu}_p$ for ^{235}U, ^{238}U, and ^{239}Pu," NEANDC(E) 238/L, Centre d'Etudes de Bruyères-le-Châtel (1986); J. Fréhaut, A. Bertin, and R. Bois, "Mesure de $\bar{\nu}_p$ et $\bar{E}_\gamma$ Pour La Fission de ^{232}Th, ^{235}U et ^{237}Np Induite Par des Neutrons d'Energie Comprise Entre 1 et 15 MeV," Int. Conf. on Nucl Data For Science and Tech., Antwerp, Netherlands, Sept. 6-10, 1982, p. 78.

23. J. Raynal, "Optical-Model and Coupled-Channel Calculations in Nuclear Physics," IAEA SMR-9/8, Int. At. En. Agency (1970).

24. P. G. Young, "Rare Earth-Actinide Potentials: ^{165}Ho, ^{238}U, ^{242}Pu," in Applied Nuclear Science Research and Development Semiannual Progress Report (Cps. E. D. Arthur and A. D. Mutschlecner) LA-10689-PR (1986) p. 48.

25. G. Haouat, Ch. Lagrange, J. Lachkar, J. Jary, Y. Patin, and J. Sigaud, "Fast Neutron Scattering Cross Sections for Actinide Nuclei," Int. Conf. on Nuclear Cross Sections for Technology, Knoxville, Tennessee (Oct. 22-26, 1979) p. 672.

26. C. L. Dunford, "A Unified Model for Analysis of Compound Nucleus Reactions," Atomics International report AI-AEC-12931 (1970).

27. P. G. Young and E. D. Arthur, "GNASH: A Preequilibrium Statistical Nuclear-Model Code for Calculation of Cross Sections and Emission Spectra," Los Alamos Scientific Laboratory report LA-6947 (Nov. 1977); E. D. Arthur, "The GNASH Preequilibrium-Statistical Model Code," Lecture at the Workshop on Applied Nuclear Theory and Nuclear Model Calculations, Trieste, Italy, February 10-12, 1988 (Los Alamos informal document LA-UR-88-382).

28. A. Gilbert and A. G. W. Cameron, "A Composite Nuclear-Level Density Formula with Shell Corrections," Can. J. Phys. 43, 1446 (1965).

29. Y. A. Ellis-Akovali, Nucl. Data Sheets 40, 523 (1983); E. N. Shurshikov, M. F. Filchenkov, Yu. F. Jaborov, and A. I. Khovanovich, Nucl. Data Sheets 38, 277 (1983).

30. P. D. Kunz, "DWUCK - A Distorted-Wave Born Approximation Program," unpublished (available from P. D. Kunz, University of Colorado, Boulder, Col.).

31. P. G. Young, E. D. Arthur, M. Bozoian, T. R. England, G. M. Hale, R. J. LaBauve, R. C. Little, R. E. MacFarlane, D. G. Madland, R. T. Perry, and W. B. Wilson, "Transport Data Libraries for Incident Proton and Neutron Energies to 100 MeV," Los Alamos National Laboratory report LA-11753-MS (July 1990).

II. DATA PROCESSING

A. NJOY 89 (R. E. MacFarlane)

The newest version of the NJOY Nuclear Data Processing System,[1] called NJOY 89, was released in May of 1989. Subsequently, 34 additional "updates" were made to produce the revision current at the end of 1989, "NJOY 89.34." This version features changes designed to support the new ENDF-6 format,[2] which will be used for both the ENDF/B-VI and the JEF-II evaluated nuclear data libraries, and it includes other modifications designed to enhance portability and fix errors found during the last two years. Many of these modifications were contributed by the large community of NJOY users that is developing around the world, especially those in Europe. The following paragraphs describe the main changes made to each module of the code.

1. NJOY. The NJOY module is the driver program that calls in other modules on request, and it also contains a library of common subroutines used by the other modules. There were only minor changes made for this version. The default for character handling in NJOY 89 is for Cray computers; that is, for 64-bit words containing 8 ASCII characters per word.

2. RECONR. The RECONR module is used to reconstruct the cross section vs energy functions $\sigma(E)$ from ENDF resonance parameters and nonlinear interpolation laws. The result is written as a pointwise ENDF, or PENDF, file in which each reaction is represented by a table of values of E and σ using linear interpolation, and all the energy values are members of a single unionized energy grid.

One of the important changes in the ENDF-6 format is the reintroduction of the Reich-Moore resonance representation. Although this format was originally introduced for ENDF/B-IV, its use was forbidden for ENDF/B-V because of its impact on codes like MC^2-II[3] that use resonance parameters directly to obtain effective resonance integrals that include the complex effects of interference between resonances. However, the Reich-Moore approach includes both multilevel and multichannel effects that are necessary to explain modern high-resolution experimental data for materials like ^{235}U. In addition, the single-channel version of the representation does a very good job of fitting cross sections for other important materials like iron, nickel, and chromium. The Oak Ridge National Laboratory (ORNL) SAMMY code makes extremely effective use of the Reich-Moore formulas. Recent theoretical work by Fröhner[4] and Hwang[5] define analytic methods that remove some of the previous objections to the Reich-Moore format, and many other users need only the detailed kernel broadening method incorporated in the BROADR module (which is not sensitive to the particular resonance representation used). Therefore, in order to gain the advantages and with due regard for the risks, the Reich-Moore representation was included in the ENDF-6 format, and the subroutine CSRMAT was added to

NJOY 89 to process it. This subroutine is based on the work of M. Bhat and C. Dunford of the National Nuclear Data Center, and it has already received some international verification attention thanks to the work of D. C. "Red" Cullen.

The Reich-Moore representation has no provision for treating overlap of the elastic or capture reactions with inelastic and particle producing reactions. Since such overlaps are common in the structural materials, a new representation called the "Hybrid R-Function" representation was developed for the ENDF-6 format. In this method, elastic scattering and radiative capture are treated exactly as in the scalar version of Reich-Moore method (no fission), but competing reactions like (n,n'), (n,p), or (n,α) are treated using the single-level Breit-Wigner line shape. Provisions are made to tabulate a background R-function, optical model phase shifts, and charged-particle penetrabilities, or these functions can be computed from simple hard-sphere formulas. The presence of these features promises to allow this method to be used to quite high energies. The new subroutine CSHYBR is also based on the work of C. Dunford with extensions and adaptations to the NJOY environment.

There is a third new resonance representation in the ENDF-6 format: the Generalized R-Matrix representation. It was developed by C. Lubitz of the Knolls Atomic Power Laboratory to include all of the capabilities needed for a full R-Matrix definition of the cross sections for all reactions for light, medium, and heavy nuclei. The Reich-Moore and the R-Function approaches are subsets of this new method, but the Lubitz approach is much more general. However, with this generality comes some increase in complexity, and the ENDF/B-VI evaluators do not intend to use this format in the near future. This version of NJOY cannot process the Generalized R-Matrix representation, but it is hoped that this capability will be added as soon as realistic test cases are available.

The ENDF-6 format includes an option to tabulate an energy-dependent scattering radius. It is not implemented. There is also a related option to use the ENDF value for the scattering radius instead of the so-called "channel radius" in calculating penetrabilities and shift factors. This option is needed for ENDF/B-VI evaluations from ORNL, and it has been implemented.

All three of these new resolved resonance representations can be used to compute detailed angular distributions directly from the resonance parameters if the evaluator says so by setting the LAD parameter. In such evaluations, the evaluator still provides the conventional (more approximate) angular distributions in File 4 for users who are not prepared to use the resonance parameters. Several of the ENDF/B-VI evaluations from the Oak Ridge National Laboratory will permit this calculation, but unfortunately, the necessary coding has not yet been added to RECONR. This is a high priority for an early update.

The unresolved range has been a problem for both evaluators and users for a long time. It is assumed that the cross sections for the resonance reactions can be obtained from a set of average

resonance parameters by averaging theoretical distributions of resonance widths and spacings. Infinitely-dilute or thin-sample cross sections can be computed using simple formulas. Self-shielded cross sections can be computed analytically by expanding the resonance-resonance overlaps and integrating over the distributions for resonance widths and spacings, or they can be produced statistically by averaging a number of ladders of resonances drawn from the appropriate distributions.

This model implicitly assumes that there are enough resonances in the vicinity of the energy of interest to justify the use of statistics. This assumption is violated for the existing evaluation for ^{235}U in the region just above 82 eV, where some of the fluctuations in the unresolved resonance parameters are actually trying to represent partially resolved resonances showing up in old poor-resolution data. This problem is being attacked in modern evaluations by using high-resolution experimental data and modern fitting codes to extend the resolved range to higher energies. Figure II-1 shows an example of this improvement.

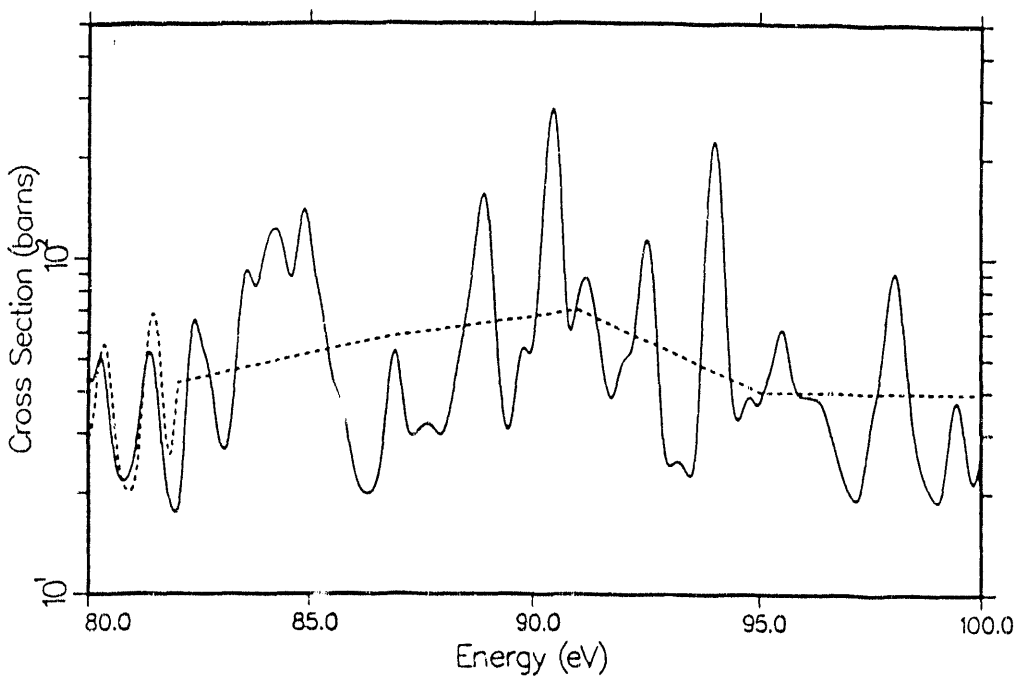

Fig. II-1. Test of the preliminary ENDF/B-VI Reich-Moore evaluation for ^{235}U (solid) compared with ENDF/B-V (dashed) where this range was unresolved.

Once the lower limit of the unresolved range has been increased sufficiently, the unresolved parameters and cross sections should be fairly smooth functions of energy. However, measurements for ^{235}U show additional "intermediate" structure. It has been suggested that this structure is due to the double-humped fission barrier.[6] If this is the case, the simple Porter-

Thomas distributions used in the ENDF representation are not correct. Even if one were to install more complex distributions, there would be no way to make the peaks and valleys of the calculated fluctuations line up with the peaks and valleys of the data. For ENDF/B-V, a rough attempt was made to represent some of the largest fluctuations using variations in the average resonance parameters, but there is no reason to believe that these parameters give good self-shielded results. In addition, the large number of energy grid points used (135) made processing this file very expensive.

In order to alleviate this problem, the ENDF-6 format has introduced the LSSF option. When this option is set, File 3 contains the infinitely-dilute unresolved cross sections on a grid fine enough to represent all the observed intermediate structure to the evaluator's satisfaction. File 2 contains a set of average unresolved parameters on a coarser energy grid. The actual cross section at a desired energy is obtained by multiplying the value interpolated from File 3 times a self-shielding factor computed from the resonance parameters (see UNRESR and GROUPR). With this representation, a user who is interested in thin samples---perhaps for dosimetry---where self shielding is not too important can do detailed calculations on a fine energy grid, while a user working with mixtures or thick samples can do a self-shielding calculation using conventional multigroup methods where the intermediate structure is not too important.

3. BROADR. The BROADR module Doppler broadens the cross sections on its input PENDF tape and writes the results on a new PENDF tape. The accurate kernel broadening method is used, and the results are independent of the particular resonance representation used. In addition, smooth cross sections and resonance-region backgrounds are correctly broadened. The changes to BROADR required for the ENDF-6 format were trivial. An error in indexing during thinning was fixed.

4. UNRESR. The UNRESR module uses an analytic method to compute self-shielded cross sections versus temperature T and background cross section σ_0 and writes them onto the PENDF tape using a specially defined section of File 2. No important changes were required for the ENDF-6 format, but the user should be aware of the LSSF option described above (see RECONR). When this option is used, the unresolved cross sections are computed as products of infinitely-dilute cross sections from the fine energy grid in File 3 and shielding factors computed from the unresolved resonance parameters on a coarser grid in File 2. As far as UNRESR is concerned, the calculation proceeds as before, except the contribution from File 3 (which is not a background in this case) is not added in. The GROUPR module then reads the special section of File 2 from the PENDF tape, interpolates for the appropriate self-shielded cross sections *vs* σ_0

from the coarse File 2 grid, divides each one by the corresponding infinitely-dilute value, and multiplies by a new infinitely-dilute cross section interpolated from the finer energy grid in File 3.

5. HEATR. The HEATR module computes the heat production and damage energy production cross sections and adds them to the PENDF tape. This calculation has been a difficult problem for previous ENDF libraries because the format lacked the detailed energy-angle distributions for neutrons and charged particles needed to get good results at higher energies; also many of the evaluations had severe energy-balance problems.[7] A number of the new features of the ENDF-6 format were added specifically to alleviate these problems. As a result, the NJOY 89 version of HEATR has many changes.

The local heat produced by a nuclear reaction comes from the kinetic energy of the charged products, including the recoil nucleus. Neutrons or photons emitted from the reaction travel elsewhere before eventually causing additional heating by inducing other reactions. However, the older ENDF/B libraries do not contain these energies.

One way around this deficiency is the "energy-balance method." The energy carried away by neutrons and photons is subtracted from the available energy. The result should be the energy of the remaining charged particles. The problem with this method is that this difference is often small compared to the available energy. Therefore, modest errors in the photon or neutron emission tables can lead to very large errors in the local heating. As an example, if the evaluator gives a value for the photon average energy that is too large, the resulting heat production value can be negative. On the other hand, this excess photon energy will be redeposited when the photons react elsewhere in the system. Clearly, the energy-balance method conserves total system heating. Errors in the evaluation lead to problems with heat distribution.

In NJOY terminology, the result obtained using the energy-balance method is called "heating," and it is written on the PENDF tape using MF=3 and MT=301.

In some cases, the energy carried away by charged particles can be computed by conservation of momentum. This is clearly true for elastic and discrete-level inelastic scattering, and an approximate relation is useful for radiative capture. Continuum inelastic scattering is a problem because energy-angle correlations can be significant, but a kinematic value can be obtained by assuming isotropy. For particle-producing reactions, kinematic limits can sometimes be established. For example, after an (n,α) reaction, the α could go to the ground state with no photon emission at all (maximum heating), or the α could come out with a very small energy leaving most of the rest of the available energy with the photons (minimum heating).

The upper kinematic limit provides a reasonable conservative estimate of the heating. It is called "KERMA" in NJOY, and it is stored on the PENDF tape using MF=3 and MT=443. The NJOY KERMA (Kinetic Energy Release in MAterials) is very similar to that computed by the MACK code.[8]

Comparisons of the NJOY heat and KERMA values make good checks on the energy-balance consistency of evaluations. An example is shown in Fig. II-2. The MATXSR module stores both types of heating cross sections in the library. The TRANSX user can choose which one to use based on plots like Fig. II-2 and the needs of his calculation. It is hoped that the new evaluations in ENDF-6 format will not have similar problems.

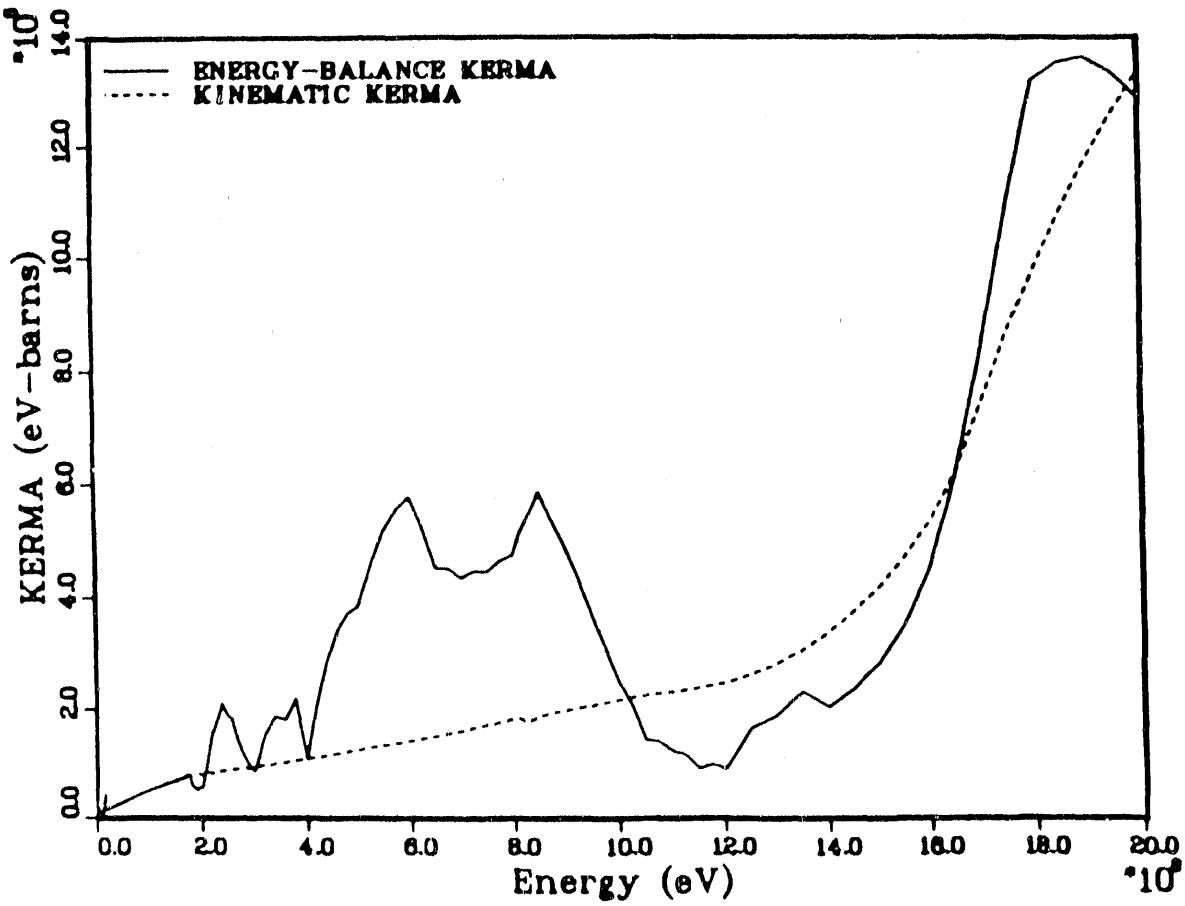

Fig. II-2. Comparison of heating (solid) with kinematic KERMA (dashed). The solid line should always be lower than the dashed line.

The fast recoil nucleus from a reaction causes displacement damage, which is often represented by DPA (displacements per atom). HEATR computes a damage energy production cross section (in eV-barns) that can be used to calculate DPA. It requires an integration over the energy spectrum of the recoil nucleus. Before the ENDF-6 format was introduced, this spectrum was obtained from the kinematics formulas used to compute KERMA as described above. An exception was made for reactions like (n,p) and (n,α), where a simple model based on a Coulomb barrier was used. Reactions like (n,np) and (n,nα) were treated like (n,n') reactions. This turned out to be a bad approximation. In practice, much of the recoil of such reactions comes from the

charged-particle emission; the neutron doesn't usually contribute very much recoil energy. Therefore, the 1989 version of HEATR treats these reactions like (n,p) and (n,α) reactions instead. The ENDF-6 format allows for improvement here.

In the new ENDF-6 format, evaluators are encouraged to include energy-angle distributions for all the emitted particles---including the residual nucleus---in File 6. If File 6 uses "Law 1" in the laboratory system (that is E,E', μ ordering), it is easy to integrate over the spectrum for each particle to find the average energy. These values are then multiplied by the associated yield and cross section, and added into both the heat and the KERMA. For "Law 7" (E, μ, E' order), the average energy is first computed by integrating over the spectrum for each μ value, then the results are integrated over μ. For "Law 1" data in the center-of-mass system, the E' integration is done adaptively using the H6CM routine from GROUPR to generate the laboratory-frame integrand. This procedure is discussed in more detail below.

Parallel methods can be used to compute the damage function at the same time as the heating. Since the evaluation gives the recoil spectrum directly, the burden of getting good results for the damage has been shifted from HEATR to the evaluator. When the evaluation is done using a nuclear model code (the modern practice), the evaluator has access to intermediate results that can aid in calculating good estimates for the recoil.[9]

A few materials in ENDF/B-V (notably silicon) include angular distributions in File 4 and energy distributions in File 5 for the discrete levels and continuum of reactions like (n,p) and (n,α). The formulas needed to calculate the recoil from such reactions are very similar to those for neutron levels except for some slight extensions to the kinematics relationships to allow the outgoing particle mass to be different from the incoming particle mass. The results are included in HEATR's kinematic limits, thereby reducing the uncertainty band between the low and high limits, and they are used directly in the calculation of damage.

6. THERMR. The THERMR module is used to compute neutron scattering at low thermal energies where the binding of the scatterer in a material or the motion of atoms in a gas is important. The results are written on the PENDF tape using MT numbers in the range 221 to 250 in Files 3 and 6. The File 6 format is nonstandard. The methods used for thermal scattering calculations haven't really changed since the original work[10] was done for ENDF/B-III. However, a number of changes were made in the the File 7 format for ENDF-6 in order to include some additional parameters that earlier users had to provide separately. Also, the earlier use of File 3 and File 4 for part of the thermal data has been eliminated; File 7 is completely self contained.

Coherent elastic scattering occurs for powdered crystalline materials like graphite, Be, and BeO. These data used to be tabulated in Files 3 and 4 on the ENDF thermal tapes as P_0 through P_3

cross sections. In the new ENDF-6 format, the quantity $C(E) = E\sigma_{coh}(E)$ is given as a function of E and T using MF=7 and MT=2. It has a stair-step form with jumps at the Bragg edges E_i. The complete energy-angle cross sections can be reconstructed using

$$\sigma_{coh}(E) = C(E)/E \,, \tag{1}$$

and

$$\sigma_{coh}(E,E',\mu) = \frac{1}{E}\sum_{E_i<E}\left[C(E_i) - C(E_{i-1})\right]\delta(\mu - \mu_i)\,\delta(E - E') \,, \tag{2}$$

where

$$\mu_i = 1 - \frac{E_i}{E} \,. \tag{3}$$

The GROUPR module uses this approach to generate multigroup cross sections for coherent elastic scattering.

Incoherent elastic scattering occurs in hydrogenous materials like polyethylene and ZrH. It depends on a characteristic cross section σ_b and a Debye-Waller factor $W/(T)$:

$$\sigma_{iel}(E,E',\mu) = \frac{\sigma_b}{2}\, e^{-2WE(1-\mu)}\,\delta(E - E') \,. \tag{4}$$

In previous versions of THERMR, the necessary parameters were tabulated in data statements. Now they are given in MF=7 and MT=2. The evaluation completely controls the result.

Incoherent inelastic scattering and the similar contribution due to coherent inelastic scattering are computed from a scattering law $S(\alpha,\beta)$ tabulated in File 7. The methods are the same as before except for the use of the short-collision-time (SCT) approximation for α and β values that are outside the range of the table. The SCT approximation requires an effective temperature value. In early versions of THERMR, this value was read from input cards; later versions used internal data statements. In either case, the numbers were obtained from the original GA report.[10] The new ENDF-6 version of File 7 includes a direct tabulation of the effective temperature. This gives the evaluator complete control of the data, and allows the evaluation to be changed without altering the code.

In the existing thermal evaluations, BeO and benzine give an $S(\alpha,\beta)$ for the molecule renormalized to be used with the cross section for the dominant scatterer (Be or H). These cases require that effective temperatures be given for both scattering nuclei. The new format allows this, and THERMR handles the calculation.

A number of other miscellaneous changes were also made. An option was added to allow THERMR to be used to calculate free-gas scattering at high temperatures. For $T > 3000^{o}$, EMAX and the incident energy grid are scaled by $T/300$.

In the other limit, the capabilities of THERMR to handle cold moderators like liquid hydrogen were improved by allowing smaller values of $S(\alpha,\beta)$ (as low as 10^{-99}), and allowing for $S(\alpha,\beta)$ functions that are not symmetric in β. This is necessary for working with ortho- and para-hydrogen. Additional incident energy points were added to the standard grid to follow the liquid hydrogen cross sections.

Earlier version of THERMR did not use a tight enough error criterion in fitting sharp features, and this sometimes led to noticeable problems in the integrated cross section. The criteria have been tightened up for NJOY 89.

7. GROUPR. The GROUPR module is used to generate multigroup cross sections and transfer matrices for neutrons, photons, and charged particles. There are massive changes in the 89 version of this module. The most noticeable ones have to do with reaction and particle selection, File 6 processing, and charged particles.

The user controls which reactions and data types (for example, cross sections or transfer matrices) GROUPR generates by giving a set of MFD, MTD, and MTNAME parameters. Old-time users will remember that this had to be done in exhausting detail. Newer versions of the code provided automatic shortcuts. These shortcuts have been extended and improved in NJOY 89 to include charged-particle reactions, and the MTNAME strings are now generated automatically. Most reactions and particles of interest can now be processed using the following:

3/ do all reactions in File 3 on input PENDF
6/ do all matrix reactions in ENDF directory
13/ do all photon production cross sections
16/ do all photon production matrices
21/ do all proton production matrices
22/ do all deuteron production matrices
23/ do all triton production matrices
24/ do all ^{3}He production matrices
25/ do all α production matrices
26/ do all A > 4 production matrices

Some use of specific MFD and MTD input lines are still required for fission data, special quantities like $\bar{\mu}$, and thermal cases. The identity of the incident particle is recognized automatically.

At the current time, the group structure for both incoming and outgoing charged particles must be the same as the neutron group structure. A different structure is allowed for photons.

If the File 6 data is expressed as a continuous energy-angle distribution (Law 1) in the laboratory system, it is fairly easy to generate the multigroup transfer matrix. As usual for GROUPR, the task is to calculate the "feed function" (the Legendre moments for transferring to all possible secondary energy groups starting with incident energy E). The E' integration is controlled by the GETMF6 subroutine, which calls F6LAB to generate the integrands. The only problems here are handling the new ENDF-6 interpolation laws for two-dimensional tabulations (for example, unit base) and converting tabulated angle functions into Legendre coefficients (which is done with a Gauss-Legendre quadrature of order 8).

If the File 6 data is given in the angle-energy form (Law 7), GROUPR converts it to the Law 1 form using subroutine LL2LAB. It does this by stepping through an E' grid that is the union of the E' grids for all the different angles given. At each of these union E' values, it calculates the Legendre coefficients using a Gauss-Legendre quadrature of order 8, and checks back to see if the preceding point is still needed to represent the distribution to the desired degree of accuracy. Now GETMF6 and F6LAB can be used to complete the calculation as above.

If the File 6 data is expressed in the CM system, or if the phase-space option is used, more processing is necessary to convert to the LAB system. This conversion is done for each incident energy E given in the file. The grid for laboratory secondary energy E'_L is obtained by doing an adaptive reconstruction of the emission probability $p_{L\ell}(E,E'_L)$ such that each Legendre order can be expressed as a linear-linear function of E'_L. This part is done in subroutine CM2LAB. The values for $p_{L\ell}(E,E'_L)$ are obtained in subroutine F6CM by doing an adaptive integration along the contour E'_L = const in the $E'_C\mu_C$ plane using μ_L as the variable of integration:

$$p_{L\ell}(E,E'_L) = \int_{\mu_{min}}^{+1} p_C(E,E'_C,\mu_C)\, P_\ell(\mu_L)\, J\, d\mu_L , \tag{5}$$

where μ is a scattering cosine and L and C denote the laboratory and center-of-mass (CM) systems, respectively. The Jacobian of the transformation is given by

$$J = \sqrt{\frac{E'_L}{E'_C}} = \frac{1}{\sqrt{1 + c^2 - 2c\mu_L}} , \tag{6}$$

and the cosine transformation is given by

$$\mu_C = J(\mu_L - c) . \tag{7}$$

The constant c is given by

$$c = \frac{1}{A+1}\sqrt{\frac{E}{E'_L}} \quad , \tag{8}$$

where A is the ratio of the atomic weight of the target to the atomic weight of the projectile. The lower limit of the integral depends on the maximum possible value for the CM secondary energy as follows:

$$\mu_{min} = \frac{1}{2c}\left(1 + c^2 - \frac{E'_{Lmax}}{E'_L}\right), \tag{9}$$

where

$$E'_{Lmax} = E\left(\sqrt{\frac{E'_{Cmax}}{E}} + \frac{1}{A+1}\right)^2 . \tag{10}$$

An example of the integration contours for this coordinate transformation is given in Fig. II-3.

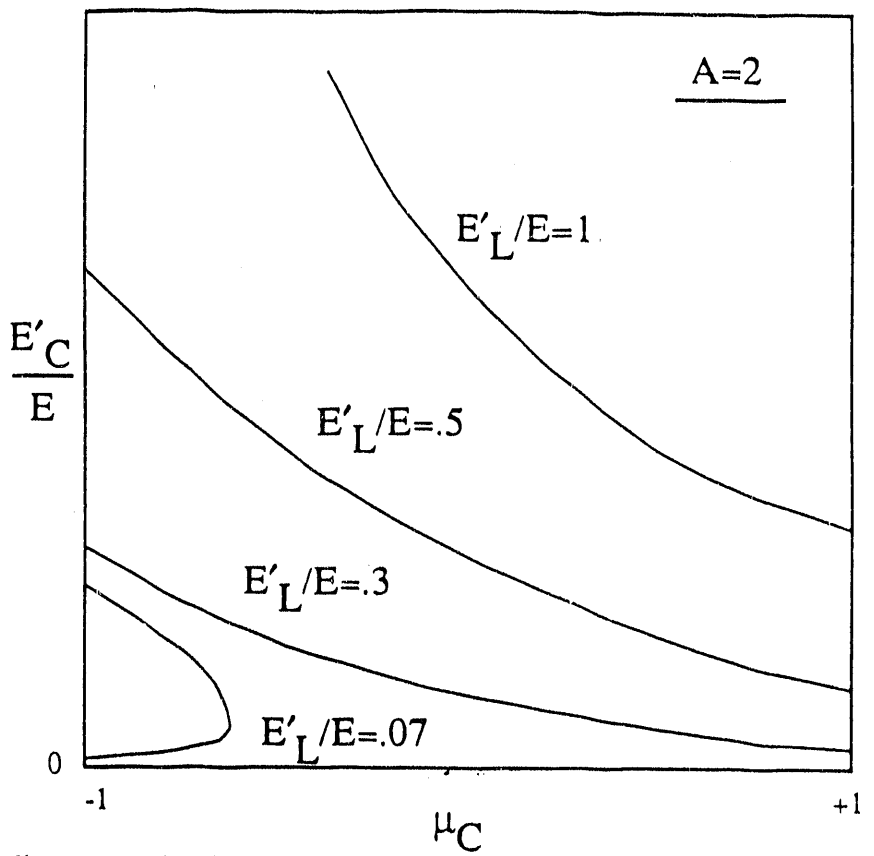

Fig. II-3. Coordinate mapping between center-of-mass and laboratory reference frames for A=2.

The CM energy-angle distribution can be given as a set of Legendre coefficients or a tabulated angular distribution for each possible energy transfer $E \rightarrow E'$, as a "precompound fraction" $r(E,E')$ for use with the Kalbach-Mann[11] or Kalbach[12] angular distributions, or as parameters for a phase-space distribution. The first three options are processed using F6DDX, and the last using F6PSP. The Kalbach option leads to a very compact representation. Kalbach and Mann examined a large number of experimental angular distributions for neutrons and charged particles. They noticed that each distribution could be divided into two parts: an equilibrium part symmetric in μ, and a forward-peaked preequilibrium part. The relative amount of the two parts depended on a parameter r, the preequilibrium fraction, that varied from zero for low E' to 1.0 for large E'. The shapes of the two parts of the distributions depended most directly on E'. This representation is very useful for preequilibrium statistical-model codes like GNASH,[13] because they can compute the parameter r, and all the rest of the angular information comes from simple universal functions. More specifically, Kalbach's latest work says that

$$f(\mu) = \frac{a}{2\sinh(a)} \left[\cosh(a\mu) + r \sinh(a\mu)\right] , \qquad (11)$$

where a is a simple function of E, E', and B_b, the separation energy of the emitted particle from the liquid-drop model without pairing and shell terms. The separation energies are computed by function SEPE. It has a problem for elemental evaluations, because it needs an A value for the calculation, and it is difficult to guess which A value is most characteristic of the element. A short table is included in the function, and an "error in sepe" will result if the function is called with an element that doesn't appear in the table. Similar routines appear in HEATR and ACER (SEPH and SEP, respectively). A better long-range solution would be desirable.

File 6 can contain angular distributions for discrete two-body scattering (see Law 3). It can also declare that a particular particle is the recoil particle from a two-body reaction (Law 4), in which case the appropriate angular distribution is obtained from the corresponding Law 3 subsection by complementing the angle. The representation of the angular distribution for these laws is almost identical to that in File 4, and the new update to GROUPR simply rearranged the existing coding into a new subroutine GETDIS to handle the calculation. Of course, the kinematics formulas in GETDIS had to be extended slightly to allow the incident and outgoing particles to have different masses (see Appendix C of the preliminary ENDF-6 manual.[2]).

Coulomb scattering only occurs in the elastic channel, and this calculation also uses the GETDIS subroutine. The problem with Coulomb scattering is that the basic Rutherford formula becomes singular at small angles. In practice, this singularity is removed by the screening effects of the atomic electrons. The forward transport of charged particles in this screening regime is

usually handled by continuous-slowing-down theory by using a "stopping power." The new ENDF-6 format allows for three different ways to handle the large-angle scattering regime. First and most general is the Nuclear Amplitude Expansion:

$$\sigma = |\text{nucl} + \text{coul}|^2$$
$$= \sigma_{\text{nucl}} + \sigma_{\text{coul}} + \text{interference} \qquad (12)$$

The Coulomb term is given by the Rutherford formula, a Legendre expansion is defined for the nuclear term, and a complex Legendre expansion is defined for the interference term. This representation cannot be generated directly from experimental data; an R-matrix or phase-shift analysis is necessary.

A method very closely related to experiment (σ_{exp}) is the Nuclear plus Interference (NI) formula:

$$\sigma_{NI}(\mu,E) = \sigma_{\text{exp}}(\mu,E) \ , \qquad (13)$$

where the function is only defined for angles with cosines $\mu < \mu_{\text{max}}$. The minimum angle is usually taken to be somewhere around 20° (GROUPR uses $\mu_{\text{max}} = .96$). This function is still ill-behaved near the cutoff, and it must be tabulated. The third option is the "residual cross section expansion":

$$\sigma_R(\mu,E) = (1 - \mu)\left[\sigma_{\text{exp}}(\mu,E) - \sigma_{coul}(\mu,E)\right] . \qquad (14)$$

The $(1 - \mu)$ term removes the pole at the origin. The residual is uncertain, but it is usually small enough that the entire curve can be fitted with Legendre polynomials without worrying about what happens at small angles. Fig. II-4 shows an example of a typical residual cross section. In practice, both the nuclear amplitude expansion and the nuclear plus interference representation are converted to the residual cross section representation in subroutine CONVER. GETDIS only has to cope with the one representation.

As usual, a few errors in GROUPR were fixed. A temperature dependence was added to the the Maxwellian part of the CLAW weight function. When used with the new high-temperature option in THERMR, and taking advantage of the existing capabilities of BROADR, this option provides for generating free-gas upscatter matrices for materials at very high temperatures.

In addition, the VITAMIN-E weight function, the VITAMIN-E group structure, and the VITAMIN-J group structure were added to the list of built-in input options.

Updates included the addition of processing for tabulated photon distributions, a tightening of the grid for weight functions (this leads to significant changes in the test problem results,

particularly for elastic removal), a fix to the storage allocation for delayed neutron spectra, and changes to allow for discrete levels in File 12 (silicon).

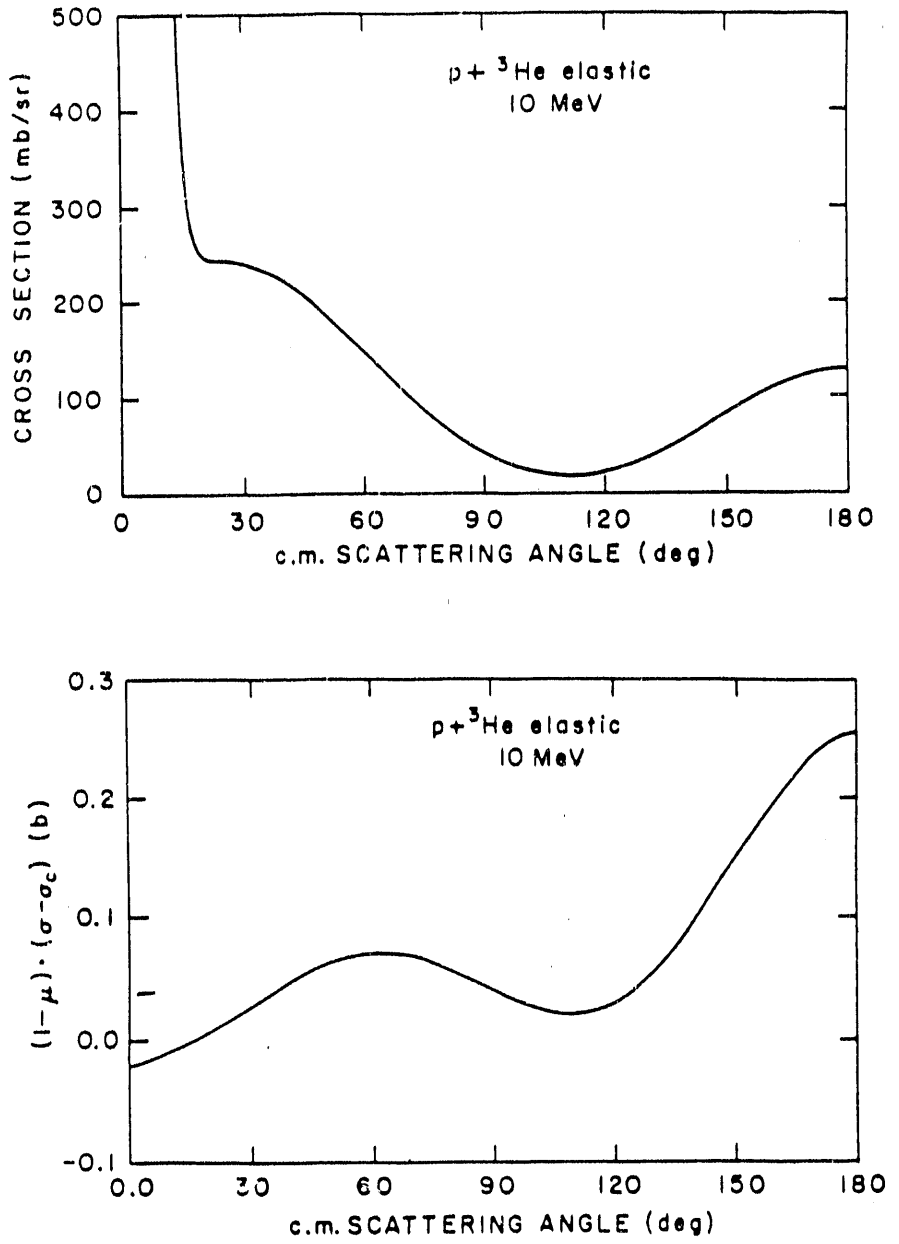

Fig. II-4. (top) A typical angular distribution for charged-particle elastic scattering showing the singular behavior at small angles, the strong interference feature, and nuclear scattering at large angles. (bottom) The residual cross section corresponding to the figure above. Note the reasonable behavior at small angles. The actual value there is not important, and it can easily be forced to zero.

8. GAMINR. The GAMINR module is used to compute cross sections for gamma ray interactions with atoms. The only updates needed for the ENDF-6 format were some changes in MT numbers. In order to make more room for MT numbers to describe charged-particle levels, MT 602 (photoelectric absorption) was changed to 522, and MT 621 (a private value used for photon heating) was changed to 525.

In addition, it was found that the cutoff used in calculating the incoherent scattering integral was too large, and there was an error in a previous patch to the incoherent result. Photon interaction libraries should be regenerated with the 89 version.

9. ERRORR and COVR. The ERRORR and COVR modules are used to compute and format cross section covariances. There are significant changes in the covariance files for the ENDF-6 format, but so far no updates to handle the changes have been made. Several small errors were patched. The DISSPLA plotting in COVR was modified to improve portability through increased use of character data. (Caution: not all versions of the DISSPLA library allow character data).

10. MODER. The MODER module is used to convert back-and-forth between coded file modes (that is, ASCII, BCD, EBCDIC, etc.) and the NJOY blocked-binary format. It can also be used to build a new ENDF, PENDF, or GENDF tape containing materials selected from several input tapes. It was necessary to add a few sections of coding to work with new formats introduced by the ENDF-6 specifications.

11. DTFR. The DTFR module is used to generate tables for transport codes that can accept the DTF format. It also has a capability for plotting the edit cross sections, the neutron or photon transport matrix, and the photon production matrix. A few minor changes were made in this module to improve portability between different computer systems, to increase the size of the problems that can be run, and to check for some kinds of input errors.

12. CCCCR. The CCCCR module is used to generate the CCCC standard interface file ISOTXS, BRKOXS, and DLAYXS using output from GROUPR. The only change made for the 89 version was the removal of the WOT8 routine because of poor portability.

13. MATXSR. The MATXSR module is used to convert multigroup data from GROUPR into the MATXS format. With ENDF-6 data, a MATXS library can contain cross sections and transfer matrices for neutrons, photons, and charged particles. The format always allowed for this generality, but some changes in the naming conventions have been made for NJOY 89. This means that MATXS files generated with the new version will not be consistent

with previous versions. In addition, the TRANSX code,[14] which is used to produce libraries for transport codes from MATXS files, must be changed to recognize the new names.

14. ACER. The ACER module is used to produce libraries in the ACE format (A Compact ENDF) for the MCNP continuous-energy Monte-Carlo code.[15] At this time, MCNP and ACER have only been updated to handle one of the File 6 formats, namely, "Law 1" tabulations in the center-of-mass frame using the Kalbach angular distribution systematics. A special sampling scheme was developed for this case. The MCNP code already had logic to select a secondary energy E' from a distribution. The problem was to select an emission cosine μ for this E'. First, the Kalbach distribution is written in the form

$$f(\mu) = \frac{a}{2\sinh(a)} \left[(1 - r)\cosh(a\mu) + re^{a\mu}\right] . \tag{15}$$

Now select a random number R_1. If $R_1 < r$, use the first distribution in Eq. (15). Select a second random number R_2, where

$$R_2 = \int_{-1}^{\mu} \frac{a\cosh(ax)}{2\sinh(a)}\, dx = \frac{\sinh(a\mu)}{2\sinh(a)} + \frac{1}{2} . \tag{16}$$

Therefore, the emission cosine is

$$\mu = \frac{1}{a} \sinh^{-1}\left[(2R_2 - 1)\sinh(a)\right] . \tag{17}$$

If $R_1 \leq r$, use the second distribution in Eq. (15). Select a random number R_2, where

$$R_2 = \int_{-1}^{\mu} \frac{ae^{ax}}{2\sinh(a)}\, dx = \frac{e^{a\mu} - e^{-a}}{e^{a} - e^{-a}} , \tag{18}$$

and emit a particle with cosine

$$\mu = \frac{1}{a} \ln\left[R_2 e^{a} + (1 - R_2) e^{-a}\right] . \tag{19}$$

The ACE format for the File 6 data is similar to the format used for other continuous energy distributions, namely, a cumulative distribution function. To this are added tables for the preequilibrium ratio r and the Kalbach slope parameter a.

It is important to add two additional sampling schemes to MCNP as soon as possible. The new evaluations from Oak Ridge use "Law 1" tabulated distributions in the laboratory system with a Legendre representation of the angular distribution for a particular $E \rightarrow E'$. The new ^{9}Be evaluation from the Lawrence Livermore National Laboratory uses "Law 7" (that is, E,μ, E' ordering).

A number of miscellaneous fixes were made in ACER, several contributed by European users. Some of them were to improve portability or to clean up obsolete coding. In addition, an error in Law 44 histograms was fixed, logic was added to make sure that thinning does not remove any thresholds, the print-out for "type 1" output was updated, and an error in the endpoint of the photon production cross section was repaired. More recent updates include a patch to set the thermal PENDF unit number and changes to allow for charged-particle levels in File 12 (silicon).

15. POWR. The POWR module is used to generate multigroup libraries for the Electric Power Research Institute codes EPRI-CELL and EPRI-CPM. No changes have been made.

16. PLOTR. The PLOTR module is used to generate plots of ENDF, PENDF, or GENDF cross sections, or of experimental data. Multiple curves from any of these sources can be overplotted, and the data points can have error bars. All the normal combinations of scales are provided, and curves can be labeled with tags and arrows or with a legend block. Angular distributions from File 4 or certain sections of File 6 can be shown in 3-d perspective plots. Energy distributions from File 5 can also be shown as perspective plots. With File 6 data, perspective plots can be constructed for any of the emitted particles. In addition, 2-d plots can be made of selected spectra extracted from File 6 for a specified particle and incident energy.

The most notable changes made for NJOY 89 were a capability to plot the "Law 7" form of File 6, improved axes for the 3-d perspective plots, and changes to improve portability. Examples of the current 3-d plots are shown in Figs. II-5 and II-6.

PLOTR needs several additional capabilities in the near future, the most important being the capability to plot single angular distributions extracted from File 4 or 6, the capability to plot File 7 data, the capability to plot Coulomb scattering data, and a better interface for selecting curves out of distributions.

PLOTR uses the DISSPLA graphics library, a product of ISSCO Graphics.

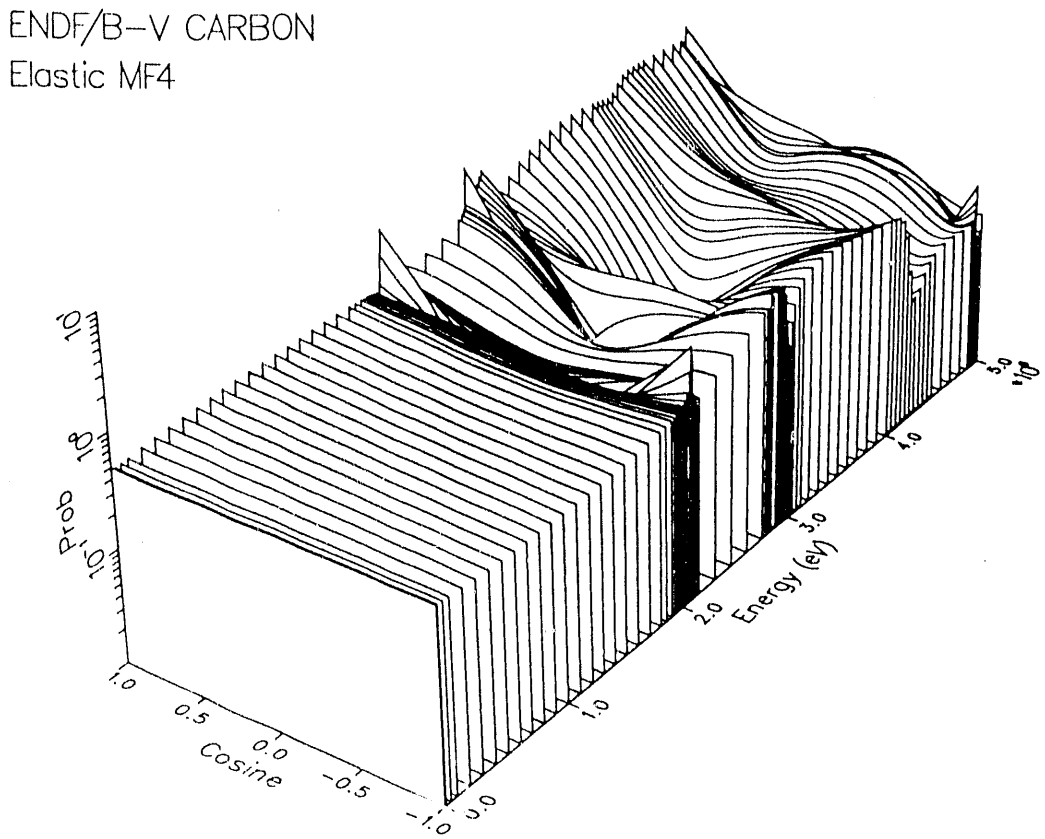

Fig. II-5. Perspective view of the carbon elastic scattering angular distribution.

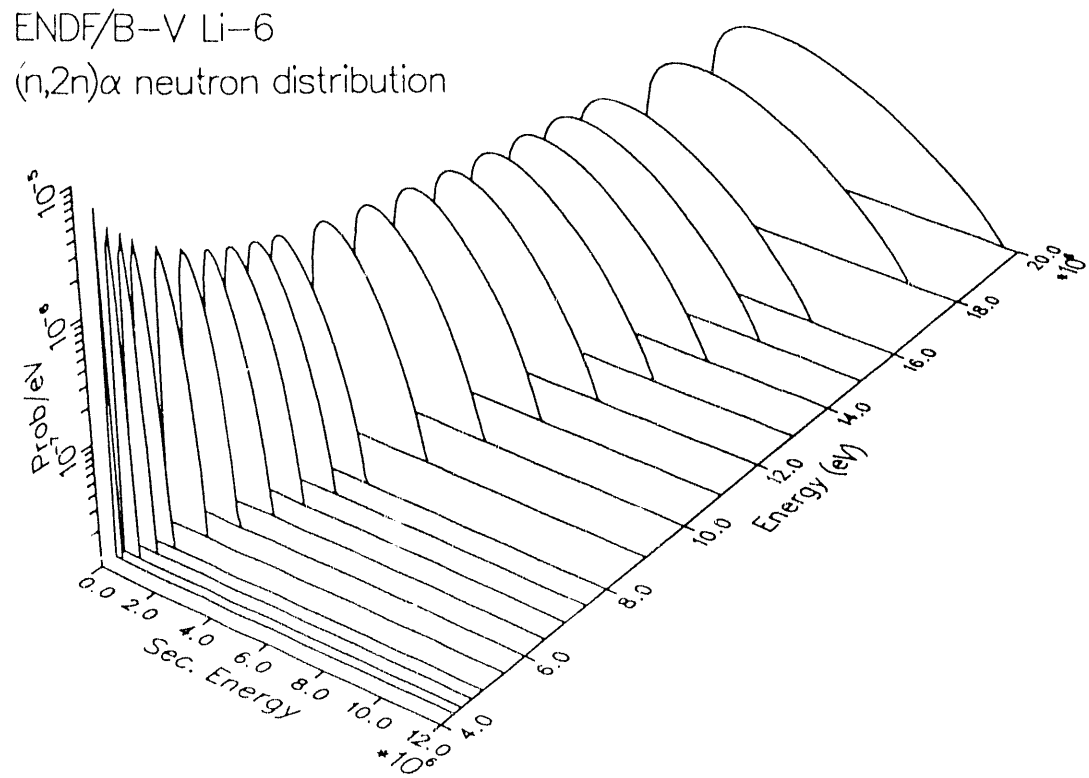

Fig.II-6. Perspective plot of the ^{6}Li (n,2n)α secondary neutron distribution.

B. MENDLIB (D. C. George and E. R. Siciliano)

Improvements to MENDLIB, the Medium Energy Nuclear Data Library Project, included:

1. Improvements to the user interface to remove the case sensitivity of responses, to allow the user to specify a range of Z and A values over which to search, and to re-arrange the order of prompts into a more logical sequence.
2. The addition of a table to the data base structure. This table contains the English words describing the units of the x and y variables. The portions of the user interface relating to retrieval, decoding, and printing of these fields were altered accordingly.
3. The creation of one master retrieval subroutine that can handle retrieval for all types of reactions. The original multiple subroutines were merged, greatly simplifying the process of modifying the code.

Efforts to acquire more data for the system, including hiring a summer student to contact prospective contributors, met with little success. At present over 20,000 data points from over 1700 measurements and 161 bibliographic references have been collected. This amount of data represents approximately 25% of available data.

C. References-Section II

1. R. E. MacFarlane, D. W. Muir, and R. M. Boicourt, "The NJOY Nuclear Data Processing System, Volume I: User's Manual," and "The NJOY Nuclear Data Processing System, Volume II: The NJOY, RECONR, HEATR, and THERMR Modules," Los Alamos National Laboratory reports LA-9303-M, Vols. I and II (May 1982). R. E. MacFarlane and D. W. Muir, "The NJOY Nuclear Data Processing System, Volume III: The GROUPR, GAMINR, and MODER Modules," Los Alamos National Laboratory report LA-9303-M, Vol. III (October 1987). D. W. Muir and R. E. MacFarlane, "The NJOY Nuclear Data Processing System, Volume IV: The ERRORR and COVR Modules," Los Alamos National Laboratory report LA-9303-M, Vol. IV (December 1985).

2. P. F. Rose and C. L. Dunford, Eds., "ENDF-102, Data Formats and Procedures for the Evaluated Nuclear Data File, ENDF," preliminary version for the ENDF-6 format available from the National Nuclear Data Center, Brookhaven National Laboratory, Upton, NY (May 1988).

3. H. Henryson, B. J. Toppel, and C. G. Stenberg, "MC^2-II: A Code to Calculate Fast Neutron Spectra and Multigroup Cross Sections," Argonne National Laboratory report ANL-8144 (1976).

4. F. H. Fröhner, "New Techniques for Multi-Level Cross-Section Calculation and Fitting," Kernforschungszentrum für Kernphysik report KFK-3081 (1980).

5. R. N. Hwang, "A Rigorous Pole Representation of Multilevel Cross Sections and Its Practical Applications," Nucl. Sci. Eng. 96, 192 (1987).

6. M. S. Moore, L. Calabretta, F. Corvi, and H. Weigmann, "Analysis of Intermediate Structure in the Fission and Capture Cross Sections of (^{235}U+n)," Phys. Rev. C 30, 214 (1984).

7. R. E. MacFarlane, "Energy Balance of ENDF/B-V" Trans. Am. Nucl. Soc. 33, 681 (1979).

8. M. A. Abdou, Y. Gohar, and R. Q. Wright, "MACK-IV, A New Version of MACK: A Program to Calculate Nuclear Response Functions from Data in ENDF/B Format," Argonne National Laboratory report ANL/FPP-77-5 (1978).

9. R. E. MacFarlane and D. G. Foster, Jr., "Advanced Nuclear Data for Radiation Damage Calculations," J. Nucl. Materials 122, 1047 (1984).

10. J. U. Koppel and D. H. Houston, "Reference Manual for ENDF Thermal Neutron Scattering Data," General Atomics report GA-8774 i (ENDF-269) revised and reissued by the National Nuclear Data Center, Brookhaven National Laboratory (1978).

11. C. Kalbach and F. M. Mann, "Phenomenology of Continuum Angular Distributions. I. Systematics and Parameterization," Phys. Rev. C 23, 112 (1981).

12. C. Kalbach, "Systematics of Continuum Angular Distributions: Extensions to Higher Energies," Los Alamos National Laboratory document LA-UR-87-4139 (1987) (to be published in Phys. Rev. C).

13. P. G. Young and E. D. Arthur, "GNASH: A Preequilibrium Statistical Nuclear Model Code for Calculation of Cross Sections and Emission Spectra," Los Alamos Scientific Laboratory report LA-6947 (November 1977).

14. R. E. MacFarlane, "TRANSX-CTR: A code for Interfacing MATXS Cross-Section Libraries to Nuclear Transport Codes for Fusion Systems Analysis," Los Alamos National Laboratory report LA-9863-MS (February 1984).

15. Judith F. Briesmeister, Ed., "MCNP--A General Monte Carlo Code for Neutron and Photon Transport, Version 3A," Los Alamos National Laboratory report LA-7396-M (September 1986).

III. NUCLEAR APPLICATIONS

A. Transmutation of Defense High Level Nuclear Wastes Using High Current Accelerators

[E. D. Arthur, P. W. Lisowski (P-17), and C. D. Bowman (P-3)]

Significant advances in the technology associated with high current linear accelerators offer attractive possibilities for new applications. One such opportunity may exist in the possible transmutation of defense high level nuclear waste using an intense accelerator-produced source of neutrons. Investigation of the application of such technology to the area of defense-generated nuclear wastes is of particular appeal now for several reasons:

1. The Department of Energy has identified cleanup of its production complex as a priority item.
2. Significant amounts of high level wastes composed of short-lived (~30 year halflife) and long-lived (>100,000 year) fission products along with higher transuranics (neptunium, americium) exist in a partitioned form.
3. The present approach for dealing with such wastes (vitrification followed by repository storage) promises to be expensive and may be open to technical criticism.
4. Long-lived fission products such as ^{99}Tc and ^{129}I dominate long-term scenarios because of their mobility and their potential impact on the biosphere. Burnup of these specific wastes could permit the technical certification required for repository or site storage options.
5. New technical advances, particularly in the area of accelerator development, offer real and implementable options for creating neutron fluxes high enough to transmute short-lived radionuclides having low interaction cross sections.
6. There is a growing national and international interest in transmutation concepts as evidenced by the Japanese OMEGA project, and study efforts such as the CURE (Clean Use of Reactor Energy) concept under development at Westinghouse Hanford Laboratory.

We have completed preliminary scoping arguments that indicate the desirability of a more complete system study of such an accelerator transmutation approach. Such a study is now beginning in Group A-3. We have also published a paper presented recently in Japan outlining the nuclear data needs for accelerator-based radionuclide transmutation.[1] Accelerator-based transmutation of defense high level nuclear wastes would concentrate on a relatively few radionuclides which exists in significant quantities in defense wastes such as those stored in single and double shelled tanks at Hanford. Candidate species include neptunium, americium, curium isotopes as well as fission products such as ^{90}Sr,^{137}Cs, ^{99}Tc, and ^{129}I. Higher order transuranics would be transmuted through fission to products having much shorter half-lives, while fission

products would be transmuted using low-energy neutron capture to stable by-product nuclei. An indication of the possible effectiveness of transmutation is indicated in Fig. III-1. The effective half-lives achieved for the cross-section curves shown and for an assumed neutron flux of 5 x 10^{15} n/cm^2/sec are compared with natural decay half-lives for three of the candidate species listed above. Such flux considerations indicate a reduction in effective time scales associated with such radionuclides of 1 to 8 orders of magnitude.

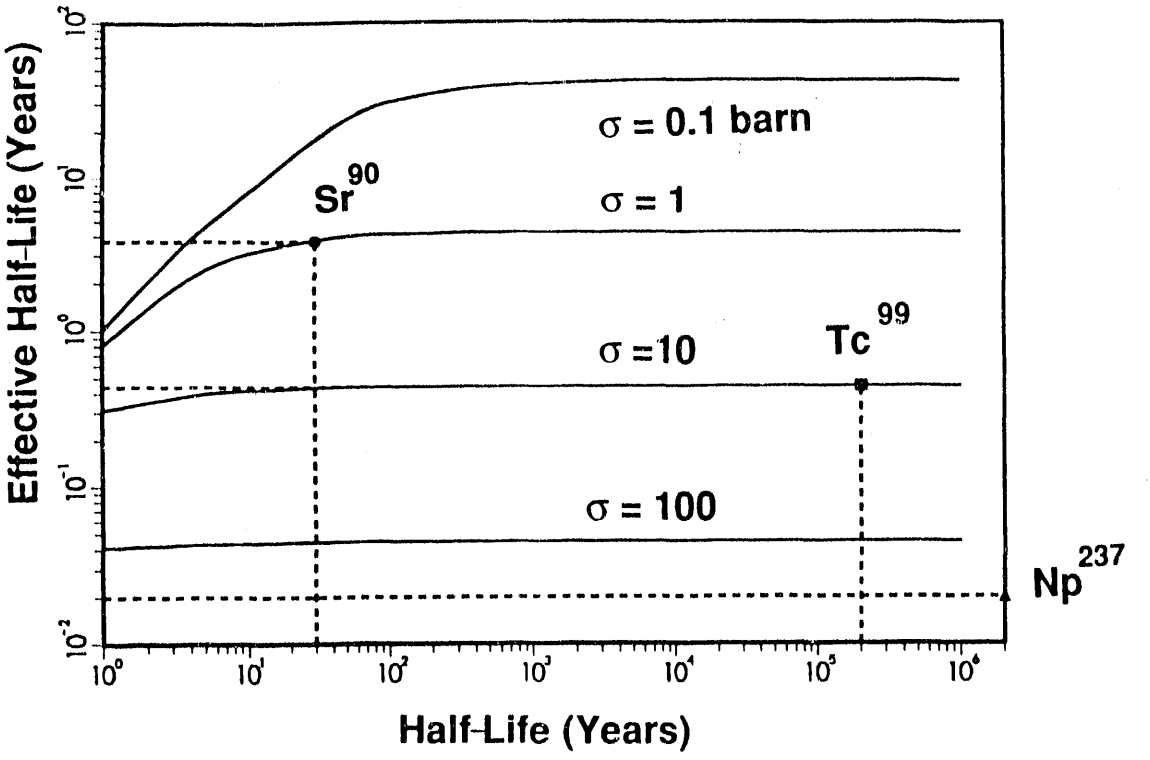

Fig III-1. Effective half-lives of radionuclides that occur in a neutron flux level of 5 x 10^{15} n/cm^2/sec.

A schematic of such an accelerator-based system for transmutation is shown in Fig.III- 2. An 1.6-GeV, 250-milliampere, continuous wave (CW) accelerator is used to produce neutrons in a flowing lead-bismuth eutectic target surrounded by a moderator such as heavy water. Neutron fluences in target configurations now under study are in the range from 10^{14} to greater than 10^{16} n/cm^2/sec, depending upon the radial distance from the spallation target. Radionuclide targets exposed in these fluences would have significant transmutation rates. Other steps indicated in the process include initial chemical separation (partitioning) that would exist prior to introduction into a neutron burnup environment, target fabrication, repartitioning after burnup levels of 30-50% are reached, and repackaging of materials into new targets for further irradiation.

Neutron economy arguments, based upon the isotopes and reaction processes involved (capture-to-fission ratios, *e.g.*), as well as the neutron fluxes expected from such an accelerator neutron source (> 10^{27} neutrons produced per year), indicate that defense waste amounts on the order of one-to-two thousand kilograms could be transmuted within decade-like time scales. In order to improve upon such estimates, we have developed, and are now testing, simple models that include burnup and cycle times associated with target removal, fabrication, and repartitioning. These will be used to generate time estimates for dealing with specified quantities of the radionuclide species listed earlier.

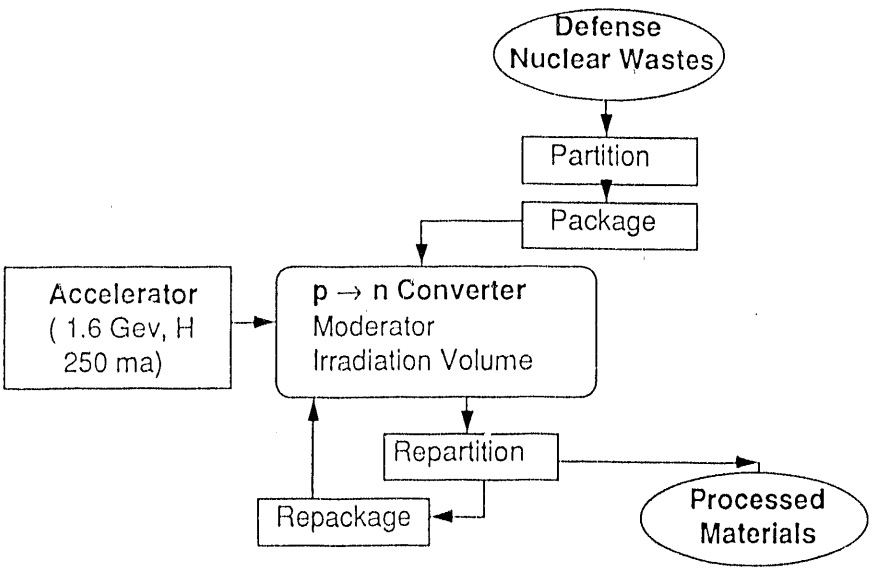

Fig III-2. Schematic of an accelerator-based system for transmutation of defense high-level nuclear wastes.

B. Application of Fission-Product, Actinide, and Activation Data (T. R. England and W. B. Wilson)

In Section V.G the extensive effort to expand the actinide, activation, fission-product and yield data base is described. Much of that effort is motivated by needs in applications. Comments in Sec. V.G will not be repeated here except to note:

(a) Decay data exists for approximately 1100 nuclides, and this currently includes complete spectra for beta, gamma, alpha, delayed neutrons, and other emissions. Six-group delayed neutron data, including spectra, for 28 fissioning nuclides have also been generated.

(b) Fission-product yields extend over 36 fissioning nuclides at one or more incident neutron energies for ≥ 1200 products.

The data have been used in several applications by Group T-2:

(a) Nuclear background radiations required in one Los Alamos program have been extensively studied for most fuels. The results are contained in Los Alamos report LA-11151-MS, "Background Radiation from Fission Pulses," referenced in Sec. V.

(b) Inventories of radionuclides in high-exposure fuels were produced for the US Nuclear Regulatory Commission, as reported in *Nuclear Safety* 29, No. 2 (April-June 1988), again as referenced in Sec. V.

(c) The fission product yields were incorporated into the recent (14th edition) of the Chart of the Nuclides (published by General Electric Co., San Jose, California) and in a draft American Nuclear Society standard produced by the ANS 5.2 Working Group. These will also be used in many other applications along with fission physics. The data base forms the foundation for a new IAEA CRP (International Atomic Energy Agency Coordinated Research Proposal) international group.

(d) Delayed neutron measurements are discrepant. The delayed neutron data have been accepted for use by a new NEANDC/NEACRP (Nuclear Energy Agency Nuclear Data Commission) international group to help resolve the problems. In addition, a new working group within the ANS (ANS 5.8) to determine a standard for delayed neutron data has been formed.

(e) At a recent meeting of the American Nuclear Society Decay Power Working Group, it was recommended that the decay data described in Sec. V.G be used to extend the range of the standard and used wherever aggregate measurements do not exist. The spectral data are utilized for several other applications at Los Alamos.

C. Data and Code Development for Transmutation Calculations (W. B. Wilson and T. R. England)

In the past we have used earlier versions of the code CINDER in calculations of reactor fuel depletion, fission-product build-up, and aggregate properties such as neutron absorption, decay power, and decay spectra.[2-6] The REAC and REAC*2 codes have been used in calculations of transmutation in non-fissioning systems.[7-8] CINDER versions have required the formation of a set of transmutation chains for a range of applications, restricting the applications to spectral limitations assumed in chain formation. REAC and REAC*2 do not include neutron absorption reactions on nuclides that are not initially present in a time step.

A new code, CINDER'90, is being developed that does not require a pre-existing transmutation chain structure. The general CINDER algorithm is used in the solution of chains formed during the calculation; in this process all paths produced by the transmutation of a nuclide are followed until significance is lost. Libraries have been developed from data processed from

ENDF/B-V and preliminary ENDF/B-VI,[9] The Table of Isotopes,[10] The Chart of the Nuclides,[11] nuclear model code calculations,[12] and the REAC code library.[8]

Accelerator activation studies have used LAHET[13] (Los Alamos High Energy Transport)-calculated spallation/fission product yields from all reactions except neutrons below 20 MeV plus the binned neutron flux for $E_n \leq 20$ MeV. CINDER'90 has been used to follow the temporal transmutation by decay and neutron absorption below 20 MeV of all initially present and yielded nuclides.

D. Ion Induced Thick-Target Nuclide Production and Radiation Sources [W. B. Wilson, M. Bozoian, R. T. Perry (N-12), and P. G. Young]

Our activity in ion reaction data has grown from low-energy reactions of decay α's in (α,n) reactions on light targets[14] to medium-energy reactions of protons and α's with a range of targets.[15-18] This extension has relied heavily upon nuclear model code results, producing reaction cross sections and thick-target yield values with rather large uncertainties but useful in a variety of applications. The range of particles and energies studied to date are given in Table III-I.

TABLE III-I

TARGETS AND ENERGIES FOR WHICH THICK TARGET YIELDS HAVE BEEN CALCULATED

	Particle Energy, MeV	
Target	Protons	Alphas
$_4$Be	≤ 100	≤ 50
$_5$B		≤ 50
$_6$C	≤ 100	≤ 50
$_7$N		≤ 50
$_8$O	≤ 100	≤ 50
$_9$F		≤ 50
$_{10}$Ne	≤ 100	≤ 50
$_{11}$Na		≤ 50
$_{12}$Mg		≤ 50
$_{13}$Al	≤100	≤ 50
$_{14}$Si	≤ 100	≤ 50
$_{15}$P		≤ 50
$_{17}$Cl		≤ 50
$_{26}$Fe	≤ 50	
$_{27}$Co	≤ 50	
$_{28}$Ni	≤ 50	
$_{29}$Cu	≤ 100	
$_{74}$W	≤ 50	
$_{83}$Bi	≤ 100	

E. References-Section III

1. C. D. Bowman, P. W. Lisowski, and E. D. Arthur, "Spallation-Based Science and Technology and Associated Nuclear Data Requirements," Proc. 2nd Int. Symp. on Advanced Nuclear Energy Research-Evolution by Accelerators, Mito, Japan, January 24-26, 1990, p. 149.

2. T. R. England, "CINDER--A One-Point Depletion and Fission Product Program," Bettis Atomic Power Laboratory report WAPD-TM-334 (Rev) (1964).

3. T. R. England, R. Wilczynski, and N. L. Whittemore, "CINDER-7: An Interim Report for Users," Los Alamos Scientific Laboratory report LA-5885-MS (April 1975).

4. T. R. England, W. B. Wilson and M. G. Stamatelatos, "Fission Product Data for Thermal Reactions, Part 1: A Data Set for EPRI-CINDER Using ENDF/B-IV," Los Alamos Scientific Laboratory report LA-6745-MS (December 1976). [Also published as EPRI NP-356, Part 1.]

5. T. R. England, W. B. Wilson, and M. G. Stamatelatos, "Fission Product Data for Thermal Reactors, Part 2: Users Manual for EPRI-CINDER Code and Data," Los Alamos Scientific Laboratory report LA-6746-MS (December 1976). [Also published as EPRI NP-356, Part 2.]

6. W. B. Wilson, T. R. England, R. J. LaBauve, and D. C. George, "CINDER-3 Depletion Code for Class VI computers," Trans. Am. Nucl. Soc. 46, 724 (1984).

7. F. M. Mann, "Transmutation of Alloys in MFE Facilities as Calculated by REAC," Hanford Engineering Development Laboratory report HEDL-TME 81-37 (August 1982).

8. F. M. Mann, "REAC*2: Users Manual and Code Description," Westinghouse Hanford Company report WHC-EP-0182 (December 1989).

9. ENDF/B-V and ENDF/B-VI, Evaluated Nuclear Data File, maintained and distributed by the National Nuclear Data Center, Brookhaven National Laboratory, Upton, New York.

10. C. Michael Lederer and Virginia S. Shirley, Eds. Table of Isotopes, Seventh Edition (John Wiley and Sons, Inc., New York, 1978).

11. F. William Walker, Josef R. Parrington, and Frank Feiner, Eds., Nuclides and Isotopes, Fourteenth Edition (General Electric Company, San Jose, California, 1989).

12. E. D. Arthur, M. Bozoian, D. G. Madland, R. T. Perry, W. B. Wilson, and P. G. Young, "Application of Nuclear Models to the Calculation of 20-100 MeV Neutron Induced Reaction Data," presentation at IAEA Advisory Group Meeting on Nuclear Theory for Fast Neutron Data Evaluation, October 12-16, 1987, Beijing, China (Los Alamos National Laboratory document LA-UR-87-3383).

13. R. E. Prael and H. Lichtenstein, "User Guide to LCS: The LAHET Code System," Los Alamos National Laboratory document LA-UR-89-3014 (September 1989).

14. W. B. Wilson, M. Bozoian, and R. T. Perry, "Calculated α-Induced Thick Target Neutron Yields and Spectra, with Comparison to Measured Data," Proc. Int. Conf. on Nuclear Data for Sci. Tech., May 30-June 3, 2988, Mito, Japan (1988), pp. 1193-1197.

15. W. B. Wilson, T. R. England, R. J. LaBauve, and J. A. Mitchell, "Calculated Radionuclide Inventories of High-Exposure LWR Fuels," Nuclear Safety 29, 177 (1988).

16. W. B. Wilson, E. D. Arthur, M. Bozoian, R. T. Perry, and P. G. Young, "Calculated Proton-Induced Thick-Target Neutron and Gamma Yield Spectra for $E_p \leq 100$ MeV," Trans. Am. Nucl. Soc. 60, 273 (1989).

17. M. Bozoian, R. T. Perry, and W. B. Wilson, "Calculated α-Induced Thick-Target Neutron and Radionuclide Yields for $E_\alpha \leq 50$ MeV," Proc. Workshop on High Energy and Heavy Ion Beams in Materials Analysis, June 14-17, 1989, Albuquerque, New Mexico (1990), pp. 51-59.

18. W. B. Wilson, E. D. Arthur, M. Bozoian, and R. T. Perry, "Calculated Proton-Induced Thick-Target Neutron and Radionuclide Yields for $E_p \leq 100$ MeV," Proc. Workshop on High Energy and Heavy Ion Beams in Materials Analysis, June 14-17, 1989, Albuquerque, New Mexico (1990), pp. 39-49.

IV. REACTIONS

A. Double-Differential Cross-Section Calculations Based on a Monte-Carlo Formulation of the Multistage Preequilibrium Model[1,2] [M. Bozoian and R. E. Prael (X-6)]

The intranuclear cascade model employed in the HETC/LAHET Monte-Carlo code underpredicts double-differential cross-section back-angle scattering in the intermediate emission energy range of 50-250 MeV. The GNASH multistage preequilibrium, statistical nuclear model has been adapted to the Monte-Carlo algorithm and implemented in HETC/LAHET in order to improve these back-angle calculations. Figures IV-1 and-2 show LAHET alone and LAHETprq1, where "prq1" refers to the interface between the cascade and preequilibrium models defined in terms of the residual nuclear state obtained after a single execution of a Bertini model intranuclear cascade calculation, compared with recent Los Alamos data.[3]

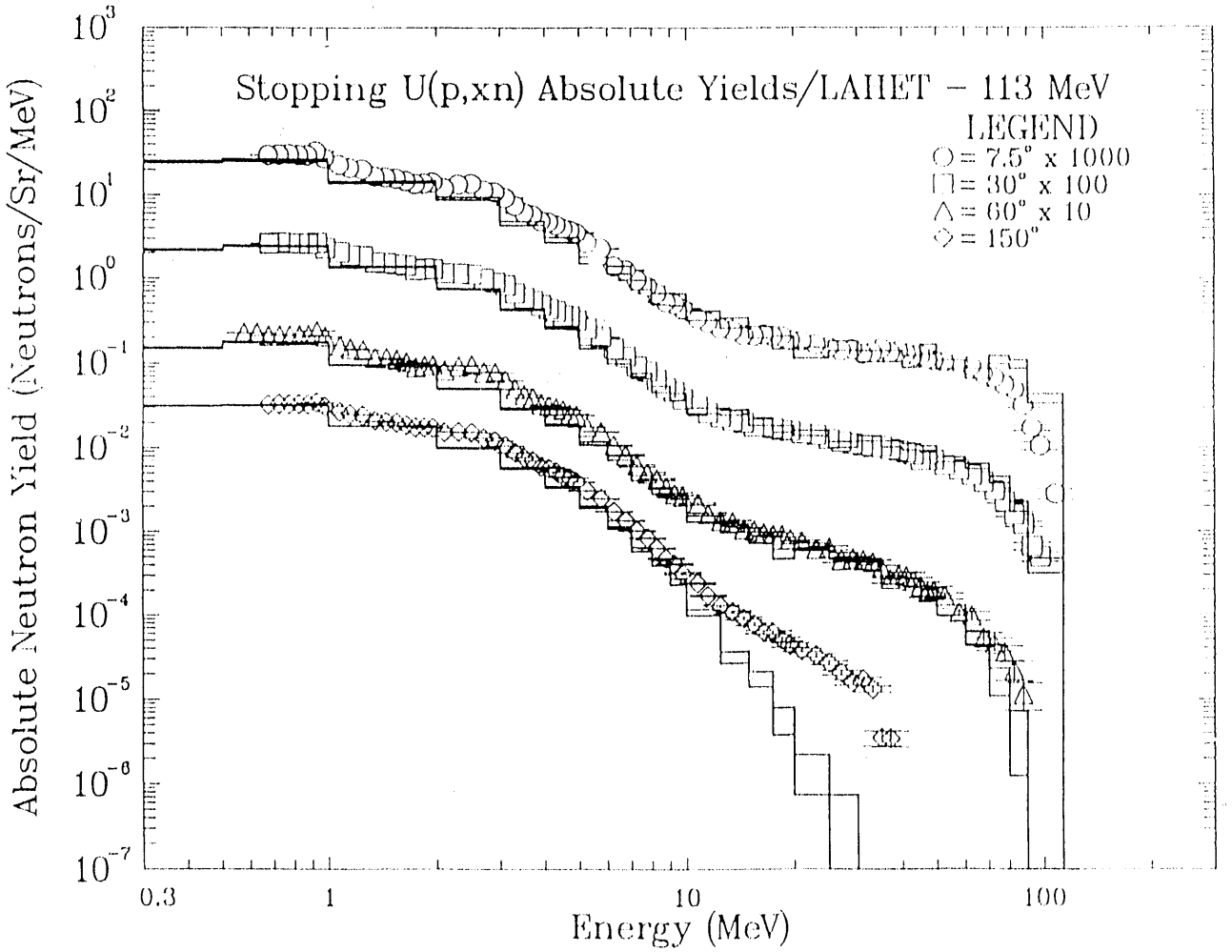

Fig. IV-1. Neutron yield for 113-MeV p + ^{238}U, LAHET alone.

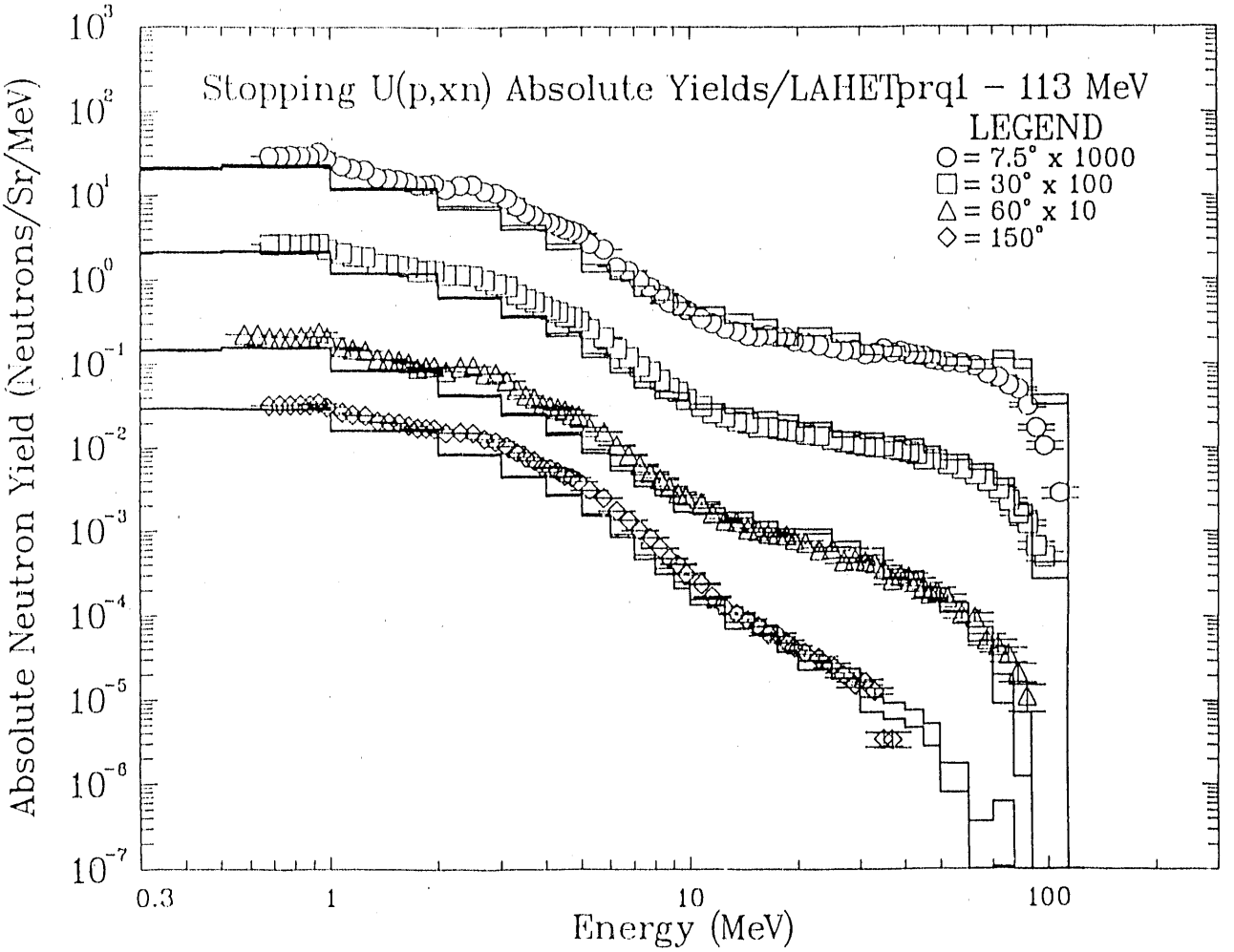

Fig. IV-2. Neutron yield for 113-MeV p + ^{238}U, LAHET with preequilibrium.

B. Quasi-Free Scattering (QFS) in the Preequilibrium Region (R. D. Smith, M. Bozoian, E. D. Arthur)

We have developed a model for inclusive proton-nucleus scattering that covers the preequilibrium region.[4,5] This model is based on (a) single-step quasi-free scattering, and (b) the exciton model, which describes emission from 3p2h and higher configurations. We have compared the model with data for various nuclei at incident energies from 60 to 200 MeV. Figure IV-3 shows the calculated (p,p') spectra with respect to both the pure exciton and QFS plus exciton models for ^{54}Fe, ^{58}Ni, and ^{27}Al. The systematics of angle-dependent energy spectra are well reproduced by the model, with the exception of the large-energy-loss region at very forward angles. We find the single-step quasi-free scattering constitutes 60% to 80% of the reaction cross section in medium-heavy nuclei and about 50% in heavy nuclei. The preequilibrium region is therefore dominated by direct single-step reactions.

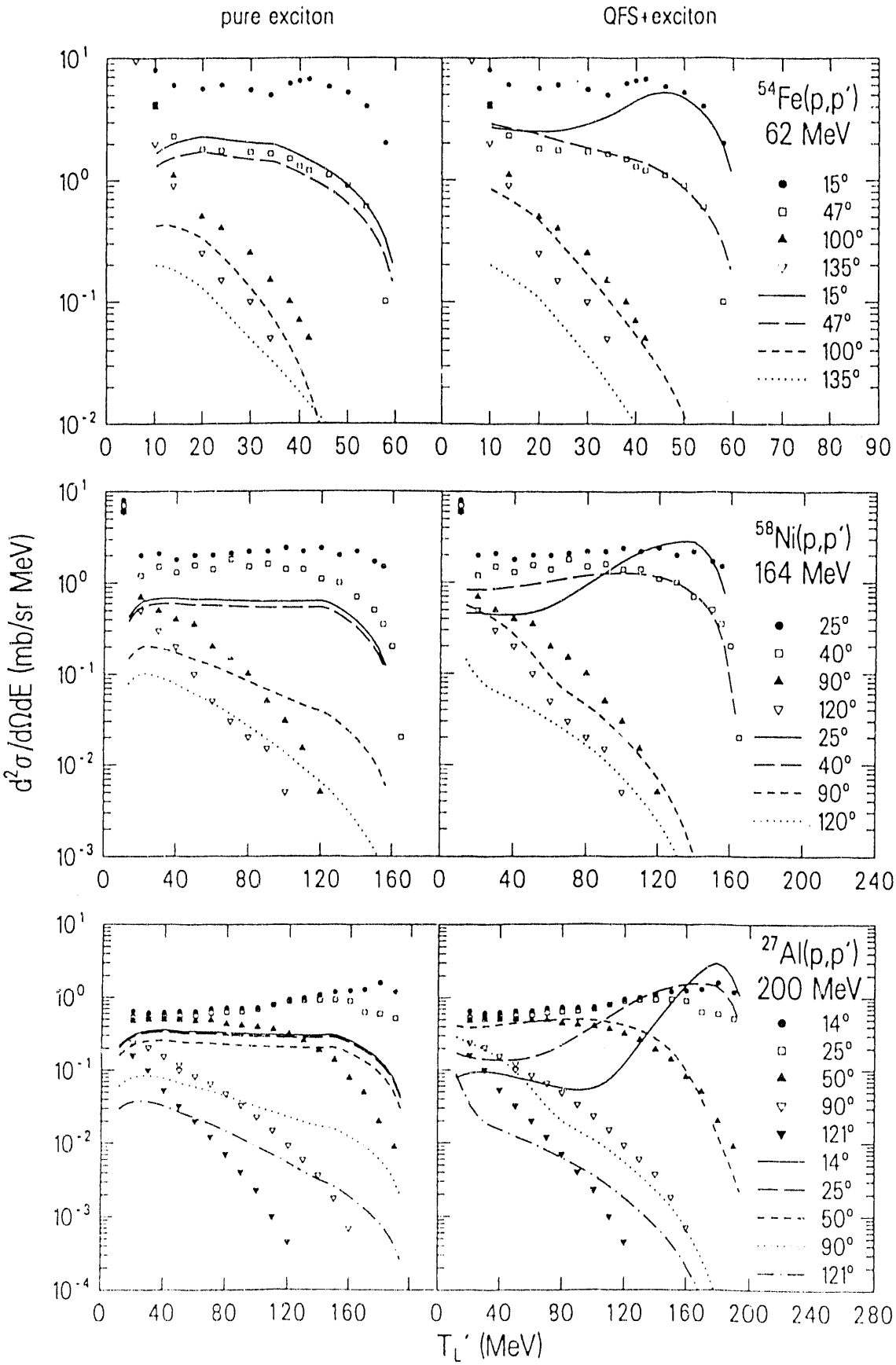

Fig. IV-3. Calculated (*p*,*p'*) spectra in the pure exciton and QFS + exciton models.

C. Phenomenology of Quasi-Free Scattering [C. Kalbach-Walker (Consultant to T-2), M. Bozoian]

The report "Phenomenology of Quasi-Free Scattering" was completed as a Los Alamos National Laboratory informal document (LA-UR-89-3047) and submitted to Physical Review C in late October 1989. The systematics of quasi-free scattering have been parameterized for incident proton energies of 100-1000 MeV on a variety of targets. The observed position of the quasi-free scattering peak at various emission angles closely tracks the kinematics for free nucleon-nucleon scattering. The peak widths are a function of the incident energy and of sin θ in the N-N center-of-mass. The angle-integrated cross section is described in terms of a peripheral interaction with a single nucleon in the target nucleus and has a threshold of 150-200 MeV. The angular variation of the cross section is either nearly isotropic or, at higher energies, exponential in cos θ. The simple parameterization derived here allows a semi-quantitative estimate of QFS peaks with no adjustable parameters.

D. 98-MeV Deuterons Incident on ^{27}Al and ^{238}U [M. Bozoian, E. D. Arthur, J. Martin (Air Force Weapons Laboratory)]

We have performed preliminary calculations of 98-MeV deuterons incident on ^{27}Al and ^{238}U using an evaporation version of GNASH that incorporates a Serber stripping model. In both cases we have approximated the transmission coefficients as being lumped into the s-wave after determining the reaction cross sections at several energies (up to 100 MeV) based on the Daehnick *et al.* potential.[6] Figures IV-4, -5 and -6 show the neutron emission spectra at 15° and 60° and the gamma emission spectra at 45°, respectively, for the ^{27}Al target. Figures IV-7 and -8 show the neutron emission spectra at 30° and at 105° for the ^{238}U target. In the latter case the GNASH version gn88c1 was used to find the multichance neutron spectra, whereas the GNASH version gn88c4 was used to determine the neutron spectra from the de-excitation of the fission fragments of ^{240}Np and related compound systems obtained after multichance neutron emissions. The fission fragments and their excitation energies were found from a scission-point model, discussed in Sec.V-D of this report. The multichance neutrons were assumed to be described by angular distribution systematics, whereas the fission neutrons were assumed to be emitted isotropically.

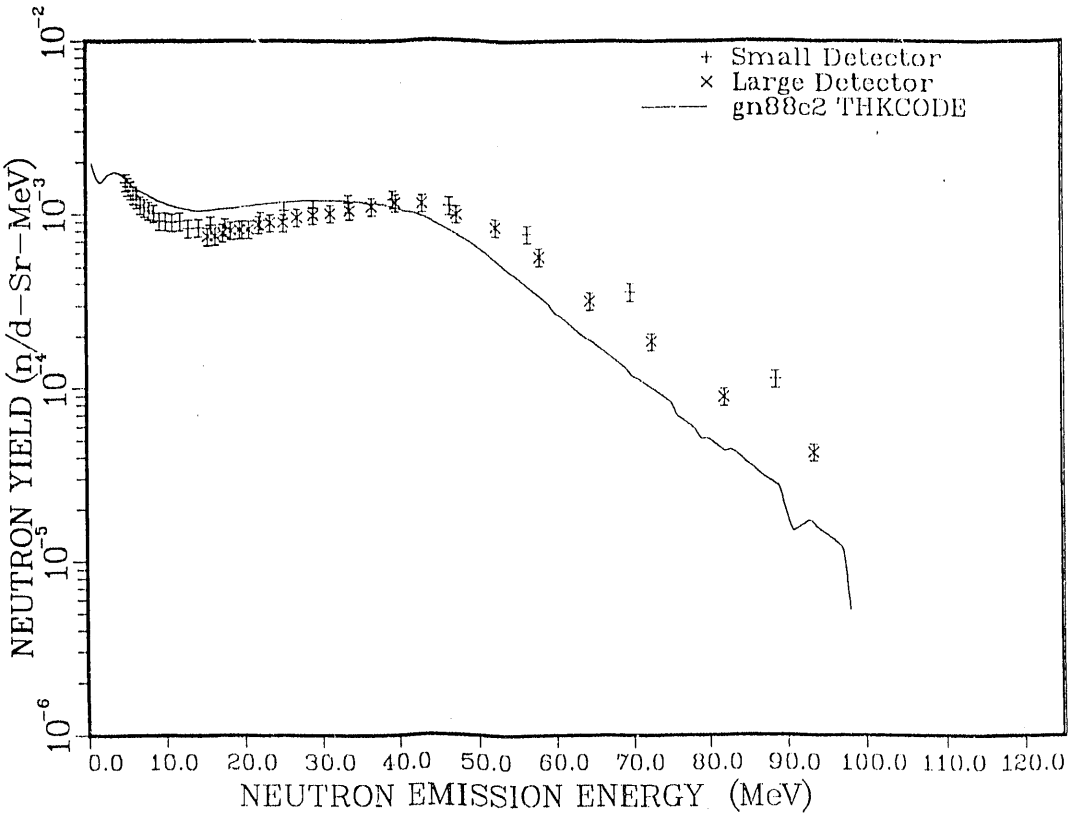

Fig. IV-4. 98-MeV deuterons plus ^{27}Al at 15°.

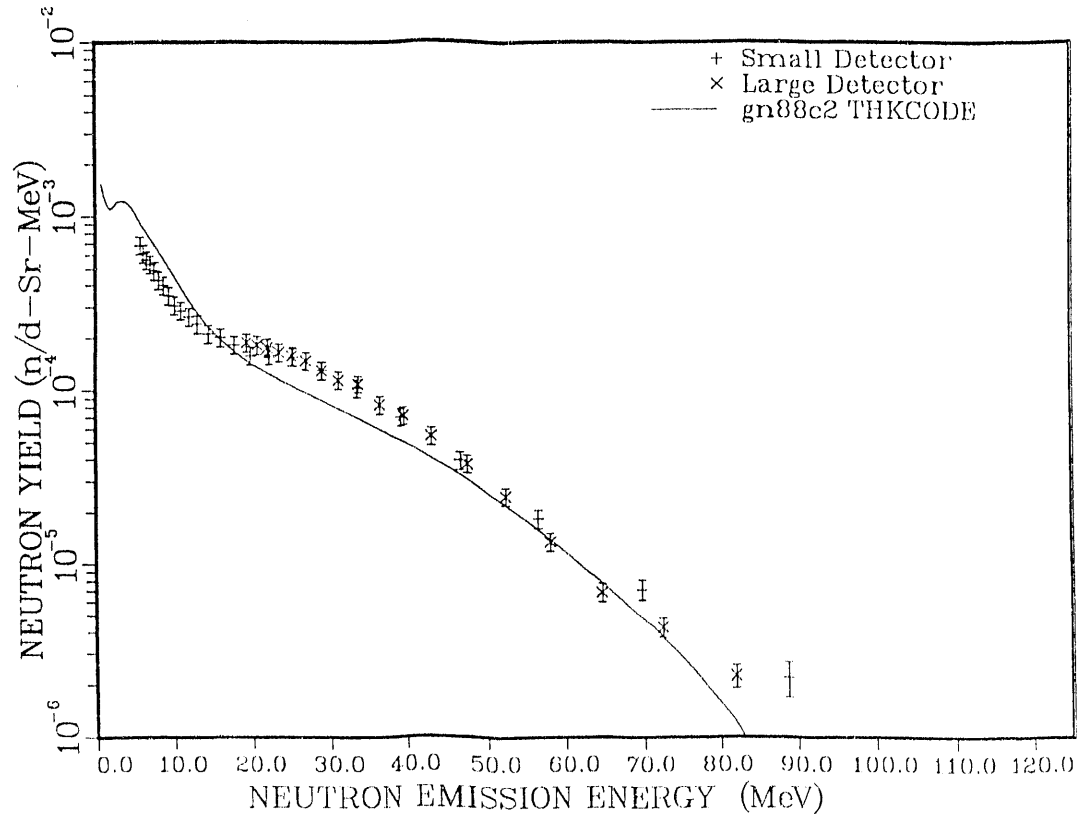

Fig. IV-5. 98-MeV deuterons plus ^{27}Al at 60°.

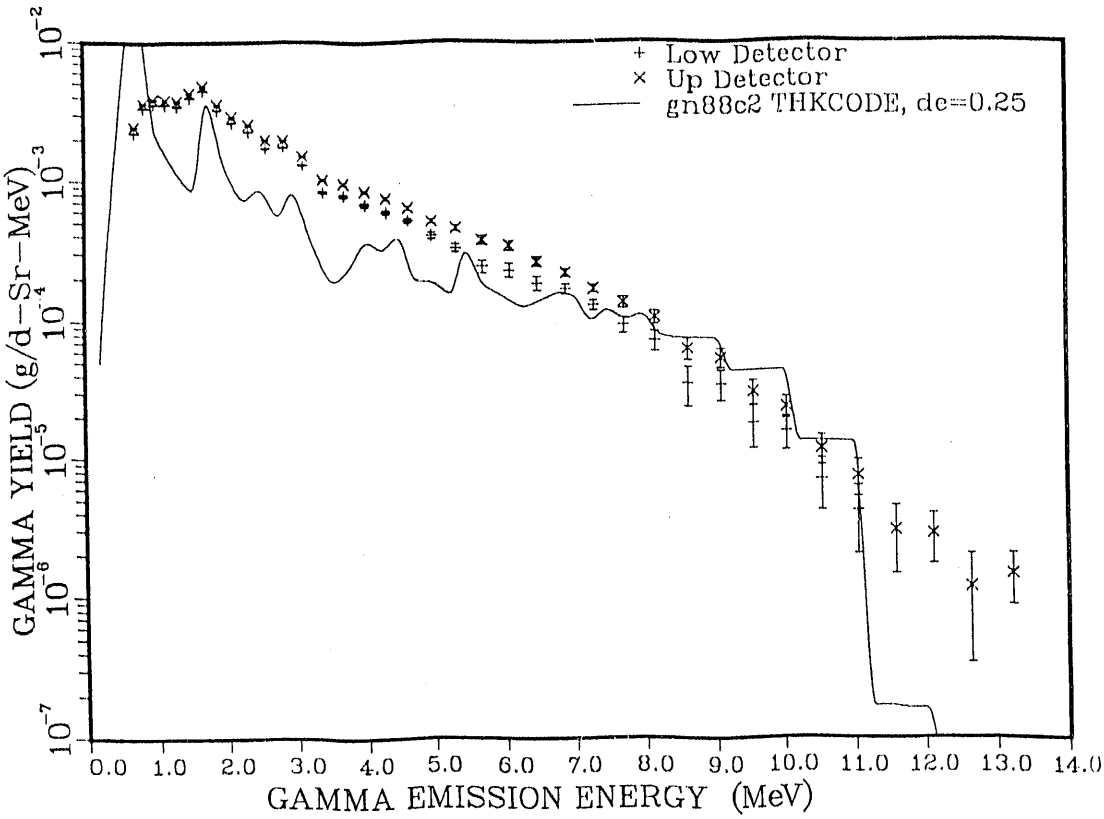

Fig. IV-6. 98-MeV deuterons plus ^{27}Al at 45°.

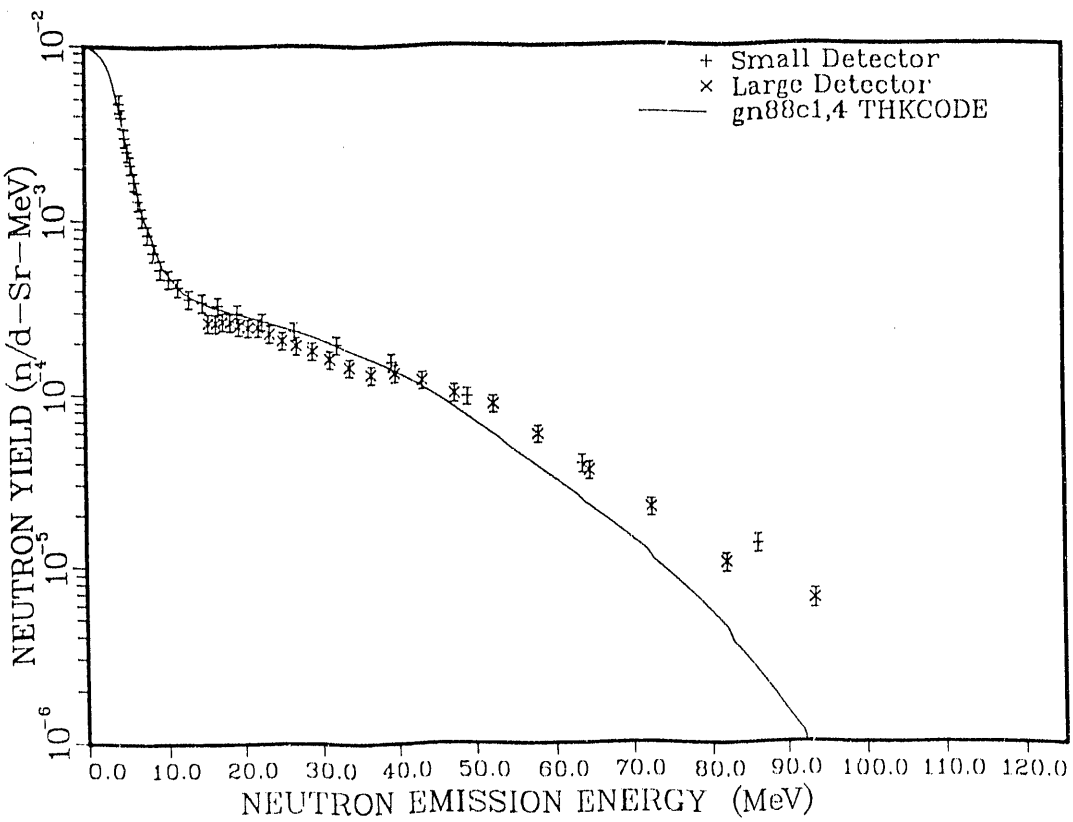

Fig. IV-7. 98-MeV deuterons plus ^{238}U at 30°.

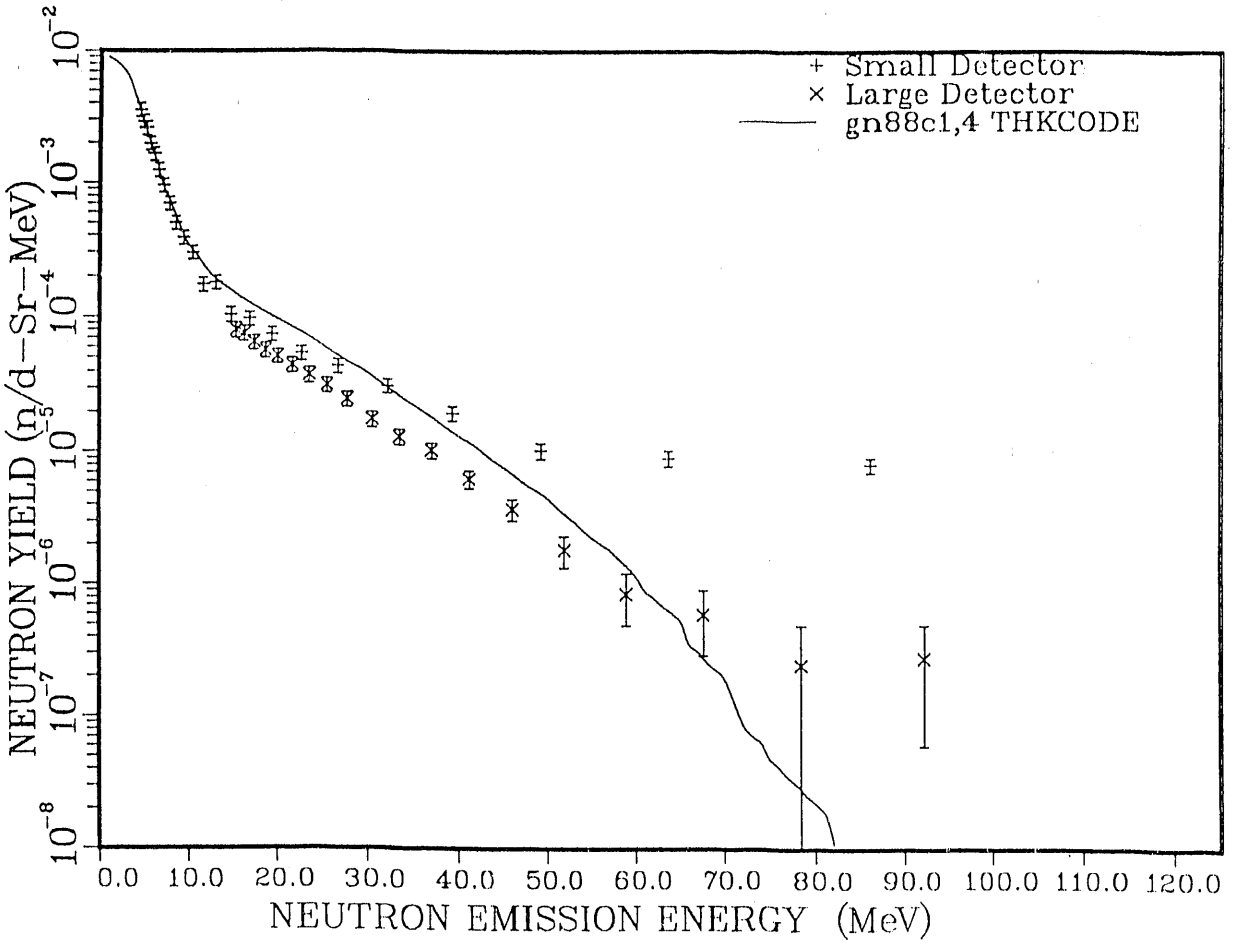

Fig. IV-8. 98-MeV deuterons plus ^{238}U at 105°.

E. Correction for Truncation in Coupled-Channels Optical Potentials [D. G. Madland, V. A. Madsen (Oregon State Univ.), and L. F. Hansen and V. R. Brown (Lawrence Livermore Nat. Lab.)]

Coupled-channel calculations using the same optical-model parameter set for all coupled states have been compared for rotational and harmonic vibrator sequences, truncating all states of the sequence above a certain nuclear energy level. It was found that the inelastic cross section for the highest included state is somewhat larger than a coupled-channel calculation that includes the next state of the sequence. This effect is due to the absence of the absorption taking place through the truncated state. Except at very low bombarding energies, the cross sections for lower states in the sequence are virtually unaffected by the truncation. Approximate formulas have been derived and tested for correcting the optical potential of the highest included state. Good agreement is

obtained with coupled-channel calculations that include these higher states explicitly. Application has been made to the problem of obtaining inelastic deformation parameters β with distorted-wave Born approximation and with different coupling schemes. This work has been published.[7]

F. Initial Deuteron-Nucleus Global Optical-Model Potential for NPB Target Discrimination Calculations (D. G. Madland)

A first-pass approximate global optical-model potential for deuteron-nucleus scattering has been determined for incident deuteron energies E_d in the range 10 MeV $\leq E_d \leq$ 200 MeV and for target mass numbers in the range $27 \leq A \leq 238$. This potential is based upon the potential of Daehnick *et al.*,[6] which is applicable to the energy range 12 MeV $\leq$ 90 MeV. The total reaction cross section observable was singled out in this study for the purposes of the applied programs. This work has been published.[8]

G. Dirac Optical Potentials for Nucleon Scattering by ^{208}Pb at Intermediate Energies [D. G. Madland and R. Kozack (Brandeis Univ.)]

We have performed a global analysis of intermediate energy nucleon plus ^{208}Pb scattering data using the Dirac phenomenology. Proton elastic differential cross sections, analyzing powers, spin rotation functions, and total reaction cross sections, together with neutron total cross sections, spanning an incident energy range of 80-800 MeV, were used in the determination of a Dirac scalar-vector global potential. Two of the six energy dependencies studied (logarithmic and exponential) were selected to construct best-fit nucleon-nucleus potentials for the reduced incident-energy interval of 95-300 MeV. These potentials reproduce the experimental data uniformly well within the reduced energy interval. The parameters of both potentials are given in Table IV-I and comparisons between experiment and the predictions of the logarithmic potential are shown in Figs. IV-9 through IV-11.

The inclusion of neutron total cross-section data has provided a means for determining the isovector strengths of the nucleon-nucleus potentials and, thereby, the capability for prediction of other (unmeasured) neutron scattering observables. This has been done and is discussed in Section IV-I. Finally, the correlations and ambiguities among the parameters of the potentials have been analyzed. This work has been published.[9]

TABLE IV-I

BEST FIT POTENTIALS FOR NUCLEON + ^{208}Pb SCATTERING
IN THE ENERGY INTERVAL $95 \leq T \leq 300$ MeV*

Logarithmic Model

Scalar real: $SR = -570 + 23.1\ ln\ T \mp 307\varepsilon$

$r_0 = 1.105$, $a = 0.692$

Scalar imaginary: $SI = 237 - 42.0\ ln\ T \mp 71.1\varepsilon$

$r_0 = 1.157$, $a = 0.512$

Vector real: $VR = 532 - 37.4\ ln\ T \pm 235\varepsilon$

$r_0 = 1.109$, $a = 0.664$

Vector imaginary: $VI = -189 + 28.9\ ln\ T \pm 54.2\varepsilon$

$r_0 = 1.149$, $a = 0.633$

Exponential Model

Scalar real: $SR = (-491 \mp 362\ \varepsilon)\ \exp(-T/5440)$

$r_0 = 1.102$, $a = 0.700$

Scalar imaginary: $SI = (52.6 \mp 125\ \varepsilon)\ \exp(-T/164.2)$

$r_0 = 1.153$, $a = 0.488$

Vector real: $VR = (399 \pm 287\ \varepsilon)\ \exp(-T/1686)$

$r_0 = 1.105$, $a = 0.676$

Vector imaginary $VI = (-54.8 \pm 60.4\ \varepsilon)\ \exp(-T/512.2)$

$r_0 = 1.137$, $a = 0.647$

*Strengths are in MeV and geometry is in fm; the upper (lower) signs refer to neutrons (protons).

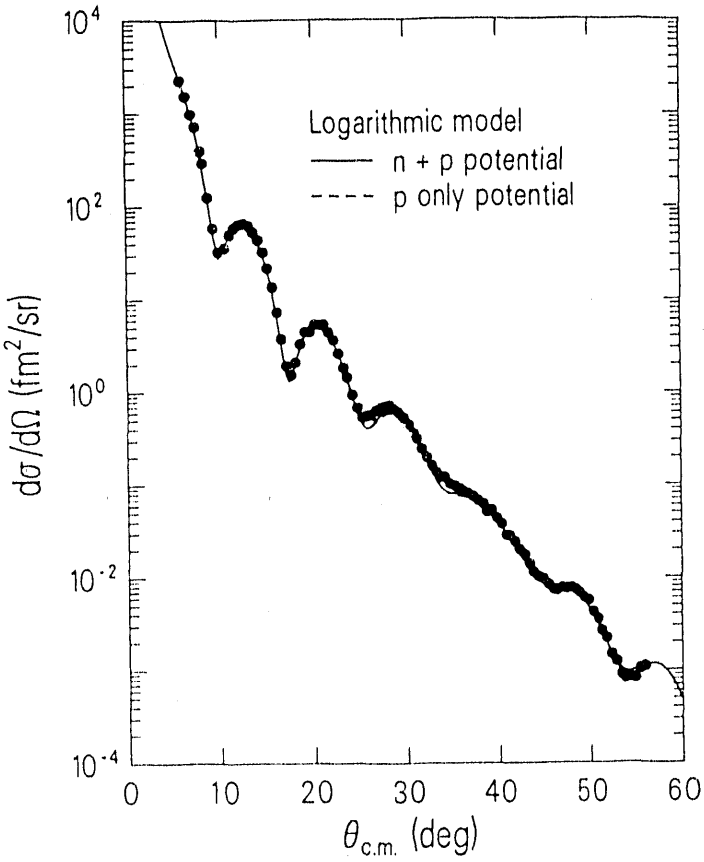

Fig. IV-9. Differential cross section for p + ^{208}Pb elastic scattering at 200 MeV in the logarithmic model. The solid curve is obtained in a calculation using the global potential (Table IV-I) that has been determined by simultaneously fitting the neutron and proton data. The dashed curve is from a calculation using a global potential in which only the proton data have been fit. Experimental data are from Ref. 10.

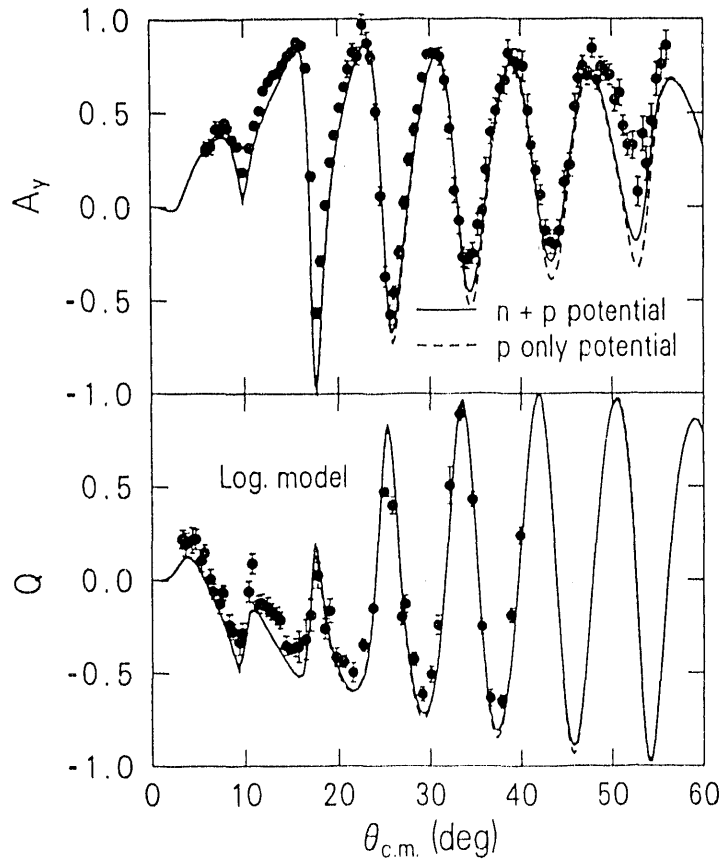

Fig. IV-10. Spin observables for p + ^{208}Pb elastic scattering at 200 MeV in the logarithmic model. The curves have the same meaning as in Fig. IV-9 and the experimental data are from Ref. 10.

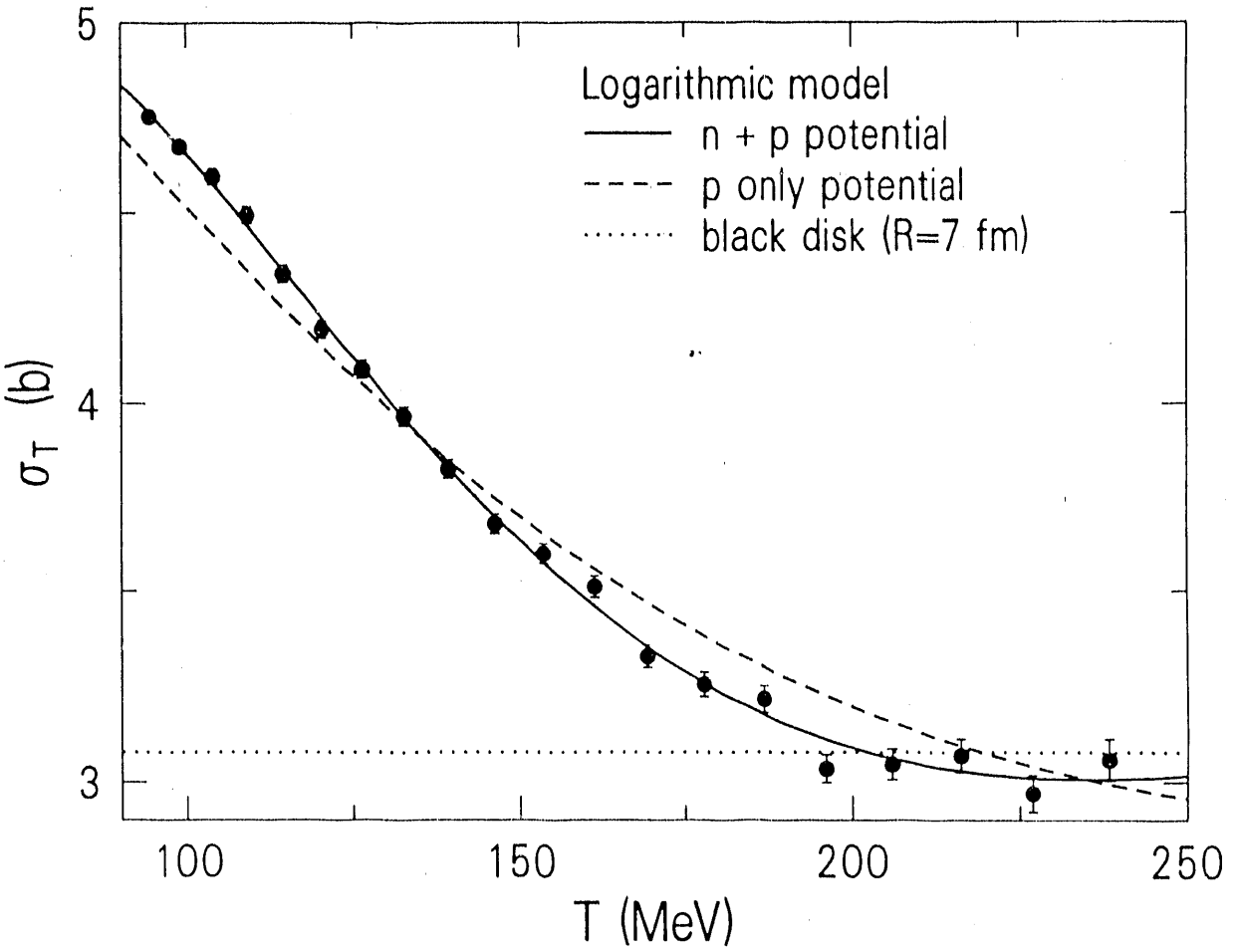

Fig. IV-11. Total cross sections for n + ^{208}Pb scattering from 95-250 MeV in the logarithmic model. The curves have the same meaning as in Fig. IV-9 and the experimental data are from Ref. 11.

H. Deuteron-Nucleus Optical Potential Analysis at Medium Energies (E. R. Siciliano, D. G. Madland, and L. C. Liu)

We have considered deuteron-nucleus (d-A) elastic scattering in the energy range of 45-200 MeV. Over this range we have demonstrated that the phenomenological optical-model potential of the type used by Daehnick *et al.*[6] for the 12-90 MeV region can provide satisfactory fits to the existing experimental differential cross sections, spin observables, and integrated observables, provided that the potential parameters are slightly altered.[10] To gain some insight into this potential, we compare it with various first-order microscopic potential models based upon phenomenological nucleon-nucleon interactions. We also consider the role that the explicit breakup channel has upon elastic scattering. Our progress on this topic was presented at the Spring 1990 American Physical Society meeting in Washington, D.C.[12]

I. Prediction of Intermediate-Energy Neutron Scattering Observables from a Dirac Optical Potential [D. G. Madland and R. Kozack (Brandeis Univ.)]

Using a Dirac scalar-vector global optical potential for nucleon + ^{208}Pb scattering,[9] we have performed calculations of unmeasured neutron + ^{208}Pb scattering observables. These show remarkable differences when compared with the corresponding proton + ^{208}Pb scattering observables, which have been measured. Examples for the differential cross section and spin observables at 100 MeV are shown in Figs. IV-12 and IV-13. The origins of the differences have been determined by performing calculations for a "gedanken" projectile with a proton isovector interaction and a neutron Coulomb interaction. These differences have stimulated proposals within the experimental neutron physics community for measurements that test these findings. This work has been published.[13]

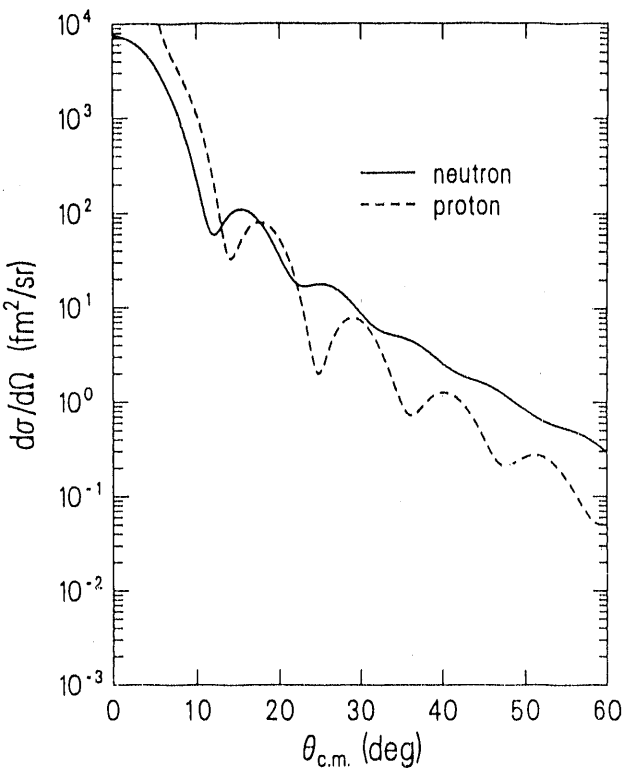

Fig. IV-12. Differential cross sections for nucleon + ^{208}Pb elastic scattering at 100 MeV. The solid curve is the prediction obtained for neutron scattering, while the dashed curve is the prediction obtained for proton scattering. A Dirac scalar-vector global potential with a logarithmic energy dependence has been used for both predictions.

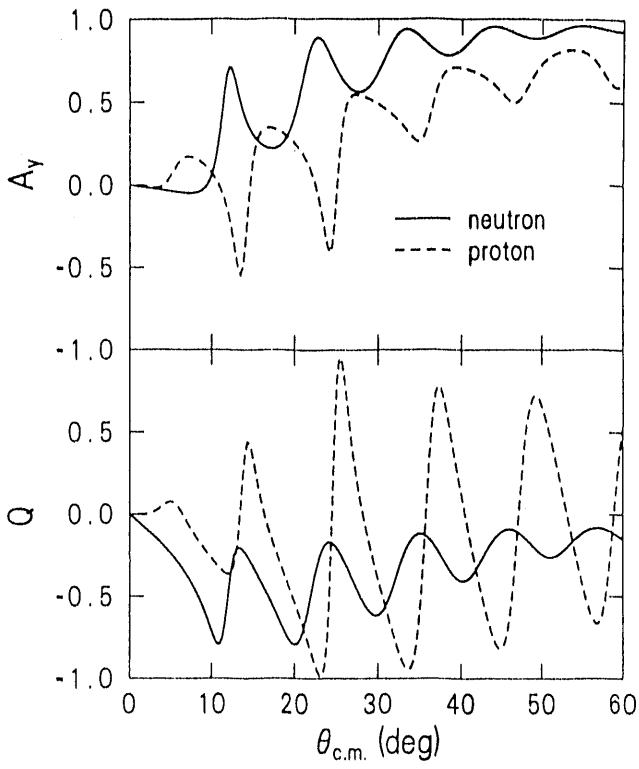

Fig. IV-13. Spin observables for nucleon + ^{208}Pb elastic scattering at 100 MeV. The solid and dashed curves have the same meaning as in Fig. IV-12.

J. Electrodisintegration of the Deuteron [L. C. Liu and R. M. Thaler (Case Western Reserve Univ.)]

There is much interest in the mass and energy dependence of deuteron reaction cross sections. Because reaction cross sections have only been measured at energies between 20 and 25 MeV,[14,15] the desired energy dependence must be calculated theoretically. Predictions are often obtained through the use of the imaginary part of deuteron-optical potentials determined from fits to deuteron-nucleus differential elastic scattering cross sections at various energies. However, in all optical model analyses of which we are aware, the imaginary part of the deuteron optical potential has been implicitly assumed to arise only from nuclear processes.[6] Accordingly, the range of this absorptive potential has been constrained to values roughly compatible with the range of the nuclear force. We have shown that for nuclei having a large charge, the electric breakup process of the deuteron can be a considerable fraction of the expected total deuteron reaction cross section at low energies. The electrodisintegration process cannot be fully simulated by nuclear absorption mechanisms because it is so long-ranged. Consequently, the use of the imaginary part of the deuteron-nucleus optical potential determined without the consideration of electrodisintegration might lead to unrealistic predictions for the mass and energy dependence of deuteron reaction cross sections.

The electric disintegration of the deuteron was considered as early as 1935 by Oppenheimer,[16] by Dancoff[17] in 1947, and by Mullin and Guth[18] in 1951. However, as has been shown in Ref.19, these early attempts are unreliable. More recently, Kleinfeller *et al.*[20] have been interested in the electrodisintegration process in the context of heavy-ion reactions. We have considered the deuteron electrodisintegration in the absence of nuclear breakup processes in order to compare it with nuclear reaction processes. The cross sections were evaluated within the theoretical framework of a modified Born approximation (MBA) in which the monopole term of the Coulomb interaction is separated out to ensure the orthogonality-scattering constraint.[15]

The calculated energy dependences for three representative nuclei (^{208}Pb, ^{58}Ni, and ^{13}Al) are given in Fig. IV-14. In our calculations we used the deuteron wave function of the Paris Group[21] and experimental nuclear charge densities.[22] We see that in the region of 25 MeV the electrodisintegration cross section of the deuteron, as induced by the Coulomb field of ^{208}Pb is ~ 1500 mb or about 65% of the observed total deuteron reaction cross section,[14,15] and remains at the level of half barn at ~ 100 MeV. Because the Coulomb interaction is proportional to Z, the electric disintegration cross section decreases as the charge of the target nucleus decreases. In the case of ^{58}Ni and ^{13}Al, electrodisintegration represents only ~ 18% and ~ 7% of the observed total deuteron reaction cross section at 25 MeV. We found from our calculations that the electrodisintegration contributes to at least 25% of the total deuteron reaction cross section for targets with $Z \gtrsim 40$ in the energy region of 25 MeV.

In conclusion, these results will significantly affect the interpretation of the observed deuteron reaction cross sections as well as the use of the existing deuteron optical potentials to make predictions for the energy dependence of the deuteron reaction cross sections. Since the interaction range, the mass/charge and energy dependence of the electrodisintegration are all different from those of the nuclear processes, we believe that in future analyses of deuteron elastic scattering from nuclei with atomic number greater than that of zirconium, the electrodisintegration of the deuteron must be included explicitly.

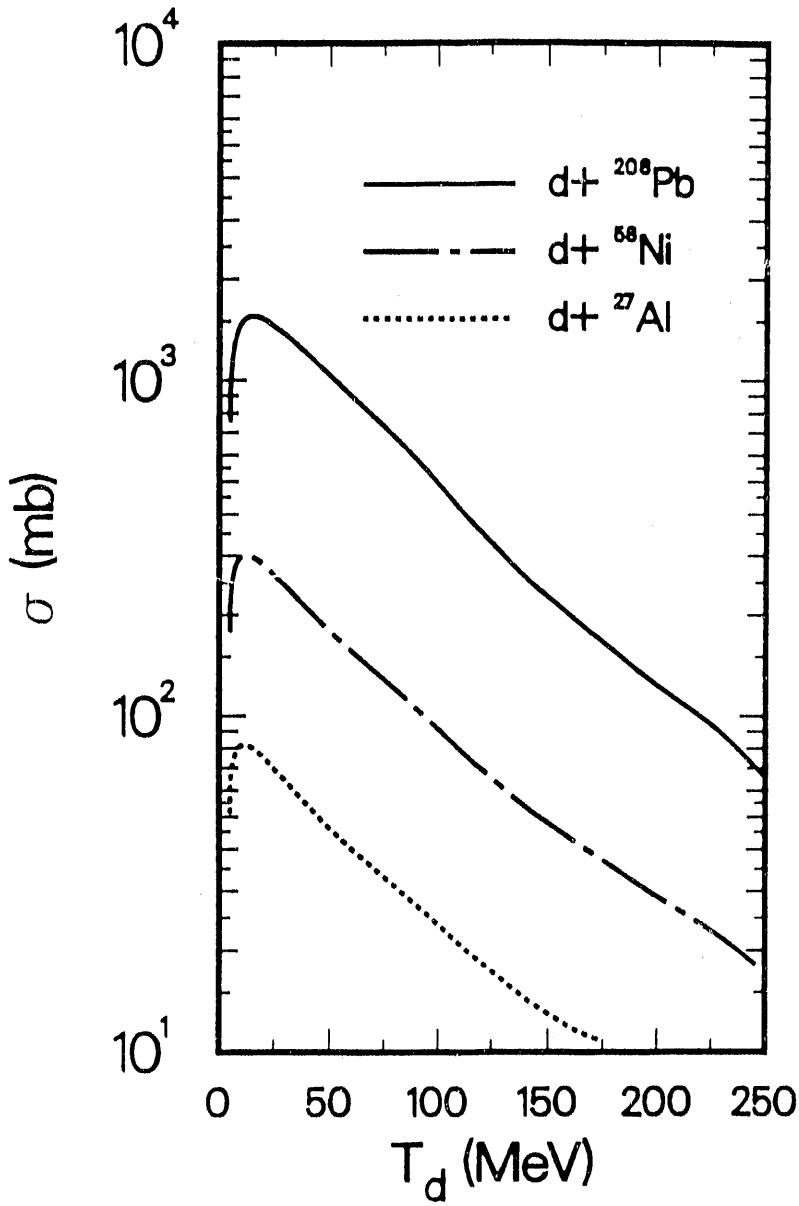

Fig. IV-14. Energy dependencies of the calculated total deuteron electrodisintegration cross sections for ^{208}Pb, ^{58}Ni, and ^{13}Al.

K. Dynamics of Pion Double-Charge-Exchange Reactions [Q. Haider (Fordham Univ.) and L. C. Liu]

The main interest in pion-nucleus double-charge-exchange (DCX) reactions stems from the fact that any leading process of DCX must involve two different nucleons, a feature that is not present in most other nuclear phenomena where two-nucleon processes appear only as higher-order corrections. Thus, pion DCX reactions are ideal for the study of short-range nucleon-nucleon correlations, as pointed out long ago by Ericson and Ericson[23] and by Koltun.[23] In recent years, a large amount of good quality data from LAMPF, SIN and TRIUMF has become available.[24-30] These data have played a decisive role in improving our understanding of the DCX dynamics.

We have studied the reaction $^{14}C(\pi^+,\pi^-)^{14}O$(DIAS) at pion energies 50 to 300 MeV, within the framework of two successive single-charge-exchange mechanisms.[31] In the following we report the most significant findings of our investigation, while referring to Ref. 32 for details of other important results concerning effects on DCX arising from nuclear structure, double spin-flip, nuclear recoil, nuclear binding, and reaction pathway.

In brief, our study has revealed that theoretical DCX cross sections are extremely sensitive to the off-shell πN model used. The observed sensitivity is shown in Fig. IV-15, where the solid curve is obtained with the use of a unitary off-shell πN model of Ernst and Johnson.[33] The dash-dotted and dashed curves represent the results given by the use of an *ad hoc* off-shell model having a monopole form factor with a cutoff range parameter of 1500 and 690 MeV/c, respectively. It is noteworthy that, because of the success of phenomenological meson-exchange potentials of the NN interaction,[34] the monopole model has been extensively adopted to describe the πN interaction in pion-nucleus reactions.

The crucial differences between the Ernst-Johnson (EJ) model and the monopole model are: (a) the EJ model is constrained by off-shell unitarity and the monopole model is not; (b) the EJ model reproduces the pN phase shifts, while the monopole model does not. As a result, the pN interaction ranges of the EJ model differ drastically from those used in the monopole models. More importantly, the requirement of reproducing the πN phase shifts has led to different interaction ranges for different πN partial-wave channels in the EJ model. In the literature, the range of the monopole model is either treated as a completely free parameter or is made to vary between 1.0 to 1.5 GeV/c, as inspired by phenomenological NN potentials.[35] Further, as in the NN potentials, only one single range is assigned to the πN P11 channel. However, as noted and emphasized in Ref. 32, the single-range monopole model cannot reproduce experimental P11 phase shifts. In view of the important contribution by the P11 πN interaction at pion energies below ~ 80 MeV, we conclude that theoretical results obtained with monopole form factor with an

ad hoc range parameter cannot be trusted, and that the fit of 50-MeV data by the dash-dotted curve in Fig. IV-15 is coincidental.

Figure IV-15 also indicates that the sequential pion single-charge-exchange mechanism alone is not sufficient to account for the observed DCX cross sections at 50 MeV, although the calculated cross sections are increased by nearly two orders of magnitude with the inclusion of all intermediate nuclear states. (Compare the solid and dotted curves.) This existing discrepancy between the theory and the experiment suggests strongly that other reaction mechanisms are important. However, the study of effects of these other mechanisms and of NN short-range correlations can only be meaningful when realistic πN off-shell models, such as the EJ model, are used.

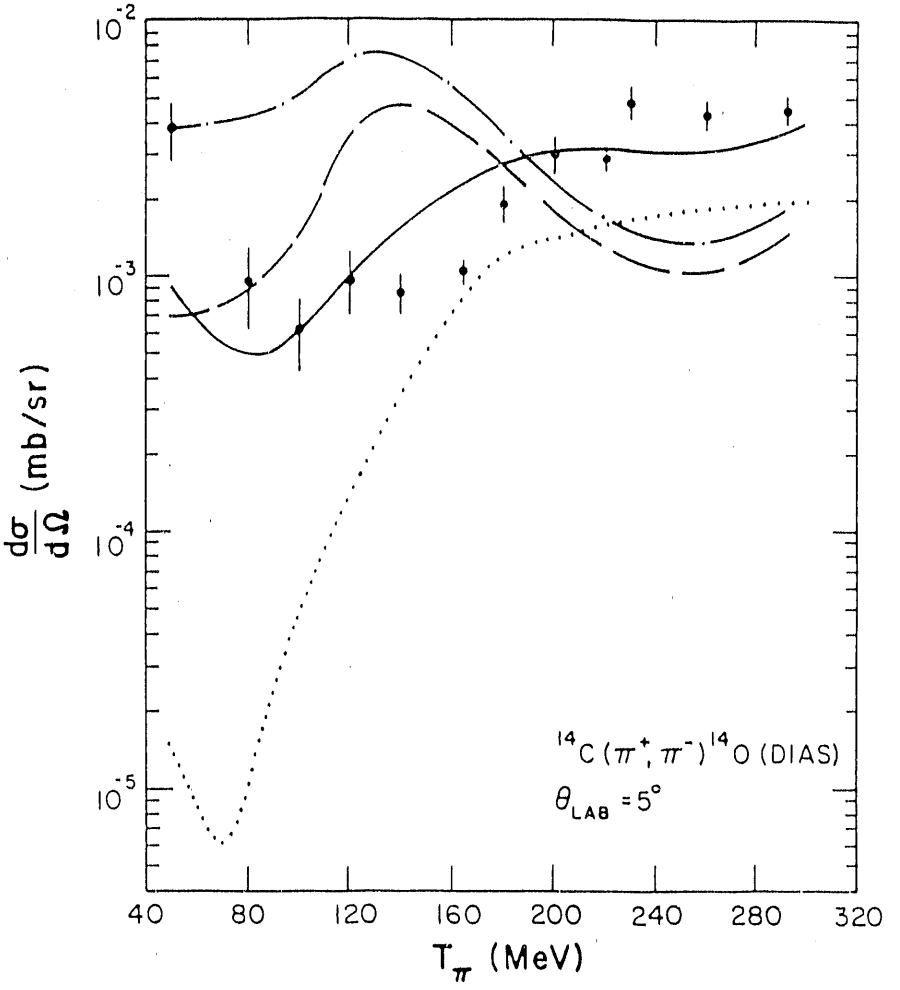

Fig. IV-15. Comparisons between the data[27] and the 5^0-excitation functions calculated with the Cohen-Kurath nuclear wave function[35] and the distortion of the external pions. The dot-dashed and long-dashed curves were obtained with monopole off-shell πN models of A = 1500 and 690 MeV/c, respectively, and also with the frozen-nucleon approximation. The solid curve was obtained with the EJ model and included nuclear recoils and medium modifications on the πN interaction. All three curves included the contributions from all intermediate nuclear states. The dotted curve had the same inputs as the solid curve except that it only took into account the contribution of the intermediate analog nuclear state.

L. Two-Nucleon Correlations in Pion Double Charge Exchange [E. R. Siciliano, M. B. Johnson (MP-DO), and H. Sarafian (Penn. State Univ. at York)]

A thorough understanding of pion-nucleus double charge exchange (DCX) is extremely important because DCX is one of the few basic reactions that directly involves the scattering from two bound nucleons. Thus, the DCX reaction has the potential of providing us with direct information about two-nucleon (2N) processes in nuclei and may help us understand the role of N-N correlations. To learn about nuclear structure, the pion-nucleus reaction mechanism must be under theoretical control. Also, because of the resonant structure of the π-N interaction, the nature of the pion-nucleus reaction mechanism changes as a function of energy.

For incident pion energies in the range of 100 to 300 MeV, there have been many measurements and corresponding theoretical calculations of DCX cross sections over the past few years. In this energy region, DCX through the Δ_{33}-N mechanism is comparable to the sequential π-N single-charge-exchange process. Recently, there have been some measurements of DCX below 100 MeV, and many theoretical groups have produced calculations in an attempt to describe the low-energy data. Unfortunately, no clear physical interpretation of the data has emerged because the different theoretical groups seem to emphasize the importance of different aspects of their calculations. One issue of particular significance (and of some controversy) is the relative importance of the short-range part of the 2N wave function and whether low-energy DCX can be used to probe quark degrees of freedom in nuclei.

To reveal some of the salient physical features inherent to DCX (particularly at low energies), we have studied the following model problem. We assume the relevant degrees of freedom to be those provided by mesons and baryons, and we work within the fixed-scatterer theoretical framework.

In the absence of elastic distortions or any other nuclear medium effects, we formulate the basic π-2N scattering operators that result from the following DCX reaction mechanisms: pion sequential charge exchange from two uncorrelated nucleons, sequential charge exchange from two correlated nucleons via explicit $\pi + \rho$ exchange, and on-shell Δ_{33}-nucleon interactions via explicit $\pi + \rho$ exchange.

In our calculations we have investigated the sensitivity of these processes to variations in the elementary vertex functions and the two-nucleon wave functions with particular emphasis on the importance of short-distance behavior. The results we have obtained indicate that for parameterizations of the off-shell pion-nucleon scattering amplitude favored by field theoretical models of the pion-nucleon scattering amplitude (with a π-N cutoff, $\Lambda_{\pi l} \approx 1$ GeV/c), pion double charge exchange is reduced by about 50% when the short-range dynamical correlation that acts between nucleons in the nucleus is considered. The extent of sensitivity to the correlation function depends upon the energy of the incident pion and also upon the amplitude to find spin-zero pairs of

excess neutrons in the nucleus. For the same value of the pion-nucleon cutoff, the empirical value of the Fermi liquid parameter $g'(\Delta\Delta)$ is also reproduced, providing independent evidence for these choices of $\Lambda_{\pi I}$. For extremely soft form factors that are sometimes used in calculations ($\Lambda_{\pi I} \leq 2.0$ fm^{-1}) we find no sensitivity of the DCX cross section to the short-range correlation function, and we are unable to obtain agreement with the empirical value of $g'_0(\Delta\Delta)$. The rho meson in sequential scattering, the DINT delta-nucleon interaction, and deltas in the nuclear wave function (DWF) all have a very small effect on the cross sections (less than 15-20%) at low energy. We conclude that low-energy pion-nucleus double charge exchange is quite sensitive to short-range dynamical correlations between nucleons.

Plane-wave cross sections were shown to have a completely different energy-dependence from that of the data. We have shown qualitatively that distorted waves calculated from optical-model fits to elastic scattering data are likely to make up for the deficiencies of the plane-wave DCX cross section, both in magnitude and energy-dependence. If these are making up the difference, then distortions are playing a substantially larger role at low energy than is conventionally thought.

A comprehensive article that gives the details of our model and the calculational results as applied to the double isobaric analog transition in ^{14}C will appear in the July 1990 issue of *Annals of Physics*.[36] The results of our calculations for the calcium isotopes will appear in *Physics Letters*.[37]

Because we are unable to calculate the magnitude of the cross section and its energy dependence without explicit consideration of pion distortions, it is difficult to be certain at the present time how much room exists in the data for contributions to the DCX cross section coming from exotic mechanisms such as π–π scattering, absorption, or six quark bags. Careful evaluations of the remaining mechanisms are in progress. Another factor in determining the magnitude of the cross section is the momentum dependence of the nuclear form factor. We have found that the magnitude of the DCX cross section varies as the sixth power of the single-particle oscillator parameter. Both the form factor and the distortions can be constrained by appropriate data, in particular reliable single charge exchange out to large angles for the intermediate nuclear states in ^{14}O accessible in sequential scattering. Such data may be taken with the use of a high resolution neutral meson spectometer such as that currently under development at LAMPF.

We believe that the weight of the evidence indicates that low-energy DCX is dominated by sequential pion scattering and that this reaction mechanism is sensitive to short-range dynamical correlations. We do not yet know whether this observation can be turned into a practical method for learning about the correlations. One possibility would be to use the observation that the sensitivity to correlations is dependent on the spin content of the excess neutron pairs. One would

thus want to compare cross sections on different nuclei having spin content known from other sources such as spectroscopic studies in the shell model.

The double isobaric analog transitions that we have studied thus far represent only one class of double charge exchange. A large class of non-analog transitions exists, and with higher intensity of the pion beams, these may be studied experimentally. We are hopeful that by an appropriate choice of final states, one can use the nucleus as a filter for amplitudes that convey more specific information about the reaction. Such final states are capable of being studied with our formulation. We look forward to exciting theoretical and experimental studies in the near future.

M. Microscopic Field Theoretical Treatment of Ultrarelativistic Nucleus-Nucleus Collisions
[A. J. Sierk, J. R. Nix, and R. J. Hughes (P-15)]

We have made progress on a new approach for treating ultrarelativistic nucleus-nucleus collisions in terms of a classical relativistic field theory corresponding to the exchange of vector ω mesons. The Lagrangian density appropriate to N nucleons of mass M interacting through the exchange of vector mesons of mass m with coupling constant g leads to covariant equations of motion for the N nucleons, which we convert into the integral equations

$$d_i^{\mu}(\tau_i) = \int_{\tau_1}^{+\infty} d\tau_i' \left[\frac{3}{2g^2} \left(g F_{ext}^{\mu\nu} u_{i\nu} + f_i^{\mu} \right) + u_i^{\mu} a_i^{\nu} a_{i\nu} \right] \exp\left[-\frac{3M}{2g^2} (\tau_i' - \tau_i) \right] . \quad (1)$$

Here τ_i is the proper time of nucleon i, a_i^{μ} is its four-acceleration, u_i^{μ} is its four-velocity, $F_{ext}^{\mu\nu}$ is the external field-strength tensor at nucleon i due to the other nucleons and f_i^{μ} is the self-interaction due to the nonzero meson mass. Because the integrations in Eq. (1) are over *future* proper times, we solve these equations iteratively, with the positions and four-velocities that enter determined by use of a finite-difference method.

Because of large nonlinearities associated with both the radiation reaction and the self-interaction, we have thus far been unable to obtain converged solutions corresponding to realistic values of m and g^2. We have obtained solutions both for a massless vector field with the full value of g^2 and for a massive vector field with a value of g^2 that is 20% of the original value. Figures IV-16 and IV-17 are examples of the latter for a single nucleon incident on a scattering center that remains fixed in the laboratory system. Whereas the Yukawa contribution to the transverse force is a narrow spike near the position of the scattering center, the contributions from the radiation reaction and self-interaction extend over large distances on both sides of the scattering center. On the other hand, the Yukawa contribution to the transverse acceleration extends over a large distance

only in front of the scattering center, which can be understood from the integration in Eq. (1) of an exponential times a narrow spike. Because the range of the exponential is proportional to g^2, both the transverse kinetic energy imparted to the projectile and the radiated energy will be larger than that shown in Fig. IV-17.

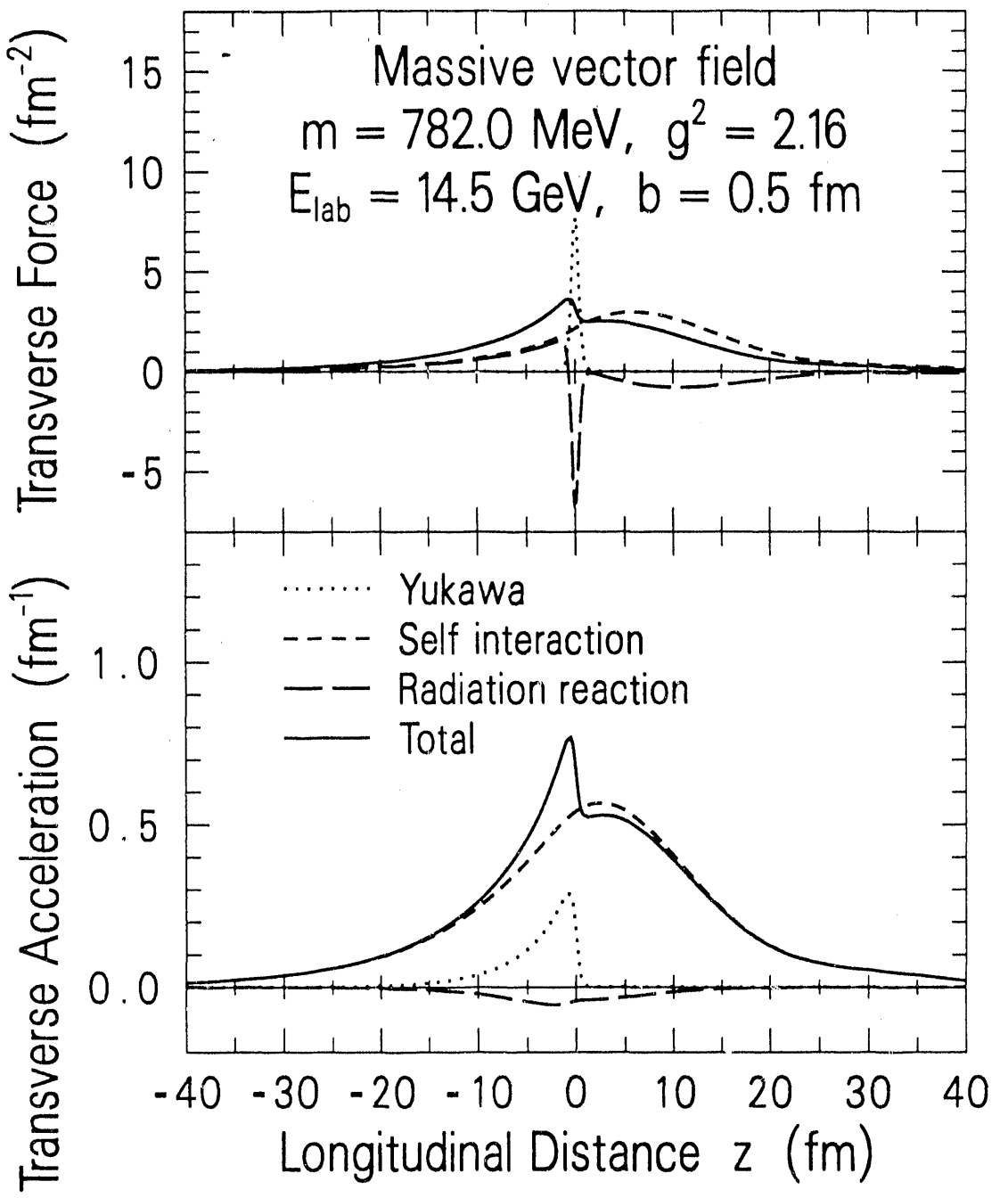

Fig. IV-16. Contributions to the transverse four-force and transverse four-acceleration.

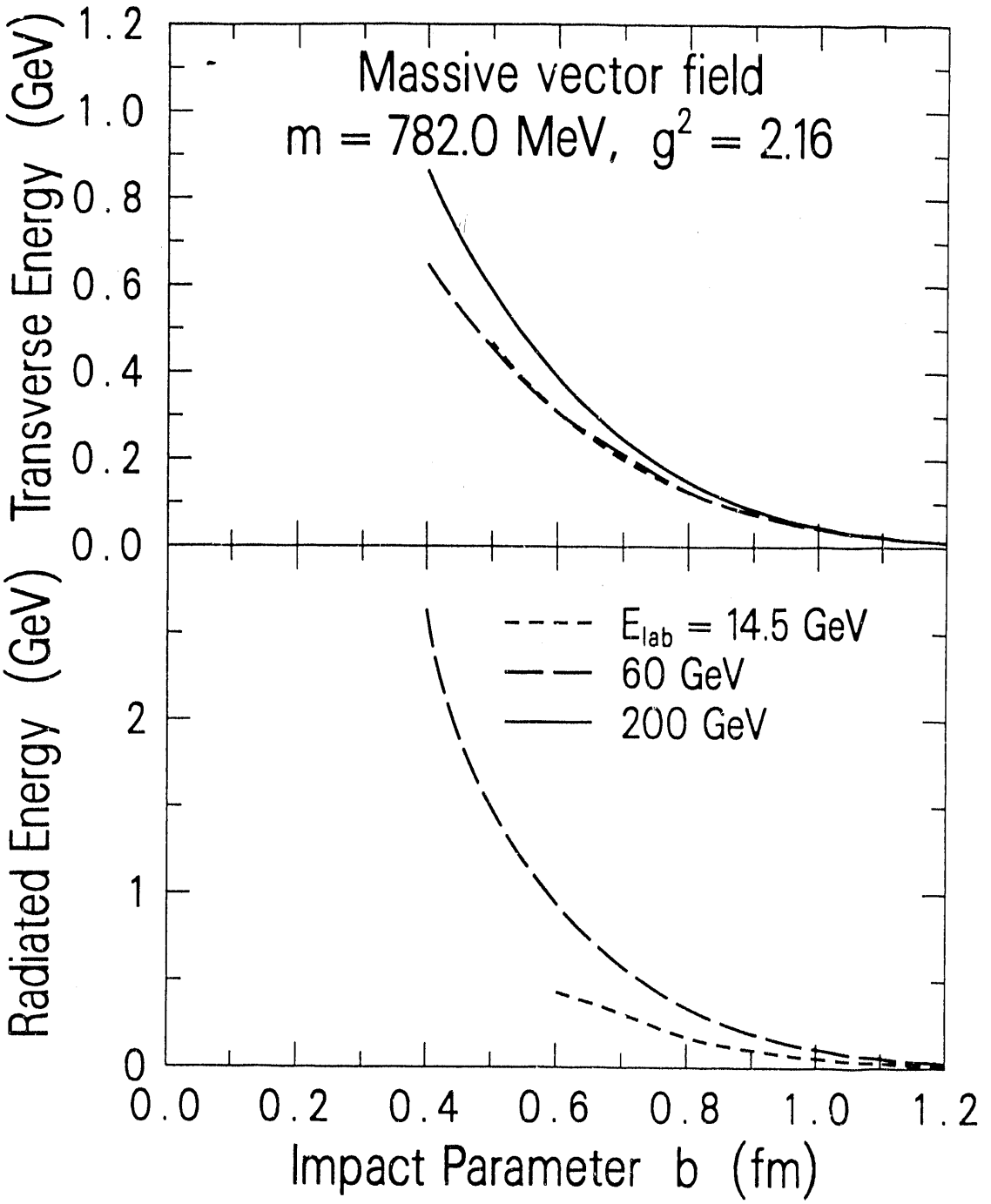

Fig. IV-17. Dependencies upon impact parameter of the transverse kinetic energy and total radiated energy.

We conclude that a classical relativistic field theory corresponding to the exchange of vector ω mesons provides a logical approach for studying the effects of relativistic retardation, nonequilibrium phenomena, interactions with correlated clusters of nucleons, and particle production in ultrarelativistic nucleus-nucleus collisions, but some formidable computational difficulties must be overcome before these virtues are realized.

N. Pion-Nucleus Elastic Scattering in the Microscopic Local Delta-Hole Model [C. Garcìa-Recio and L. L. Salcedo (Univ. of Granada); E. Oset and M. J. Lòpez (University of Valencia) and D. D. Strottman]

The early recognition of the peculiarities of pion-nuclear reactions around resonance led to the development of the Δ-hole model. Medium corrections to pion-nucleus scattering have been included in either a phenomenological complex Δ spreading potential, which was fitted to the pion-nucleus elastic scattering data, or by microscopic evaluations of the Δ self-energy in the nuclear medium. The microscopic calculation included the ΔN to NN channel, which leads to two-nucleon pion absorption in the related pion-nuclear problem. Under certain reasonable approximations, the non-local information contained in the set of nuclear matrix elements obtained in the microscopic approach could be approximated by a linear function of the density, the strength of which for the imaginary part agreed qualitatively (20 - 30% smaller) with the empirical determination. Thus, the Δh model approach, with the renormalization of the Δ properties in the nuclear medium, is a natural way to proceed in the energy regime close to the Δ resonance.

Although a knowledge of the Δ self-energy is sufficient to evaluate the elastic differential cross section and the total cross section via the optical theorem, the separation into the different reaction channels requires more information. This is the point where a many-body calculation has its maximum strength because it allows for a separation of the contribution from the different pion-nuclear reaction channels: absorption, quasi-elastic, single-charge exchange and double-charge exchange. The success of such a separation was previously shown,[38] where, by means of an eikonal approximation, the separation of the reaction channels was reduced to the solution of a set of coupled differential equations. However, only integrated cross sections could be obtained by this method, including elastic cross sections. The removal of the eikonal condition and the interest in calculating both differential and double differential cross sections led to the work of Ref. 39 in which the calculated reaction probabilities were used in a computer simulation procedure.

We have constructed a microscopic model for the pion-nucleus interaction that starts from elementary couplings of mesons to nucleons and isobars and uses a systematic many-body expansion in the number of ph excitations, up to the level of three-particle, three-hole excitations in the absorption channel, where convergence is found. The model not only provides the optical potential with no free parameters, but more importantly, it provides the separation of its imaginary part into different pieces that are related to the reaction probabilities. We have shown the consistency of the model with the elastic differential cross sections in a variety of nuclei and different energies around resonance. As an example, in Fig. IV-18 results are shown for pion scattering on ^{208}Pb; results for other nuclei are comparable. Our results compare fairly well with the experimental differential cross section for different nuclei and energies around the resonance, providing a new consistency check of our model as a tool with which to describe in a unified way the different pion-nuclear reactions.

The consistency of the model with the different reaction cross sections implies that the essential features of the reaction mechanisms have been properly incorporated into the model. We should note that in different reactions, such as pion single-charge exchange and double-charge exchange exclusive reactions, pion-induced pion production, nuclear photo production, etc., the influence of the different pion reaction channels in the propagation of the pions through the nucleus will be different. (Recall that the density dependence of each of the different channels is different and different reactions will explore different regions of the nucleus.) Hence, the use of an optical potential consistent with each of the different reaction channels is very important if one aims at a global understanding of these reactions.

On the other hand, the global study we have carried out with this model shows clearly that a consistent many-body treatment of the pion-nuclear problem is possible, that one obtains a unified picture for the different pionic reactions, and it provides a good insight into the details of the reaction mechanics.

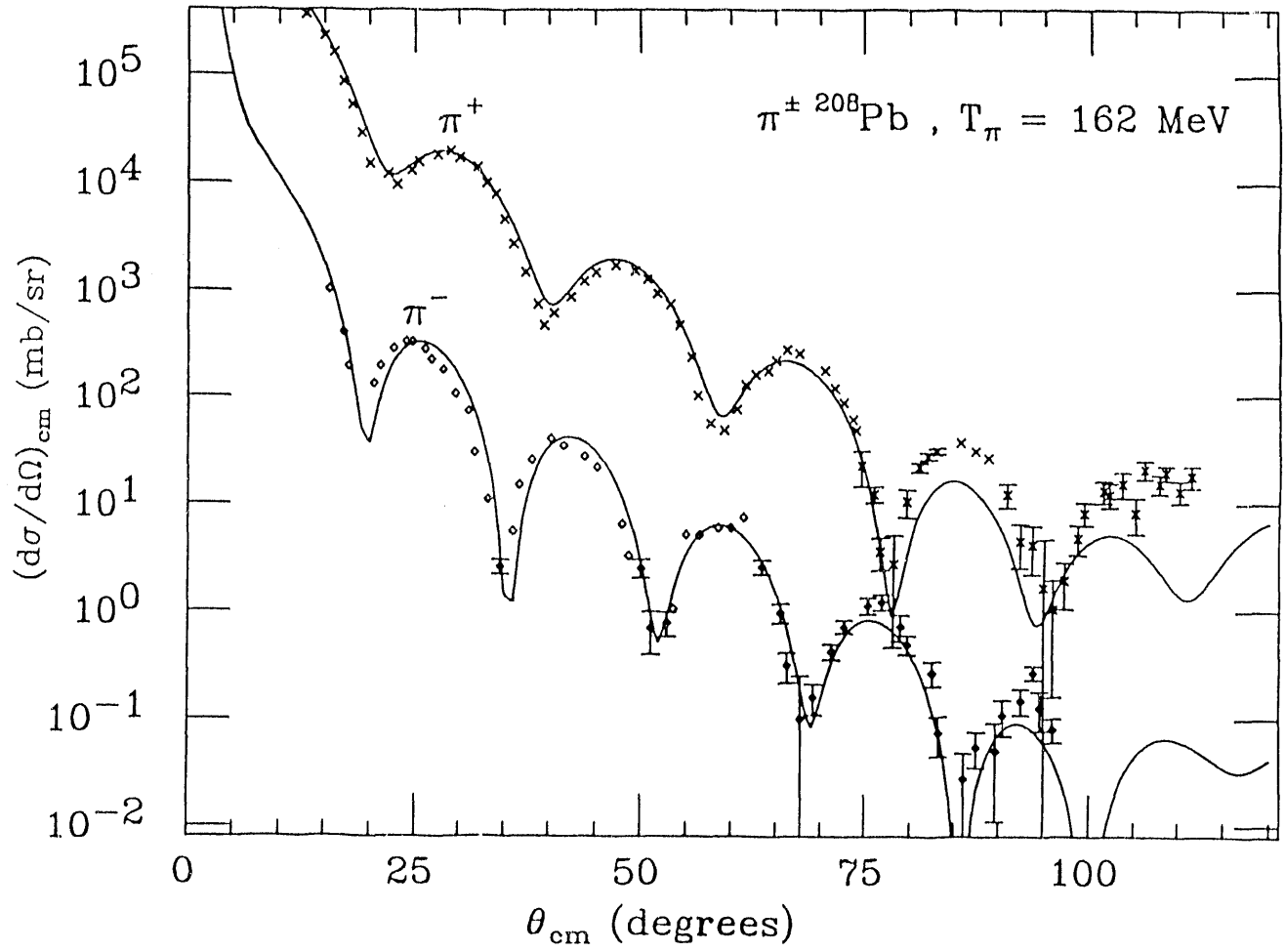

Fig. IV-18. Differential cross section for π^+ and π^- scattering on ^{208}Pb at T_π = 162 MeV. The experimental data are from Ref. 40.

O. Pion-Nucleus Single-Charge Exchange Above the Resonance [E. Oset (University of Valencia) and D. Strottman]

Recent experiments[41] of the (π^+,π^0) reaction on nuclei have extended measurements of the pion-induced single-charge exchange reaction (SCX) into the hitherto unexplored energy regime above the $\Delta(3,3)$ resonance. These experiments found that the cross section at forward angles increases with increasing energy of the projectile, in contrast with the behavior of single-charge exchange on a free nucleon.

One may obtain a qualitative understanding of the apparent anomalous behavior of the excitation function by considering the competition between distortion and charge exchange on a single nucleon. In the region of the (3,3) resonance, pions are strongly absorbed and the SCX reaction is correspondingly suppressed. As one moves higher in energy, away from the (3,3) resonance, the amplitude for charge exchange on a free nucleon slowly decreases, but the distortion of the pion wave rapidly decreases. The actual calculated forward scattering cross section can only be determined by more quantitative, detailed considerations, but this argument suggests it should not be surprising that the SCX reaction on a nucleus will have a much different energy dependence than it does on a free nucleon.

In the energy region of the resonance and below, only the s- and p-partial waves need to be included in calculations. However, above the resonance, additional partial waves need to be included in calculations. An examination of the FP84 phase shift solution of Arndt *et al.** demonstrates that the D_{31} phase shift becomes important above 250-MeV pion energy and the F_{51} should be included above 450 MeV. Thus, the usual programs used to calculate pion-induced reactions at lower energies and those that are based on the dominance of the s- and p-waves are not applicable in this higher energy regime.

We have used a microscopic model based on the Glauber theory of multiple scattering to study the SCX reaction above the (3,3) resonance. Shell model wave functions were obtained from diagonalizing the Cohen-Kurath interaction; the calculation had no free parameters. In Fig. IV-19, one can note the importance of each of the partial waves. Clearly, above the resonance one must include the d wave and above 450 MeV, also the f wave. Our results for ^{7}Li and ^{14}C follow closely the shape of the experimental data but exceed experiment by about 25% and 33%, respectively. The standard Glauber theory was modified to include pion absorption. The evaluation of the absorption probability relied upon detailed work[42] around the resonance and is compatible with experimental cross sections. The extrapolation of these results to energies above the resonance was performed, assuming a model similar to those used around the resonance and including the modification of phase space with energy. The result was a decreasing function of the absorption probability on two and three nucleons as the pion energy increased. This absorption

* This information was provided by R. A. Arndt, Physics Dept., Virginia Polytechnic Inst., in 1987.

probability resulted in reductions of the cross section by a small amount for ^{7}Li and 6-15% for ^{14}C, implying the effects of absorption become increasingly important for heavier nuclei. We have also found that, as the energy increases, the effects of pion absorption on the SCX cross section become less important. This further suggests that Glauber theory will become increasingly accurate as the pion energy increases.

The reliability of Glauber theory at higher energies is based, in part, on a decreased role played by absorption. As one goes away from resonance our extrapolation is also less reliable. It is therefore very important to perform experiments on pion absorption at high energies to test these theoretical predictions and then to set limits on the importance such many-body processes can have on different pion-nucleus reactions. This information is needed not only for the current work but also in other aspects of physics, such as photonuclear reactions, antiproton annihilation and heavy ion reactions. The experimental investigation of pion absorption should be considered of high priority in the next phase of experiments on pion-nucleus reactions at high energies.

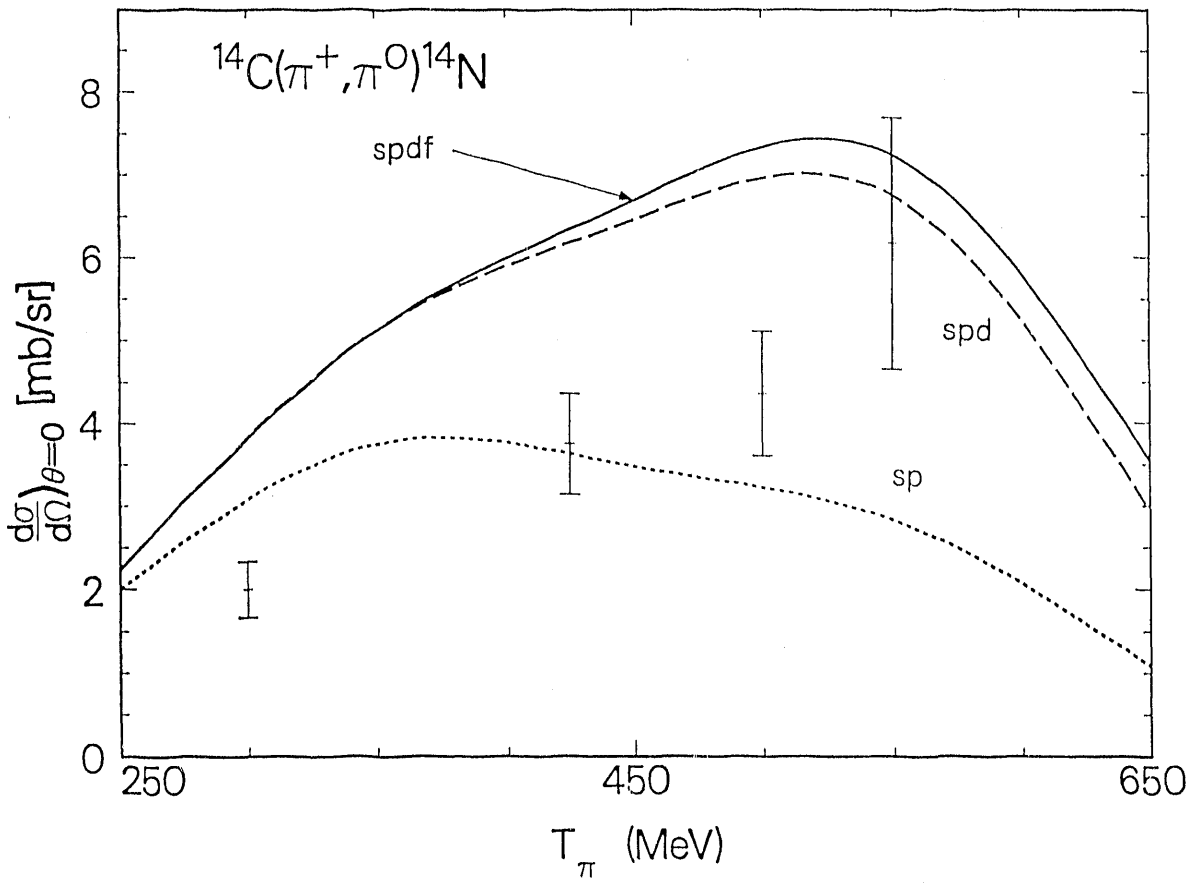

Fig. IV-19. Excitation function for the reaction $^{14}C(\pi^+,\pi^0)$ in the laboratory system calculated with three different assumptions regarding the number of partial waves. The experimental points are from Rokni *et al.*[41] and Sennhauser *et al.*[41]

Fig. IV-20 shows the results for SCX from 600 to 1400 MeV, essentially the energy regime in which PILAC will be used. The resonance-like structure above 800 MeV is due to contributions from the f wave. The g wave becomes increasingly important as the energy increases. Of particular interest is the minimum in the forward cross section around 1.2 GeV. Although the πN phase shifts are poorly known in this region, it suggests a number of possible experiments to look for new processes.

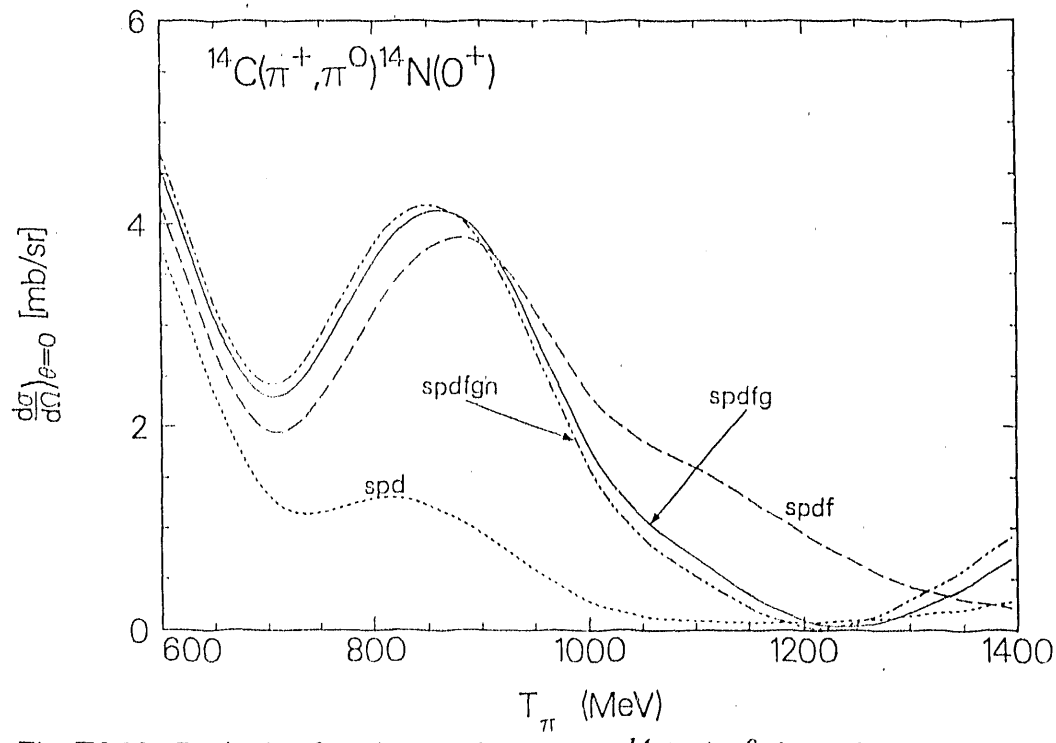

Fig. IV-20. Excitation function for the reaction $^{14}C(\pi^+,\pi^0)$ in the laboratory system calculated with four different assumptions regarding the number of partial waves.

P. Pion Distributions from the Fluid Dynamical Model of Ultra-relativistic Heavy Ion Collisions [E. F. Johansen, A. K. Holme, and L. P. Csernai (University of Bergen); Minzhuan Gong (Michigan State University); and D. D. Strottman]

Recent AGS and SPS experiments lead to the conclusion that in central heavy ion collisions hadronic matter is strongly stopped and a significant portion of the incident energy can be observed in transverse directions. The normalized pseudorapidity distributions of charged secondaries are strongly peaked at mid-rapidities for 14.6, 60, and 200 GeV/nucleon O+Ag/Br collisions and do not show any development of a central plateau. The present data from WA-80 and NA-35 also indicate that the stopping of baryons is strong at energies up to 200 GeV/nucleon. At the lower energies (14.5 and 60 GeV) there is evidence for complete stopping in central collisions where no energy is detected around zero degrees in calorimeters.

Thus it is not illogical to attempt a description of these latter two reactions in terms of a one-fluid hydrodynamical model in which there is complete stopping. The aim of current calculations and experiments is to determine under what conditions a quark-gluon plasma (QGP) is formed in heavy ion collisions. We have for the first time performed three-dimensional calculations using an equation of state (EOS) with a phase transition. Also, the breakup mechanism of the fluid cells is important if we intend to describe observable quantities, because the random thermal motion of particles is not negligible and must therefore be included.

For our numerical fluid dynamical study we used a phenomenological EOS reproducing the characteristic phase diagram of the QGP phase transition. It is composed of a nuclear part which is described by the Sierk-Nix parameterization, a QGP part which is given by the bag model EOS, and a mixed phase which is obtained by Maxwell construction. Nucleons and pions as well as nonstrange quarks and gluons were considered. Our EOS has a first order phase transition. The critical temperature at n = 0 is T_c = 216 MeV, consistent with recent lattice QCD results: T_c = 177-276 MeV. The energy density increases monotonically with T until T_c is reached where the critical energy density is e_{cH}(n=0)=280 MeV/fm^3.

At breakup the local pion momentum distribution at a space-time point x is assumed to be a relativistic Bose distribution: $f^{\pi}(x,p;U^{\mu},T)$. The pions are emitted in their own local rest frame and their number is proportional to T^3. At the breakup each fluid cell is moving with the velocity $U^{\mu} = \gamma(1, \beta_{//}, \beta_{\perp}) = \gamma_{\perp}(\cosh(y_0), \sinh(y_0), v_{\perp})$, where y_0 is the rapidity of the fluid cell and the other variables provide the usual decomposition of the four-velocity.

The total pion multiplicity in the calculation is sensitive to the EOS. For example at 14.5 GeV/nucleon the phase transition to QGP yields a total pion multiplicity (π^+, π^0, π^-) 60 while the hadronic EOS yields about 40 at 10 fm/c breakup time, when the volume average of the density dropped to normal nuclear density in both cases. Earlier breakup times yield a higher pion multiplicity for both EOS's; later breakup times yield a smaller one. At 8 fm/c breakup time the pion multiplicities are 75 (50) for QGP (hadronic) EOS. The higher pion multiplicity in case of QGP EOS can be understood as a consequence of the reduced collective flow and thus a larger part of the energy is thermalized.

The pion transverse momenta, $p_{\perp}$, at 14.5 GeV are about 480 MeV/c with both EOS's if the breakup happens at normal nuclear density; this value decreases with increasing breakup time. At 60 GeV/nucleon and at 8 fm/c breakup time the maximum pion transverse momentum, $p_{\perp}$, is 670 (860) MeV/c for QGP (hadronic) EOS at 8 fm/c, and is increasing (decreasing) with increasing breakup time. The maximum of the average $p_{\perp}$ for QGP EOS peaks at 12 fm/c breakup with 720 MeV/c.

With a phenomenological EOS describing the phase transition to QGP in a S+Pb collision at 60 GeV/nucleon a QGP was created in a volume which reached 18% of the rest volume of the projectile. For a period of 2 fm/c the plasma occupied more than 10% of the initial nuclear volume. At 14.5 GeV/nucleon pure plasma was created in a small volume only, (maximum of 6% of the projectile), and it existed for a very short time. Thus, the modification of the flow pattern was caused by the mixed phase only.

The main effects of the QGP formation are increased longitudinal and reduced transverse flow. At 60 GeV/nucleon these effects are stronger, while at the lower energy the small amount of the plasma produced and the uncertainties in breakup time make it difficult to observe a clear change in the flow experimentally. The essence of these predictions is that the transverse flow should decrease in the presence of a phase transition in a given energy region. This is due to the fact that the pressure is strongly decreased by the latent heat of the deconfinement phase transition in the mixed phase region. A more complete description of this work may be found in Phys. Lett. B229, 351 (1989).

Q. Equilibration in Relativistic Nuclear Collisions: Two-Fluid Hydrodynamics *vs* Experiment
[A. S. Goldhaber (State University of New York at Stony Brook) and D. D. Strottman]

The conditions for establishment of local thermodynamic equilibrium in a complex, rapidly evolving system are among the most puzzling and important open issues in physics. Perhaps the chief arena where this issue appears is the inflationary model for the origin of the Universe. The assumption of rapid equilibration is essential in all analyses done so far, whether of the original, new, or extended versions of inflation. One setting in which equilibration can be investigated in the laboratory, perhaps the only one involving relativistic velocities, is the collision of atomic nuclei. Exploration already has begun in the energy range up to ten GeV/nucleon in the center-of-rapidity frame.

Hydrodynamics is based on the assumption of local thermodynamic equilibrium. In the two-fluid hydrodynamics model projectile and target are treated as distinct fluids, suffering a frictional drag when they overlap. Thus, in addition to the adjustable parameters associated with the equation of state in ordinary hydrodynamics, complete definition of the model requires specification of the drag force and of the "merger" conditions under which the two fluids should be treated as one undifferentiated substance. We have reformulated the assumptions about both drag and merger in a way which strengthens the tendency towards equilibrium by comparison with that in the earliest version of this model. The new drag assumptions are consistent with data on deceleration of high-energy nucleons upon traversal of nuclei.

In the original model, the criterion for beginning merger was that the relative velocity between the two fluids approached the Fermi velocity of ordinary nuclear matter.[43,44] However, dense matter would be likely to equilibrate at higher relative velocity, and we have, therefore, introduced the more generous criterion that merger begins when the momentum per unit mass of one fluid in the rest frame of the other approaches the nucleon Fermi momentum (in nucleon mass units) of the total fluid considered as a single entity. Since Fermi momentum increases only as the 1/3 power of nucleon density, this seems a conservative way of taking into account all the particle creation and other interaction effects which tend to bring about equilibrium. In the absence of initial slowing by the drag forces, no merger occurs even with the new criterion.

We have calculated proton rapidity distributions for heavy ion reactions of 1 to 200 GeV/nucleon and have compared with experiment. Both experiment and model show some peaking of proton distributions at rapidities between the central and incident values; it is worth asking whether these represent partial "transparency," that is, slowing but not stopping of some of the incident matter--or a kind of "bounce"--hydrodynamic expansion following stopping and equilibration. Examination of the evolution described by the model strongly supports the former notion. Nevertheless, the degree of transparency is much less than one might have expected for such light collision partners, and is clearly associated with the less substantial equatorial zones in the case of head-on collisions, and with "spectator" matter for collisions at larger impact parameters. Thus, compression and equilibration should be even more noticeable for collisions of the largest nuclei.

We now work to extend the useful range of center-of-rapidity energies by another order of magnitude in order to make predictions about the target and projectile fragmentation regions and to see how far (if at all) these regions become separated in rapidity.

R. Hadronization from Supercooled Baryon-rich Quark Gluon Plasma [A. K. Holme, E. F. Staubo, L. P. Csernai (University of Bergen); Eivind Osnes Physics (University of Oslo); and D. D. Strottman]

Detonations and deflagrations have been widely discussed in the literature in relation to ultra-relativistic heavy ion reactions and to formation and decay of the Quark Gluon Plasma (QGP). While the relevance of simplified detonation studies depends on the degree of thermalization and stopping and on the dynamical speed of the phase transition with respect to the size and time span of the collision, deflagrations are bound to occur at late phases of the reaction if a first order phase transition is part of the equation of state (EOS).

For detonations (compression shocks) the density increases across the shock front, while for deflagrations (rarefaction shocks) it decreases. In previous discussions of the hadronization of a quark-gluon plasma one has considered space-like deflagrations from supercooled baryonless

plasma, space-like detonations and deflagrations from baryonless plasma, time-like deflagrations from baryonless plasma and space-like deflagrations from the phase boundary of baryon-rich plasma.

We have discussed for the first time deflagrations initiated from a supercooled, baryon-rich QGP. In this case both supercooling and a baryon-rich initial state are important features of a realistic initial state that can be reached in heavy ion collisions in the presently available energy range. In recent publications simple phenomenological EOS's were used to study hadronization by rate equations with assumed hadronization rates or by assuming adiabatic expansion during hadronization. Deflagrations from supercooled QGP would modify the outcome of these scenarios.

Recent AGS and SPS experiments have led to the conclusion that in central, heavy ion collisions hadronic matter is strongly stopped. The present data from WA-80 indicate that the stopping of baryons is strong at energies up to 200 GeV/nucleon. At the lower energies 14.5 and 60 GeV/nucleon there is evidence for complete stopping in central collisions where no energy is detected around zero degree in calorimeters. Thus it should be possible to describe these reactions in terms of a one-fluid hydrodynamical model in which there is complete stopping.

If a quark-gluon plasma is produced during the initial compression, it will be very dense and hot. Afterwards the plasma expands, isentropically or with slight entropy production due to viscosity effects, and cools. As long as the matter is in the pure quark phase, there is no 'generalized force' to initiate a hadronization. Shocks are prevented by the requirement of mechanical stability. If the expansion is very rapid there might not be enough time for an adiabatic phase transition and the plasma will become supercooled. We have studied deflagrations from supercooled baryon-rich QGP using a phenomenological EOS. The choice of the EOS is not crucial for the qualitative discussion of reaction dynamics as our studies with different EOS's have shown.

Therefore, a simple phenomenological model for the equation of state with which to discuss the phase transition region and its dependence on the parameters of the EOS was introduced. Due to its relative simplicity this EOS is also used in three-dimensional fluid dynamical calculations describing ultra-relativistic collisions. We have also discussed the collision dynamics using shock wave formalism and the hadronization of quark matter by means of deflagrations from supercooled plasma. The equation of state for hadronic matter is chosen to be as simple as possible, but still retains the "essential features," which are:

a. The nucleons behave (approximately) as an ideal gas.

b. The nuclear density saturates at $n_0 = 0.145$ fm^{-3} with a binding energy per nucleon of $E_B = -8$ MeV, and nuclear matter is rather incompressible ($K \sim 200$).

c. At higher temperatures mesons are created.

In a relativistic heavy ion collision the two nuclei hit each other with a velocity larger than the speed of sound in nuclear matter. The compression will then propagate through the matter as a shock wave. The possible final states are found by solving the Taub adiabat using normal nuclear matter as the initial state. The final deflagration is determined by the relative rates of the phase transition from QGP to hadronic matter and of the supercooling. The hydrodynamically most favored deflagration is a Chapman-Jouguet (CJ) deflagration which maximizes the entropy production. However, if we would like to maintain such a CJ deflagration from a slightly supercooled state we need a large current, *i.e.*, a large phase transition rate across the front, because the corresponding Rayleigh-line is rather steep. If the phase transition rate is not sufficiently large the QGP will supercool further and reach a state for which a smaller phase transition rate is sufficient to maintain a CJ deflagration. If the supercooling is fast and the phase transition is very slow the supercooling might reach a stage for which the final state is determined by the phase transition rate alone.

Our studies indicate that the so far unknown phase transition rates from QGP to hadronic matter determine the dynamics of the final hadronization, and small changes in this rate may cause qualitative differences in the collision dynamics. (See Ref. 45 for a complete description of this work.)

S. References-Section IV

1. R. E. Prael and M. Bozoian, "Adaptation of the Multistage Preequilibrium Model for the Monte Carlo Method (1)," Los Alamos National Laboratory document LA-UR-88-3238 (September 1988).

2. M. Bozoian and R. E. Prael, "Double-Differential Cross-Section Calculations Based on a Monte-Carlo Formulation of the Multistage Preequilibrium Model.," Trans. Am. Nucl. Soc. 60, 261 (1989).

3. M. M. Meier, R. C. Bryd, R. E. Prael, W. A. Amian, "Measurements of Neutrons from (p,χn) Reactions at Proton-Bombarding Energies Below 800 MeV," Trans. Am. Nucl. Soc. 60, 258 (November 1989).

4. R. D. Smith, M. Bozoian, and E. D. Arthur "Preequilibrium Exciton Model with Quasi-Elastic Component," Bull Am. Phys. Soc. 33, 1601 (1988).

5. R. D. Smith and M. Bozoian, "Quasi-Free Scattering in the Preequilibrium Region," Phys. Rev. C 39, 1751 (1989).

6. W. W. Daehnick, J. D. Childs, and Z. Vrcelj, "Global Optical Model Potential for Elastic Deuteron Scattering from 12 to 90 MeV," Phys. Rev. C 21, 2253 (1980); and the references contained therein.

7. V. A. Madsen, L. F. Hansen, V. R. Brown, and D. G. Madland, "Correction for Truncation in Coupled-Channels Optical Potentials," Phys. Rev. C 40, 1999 (1989).

8. D. G. Madland, "Initial Deuteron-Nucleus Global Optical-Model Potential for NPB Target Discrimination Calculations," Los Alamos National Laboratory Group T-2 informal report T-2-IR-89-1 (November 1989).

9. R. Kozack and D. G. Madland, "Dirac Optical Potentials for Nucleon Scattering by ^{208}Pb at Intermediate Energies," Phys. Rev. C 39, 1461 (1989).

10. D. A. Hutcheon, W. C. Olsen, H. S. Sherif, R. Dymarz, J. Cameron, *et al.*, "The Elastic Scattering of Intermediate Energy Protons from ^{40}Ca and ^{208}Pb," Nucl. Phys. A483, 429 (1988).

11. R. L. Schutt, R. E. Shamu, P. W. Lisowski, M. S. Moore, G. L. Morgan *et al.*,"Nucleon Scattering from ^{208}Pb at Low and Intermediate Energies," Phys. Lett. B 203, 22 (1988).

12. E. R. Siciliano, D. G. Madland, and L.-C. Liu, "Deuteron Nucleus Optical Potential Analysis at Medium Energies," Bull. Am. Phys. Soc. 35, 1395 (1990).

13. R. Kozack and D. G. Madland, "Prediction of Intermediate-Energy Neutron Scattering Observables from a Dirac Optical Potential,"Nucl. Phys. A509, 664 (1990).

14. B. Wilkins and G. Igo, "Total Reaction Cross Sections for 22.4 MeV Deuterons," Phys. Lett. 3, 48 (1962).

15. S. Mayo, W. Schimmerling, M. J. Sametband, and R.M. Eisberg, "Reaction Cross Sections for 26.5-MeV Deuterons," Nucl. Phys. 62, 393 (1965).

16. J. R. Oppenheimer, "The Disintegration of the Deuteron by Impact," Phys. Rev. 47, 845 (1935).

17. S. M. Dancoff, "Disintegration of the Deuteron in Flight," Phys. Rev. 72, 1017 (1947).

18. C. J. Mullin and E. Guth, "Electric Excitation and Disintegration of Nuclei. I. Excitation and Disintegration of Nuclei by the Coulomb Field of Positive Particles," Phys. Rev. 82, 141 (1951).

19. L. C. Liu and R. M. Thaler, "Electrodisintegration of the Deuteron in Nuclear Reactions," Los Alamos document LA-UR-89-3894 (submitted to Phys. Rev. C).

20. J. Kleinfeller, J. Bisplinghoff, J. Ernst, T. Mayer-Kuckuk, G. Baur, B. Hoffmann, R. Shyam, F. Rösel, and D. Trautmann, "Study of Inclusive Proton Spectra for Low-Energy Deuteron Reactions in Terms of Spectator Break-Up and Coulomb Dissociation of the Projectile," Nucl. Phys. A370, 205 (1981).

21. M. Lacombe, B. Loiseau, R. Vinh-Mau, J. Côte, P. Pirés, R. de Tourreil, "Parameterization of the Deuteron Wave Function of the Paris N-N Potential," Phys. Lett. 101B, 139 (1981).

22. C. W. DeJager, H. DeVries, and C. DeVries, Atomic Data and Nuclear Data Tables 14, 485 (1974).

23. M. Ericson and T. E. O. Ericson, "Optical Properties of Low-Energy Pions in Nuclei," Ann. Phys. (N.Y.) 36, 323 (1966); D.S. Koltun, Adv. Nucl. Phys., Eds. M. Baranger and E. Vogt, (Plenum, N.Y.) 3, 71 (1969).

24. R. Gilman, H. T. Fortune, K. S. Dhuga, P. H. Kutt, L. C. Bland *et al.*, "Energy Dependence of Angular Distributions in the Nonanalog Pion Double-Charge-Exchange Reaction $^{16}O(\pi^+,\pi^-)^{14}O$ at 50 MeV," Phys. Rev. C, 29, 2395 (1984); and references therein.

25. K.K. Seth, S. Iversen, H. Nann, M. Kaletka, J. Herd, H. A. Thiessen, "Angular Distributions for the Reaction $^{18}O(\pi^+,\pi^-)^{18}Ne$ and Pion Double-Charge Exchange Form Factors," Phys. Rev. Lett. 43, 1574 (1979); *ibid*, 45, 147(E) (1980).

26. S.J. Greene, W. J. Braithwaite, D. Holtkamp, W. Cottingame, and C. F. Moore, "Systematics in Pion Double-Charge Exchange," Phys. Rev. C 25, 92 (1982); P.A. Seidl, M. P. Brown, R. R. Kiziah, and C. F. Moore *et al.*, Phys. Rev. C 30, 973 (1984); *ibid* , 30, 1076 (1984); P.A. Seidl, C. F. Moore, S. Mordechai, R. Gilman, K. S. Dhuga, and H. T. Fortune, Phys. Lett. B 154, 2255 (1985).

27. M. J. Leitch, E. Piasetzky, H. W. Baer, J. D. Bowman, R. L. Burman *et al.*, "Double Analog Transition $^{14}C(\pi^+,\pi^-)^{14}O$ at 50 MeV," Phys. Rev. Lett. 54, 1482 (1985); I. Navon, Phys. Rev. Lett. 52, 105 (1984).

28. S. S. Keth, M. Kaletka, S. Iversosen, A. Saha, D. Barlow, and D. Smith, "Core Excitation Effects in Pion Double Charge Exchange," Phys. Rev. Lett. 52, 894 (1984).

29. A. Altman, R. R. Johnson, V. Wienads, N. Hessey, B. M. Barnett, B. M. Forster *et al.*, "Observation of Double Isobaric Analog Transition $^{18}O(\pi^+,\pi^-)^{18}Ne$ at 50 MeV," Phys. Rev. Lett. 55, 1273 (1985).

30. For a compilation of the data prior to 1985 and their references, see also R. A. Gilman in Los Alamos National Laboratory report LA-10524-T (1985).

31. Z. Weinfeld, E. Piasetzky, M. J. Leitch, H. W. Baer, C. S. Hishra *et al.*, "Pion Induced Transitions to Double Isobaric-Analog States at 35 MeV on $1f_{7/2}$-Shell Nuclei," Phys. Lett. B 237, 33 (1989).

32. Q. Haider and L. C. Liu, "Dynamics of Pion Double-Charge Exchange Reactions," Z. f. Physik A (in press), Los Alamos document LA-UR-89-3466.

33. D. J. Ernst and M. B. Johnson, "Simple Model of Pion-Nucleon Elastic Scattering," Phys. Rev. C 22, 651 (1980).

34. R. Machleidt, K. Holinde, and Ch. Elster, Phys. Rep. 149, 1 (1987).

35. S. Cohen and D. Kurath, "Effective Interactions for the 1p Shell," Nucl. Phys. 73, 1 (1965).

36. E. R. Siciliano, M. B. Johnson, and H. Sarafian, "Dynamical Correlations in Low-Energy Pion Double Charge Exchange," Los Alamos document LA-UR-89-3302, to be published in Ann. Phys. (1990).

37. M. B. Johnson, E. R. Siciliano, and H. Sarafian, "Dynamical Short-Range Correlations in Low-Energy Pion Double Charge Exchange on the Calcium Isotopes," Los Alamos document LA-UR-90-375, to be published in Phys. Lett. B (1990).

38. E. Oset, L. L. Salcedo and D. Strottman, "A Theoretical Approach to Pion Nuclear Reactions in the Resonance Region," Phys. Lett. 165B, 13 (1985).

39. L. L. Salcedo, E. Oset, M. J. Vicente-Vacas and C. García-Recio, "Computer Simulation of Inclusive Pion Nuclear Reactions," Nucl. Phys. A484, 557 (1988).

40. C. Olmer, D. F. Geesaman, B. Zeidman, S. Chakravarti, T. S. H. Lee *et al.*, "Elastic and Inelastic Scattering of 162-MeV Pions by ^{28}Si, ^{58}Ni, and ^{208}Pb," Phys. Rev. C21, 254 (1980) .

41. S. Rokni, H. W. Bauer, A. G. Bergmann, J. D. Bowman, F. Irom, M. J. Leitch *et al.*, "Isobaric-Analog-State Transitions in Pion Charge-Exchange Reactions Above the Δ (1232 Resonance), Phys. Lett. B 202, 35 (1988); U. Sennhauser, J. D.Bowman, M. D. Cooper, E. Piasetzky, H. W. Baer *et al.*, "Isobaric Analog States in Pion Single-Charge-Exchange Reactions on and Above the (3,3) Resonance Energy," Phys. Rev. Lett. 51, 1324 (1983).

42. E. Oset, Y. Futami, and H. Toki, "Pion Absorption in the Resonance Region," Nucl. Phys. A448, 597 (1986).

43. A. A. Amsden, A. S. Goldhaber, F. H. Harlow and J. R. Nix, "Relativistic Two-Fluid Model of Nucleus-Nucleus Collisions," Phys. Rev. C17, 2080 (1978).

44. R. B. Clare and D. Strottman, "Relativistic Hydrodynamics and Heavy Ion Reactions," Phys. Rept. 141, 177 (1986).

45. A. K. Holme, E. F. Staudbo, L. P. Csernai, E. Osnes, D. Strottman, "Hadronization from Supercooled Baryon-rich Quark-Gluon Plasma,"Phys. Rev. D40, 3735 (1989).

V. FISSION

A. Heavy-Element Fission Barriers (P. Möller and J. R. Nix)

Experimental studies of fission properties of nuclei close to ^{258}Fm sometimes show two components in the kinetic-energy distribution and rapid changes in mass distributions and spontaneous-fission half-lives with a change of only one or two neutrons or protons. These results led to the speculation that the two modes of fission were the result of two different valleys, or paths, from the single nuclear ground state to two different scission configurations. The scission configuration yielding low kinetic energies would correspond to elongated shapes and the configuration resulting in high fission-fragment kinetic energies was thought to correspond to two approximately spherical fragments.

In the top part of Fig. V-1 we show a family of shapes leading from the ground state to these two different scission configurations. Corresponding potential-energy surfaces have been calculated for several hundred heavy elements. Two examples are shown in the lower part of the figure. For ^{258}Fm the results show three fission paths indicated by arrows. The lower path, sometimes called the new path, leads to compact, spherical scission shapes with high kinetic energies and the upper path to very elongated shapes with low final kinetic energies. Thus, one finds that the structure of the calculated potential-energy surface agrees well with what was expected from experiments. However, to explain the similar spontaneous-fission half-lives for the high and low kinetic-energy modes, the paths corresponding to these two different modes cannot be very different. Therefore, it is our contention that it is a third path, the switchback path, indicated by a long-dashed line, that leads to elongated scission configurations. This path differs from the new path only in the very outermost part of the fission barrier, and one can show that the spontaneous-fission half-lives are of the same magnitude along the two lower paths even if the two outer barrier heights are somewhat different. Investigations of the stability of the potential energy in the shaded region with respect to mass-asymmetric shape degrees of freedom have shown that the saddle on the switchback path is lowered by about two MeV due to mass asymmetry, but that the lower saddle leading to spherical, compact shapes is unaffected by mass-asymmetric shape degrees of freedom.

For ^{252}Cf, seen in the middle part of the figures, access to the compact fission valley is blocked by a ridge at 8 MeV (about 10 MeV above the ground state).

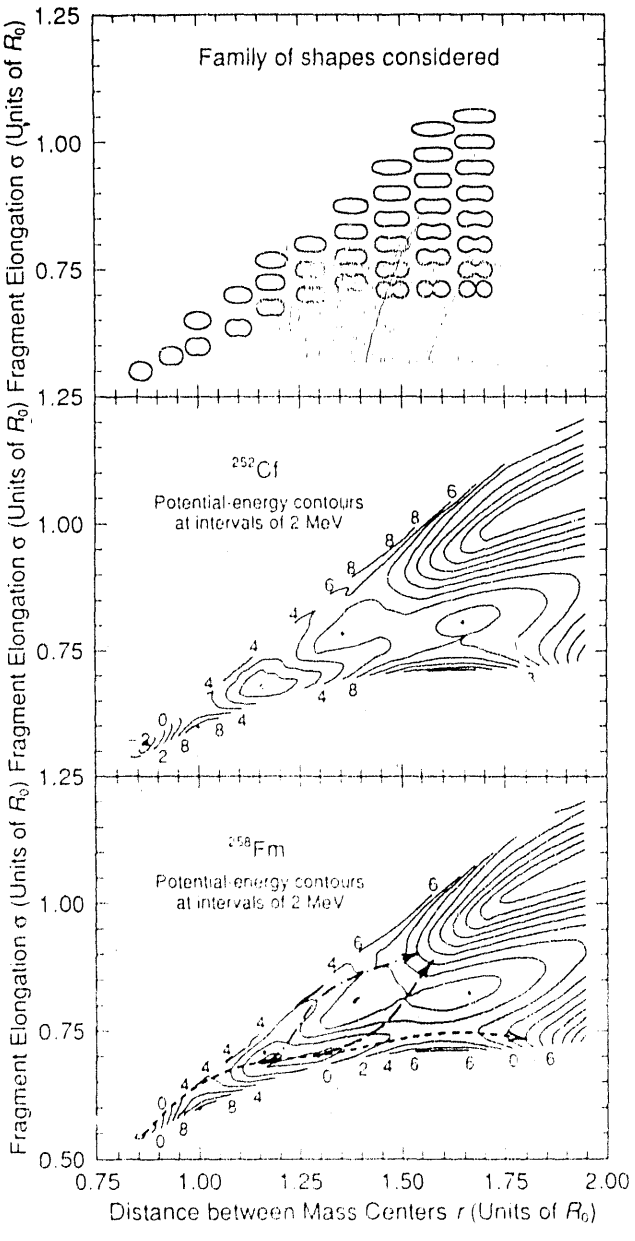

Fig. V-1. Potential-energy surfaces for ^{252}Cf and ^{258}Fm, corresponding to the nuclear shapes shown in the top part of the figure.

B. Heavy-Element Fission Half-Lives (P. Möller and J. R. Nix)

Experimental studies of fission properties of nuclei close to Fm sometimes show two components in the kinetic-energy distribution and rapid changes in mass distributions and spontaneous-fission half-lives with a change of only one or two neutrons or protons. Particularly striking is the experimental result that for Fm the spontaneous-fission half-life varies by 13 orders of magnitude with a change in neutron number from N = 152 to N = 158.

A theoretical description of these data requires a description of the fission barrier in terms of several shape coordinates. Multi-dimensional calculations of potential-energy surfaces for the heaviest actinides show several paths from the ground-state to different scission configurations. In Fig. V-2 we compare experimental spontaneous-fission half-lives to calculated ones along two

different paths for even nuclei from Z = 100 to Z = 106. The notation "old path" corresponds to shapes leading to elongated scission shapes, and "new path" to shapes leading to a compact scission configuration of two touching spheres. The new path only exists for nuclei close to ^{264}Fm. It is clear from the figure that from about N = 156, the new path becomes the dominating one and explains the rapidly decreasing half-lives in this region of large N values. As the new path is fully developed, the calculated half-lives become approximately constant with increasing neutron number, in agreement with experiment. When analyzing the discrepancies between calculations and experiment, one should recall that a change in the calculated ground-state energy by 1 MeV affects the calculated half-life by about 6 orders of magnitude.

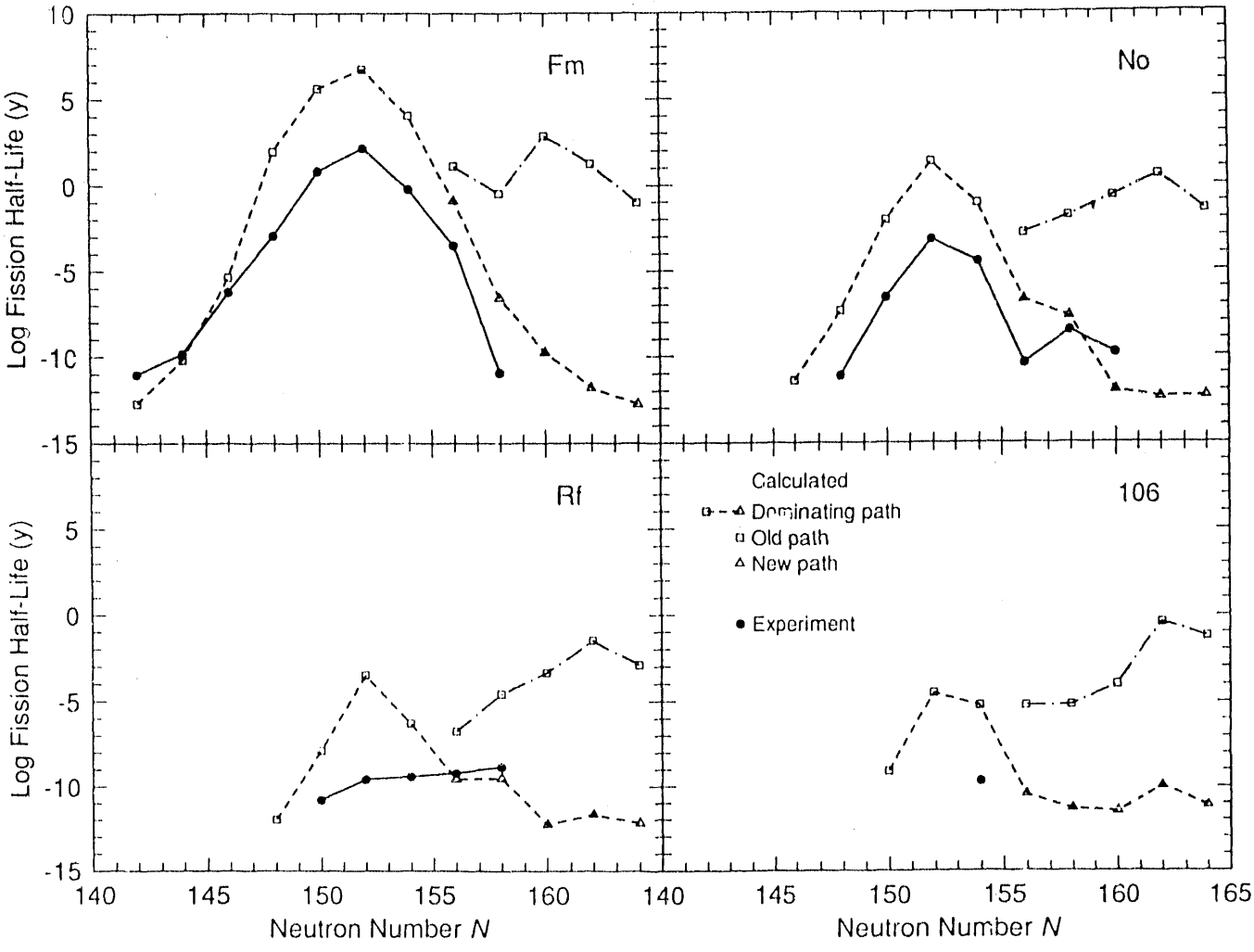

Fig. V-2. Calculated spontaneous-fission half-lives compared with experimental data, for isotopes of Fm, No, Rf, and Z = 106.

C. Theory of Neutron Emission in Fission (D. G. Madland)

The current status of the theory of neutron emission in fission was recently reviewed at the Conference on Fifty Years with Nuclear Fission.[1] Following a summary of the observables in neutron emission in fission, a brief history was given of the theoretical representations of the prompt fission neutron spectrum N(E) and average prompt neutron multiplicity $\bar{\nu}_p$. This was followed by descriptions and examples of modern approaches to the calculation of these quantities including recent advancements. Emphasis was placed upon the predictability and accuracy of the modern approaches. In particular, the dependence of N(E) and $\bar{\nu}_p$ on the fissioning nucleus and its excitation energy was discussed, as were the effects of and competition between first-, second-, and third-chance fission in circumstances of high excitation energy. Finally, properties of neutron-rich (fission-fragment) nuclei were discussed that must be better known to calculate N(E) and $\bar{\nu}_p$ with higher accuracy than is currently possible. This work has been published.[1]

D. Fission Neutron Spectra for ^{240}Pu, ^{238}Pu, and ^{242}Pu [D G. Madland, R. L. Walsh (Australian Nuclear Science and Technology Org., Lucas Height Research Labs.), and G. Chircu (Univ. of New South Wales, Australia)]

We have calculated the prompt fission neutron spectra for the spontaneous fission of ^{240}Pu, ^{238}Pu, and ^{242}Pu using the Los Alamos model[2] and incorporating center-of-mass anisotropy effects.[3] Our calculations agree well with the trends of the (somewhat scarce) experimental data for these three fissioning systems, and they are currently being used in plutonium assay work for nuclear safeguards. This work has been published.[4]

E. An Improved Model for the Calculation of Prompt Fission Neutron and Gamma-Ray Data (E. D. Arthur, M. Bozoian, D. G. Madland, P. G. Young)

An effort is underway to develop improved theoretical methods for calculation of prompt fission neutron and gamma-ray emission. The focus of the present effort is the correct description of the competition between neutron and gamma-ray emission in fission fragment deexcitations that take place immediately after prompt fission. Additionally the possible effect of non equilibrium deexcitation modes on calculated prompt fission neutron emission spectra are also being investigated. The procedures and steps occurring in prompt fission neutron and gamma ray emission spectra calculations are summarized in the paragraphs that follow.

The GNASH preequilibrium statistical model code[5,6] is used to provide multichance fission cross sections as well as average excitation energies of each fissioning compound system. Next, modeling of data associated with individual fission fragments occurs.[7] In order to effectively characterize the nature of the nuclei produced during fission, the heavy mass portion of the fission product yield distribution is sampled as an equidistant function of the mass A. This determines the

initial fission product yields from which fragment yields will be obtained. The first step in this process is the determination of the fragment mass using the chosen fission product mass and the average neutron multiplicity associated with a given fragment, *i.e.*, $A_H = A_H' + \nu/2$, where prime quantities are associated with a given fission product and unprimed ones refer to fission fragments. The average neutron multiplicity is then calculated by use of the expression

$$\upsilon = \frac{E^* - \left\langle E_\gamma^{Tot} \right\rangle}{\langle S_n \rangle + \langle \eta \rangle} \qquad (1)$$

Here E^* is the total excitation energy of the fragment pair occurring in fission, $<E_\gamma^{Tot}>$ is the average total gamma ray emission energy occurring in fission, $<S_n>$ is the average neutron binding energy, and $<\eta>$ is the average center-of-mass energy of the emitted neutrons. The average total gamma ray energy occurring in fission is obtained empirically from $<E_\gamma^{Tot}> = 0.028\ A_c + 0.09$ MeV, where A_c is the mass of the fissioning system. The total excitation energy of the fragment pair is determined from

$$E^* = \varepsilon + E_r - E_f^{Tot} \quad , \qquad (2)$$

where E_r is the energy release in fission , E_f^{Tot} is the total fission fragment kinetic energy, and ε is the excitation energy of the compound system that is provided from GNASH. The energy release in fission is computed from experimental or calculated masses. Because this calculation requires knowledge of both the heavy- and light-mass fragments, an initial value of ν must be chosen to determine A_H. The charge associated with the heavy fragment is then determined assuming a Gaussian charge distribution for a given fragment mass together with a most probable charge determined from a modified UCD (unchanged charge distribution) model. These initial Z and A values of the heavy fragment are used to find the similar light fragment quantities. Additionally, once a trial value for the Z,A of both the light and heavy fragments is known, the total fission fragment kinetic energy can be calculated using the following empirical expression

$$E_f^{Tot}(Z_L,A_L,Z_H) = \alpha \left\langle E_f^{Tot} \right\rangle + \frac{(A_H - A_c/2)}{(130 - A_c/2)} \left\{ E_f^{Tot}(Z_L,A_c\text{-}130;\ Z_H,130) - \alpha \left\langle E_f^{Tot} \right\rangle \right\}$$

for $A_c/2 \le A_H < 130$, and

$$E_f^{Tot}(Z_L,A_L;Z_H,A_H) = \left[\frac{(Z_c - Z_H)\, Z_H}{(Z_c - \overline{Z_H})\, \overline{Z_H}} \right]^2 \left[\frac{\overline{A_L^{1/3}} + \overline{A_H^{1/3}}}{A_L^{1/3} + A_H^{1/3}} \right]^2 \left\langle E_f^{Tot} \right\rangle \qquad (3)$$

for $130 \le A_H$

where $\left\langle E_f^{Tot} \right\rangle = 0.119 \left[\frac{Z_c^2}{A_c^{1/3}} \right] + 7.3\ MeV$.

An iterative procedure is then used to solve again for ν, E_r, and E_f^{Tot} until final values for the heavy and light mass fragments are obtained. Yields for a light-heavy fragment pair are then determined via systematics or from specific inputed values. In either case, corrections are applied to obtain corresponding charge yields.

With the fragment pair Z,A, yield, total excitation energy, and total kinetic energy computed from the above expressions, the remaining step involves the partitioning of the total fragment pair excitation energy between the light and heavy fragment. This can be done in several ways using the ratio of the light and heavy fragment masses, the ratio of the Fermi gas level density parameters for the respective fragments, or through the ratio of results from simple models for the density of states of the fragments (using particles in a box, for example). Two examples of the latter that give improved calculations of multiplicity *vs* fragment mass are shown in Figs. V-3 and V-4, respectively, for the cases 14.5 MeV n+^{238}U and spontaneous fission of ^{252}Cf.[8,9]

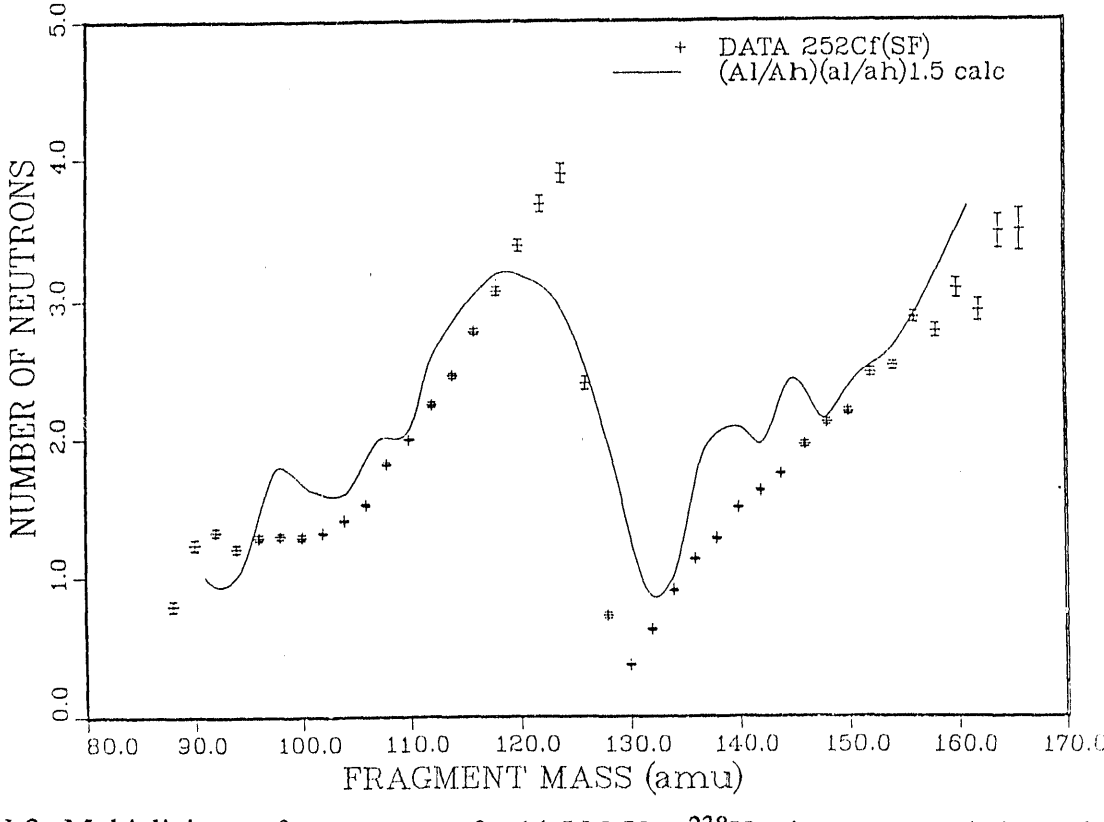

Fig. V-3. Multiplicity per fragment mass for 14.5 MeV n+^{238}U using a mass ratio in particles-in-a-box total level formula.

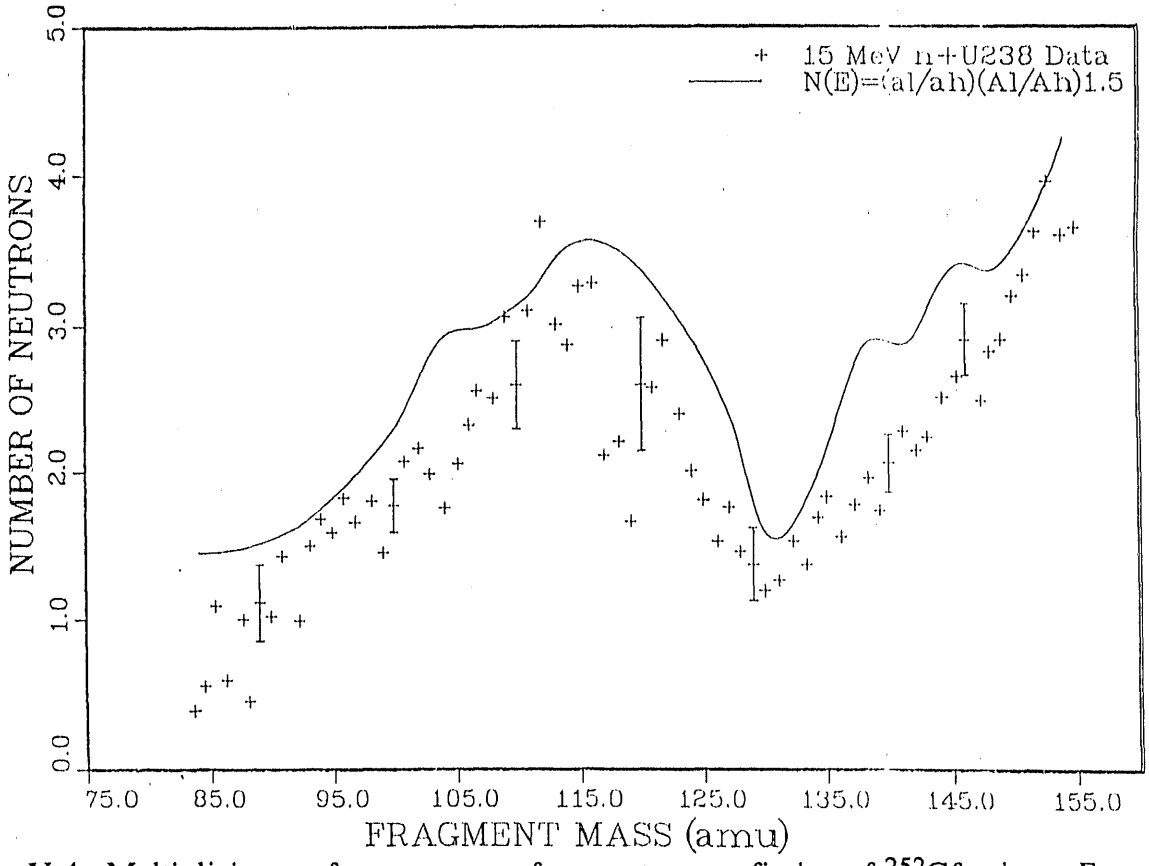

Fig. V-4. Multiplicity per fragment mass for spontaneous fission of ^{252}Cf using a Fermi-gas-level-density-parameter ratio in particles-in-a-box total level formula.

Finally, we also obtain root mean square values for the initial spin of the light and heavy fragments using a classical expression[3] that relates them to the incident energy of the projectile, an accompanying impact parameter, and the number of particles emitted prior to fission of a given compound system. While such spin information is necessary for fragment deexcitation calculations using Hauser Feshbach statistical models (or other models that approximately conserve spin), the fragment deexcitation model described next does not require this input data since evaporation model methods are currently used in it.

After the above information has been determined, the calculation of the neutron and gamma ray emission occurring from the deexcitation of individual fission fragments is made using a streamlined version of the GNASH code that employs a Weisskopf-Ewing model to compute equilibrium emission. The formalism for inclusion of particle-gamma ray competition follows a method originally developed by Buttner *et al.*[10] and is described in Ref. 6. Within this evaporation model framework, multistage particle processes are followed and detailed optical model penetrabilities and nuclear level density information is used to calculate particle and gamma ray partial widths.

The calculation of fission fragment deexcitation also includes contributions from nonequilibrium emission processes that are computed using a closed form version of the exciton preequilibrium model.[11] This model is used in the calculation of fragment deexcitation because of the relatively high excitation energies that occur in many fragments where equilibrium reaction assumptions may not be valid. The exciton preequilibrium model assumes that the deexcitation of the compound system proceeds through a series of stages each described by a given particle-hole configuration until equilibrium is reached. This process involves stages that are initially made up of a few excitons while latter stages close to equilibrium include significant numbers of particle-hole pairs. The nonequilibrium contribution to the cross section is computed via the expression

$$\frac{d\sigma}{d\varepsilon} = \sigma_R \sum_n \left[\frac{\rho_{n-1}(U)}{\rho_n(E)}\right]\left[\frac{W_c(\varepsilon)}{W_c(\varepsilon) + W^+(E)}\right] D_n \, d\varepsilon \ . \qquad (4)$$

Here n refers to the number of excitons (n=particle + hole) and σ_R is the reaction cross section at a given incident energy. The term in the first bracket is related to the number of excitons that can be emitted with channel energy ε and is computed from the phase space represented by the exciton state densities in the compound and residual nuclear systems. The second bracket represents the probability that particle emission will occur. Here $W_c(\varepsilon)$ is the overall particle emission fraction while W^+ represents the fraction of the process that leads to higher exciton configurations. D_n is a depletion factor that accounts for population loss to the $(n+1)^{th}$ stage from preceding stages.

The initial particle-hole configuration normally assumed in particle-induced reactions consist of two particles and one hole. Here we do not have an incident particle in the initial state of the deexcitation of a fragment, so we have assumed the simplest one particle, one hole configuration with which to begin calculation of the contribution given by Eq (4). In doing so we have also adjusted the normalization constant that determines the magnitude of W^+ to better match data for ^{252}Cf that we used to benchmark our calculational procedure. This quantity involves an empirical normalization of the residual terms appearing in the matrix element describing two-body interactions. This factor determines the rate at which a system proceeds to higher exciton configurations and is normally equal to about 150 MeV.[7] From our adjustments to ^{252}Cf neutron emission spectra data we determined a value of 400 MeV.[7] Figure V-5 provides an example of the comparisons made to determine the overall normalization for W^+. Here we plot the ratio of our calculated and the measured spectrum[12] to that produced using a Maxwellian representation with a temperature of 1.42 MeV. These calculations that include a nonequilibrium component reproduce these data quite well.

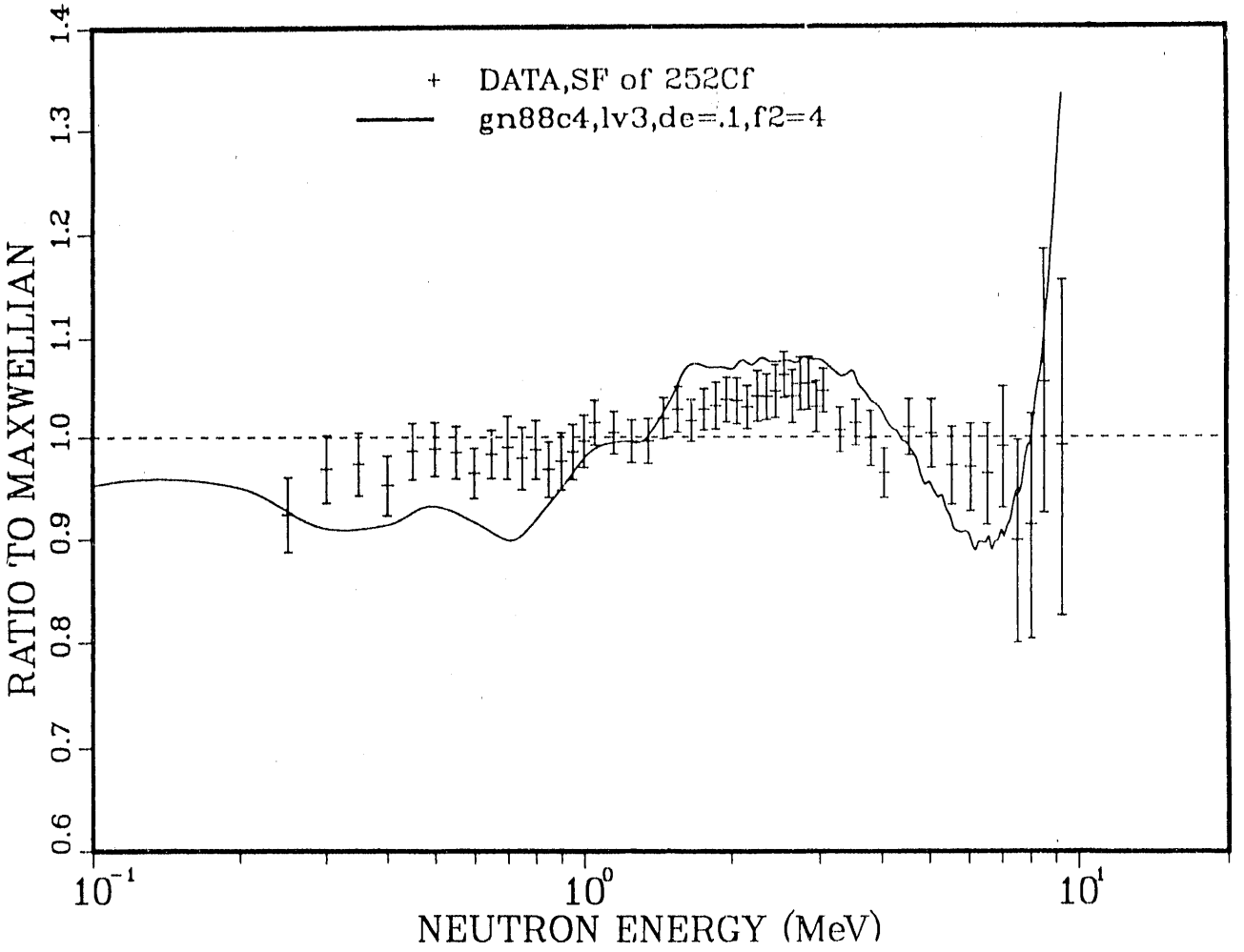

Fig. V-5. A comparison of the prompt fission neutron spectrum for ^{252}Cf calculated using the methods described in the text with the Poenitz data.

In addition to comparisons for ^{252}Cf, we have also calculated prompt fission neutron emission spectra for incident energies of 0.6, 7, and 14 MeV. Prompt fission gamma-ray emission spectra were also calculated for 14 MeV-neutron induced fission of ^{235}U and compared to the data of Ref. 13. We found a significant underprediction for gamma-ray energies below 2 MeV, which we attribute to the inherent neglect of angular momentum effects in evaporation model calculations of gamma-ray cascades. In order to correct this deficiency, we are pursuing the implementation of a streamlined Hauser-Feshbach model for the calculation of gamma-ray emission from fragment deexcitation.

F. Calculation of Medium Energy Nucleon-Nucleus Fission Cross Sections (E. D. Arthur and P. G. Young)

An intensive effort has been underway to develop and apply models appropriate for realistic description of nucleon-induced fission up to incident energies of 100 MeV. Results from this effort are discussed in detail in Ref. 14. Specifically, most of the effort has concentrated on models that provide more physics insight to higher energy fission processes than do those that are generally utilized in intranuclear cascade evaporation code calculations. Those appearing in intranuclear cascade codes such as NMTC and HETC, are based upon systematics or simple theoretical parameterizations[14] of (Γ_n/Γ_f) where the Γs refer to the neutron and fission width, respectively. Such models parameterize the behavior of these ratios as a function of mass, charge, and sometimes, excitation energy. The present calculations employ a more detailed treatment of the fission channel based upon the Bohr-Wheeler formalism[15] for fission penetrabilities as well as explicit calculation of fission transition state spectra and densities occurring at the fission saddle point. Although we still must determine the barrier parameters empirically, we are interested in the determination of the systematics of barrier parameters as more compound systems are reached at higher energies. We are also pursuing a preliminary investigation of fission dynamics for fission occurring at high excitation energies in a given compound system. From recent heavy-ion experimental[16] and theoretical work,[17] one expects that the time scale involved in reaching the scission point is significantly longer than that for neutron emission at high excitation energies. Thus, instances may occur where the assumption of statistical equilibrium is not valid, and particle emission can occur before the fissioning system can reach the scission point. As described below we have approximated these effects and have investigated their impact on total calculated fission cross sections as well as on cross sections associated with specific multichance fission components.

As a basis for further discussion of barrier systematics and fission dynamics, we examined the multichance fission contributions that make up the total fission cross section at higher nucleon energies. Figure V-6 illustrates multichance contributions to ^{237}Np(n,f) cross sections for incident energies between 20 and 100 MeV. As described in Ref. 14, these were part of an analysis of new higher energy fission data recently measured at Los Alamos.* In Fig.V-6 we compare contributions from neptunium compound systems ranging in mass number from 237 to 230. Contributions from the ^{238}Np compound system are not shown because preequilibrium particle emission essentially exhausts reaction strength for fission of this system because of the faster time scale associated with particle emission. Here at energies above 40 MeV, the total fission cross section is made up of almost equal contributions from several fissioning neptunium systems. At

* This information was provided by P. W. Lisowski, Los Alamos National Laboratory in early 1989.

energies of 80-100 MeV, seven systems contribute to the total fission cross section in roughly equal parts of 0.2 barns.

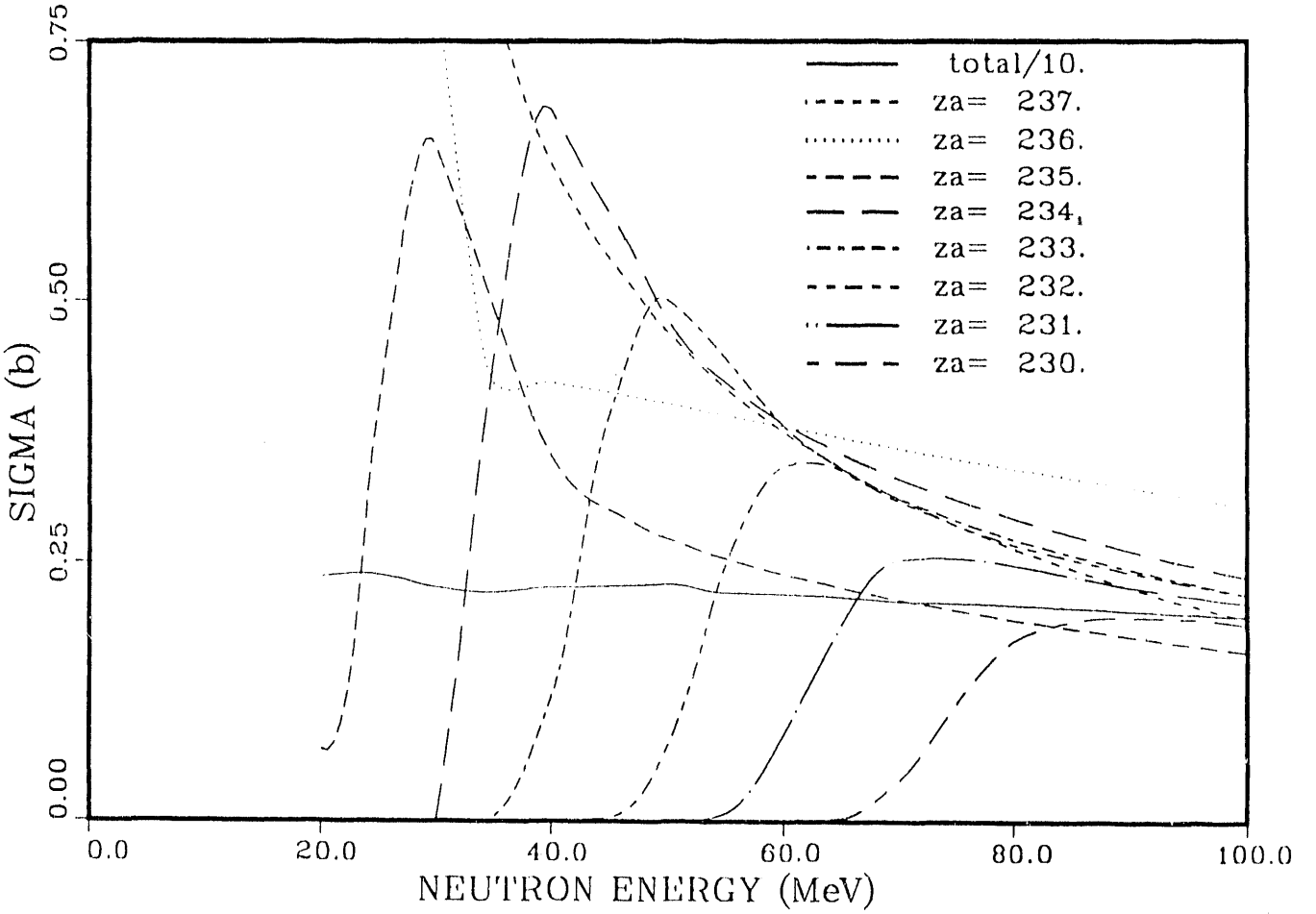

Fig. V-6. Calculated multichance fission components of the total n + ^{237}Np fission cross section for incident energies between 20 and 100 MeV.

The systematics of neptunium compound system fission barriers are shown in Fig. V-7 where their values are compared with neutron separation energies appropriate for these compound nuclei. This figure shows a conclusion reached from our analyses, indicating that, in order to achieve reasonable multichance fission components (as well as a reasonable total fission cross section), barrier heights should be commensurate in magnitude with the neutron binding energy of the system. For the more proton-rich (lighter) neptunium isotopes, the neutron binding energy generally increases, reaching a value near 7.5 MeV in some instances. This trend led us to increase barrier heights for proton-rich systems, resulting in systematics that are counter to results obtained from liquid drop barrier calculations[18] that employed ground state mass corrections.* These results

* This information was provided by D. G. Madland, Los Alamos National Laboratory in 1988.

are in partial disagreement with certain results obtained from analyses using charged-particle fission probability data.

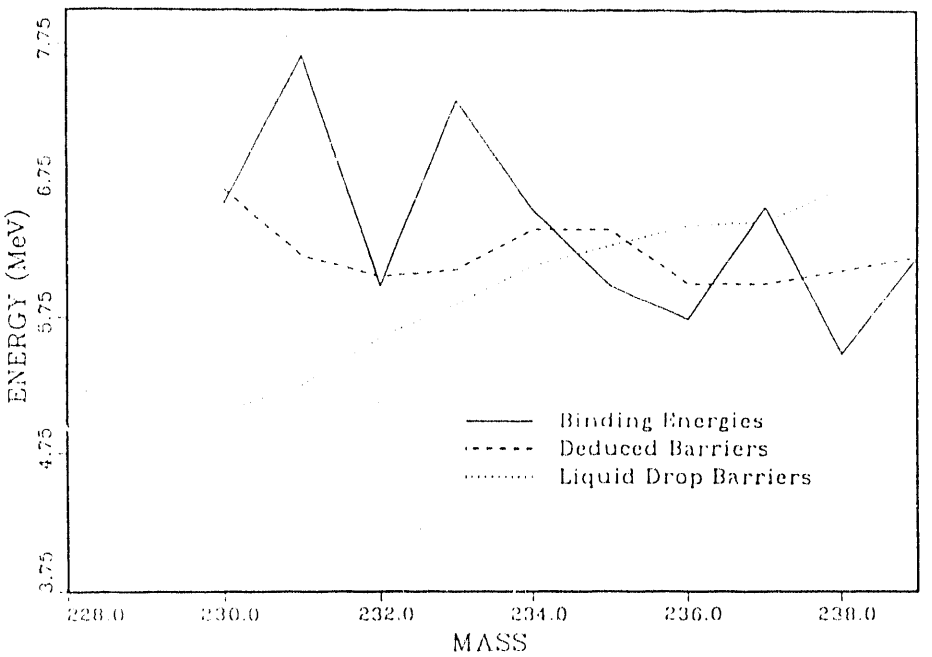

Fig. V-7. Systematics of neptunium compound system fission barrier heights as determined from this analyses. Also shown are neutron separation energies and barrier height predictions from the liquid drop model.

A final area in which we have begun investigation of fission phenomena at high incident (and excitation) energies involves the influence of fission dynamics on predicted fission cross sections. This area has been of recent interest for heavy-ion reaction induced fission and has been investigated through Fokker-Planck diffusion calculations performed by Nix, Hoffman, Weidenmüller and others (see Ref. 17). Such calculations have examined characteristic diffusion rates and times to reach either fission saddle or scission points in various over or underdamped fissioning systems. At high excitation energies (around 100 MeV) such calculations indicate significant departures from results obtained using standard Hill-Wheeler penetrabilites that assume the existence of statistical equilibrium in a fissioning system. The most immediate modification of the Hill-Wheeler calculated width is due to Kramers,[19] which involves a multiplicative factor that includes a viscosity coefficient *b* associated with the fission process. In the present work we have not replaced our Hill-Wheeler fission widths because the factors occurring in the Kramers expressions would uniformly reduce the fission widths for most compound systems occurring in our calculations. In order to reproduce available experimental data, we would then have to readjust barrier heights and state density enhancement factors so that the resulting fission cross section would probably not change significantly. Instead, we have approximated master equation

calculations performed by Hassani *et al.*,[20] which explicitly include fission rates calculated via diffusion methods. For fissioning systems having temperatures of approximately 2 MeV (appropriate for excitation energies of interest here) such characteristic times for fission are on the order of 50-100 $\times$ 10^{-22} seconds.[21] We can also compute an equivalent neutron emission characteristic time from $\tau = h/\Gamma_n$, where the neutron width is determined by

$$\Gamma_n(U) = \frac{1}{\pi\rho(U)} \int_0^U d\varepsilon \sum (2\ell + 1) T_\ell \, \rho(U - \varepsilon) , \qquad (5)$$

in which T and ρ refer respectively to optical model transmission coefficients and level density data. Characteristic neutron emission times computed at an excitation energy U are then compared with characteristic fission time range given above. At high excitation energies, neutron emission times were found to be significantly less than these times. In such cases we bypassed our normal calculation of the fission width in the equilibrium portion of the GNASH code and allowed only particle and gamma ray emission.

As an indication of this approximation, Fig. V-8 illustrates the change in fission contributions occurring from several fissioning systems that contribute to the n + ^{237}Np reaction in the incident energy range from 60-100 MeV. The systems shown there are the same as shown earlier in Fig. V-6 where the magnitudes of various contributions to the total fission cross section were presented. Several trends are apparent from the results shown in Fig. V-8. First, the contribution from fission of the ^{237}Np compound system decreases significantly. This occurs because ^{237}Np exists at the highest excitation energy of the set considered here and neutron emission thus occurs on the shortest time scale. This means that population strength occurring in this system is available for neutron emission, which then populates compound systems occurring later in the reaction chain. This increased population is then followed by fission of these systems. Note that the fission probability of these later compound systems is not significantly affected by our fission dynamics approximation as they exist at lower excitation energies where characteristic neutron emission times are large. Because of this increased initial population, their overall fission contribution increases relative to the case where no fission dynamics effects were included. This trend continues up to higher incident energies where neutron emission times of systems such as ^{235,236}Np become short because of the higher excitation energies that are reached. These systems then exhibit a decline in their fission contribution relative to the non-fission dynamics case.

The overall effect of this crude approximation to fission diffusion on the total fission cross section is small. This occurs because of the offsetting of reduced fission probabilities for specific compound systems with increased neutron population of later stages of the reaction chain, as

discussed above. Thus, we see little effect upon our calculations at high energies using this approximation but caution that these investigations are still in a preliminary form.

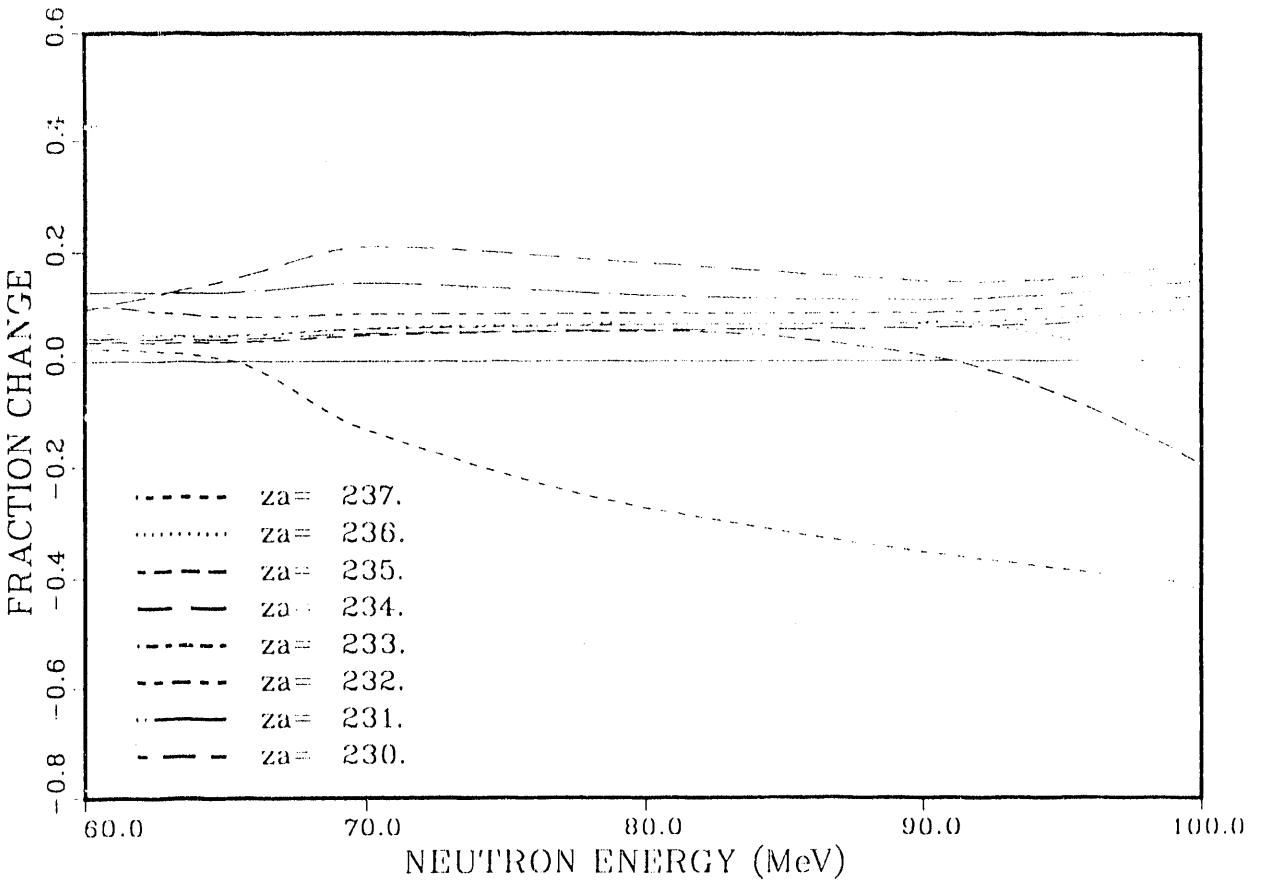

Fig. V-8. The effect on components of the calculated ^{237}Np(n,f) due to the approximation of fission dynamics as discussed here.

G. Activation, Actinide, and Fission-Product Yields and Decay Data [T. R. England, W. B. Wilson, B. F. Rider (T-2 consultant), C. W. Reich (Idaho Nat. Eng. Lab.), F. M. Mann (Hanford Eng. Dev. Lab.), R. E. Schenter (Hanford Eng. Dev. Lab.), M. C. Brady (Oak Ridge Nat. Lab.), and Jun-ichi Katakura (Japan Atomic Energy Research Inst.)]

The ENDF/B-VI National Data Files are in the process of being greatly expanded in decay and yield data. This section summarizes some preliminary results and content. References 22-25 provide summaries of the general ENDF/B-VI content; the special yield and decay data are summarized here as well.

1. Decay Data (Average Energies and Spectra: Refs. 26-35) There will be a single file of decay data for ENDF/B-VI format; Table V-I, however, shows the content in terms of activation, actinide, and fission product nuclides.

TABLE V-I

ENDF/B-VI DECAY DATA IN ACTIVATION, ACTINIDE, AND FISSION-PRODUCT FILES[a]

Data Type	Activation	Actinide	Fission-Product
Total Nuclides	149	108	> 391
Isomeric States	22	5	168
Stable	0	0	127
Delayed Neutron Precursors	0	0	271
Nuclides with Spectra	149	108	755
Gamma and/or x ray	119	98	736
Beta and/or discrete elec.	119	96	677
Positron and/or e.c.	61	0	40
Alpha	12	71	3

[a]Activation and actinide decay files are complete with limited tests. Fission-product files are not complete as of 7 November 1989 and numbers are approximate. The number of fission products having some measured spectra or average energies is 510. Theoretical values will be given for most remaining unstable nulcides and will supplement the discrete (but incomplete) spectra in 115 nuclides of the 510 set.

The activation and actinide files are complete and in an ENDF/B-VI format. These are based on an INEL (Idaho National Engineering Laboratory) evaluation, converted to the ENDF formats at HEDL (Hanford Engineering Development Laboratory). Limited testing at Los Alamos shows that several errors require correction before data are released. The amount of decay data (and number of nuclides) in these files is approximately twice that in ENDF/B-V.

Fission products present several problems because of data measured incompletely. There are no measured spectra for 30% of the products, and spectra are incomplete for at least half of the products. In some cases we know only a halflife (in several cases, we do not even have a measured halflife). In a few cases, we have a measured decay energy, but no spectra, and in many cases, we have measured spectra that are either incomplete or have the "pandemonium problem." The ENDF system requires complete data, where possible, within the time limits of evaluators, using nuclear models as necessary.

Unlike ENDF/B-V, we would like to complete a fission-product decay file that does not exhibit the pandemonium problem and has complete spectra that will reproduce the average beta, gamma, delayed neutron, *etc.* energies, either exactly or within a few per cent. This requires nuclear theory calculations for essentially all unstable products for their average energies and spectra.

This is followed by a decision for each of the nuclides that have some measured spectra as to which require supplements and the amount of each supplement.

For many nuclides there is no way to know with certainty that an average energy and its spectra are deficient. It is possible to use all decay and yield data in calculations of aggregate energies and spectra in comparisons with the many time-dependent measurements and thereby decide on the type of spectra needing model data. It is also possible to identify many nuclides as having incomplete spectra. In other cases, in which we cannot say definitively that a particular nuclide is missing spectra data, sensitivities of the aggregate spectra to particular nuclides at various decay times suggest deficiencies.

We have created several energy files and compared these with aggregate beta and gamma heating and their aggregate spectra from several fissioning systems. Here we include only a sufficient number of comparisons to demonstrate the problem as it still existed in September 1989 and the resolution as of November 1989.

Figures V-9 and V-10 show the YAYOI measurements compared with calculations using a file consisting of ENDF/B-V chain data, a preliminary version VI yield set, and an updated energy library. This energy library includes the spectral data for 510 nuclides in a preliminary INEL evaluation. However, INEL identified approximately 68 of these that should have average energies replaced by model values. Another 44 had no average energy in the initial INEL evaluation.

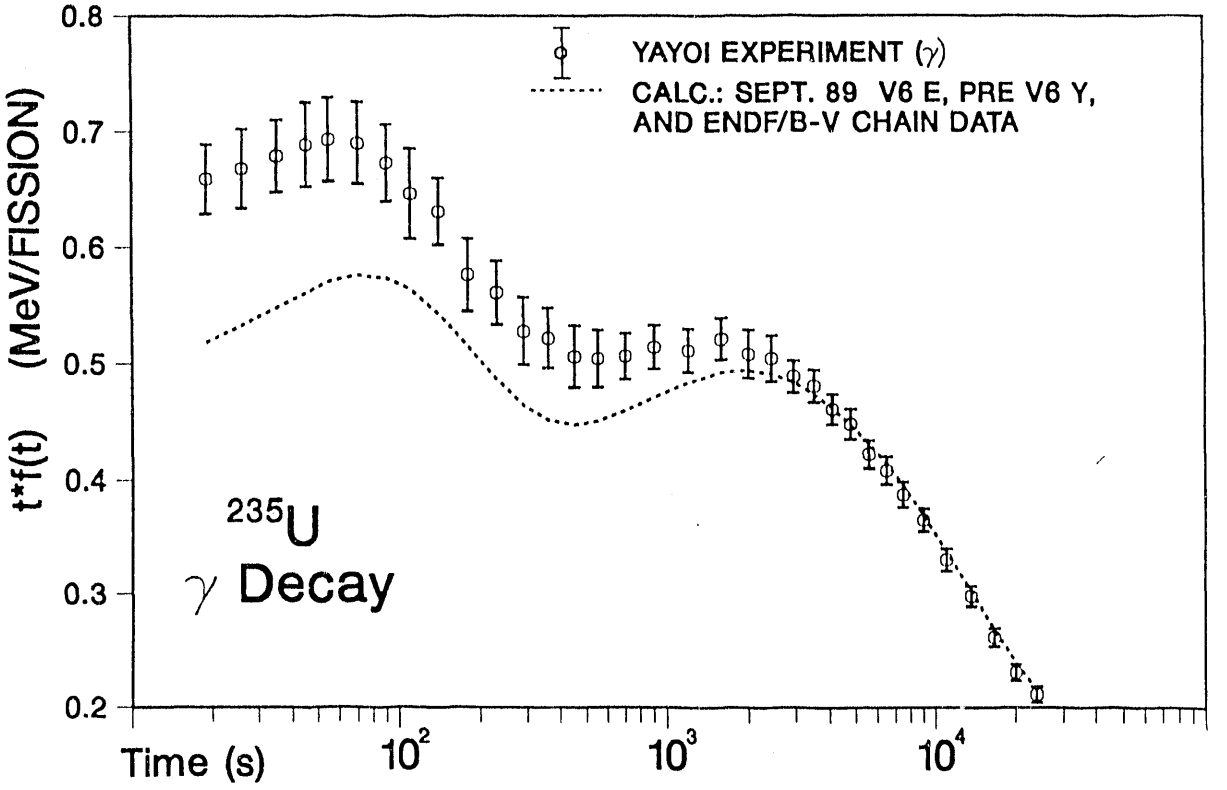

Fig. V-9. Gamma decay energy after ^{235}U fast fission (pulse).

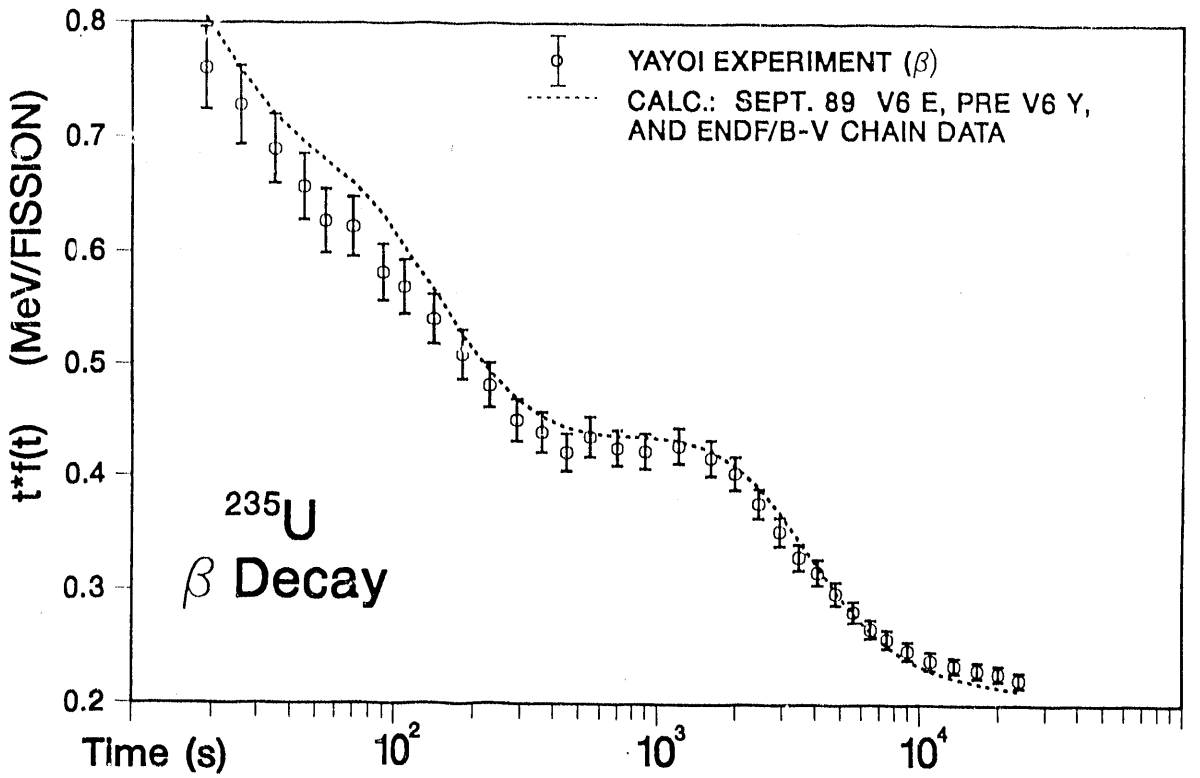

Fig. V-10. Beta decay energy after ^{235}U fast fission (pulse).

These and all unmeasured values were replaced with Gross Theory calculations of spectra and, usually, with JENDL2 energy averages. The Gross Theory Model is described in Nucl Sci. Eng. 93, 193 (1986). We modified the bin structure and the important Q_{00} parameters.

This new energy file has proven to be a considerable improvement over, *e.g.*, ENDF/B-V, but the gamma energy is still deficient at short decay times, as Fig. V-9 illustrates.

We created several additional files using various criteria for incorporating model values. From Fig. V-9 it was apparent that measured data were going to require additional supplementation with models.

The current energy library (November 1989) appears to be exceptional in the aggregate comparisons, as is shown in Figs. V-11 through V-13. The library consists of

a. Some new values from INEL for the original set of 510.
b. Approximately 115 of these are replaced with JENDL2 or other averages.
c. Spectra from Gross Theory are used to supplement measured spectra when measurements produced averages that differ by > 5% from the chosen file values.
d. Average energies and spectra using the Gross Theory code are included for all unmeasured data (> 300 nuclides).
e. Delayed neutron spectra for 271 nuclides are also included (and discussed below).

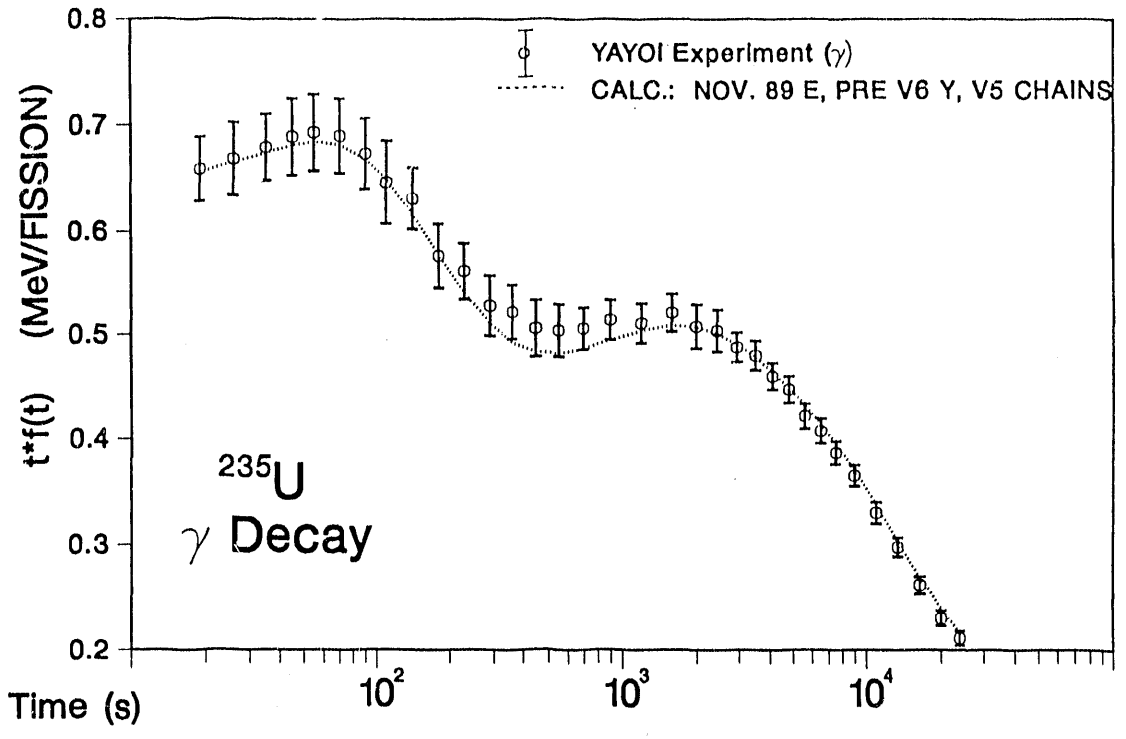

Fig. V-11. Gamma decay energy after ^{235}U fast fission (pulse).

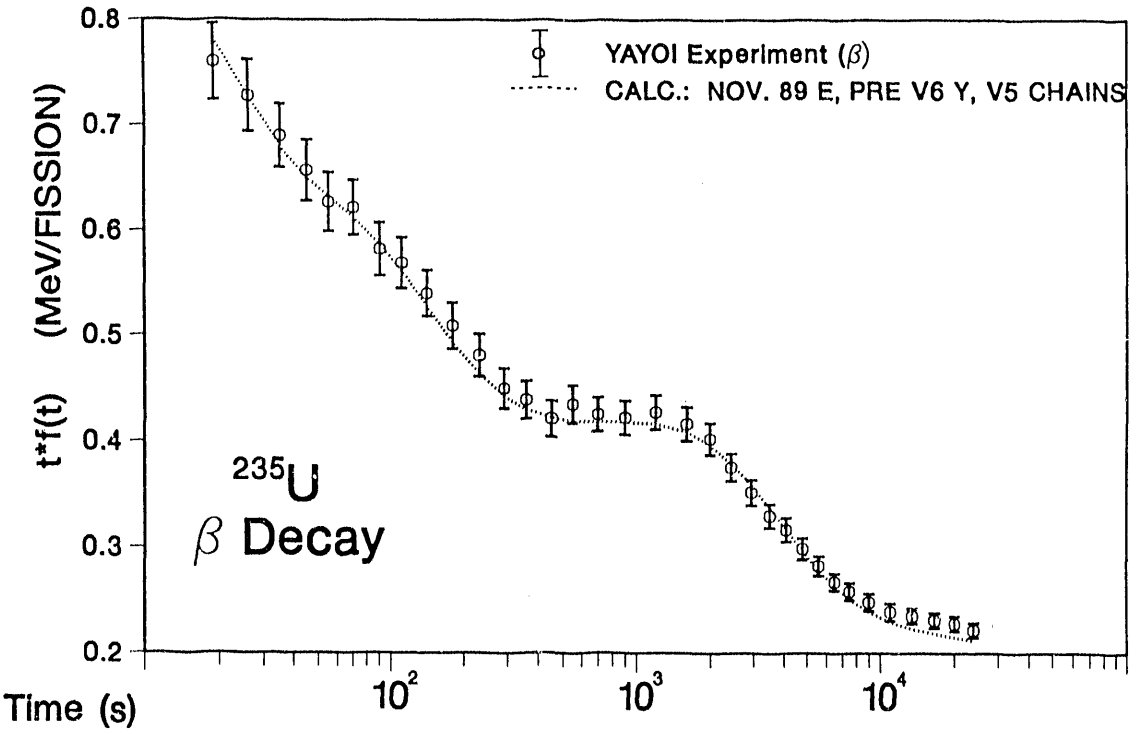

Fig. V-12. Beta decay energy after ^{235}U fast fission (pulse).

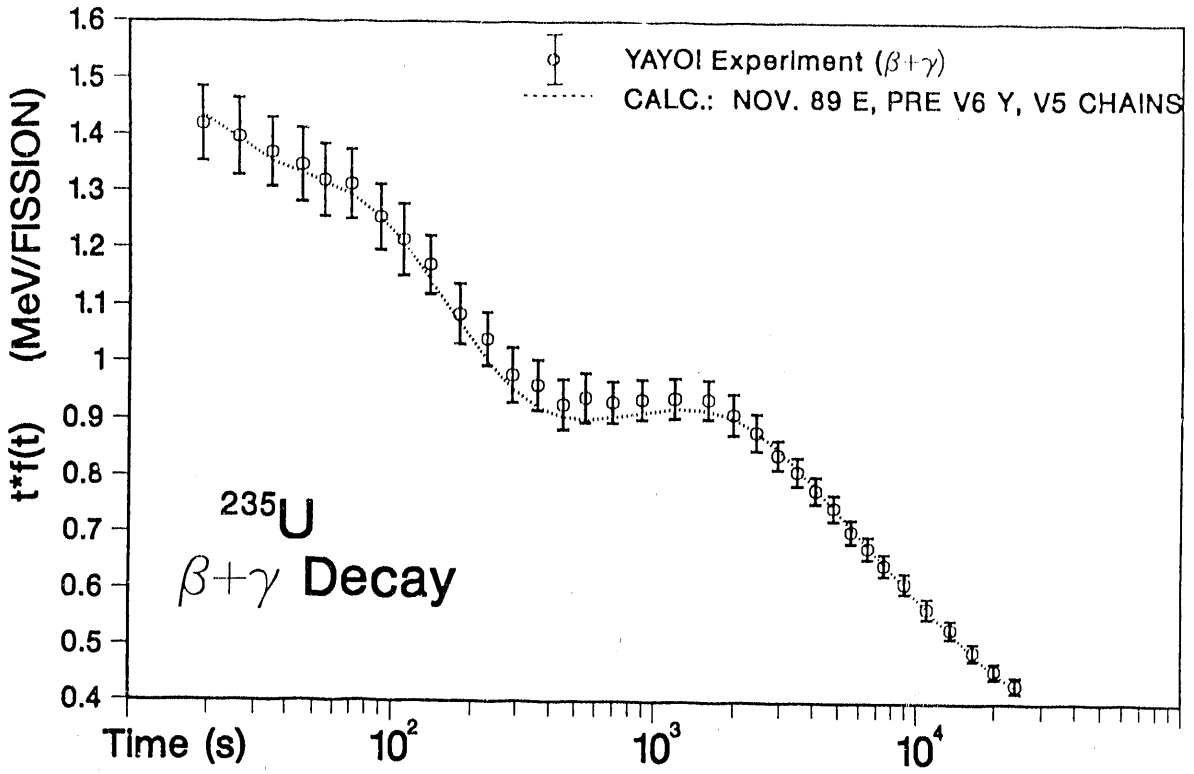

Fig. V-13. Total decay energy after ^{235}U fast fission (pulse).

We have not altered any measured transition data. These are discrete values in the files. All model supplements are given as continuous spectra, including delayed-neutron spectra. Any nuclide having a model value will also be identified in the final file along with any change made in FD or FC (normalizations).

This brief discussion is misleading as to the amount of effort expended into data improvement. We were equally concerned with deficient spectra shapes, not just their average energies. Part of the process toward enhancing the data required comparisons with several hundred measured (aggregate) spectra. Figure V-14 shows a comparison for ^{235}U between an ORNL measurement, ENDF/B-V, and the current spectral library. The improvement is evident at all energies and is several orders of magnitude improved at high energies. Figure V-15 shows the same information over a shorter energy range.

Half-lives, branchings, Q-values, spin, parity, and isomeric identifications have not yet been updated for about 350 fission products. When this is done it could alter the remarkable comparisons seen in Figs. V-11 through V-15.

It should be emphasized that some energy supplements could be (and probably are) incorrect for an individual nuclide. This is normal for model values. The aggregate is greatly improved over version V, and we have retained the measurements in the files in a recoverable way for users.

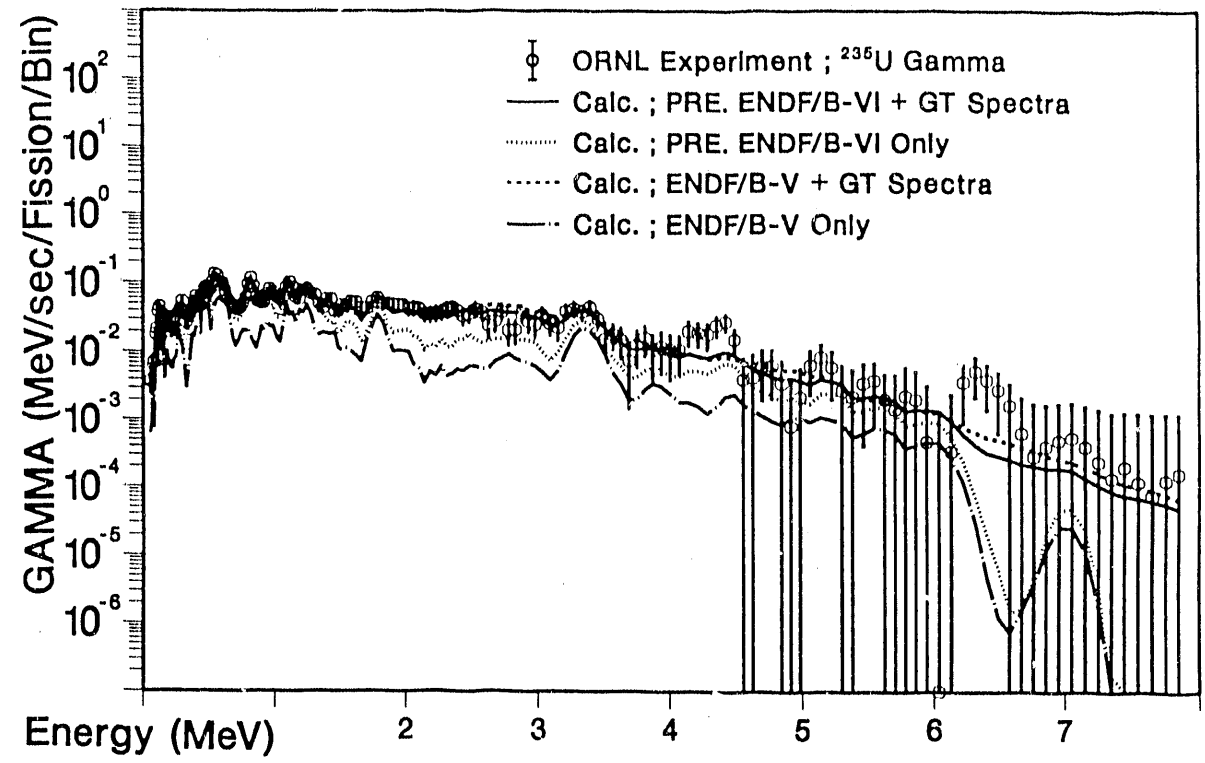

Fig. V-14. Gamma spectrum after ^{235}U thermal neutron fission ($T_{cool.}$ = 2.7 s).

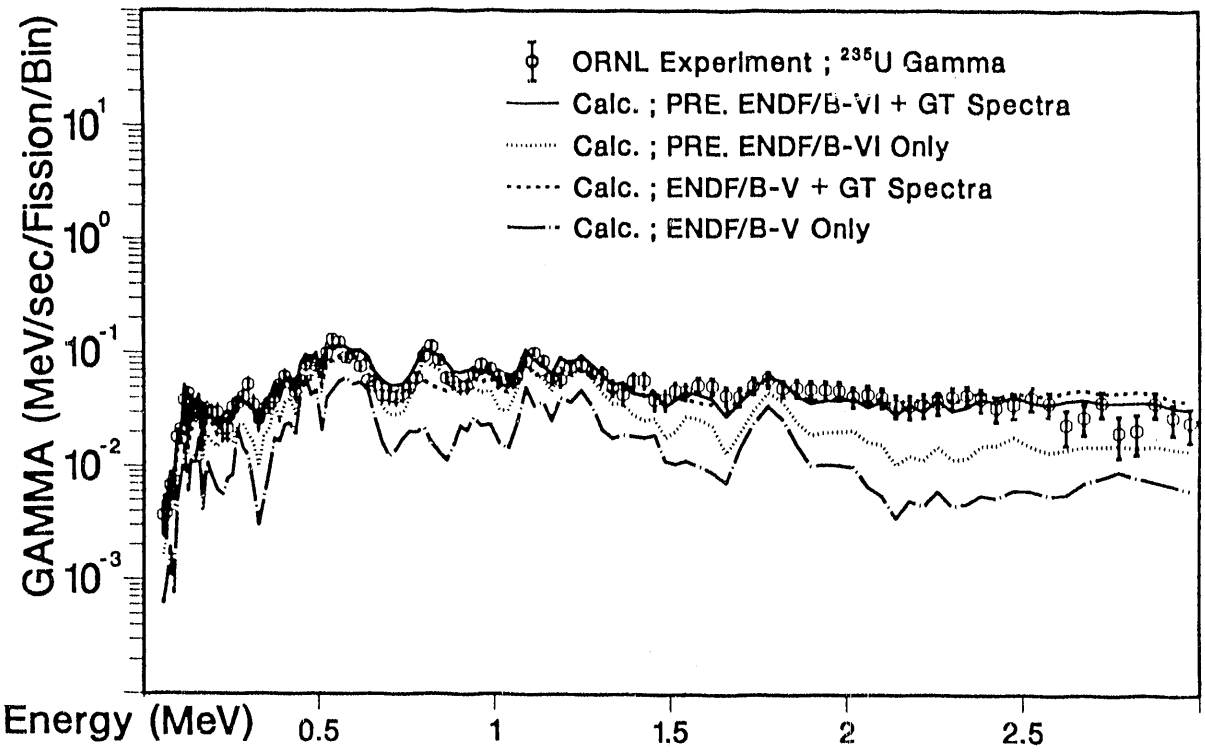

Fig. V-15. Gamma spectrum after ^{235}U thermal neutron fission ($T_{cool.}$ = 2.7 s).

We started these files using the Evaluated Nuclear Structure Data File (ENSDF) and maintained as close an overlap as possible between ENSDF and ENDF/B-VI. The overlap had to be consistent with some directly measured energies and ultimately with comparisons of aggregate measurements.

Spectra data measured at Studsvik, Sweden, for ~114 nuclides have been received recently. Time permitting, we will substitute some of these data where we have used nuclear models previously.

2. Delayed Neutrons (References 36-46) In addition to individual precursor data [emission probabilities (Pn) and neutron spectra] in the decay files, the ENDF system requires $\bar{\nu}_d$ (E), and its time-dependence and spectra using a few time groups. These data have been greatly extended, tested, and recently (June 1989) compared with new measurements of pulse spectra.

Temporal group data can be obtained from aggregate measurements, as has been the practice in earlier versions of ENDF, or from summation calculations using precursor data [emission probabilities (Pn), spectra, halflives, branchings, and fission product yields]. Until recently the precursor data were not sufficiently complete for the latter approach. Measurements were limited to a few fissionable nuclides and even more limited in the range of measured aggregate spectra.

We now have a complete set of data for 271 precursors. It includes all known Pn and spectral measurements, supplemented with model calculations, in 10-keV bins from 0-~10 MeV. All of these data will be included in the decay files.

For 28 fissioning nuclides we have calculated the aggregate time-dependence and approximated this with six temporal groups (abundances, halflives and consistent group spectra). The group spectra are in 10-keV bins extending from 0-3 MeV. [ENDF/B-V used 28 bins from ~ 79 keV to 1.2 MeV. Such data were available for only six fissioning nuclides; it was also assumed that the group spectra for time Group 6 (and usually Group 5) was the same as Group 4]. This precursor work has extended over several years and is well documented in the noted references.

Having a fiducial data base permits an answer to some existing questions (discussed in the earlier references):

(a) Six-groups are an adequate representation; nine would be better, but unnecessary for most applications; more than nine-groups is not likely to be needed in applications.

(b) There is only a very weak spectral dependence on the energy of the incident fission neutron; this is fortunate because ENDF/B formats permit only such dependence on $\bar{\nu}_d$ (the lack of dependence is confirmed by the recent experiments).

We do not expect the new data to produce significant changes in most types of reactor calculations, but we have already used the data in other problems where its difference from ENDF/B-V appears very significant. The difference in energy range has been confirmed by recent, unpublished Los Alamos measurements. Figure V-16 compares group spectra for ^{235}U fission over 0-1 MeV between ENDF/B-V and -VI.

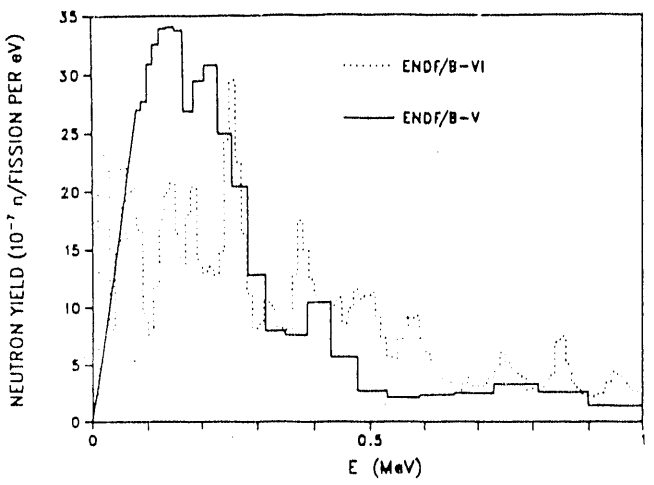

Fig. 16(a). Group 1 normalized ν_d spectra ^{235}U.

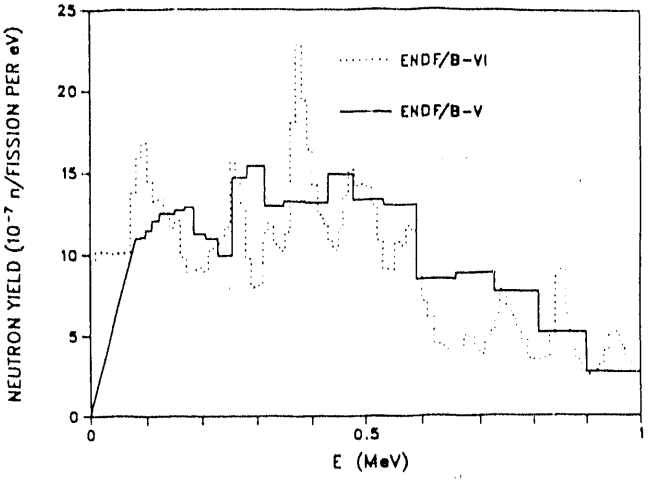

Fig. 16(b). Group 2 normalized ν_d spectra ^{235}U .

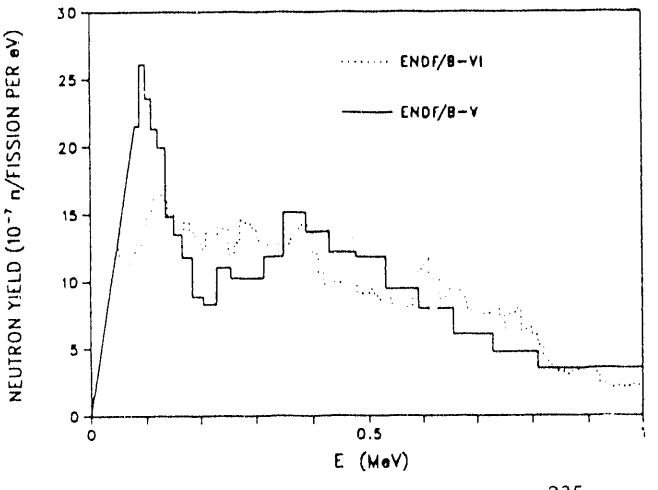

Fig. 16(c). Group 3 normalized ν_d spectra ^{235}U.

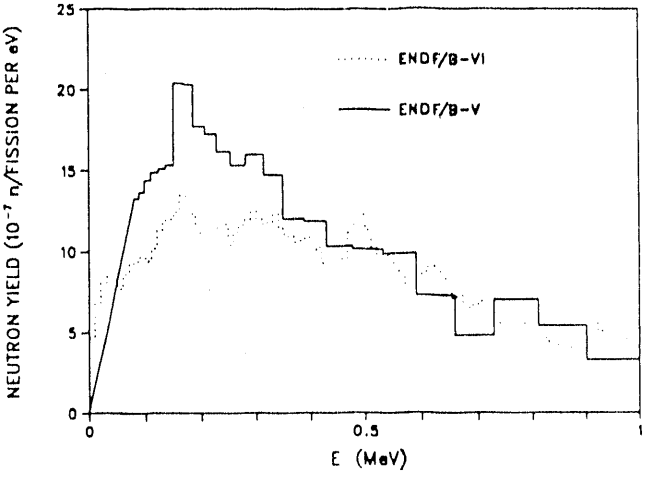

Fig. 16(d). Group 4 normalized ν_d spectra ^{235}U .

Fig. V-16(a-f) Comparison of ENDF/B-V on ENDF/B-VI group spectra.

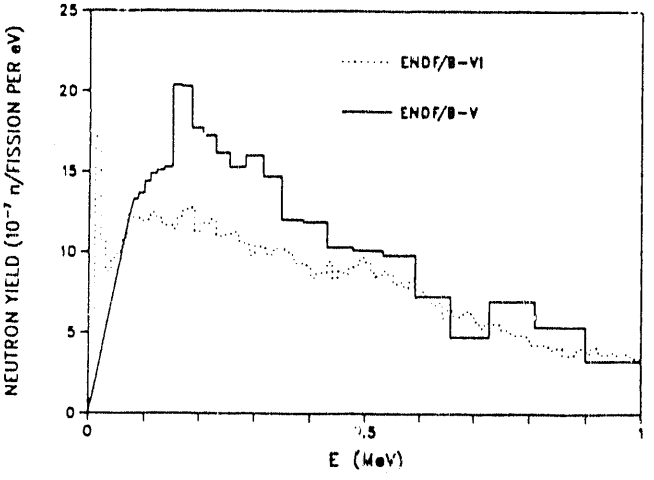

Fig. 16(e). Group 5 normalized ν_d spectra ^{235}U.

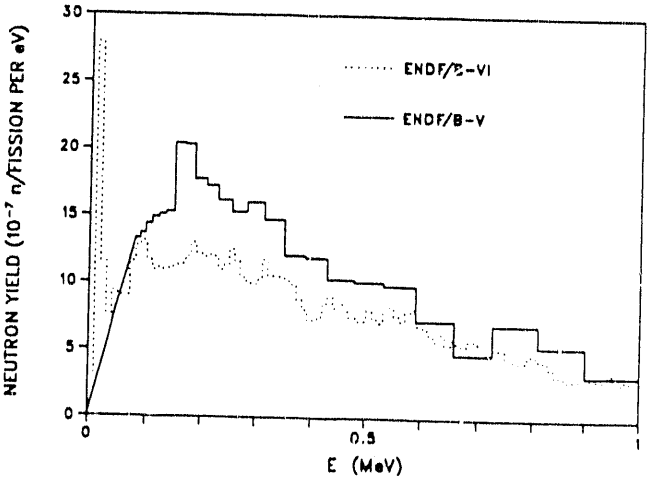

Fig. 16(f). Group 6 normalized ν_d spectra ^{235}U.

Fig. V-16 (a-f). Comparison of ENDF/B-V on ENDF/B-VI group spectra (cont.).

The University of Lowell has recently completed time-of-flight spectra measurements for delayed neutrons from ^{235}U, ^{239}Pu, and ^{238}U fission pulses. Comparisons with their ^{235}U data and the new group data in ENDF/B-VI have been made. Their ^{239}Pu and ^{238}U measurements were made available in June 1989. Comparisons for all three fuels are shown in Fig. V-17 at three decay intervals. These are total spectra (ENDF/B-VI group values are summed) following decay from a fission pulse. Data generally agree within measured uncertainties. The largest uncertainty in measurements are the ^{239}Pu values (100-50% at small energies). We are currently trying to understand the differences that do exist but the agreement is generally very good, particularly for such pulse spectra.

The delayed neutron temporal group data will not be entirely consistent with yield and decay data files. As noted below, the yield files are not yet complete; however, an evaluation of yields subsequent to ENDF/B-V was used. Some Pn values based on recent measurements at Studsvik, Sweden, may also change the values in the current decay files.

3. Yields (References 47-50) Table V-II shows the yield sets to be incorporated into ENDF/B-VI. A preliminary set of data for 50 sets was completed in March 1989 and the additional 10 sets listed at the bottom of this table were completed in August. [The latter evaluation used funds from the Japan Atomic Energy Research Institute (JAERI) to Oak Ridge National Laboratory and then to Los Alamos in the Japan/US actinides program.]

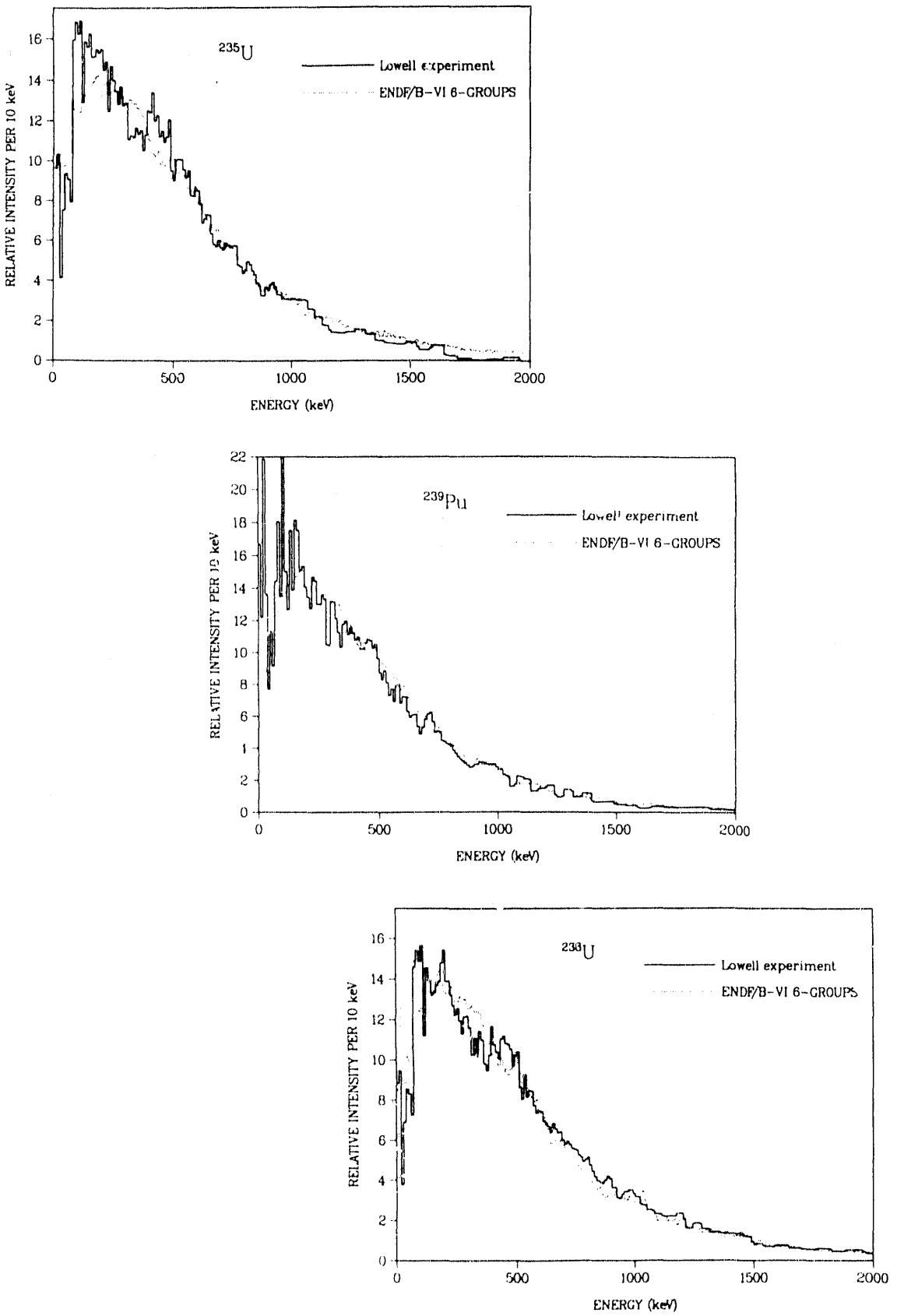

Fig. V-17. Pulse spectra comparisons with Lowell measurements at 0.17-0.37 seconds.

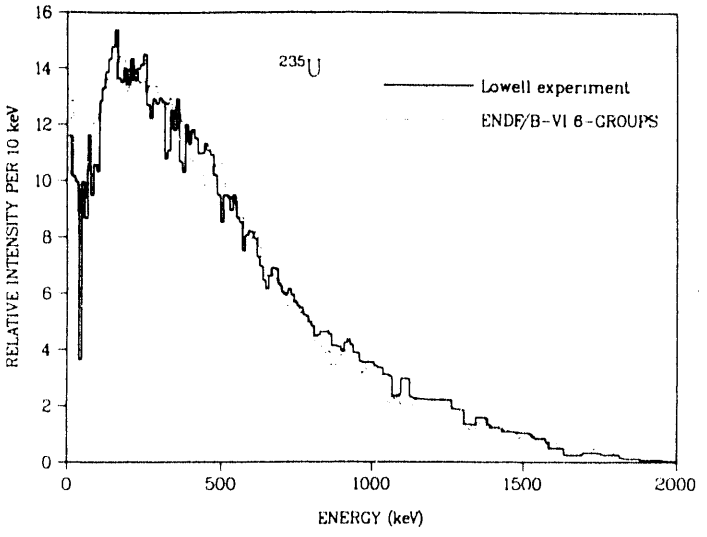

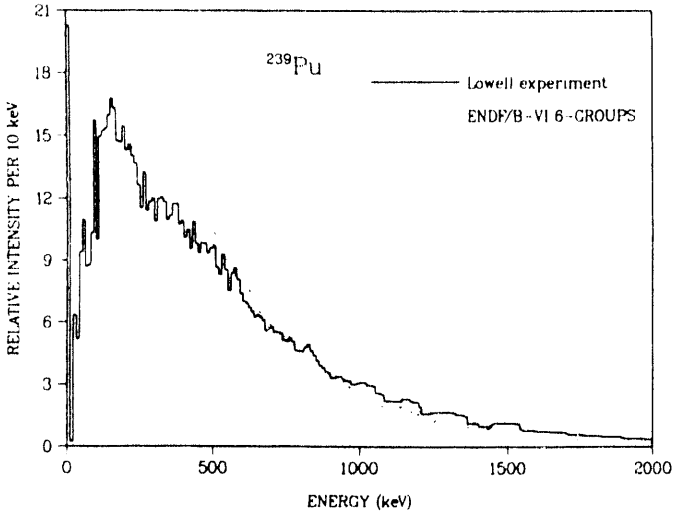

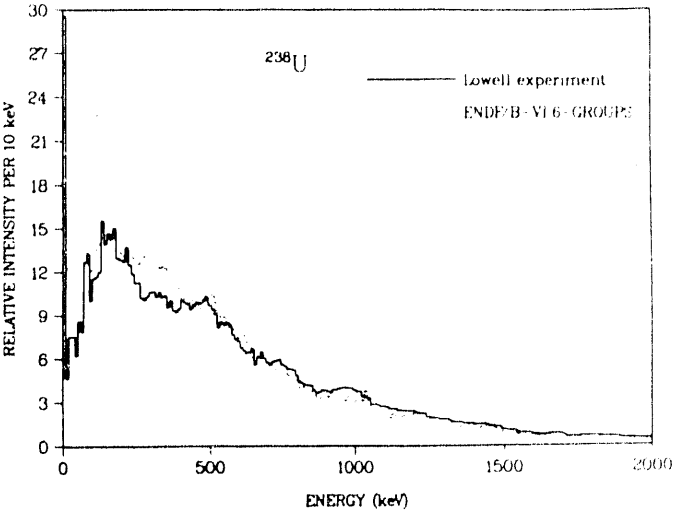

Fig. V-17 (cont.). Pulse spectra comparisons with Lowell measurements at 0.17-1.25 seconds.

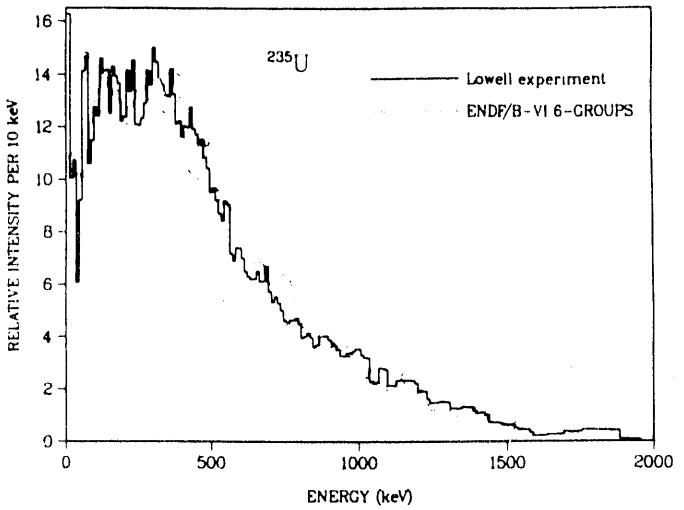

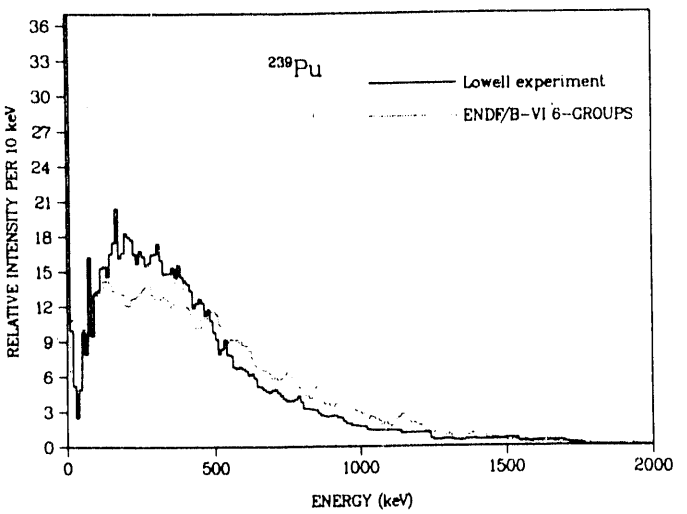

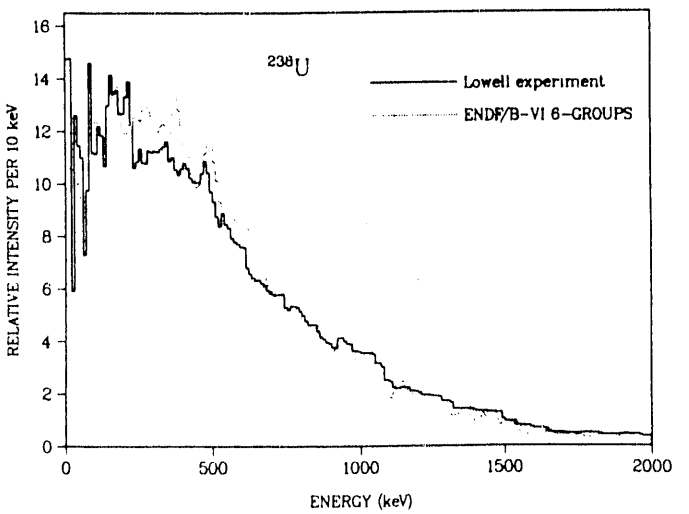

Fig. V-17 (cont.). Pulse spectra comparisons with Lowell measurements at 4.7-10.2 seconds.

TABLE V-II

EVALUATED YIELD SETS FOR ENDF/B (SET JM)

Fissionable Nuclide	Fissionable Nuclide
^{227}Th (T)	^{242}Pu (F)
^{229}Th (T)	^{241}Am (T, F, H)
^{232}Th (F, H)	^{42m}Am (T)
^{231}Pa (F)	^{243}Am (F)
^{232}U (T)	^{242}Cm (F)
^{233}U (T, F, H)	^{244}Cm (S)
^{234}U (F, H)	^{245}Cm (T)
^{235}U (T, F, H)	^{248}Cm (S)
^{236}U (F, H)	^{249}Cf (T)
^{237}U (F)	^{250}Cf (S)
^{238}U (S, F, H)	^{251}Cf (T)
^{237}Np (F, H)	^{252}Cf (S)
^{238}Np (F)	^{253}Es (S)
^{238}Pu (F)	^{254}Es (T)
^{239}Pu (T, F, H)	^{254}Fm (S)
^{240}Pu (F, H)	^{255}Fm (T)
^{241}Pu (T, F)	^{256}Fm (S)

S = Spontaneous, T = Thermal, F = Pooled Fast, H = 14 MeV.

[Ten new sets completed: ^{243}Cm (T,F), ^{246}Cm (S,F), ^{244}Cm (F), ^{248}Cm (F), ^{242}Pu (T,H), ^{237}Np (T), ^{240}Pu (T). These may not be included in ENDF/B-VI.]

All data should be reevaluated using new distribution parameters as well as newly measured data; these were discussed at a recent (September 1989) IAEA CRP (Coordinated Research Program) meeting. The primary documentation for the yields will be a Los Alamos report, which will also include the number ENDF-349. A draft form of this report has been completed but data included are still the existing evaluations of March and August.

For the *primary* fissioning nuclides, it is unlikely that the use of new yield data and distribution parameters will have any significant effect on aggregate six-group delayed neutron

abundances, halflives, and normalized spectra. Any such change will have to be added in a future mod to ENDF/B-VI.

The amount of fission yield data for ENDF/B-VI is three times that of ENDF/B-V and six times that of ENDF/B-IV. There are sets of independent (direct) yields for each of the 60 cases in Table V-II (before the emission of delayed neutrons) and cumulative yields (after delayed neutron emission). Each set contains yields for 1150 to 1200 products along with one sigma uncertainties. Each set depends strongly on phenomenological models, especially for some of the sparsely measured higher mass fissioning nuclides.

The final evaluations of yields for ENDF/B-VI will include data published through February 1990. We also hope to modify some of the distribution parameters.

H. References-Section V

1. D. G. Madland, "Theory of Neutron Emission in Fission," Proc. Conf. on 50 Years with Nuclear Fission, Washington DC/Gaithersburg, Maryland, 1989 (American Nuclear Society, La Grange Park, Ill., 1989), Vol. 1, p. 429.

2. D. G. Madland and J. R. Nix, "New Calculation of Prompt Fission Neutron Spectra and Average Prompt Neutron Multiplicities," Nucl. Sci. Eng. 81, 213 (1982).

3. R. L. Walsh, "Spin-Dependent Calculation of Fission Neutron Spectra and Fission Spectrum Integrals for Six Fissioning Systems," Nucl. Sci. Eng. 102, 119 (1989).

4. R. L. Walsh, G. Chircu, and D. G. Madland, "Fission Neutron Spectra for ^{240}Pu, ^{238}Pu, and ^{242}Pu," Proc. Conf. on 50 Years with Nuclear Fission, Washington, DC/Gaithersburg, Maryland, 1989 (American Nuclear Society, La Grange Park, Ill., 1989), Vol. 1, p. 274.

5. P. G. Young and E. D. Arthur, "GNASH- A Preequilibrium Statistical Nuclear Model Code," Los Alamos Scientific Laboratory report LA-6947 (1977).

6. E. D. Arthur, "The GNASH Preequilibrium-Statistical Model Code," Los Alamos National Laboratory document LA-UR-88-382 (1988).

7. D. G. Madland, "Scission Point Fission Model for Calculating Particle and Gamma Spectra and Multiplicities Associated with Medium Energy Fission," Los Alamos National Laboratory internal report, T-2-IR-88-1, 1988.

8. E. D. Arthur, M. Bozoian, D. G. Madland, and P. G. Young, "Medium-Energy Fission Model Calculations for the 14.5 MeV Neutron-Induced Fission of ^{238}U," Bull Am. Phys. Soc. 34, 1836 (1989).

9. M. Bozoian, D. G. Madland, E. D. Arthur, and P. G. Young, "Comparison of Experimental and Calculated Neutron Energy Spectra and Multiplicities from Spontaneous Fission of ^{252}Cf," Bull. Am. Phys. Soc. 34, 1836 (1989).

10. H. Buttner, A. Lindner, and H. Meldner, "Two-Particle Emission in Nuclear Reactions," Nucl. Phys. A63, 615 (1965).

11. C. Kalbach, Zeits. für Physik A283, 401 (1977).

12. W. P. Poenitz and T. Tamura, Proc. Conf. Nucl. Data for Sci. and Tech., Antwerp, Belgium, Sept. 6-10, 1982, p. 465, D. Reidel, Dordrecht (1983).

13. D. M. Drake, E. D. Arthur, and M. G. Silbert, "Cross Sections for Gamma-Ray Production by 14-MeV Neutrons," Nucl. Sci. Eng. 65, 49 (1978).

14. E. D. Arthur and P. G. Young, "Calculation of Medium-Energy Fission Cross Section," Proc. Conf. on 50 Years with Nuclear Fission, Washington, DC/Gaithersburg, Maryland, 1989 (American Nuclear Society, La Grange Park, Ill., 1989), Vol. 2, p. 931.

15. N. Bohr and J. A. Wheeler, "The Mechanisms of Nuclear Fission," Phys. Rev. 56, 426 (1939).

16. A. Gavron, A. Gayer, J. Boissevain, H. C. Brit, T. C. Awes *et al.*, "Neutron Emission in the Fissioning ^{158}Er Composite System," Phys. Rev. C35, 579 (1987).

17. P. Grange, S. Hassani, H. A. Weidenmüller, A. Gavron, J. R. Nix, and A. J. Sierk, "Effect of Nuclear Dissipation on Neutron Emission Prior to Fission, Phys. Rev. C34, 209 (1986); J. R. Nix, A. J. Sierk, H. Hofmann, and F. Scheuter, "Stationary Fokker-Planck Equation Applied to Fission Dynamics," Nucl. Phys. A424, 239 (1984).

18. D. G. Madland, personal communication, Los Alamos National Laboratory, 1988 and Applied Nuclear Science Group informal report T-2-IR-8-2 (1988).

19. H. A. Kramers, "Brownian Motion in a Field of Force and the Diffusion Model of Chemical Reactions," Physica 7, 284 (1940).

20. S. Hasani and P. Grange, "Neutron Multiplicities in Fission Viewed as a Diffusion Process," Phys. Lett. 137B, 281 (1984).

21. Yi-Zhong and Xi-Zhen Wu, "Recent Progress in Fission Theory Based on Diffusion Models," Nuclear Data for Science and Technology, Mito, Japan, p. 667 (1988).

22. P. G. Young, "The Status of Nuclear Evaluations for Version VI of ENDF/B," Proc. Reactor Physics Conf., Jackson Hole, Wyoming, September 12-21, 1988.

23. R. Roussin, C. Dunford, R. McKnight, P. G. Young, "The Status of ENDF/B-VI," Proc. 17th Int. Conf. Reactor Shielding, Bournemouth, England, September 12-16, 1988.

24. R. Peelle, H. Condé, "Neutron Standard Data," Proc. Int. Conf. Nuclear Data for Sci. Technology, Mito, Japan, May 30-June 3, 1988, p. 1005.

25. R. McKnight, Comp., "Review of the Contents and Performance of ENDF/B-VI-I and -II," Trans. Am. Nucl. Soc. 1989 Winter Mtg., San Francisco, Calif., November 26-30, 1989, Vol. 60, pp. 609-621.

26. T. R. England, M. C. Brady, D. C. George, R. J. LaBauve, and W. B. Wilson, "DKPOWR87: A Code Using Fission Pulse Functions to Describe the Aggregate Decay Properties of LWR Fuels," Proc. Specialists' Mtg. on Data for Decay Heat Predictions, Studsvik, Sweden, September 7-10, 1987, NEACRP-302-'L', NEANDC-245 'U' (Los Alamos document LA-UR 87-2955).

27. T. R. England, R. J. LaBauve, and W. B. Wilson, "Evaluation of the Neutron Absorption Corrections G(t) of the ANS/ANSI 5.1 Decay Power Standard," Proc. of the Specialists' Mtg. on Data for Decay Heat Predictions, Studsvik, Sweden, September 7-10, 1987, NEACRP-302-'L', NEANDC-245 'U' (Los Alamos document LA-UR -87-2956).

28. T. R. England and R. E. Schenter, "The ANS Standard Curves of 1979 and Other Standards in the Light of New Experimental Information," Proc. Specialists' Mtg. on Data for Decay Heat Predictions, NEACRP-302-'L', NEANDC-245 'U" (Los Alamos document LA-UR-87-2957).

29. T. R. England, E. D. Arthur, M. C. Brady, and R. J. LaBauve, "Background Radiation from Fission Pulses," Los Alamos National Laboratory report LA-11151-MS (September 1987).

30. W. B. Wilson, T. R. England, R. J. LaBauve, and J. A. Mitchell, "Calculated Radionuclide Inventories of High-Exposure Fuels," Nuclear Safety, Vol. 29, No. 2 (April-June 1988).

31. T. R. England, F. M. Mann, C. W. Reich, and R. E. Schenter, "ENDF/B-VI Radioactive Decay and Yield Libraries," invited paper for ANS Mtg. November 26-30, 1989 (Los Alamos document LA-UR-89-2174).

32. J. Katakura and T. R. England, "Augmentation of ENDF/B Fission Product Gamma-Ray Spectra by Calculated Spectra," (draft form, to be published as Los Alamos National Laboratory report).

33. F. M. Mann, "Status of Dosimetry and Activation Data," Proc. Int. Conf. Nuclear Data for Science and Technology, Mito, Japan, May 30-June 3, 1988, p. 1013.

34. "Decay Data of the Transactinium Nuclides," IAEA Technical Report Series No. 261, International Atomic Energy Agency, Vienna (1986).

35. C. W. Reich, "Review of Nuclear Data of Relevance for the Decay Heat Problem," Proc. Specialists' Mtg. Data for Decay Heat Predictions, Studsvik, Sweden, September 7-10, 1987, NEANDC-245 'U'(1987).

36. S. A. Cox, "Delayed Neutron Data-Review and Evaluation," Argonne National Laboratory report ANL/NDM-5 (April 1974). (For ENDF/B-V, these data were updated, but unpublished, by R. E. Kaiser and S. G. Carpenter, Argonne National Laboratory-West.)

37. T. R. England, M. C. Brady, E. D. Arthur, R. J. LaBauve, and F. Mann, "Status of Evaluated Precursor and Aggregate Spectra," Proc. Specialists' Mtg on Delayed Neutrons at the University of Birmingham, Birmingham, England (September 15-19, 1986), proc. issued June 1988. (Los Alamos document LA-UR 86-2983).

38. M. C. Brady and T. R. England, "Few-Group Representation of Delayed Neutrons," Trans. Am. Nucl. Soc. 54, 342 (Mtg. Dallas, Texas, June 1987) (Los Alamos document LA-UR-87-48).

39. T. R. England, M. C. Brady, E. D. Arthur, R. J. LaBauve, and F. M. Mann, "Evaluated Delayed Neutron Precursor Data," Trans. Am. Nucl. Soc., 54, 350 (Mtg. Dallas, Texas, June 1987) (Los Alamos document LA-UR-87-49).

40. T. R. England and M. C. Brady, "Delayed Neutron Spectra by Decay Group for Fissioning Systems from ^{227}Th through ^{255}Fm," invited paper, 1988 Int. Reactor Physics Conf., Jackson Hole, Wyoming, September 18-21, 1988.

41. M. C. Brady and T. R. England, "Delayed Neutron Data and Group Parameters for 43 Fissioning Systems," Nucl. Sci. Eng. 103, pp. 129-149 (October 1989). See also M. C. Brady, "Evaluation and Application of Delayed Neutron Precursor Data," doctoral dissertation from Texas A &M (December 1988), Los Alamos National Laboratory thesis series report LA-11534 (April 1989).

42. T. R. England and M. C. Brady, "ENDF/B-VI Six-Group Delayed Neutron Data," invited paper ANS mtg., San Francisco, Calif., November 26-30, 1989 (Los Alamos document LA-UR-89-2207).

43. M. C. Brady and T. R. England, "Validation of Aggregate Delayed Neutron Spectra Calculated from Precursor Data," invited paper Int. Conf. on Physics of Reactors: Design and Computation, PHYSOR '90, Marseilles, France, April 23-26, 1990 (Los Alamos document LA-UR-90-480).

44. R. S. Tanczyn, Q. Sharfuddin, W. A. Schier, D. J. Pullen, M. H. Haghighi, L. Fisteag, G. P. Couchell, "Composite Delayed Neutron Energy Spectra for Thermal Fission of ^{235}U," Nucl. Sci. Eng. 94, 353 (1986).

45. G. Couchell, P. Bennett, M. Haghighi, E. Jacobs, D. Pullen, W. Schier, Q. Sharfuddin, R. Tanczyn, M. Villani, "Measurements of Delayed Neutron Energy Spectra of ^{235}U, ^{238}U, and ^{239}Pu," Proc. 1988 Int. Reactor Physics Conf., Jackson Hole, Wyoming, September 1988.

46. Proc. Specialists' Mtg. Delayed Neutrons, University of Birmingham, Birmingham, England, September 15-19, 1986, proc. issued June 1988 (see papers by England, *et al.*, Mann, Goulding, Reeder, Couchell, Weaver)

47. B. F. Rider and T. R. England, "Evaluation of Fission Product Yields for the USA National Nuclear Data Files," Proc. Specialists' Mtg. on Data for Decay Heat Predictions, Studsvik, Sweden, 7-10 September 1987 (NEACRP-302-'L', NEANDC-245 'U') (Los Alamos document LA-UR-87-2462).

48. T. R. England and J. Blachot, "Status of Fission Yield Data," invited paper, Int. Conf. on Nuclear Data for Sci. and Technology, Mito, Japan, May 30-June 3, 1988, S. Igarasi, Ed. (Los Alamos document LA-UR-88-1696).

49. T. R. England, B. F. Rider, and M. C. Brady, "Yield Data for the Japan/US Actinides Program," report in completion of a joint Oak Ridge/Los Alamos contract (Los Alamos document LA-UR-89-4023).

50. T. R. England and B. F. Rider, "Evaluation and Compilation of Fission Product Yields, 1989," (ENDF-349) draft form, to be published as Los Alamos report as the primary documentation for ENDF/B-VI.

VI. NUCLEAR STRUCTURE

A. Nuclear Level Density Sensitivity Studies (E. D. Arthur)

A series of calculations were performed to examine the sensitivity of calculated particle emission spectra to the level density of the following models: Gilbert-Cameron,[1] Back-Shifted Fermi Gas,[2] and the more modern phenemonological model of Ignatyuk.[3] These calculations also examined the issue of the sensitivity of new IAEA-sponsored experiments* that are under way to provide level density information through measurement of (p,n) and (n,n') emission spectra. The results of these calculations are summarized more fully in a recent review paper.[4]

Particle emission spectra offer a significant opportunity for determining level densities of the residual systems produced, as well as the validation of specific level density models. However, questions pertaining to data types, or more specifically, what reaction channels are most sensitive to level density effects must be addressed to achieve maximum benefits from such experimental data. To examine these questions, we made detailed calculations using the models listed above for the following systems: n +^{60}Ni, p + ^{59}Co, n + ^{93}Nb, and n + ^{181}Ta at low incident energies (<10-11 MeV) where preequilibrium contributions should be minimal. The parameter sets utilized in these models are described in Ref. 4. Figure VI-1 illustrates results for spectra occurring in n + ^{60}Ni reactions, while Figure VI-2 illustrates level densities occurring in residual systems populated in these respective reactions. In this example, both the neutron and proton emission spectra indicate a reduced sensitivity to level density changes. These channels dominate the Hauser-Feshbach calculation of both partial and total widths; thus, large level density changes produce relatively little impact on this ratio, and therefore on the calculated neutron and proton emission spectra. Alpha emission spectra indicate a sensitivity arising from the fact that it is a minor reaction process, so that the level density effects its decay width and therefore its competition with other channels. Discrete level data also show sensitivities to level densities for similar channel strength and competition arguments.

We also examined the differences in calculated results obtained using the Gilbert-Cameron model and that of Ignatyuk. The Ignatyuk model incorporates an energy-dependent Fermi gas parameter that has the effect of damping out shell effects at higher excitation energies. The Gilbert-Cameron model does not. We therefore chose to calculate reactions of n + ^{207}Pb up to incident energies of 50 MeV using these two models and compare the results. This is a rather extreme test because of the strong shell effects existing in the lead region, and because of the high excitation energies occurring over this calculational range.

* For example, the IAEA Coordinated Research Proposal (CRP) on Nuclear Level Densities was begun in 1988.

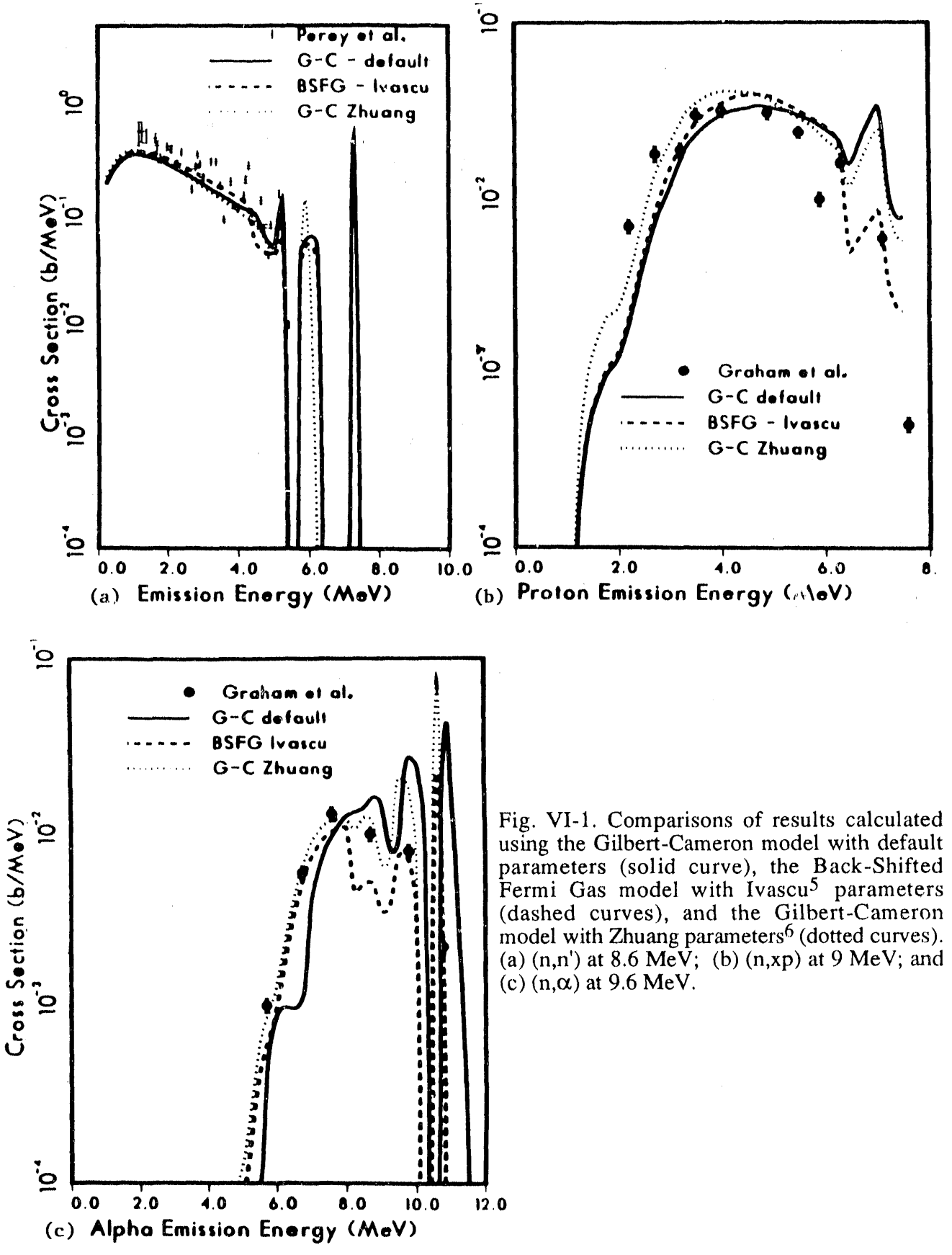

Fig. VI-1. Comparisons of results calculated using the Gilbert-Cameron model with default parameters (solid curve), the Back-Shifted Fermi Gas model with Ivascu[5] parameters (dashed curves), and the Gilbert-Cameron model with Zhuang parameters[6] (dotted curves). (a) (n,n') at 8.6 MeV; (b) (n,xp) at 9 MeV; and (c) (n,α) at 9.6 MeV.

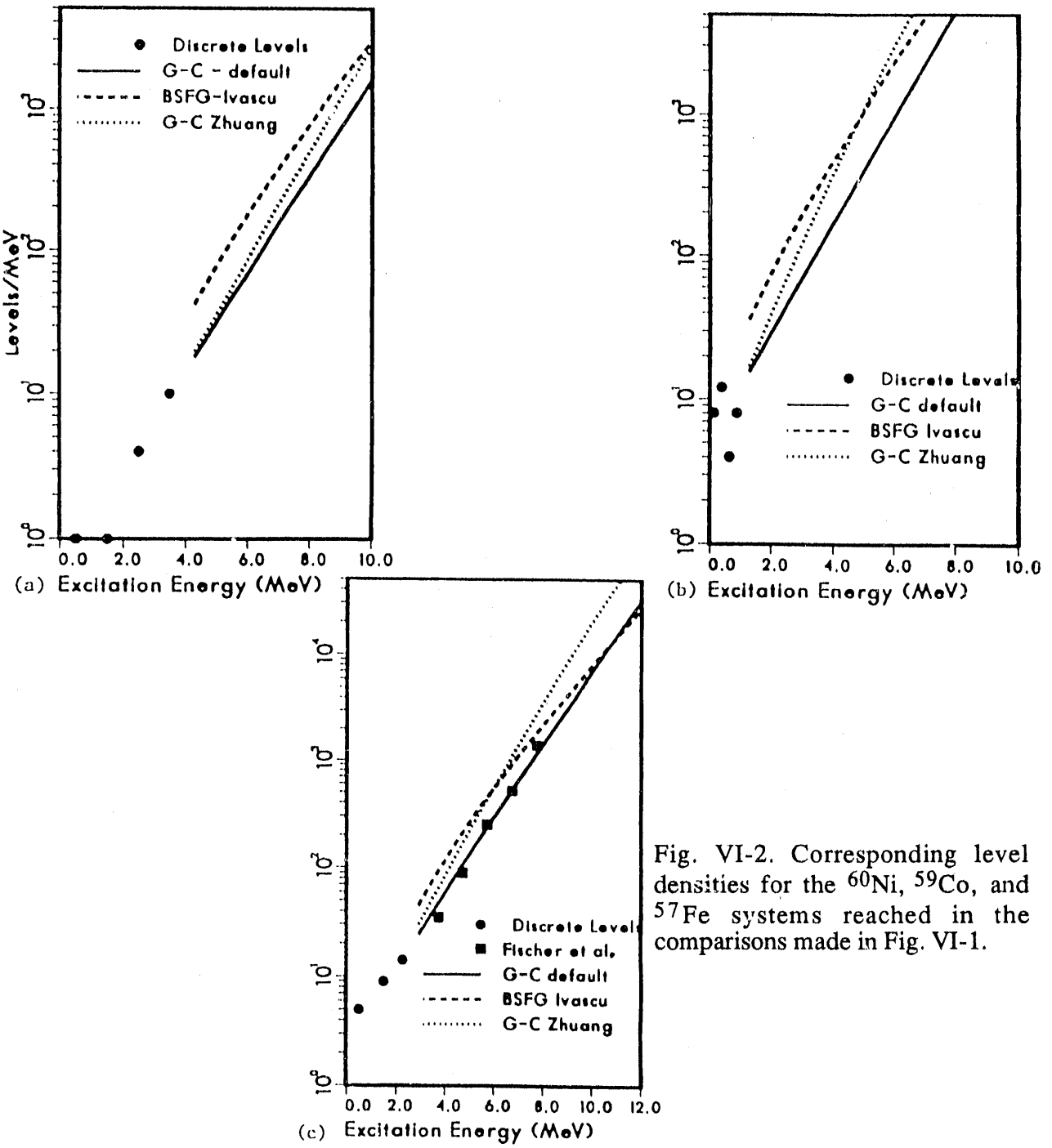

Fig. VI-2. Corresponding level densities for the ^{60}Ni, ^{59}Co, and ^{57}Fe systems reached in the comparisons made in Fig. VI-1.

Figure VI-3(a) illustrates the large differences existing between ^{208}Pb level densities predicted by these two models. Figure VI-3(b) shows the actual impact upon calculated neutron production and (n,xn) cross sections. The large level density that occurs at high excitation energies is mitigated in several ways. The first of these concerns the normalization of partial decay widths to the total width to produce Hauser Feshbach results. Here the dominant factor in the computed cross section is the relative shape of the level density rather than its magnitude. Secondly, preequilibrium emission can mask much of the high excitation energy behavior of these level

preequilibrium emission can mask much of the high excitation energy behavior of these level density models. Finally, as each multiple neutron emission channel opens, the greatest sensitivity occurs near excitation energies of 10-15 MeV in the preceding compound system that decays into the residual (n,xn) system of interest. In these excitation energy regimes, orders of magnitude differences do not exist between level densities of the two models, and this accounts for the magnitude similarities of the calculated cross sections.

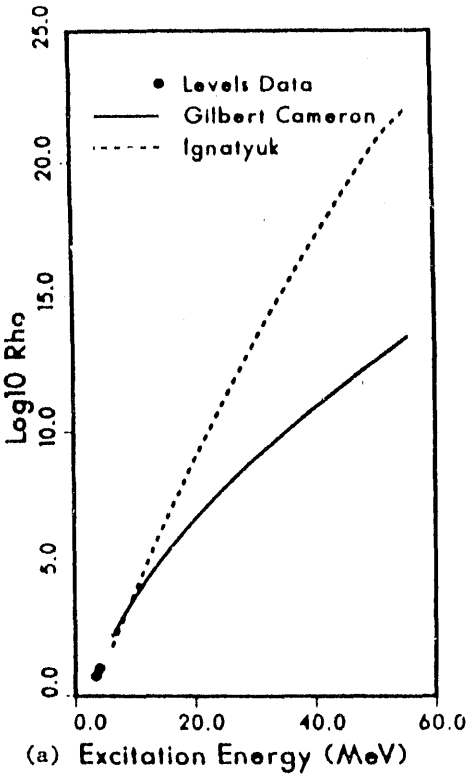

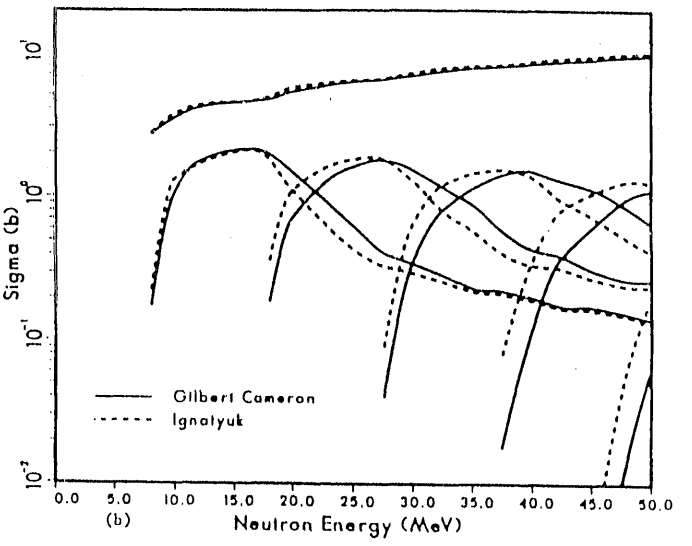

Fig. VI-3. Comparison of Ignatyuk (dashed line) and Gilbert-Cameron (solid line) formalism results. (a) Level densities for ^{208}Pb. (b) Comparison of cross sections for total neutron production, (n,xn) reactions (x = 2-6).

B. P-Wave Pion Scattering in the Los Alamos Soliton Model [M. Bolsterli and J. A. Parmentola (Harvard University)

In the Los Alamos soliton model (LASM) of the nucleon, the coupling of the pion field to the nucleon core is strong. Therefore, in order to compute phase shifts in the LASM, new techniques for dealing with the required portions of Hilbert space were developed. An expansion in the number of virtual mesons is clearly useless; instead, the expansion is in the number of *external* mesons, namely, those that are in modes orthogonal to the internal meson mode that is strongly coupled to the core. The internal mode is treated to very high order by methods appropriate to strong coupling. The one-external-meson approximation gives a result that is unitary. The results for the P33 and P11 phase shifts are shown in Fig. VI-4 for various values of the intrinsic core radius R.[7]

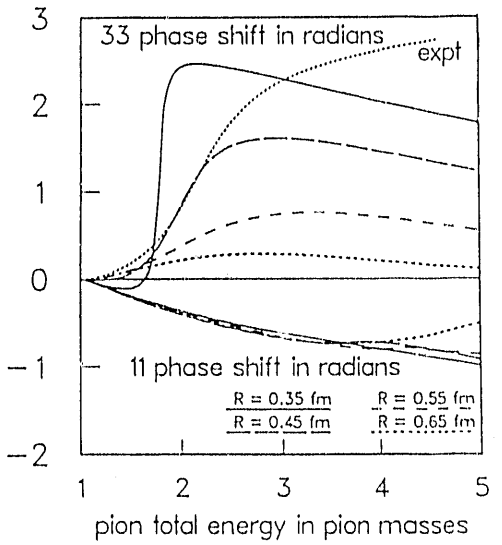

Fig. VI-4. P_{11} and P_{33} phase shifts in the LASM for various values of the intrinsic core radius R.

The P33 phase shift agrees reasonably well with the experimental data. As with many calculations, the P11 phase shift is not in agreement with the data. Within the LASM, the most interesting possibility for explaining the P11 phase shift involves excitation of the motion of the core from its 1s state to a 2s state.

C. Maximum Velocity in the Los Alamos Soliton Model and in Other Nonrelativistic Quantum Field Theories (M. Bolsterli)

In the course of a study of the nucleon electric form factor in the Los Alamos soliton model, it became clear that it is important to use momentum eigenstates, because the form factor involves an electromagnetic transition from one momentum eigenstate to another. As an example of a similar system in which the study of momentum eigenstates might be simpler, the polaron was selected for some detailed studies of momentum eigenstates. The method used was to generate the momentum eigenstates by translating localized states that consist of a core (electron) with some characteristic motion surrounded by mesons (phonons) in a coherent state. Use of these states led to the conclusion that there is a maximum velocity of the dressed core,[8] contrary to what one might expect for a nonrelativistic particle interacting with a Bose field.

The maximum velocity is the velocity V at which it becomes possible for the core to emit an on-shell meson. As the core velocity approaches V, it surrounds itself with more and more virtual mesons, and its energy and momentum grow without limit. An important question then is the value of the limiting velocity; if it is not very different from c, then the nonrelativistic model may give good results for form factors even at high momentum transfers. The maximum velocity for a core of mass M interacting with mesons of mass m turns out[9] to be $c(1 + r^2)(1 - r^2)^{-\frac{1}{2}}$, where r is the mass ratio $m/2M$. Because r is about 1/13 for the case of a nucleon core interacting with pion field, this result shows that a nonrelativistic model for the nucleon can have a maximum velocity

structure. The question arises as to whether this structure is due to nuclear structure or mainly a fluctuation phenomenon of the Porter-Thomas type.

Experimentally, it has now been shown for some of these nuclei that almost all of the discernible proton peaks have no corresponding levels that decay by γ emission. It has also been shown by others that the proton resonances observed in $^{147}_{66}Dy$ decay are correlated with those of the β-strength function and that the observed proton to γ-ray intensities are approximately a factor 20 larger than predicted by the statistical model.

To account for the strong dominance of the proton channel we are proposing a description based on the population of doorway states by β^+ decay or EC. These states are strongly hindered in their γ-ray deexcitation to more complex states, due to their simple structure. However, because of their simple structure, they couple strongly to the open-channel proton wave function. Calculations of β-strength functions in the QRPA approximation with Nilsson model wave functions support this interpretation. These calculations reproduce the average location of the β-strength and the mean spacing and number of strong GT transitions.

G. New Developments in the Calculation of β–Strength Functions [P. Möller and J. J. Randrup (Lawrence Berkeley Laboratories)]

We use a recently extended QRPA model for Gamow-Teller β-strength functions to calculate several quantities of physical interest. Relative to the initial model presented in 1984, the enhanced version may, in addition to the Nilsson model wave functions, now also use Woods-Saxon or folded-Yukawa wave functions as the starting point for determining the wave functions of the mother and daughter nuclei involved in the β decay. Pairing may be treated in either the BCS or the Lipkin-Nogami approximation. To account for the retardation of low-energy GT decay rates, we add (as in the earlier model) a simple residual interaction specific to GT decay, namely, $V_{GT} = :\beta^{1-} \cdot \beta^{2+}:$, to the Hamiltonian. This residual interaction is studied in the RPA approximation. As a final extension of the earlier model, we also allow the unpaired odd particle to be in an excited state. The enhanced model may be used to calculate β-decay properties for nuclei throughout the periodic system. Here we give some examples of results obtained. In Fig. VI-7 is illustrated calculated β-strength functions for a sequence of neutron-rich sodium isotopes.

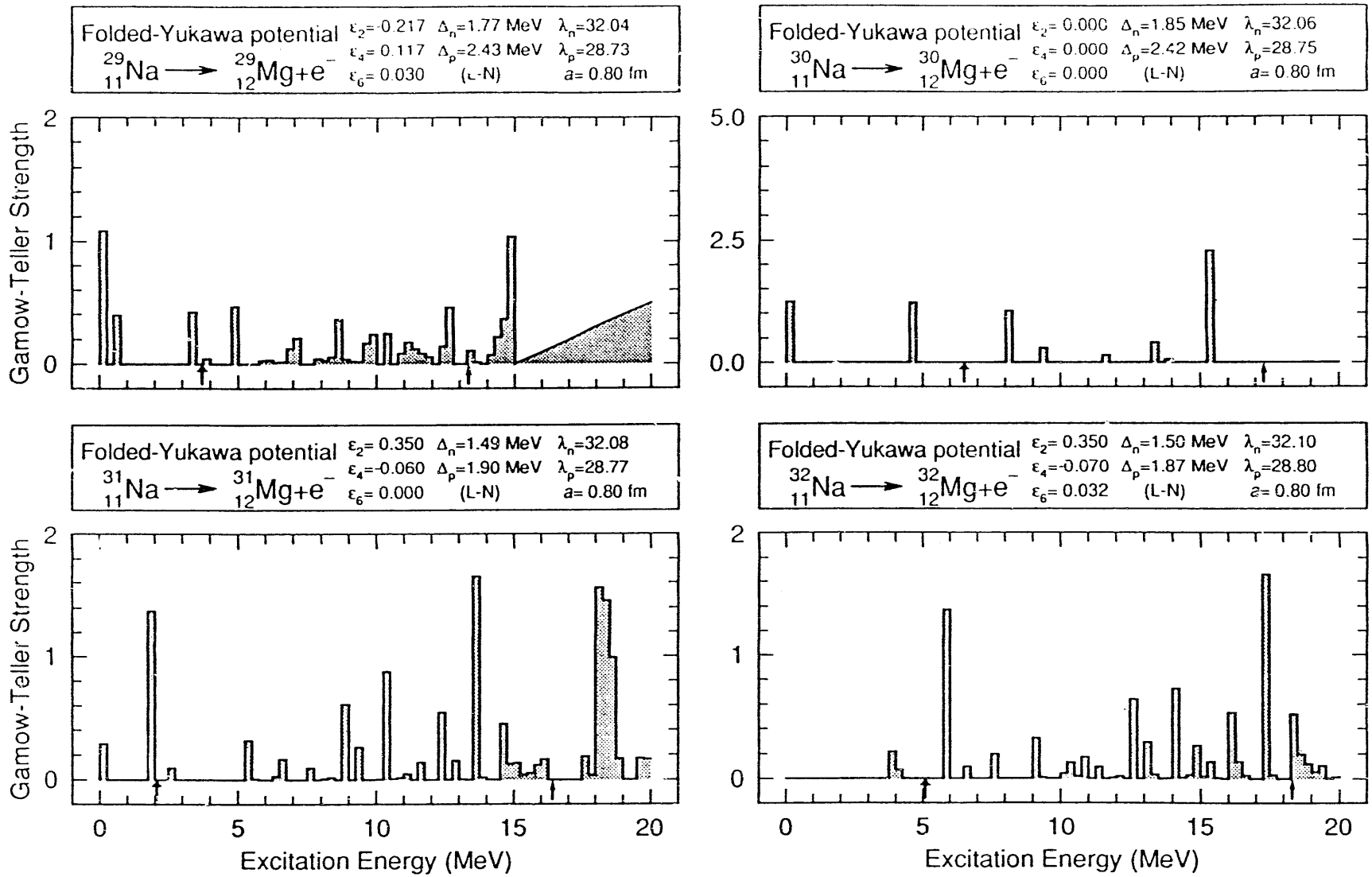

Fig. VI-7. Calculated β-strength functions for neutron-rich sodium isotopes.

Figure VI-8 shows β-decay half-lives and delayed neutron emission probabilities for these and other sodium isotopes. In Fig. VI-9 we compare β-strength functions for decay from ground-state and excited-state configurations for two nuclei. For Tc the excited state is only 0.1 MeV above the ground state. Still, the difference in half-lives between these two decays is about two orders of magnitude, both experimentally and theoretically.

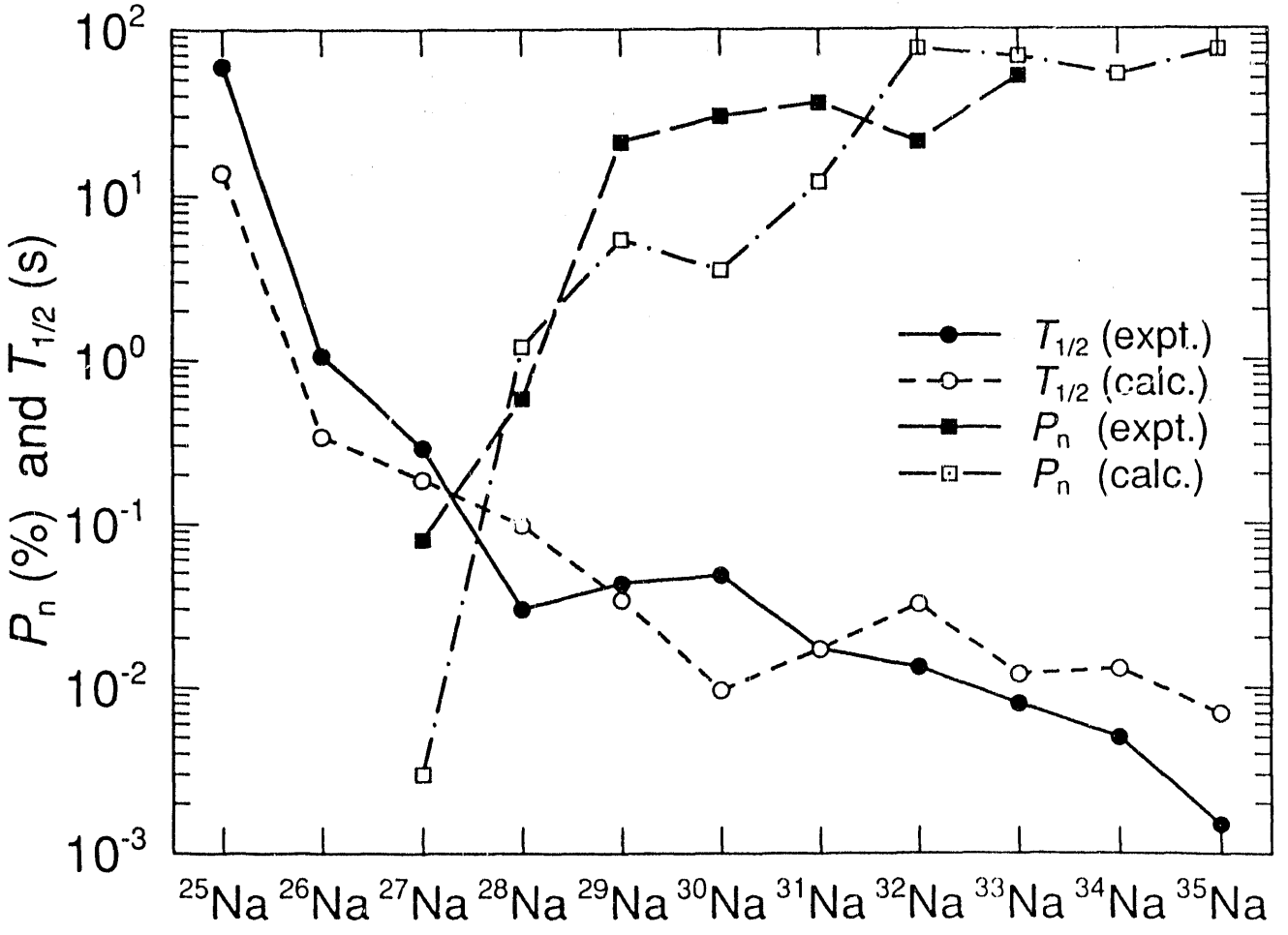

Fig. VI-8. Comparison of calculated and experimental β-decay half-lives and delayed neutron emission probabilities.

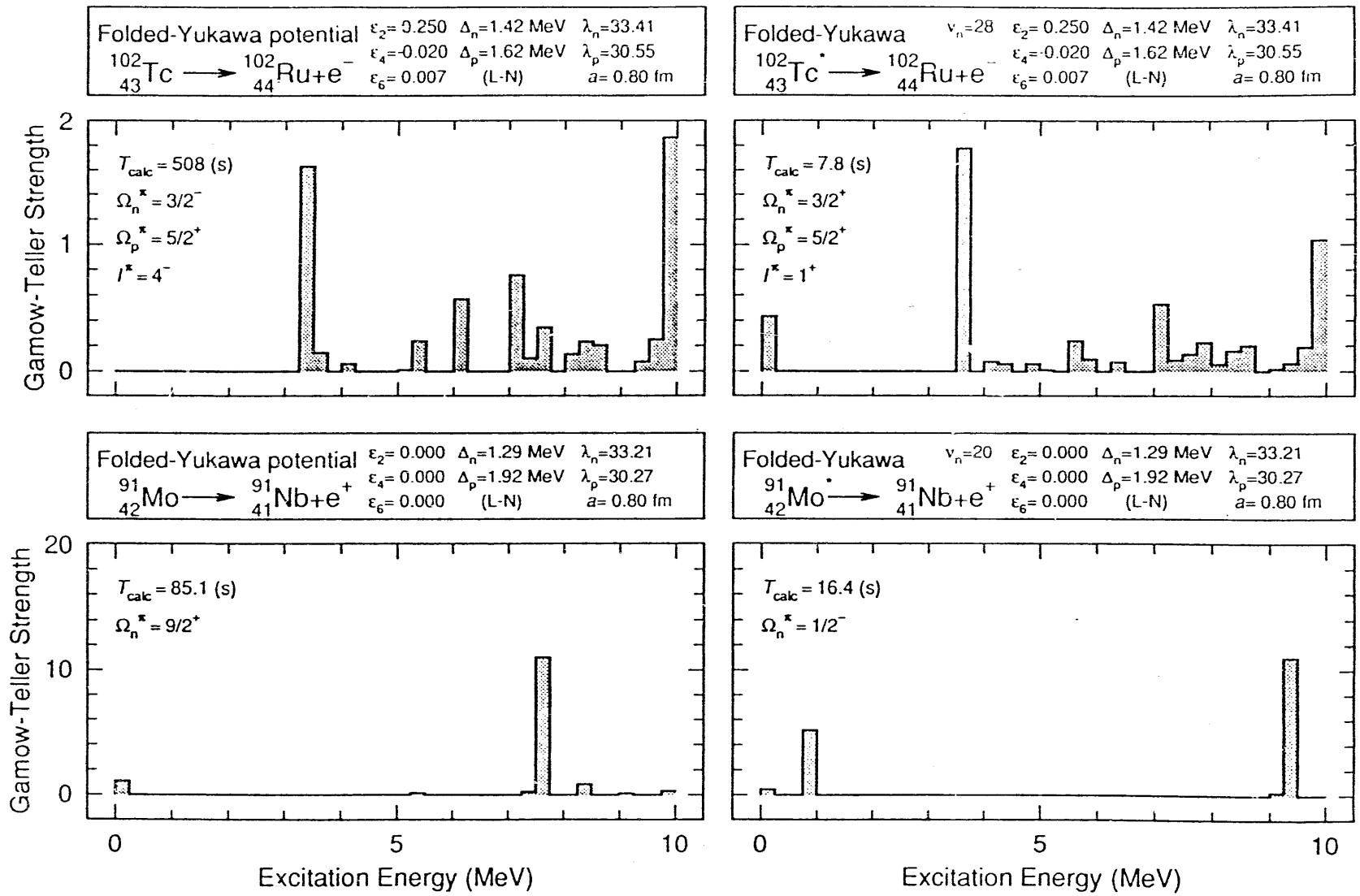

Fig. VI-9. Effect of excitation energy on calculated β-strength functions.

H. β-Decay Properties of A ≈ 80 Nuclei and Implications for Astrophysics [K.-L. Kratz, V. Harms, B.Pfeiffer and A. Wöhr (Univ. Mainz), W. Hillebrant (Inst. f. Astrophysik, MPI Garching), F.-K. Thielemann (Harvard Univ.), and P. Möller]

We have calculated β-strength functions, half-lives, and β-delayed neutron-emission probabilities for nuclei with proton numbers from about Z = 28 to Z = 37 for several values of the neutron number N. Experimentally, an odd-even staggering is observed in the solar A = 80 abundance peak. Calculations of β-delayed neutron emission based on the above strength functions, obtained in the QRPA, give good agreement between the observed and calculated *r*-abundances and strongly suggest that β-delayed neutron emission is the nuclear-physics origin behind the thus far unexplained odd-even effect in the solar A = 80 *r*-abundance peak.

For neutron-rich nickel isotopes, very detailed comparisons between calculated ground-state β-decay properties and level structure and corresponding experimental quantities have been carried out. These studies have shown that the initially unexpected short half-lives of N ≥ 36 isotopes of Cr and Ni may be explained as a result of prolate or oblate deformation predicted in this mass region. However, the studies also show that shape coexistence makes it difficult, if not impossible, to reproduce known nuclear properties such as $T_{1/2}$ for some nuclei in this region, with the present QRPA model, with any reasonable choice of deformation and parameter set. This is an expected difficulty for nuclei in transition regions between spherical and well-deformed shape, since the model assumes an identical, well-defined shape in the mother and daughter nuclei involved in the decay.

I. Actinide Nuclear-Structure Properties and Implications for Astrophysics [B. S. Meyer, W. M. Howard, G. J. Mathews (Lawrence Livermore Nat. Lab.), and P. Möller]

The theoretical study of the decay from the *r*-process line to the line of β stability requires the calculation of several nuclear-structure properties The path of the decay may be influenced by β-delayed neutron emission and fission. A determination of the branching ratios for the various decay paths requires a knowledge of fission-barrier heights, neutron separation energies, level densities, and β-strength functions. In the macroscopic-microscopic approach, the nuclear potential energy is calculated as a function of shape, and at each shape studied, one also obtains a corresponding single-particle spectrum. We have calculated fission barriers, ground-state masses, and level spectra for neutron-rich heavy elements, in the macroscopic-microscopic approach. By considering additional residual interactions, β-strength functions have been calculated that realistically account for the microscopic structure of the nucleus, including deformation effects.

For neutron-rich nuclei, we get higher fission barriers than were generally obtained 10 years ago in similar studies, and neutron-induced fission appears not to play a major role in cutting off the *r*-process path. The top of Fig. VI-10 shows regions in which the $Q\beta$ value is higher than the fission barrier. In such regions β-delayed fission is possible.

The lower part of the figure shows the regions in which one-, two-, and multi-neutron emission are possible. Calculations of β-strength functions for a limited set of nuclei show that most of the decay occurs to states below the barrier and consequently that β-delayed fission in these cases is of little importance. More definitive conclusions about the decay from the *r*-process path in the actinide region must await the inclusion of axially asymmetric shape degrees of freedom in fission-barrier height calculations and calculations of β-strength functions for all nuclei of interest.

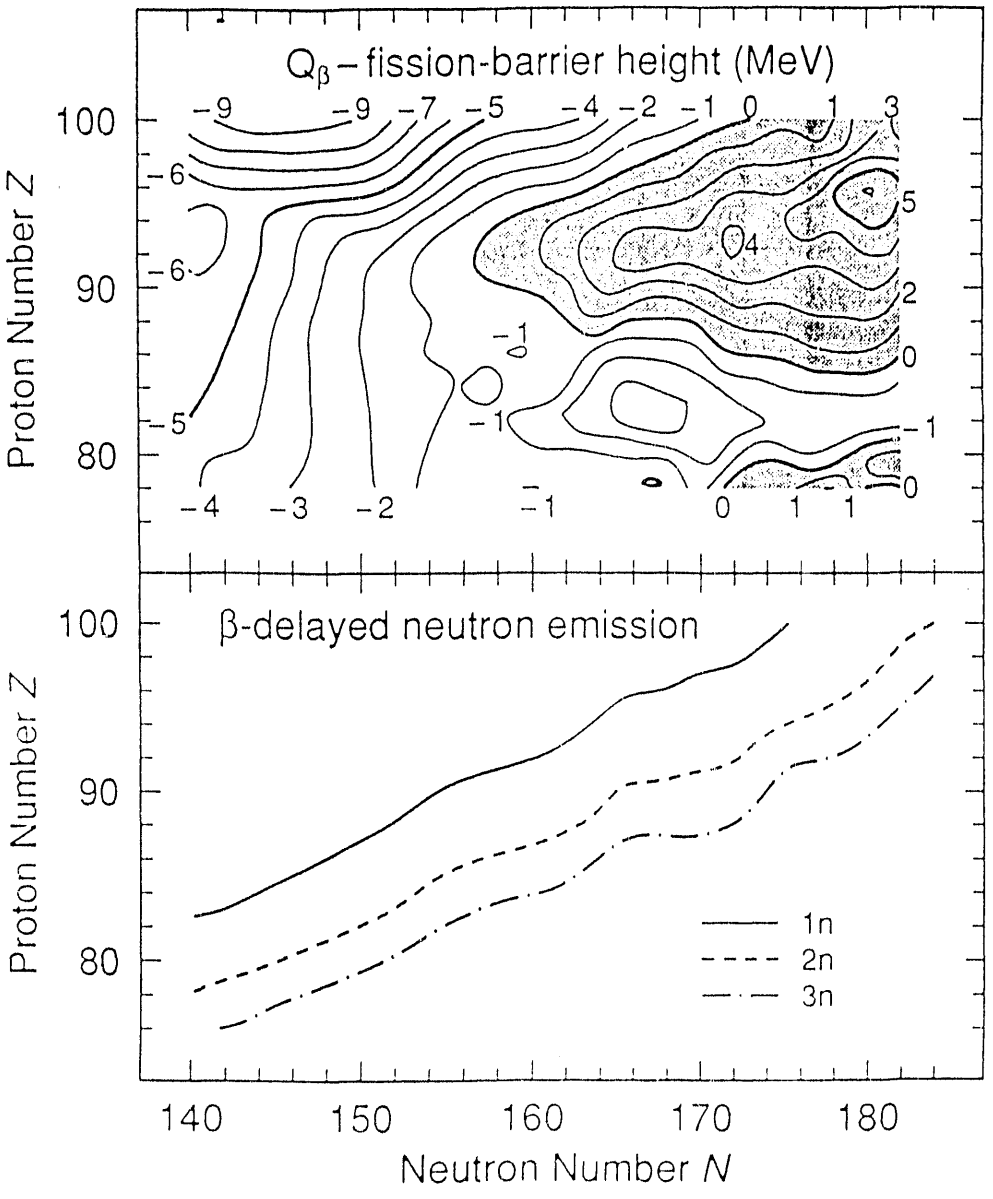

Fig. VI-10. Regions of nuclei where β-delayed fission (top) and β-delayed neutron emission (bottom) are possible.

J. Relativistic Point Coupling Model for the Description of Nuclear Ground State Properties [B. A. Nikolaus, D. G. Madland, and P. Manakos (Technische Hochschule Darmstadt)]

A point coupling approach in a manifestly non-renormalizable effective Lagrangian has recently been proposed by Manakos and Mannel,[14] which leads to an effective interaction model in the relativistic Hartree-Fock approximation. We have developed a self-consistent relativistic Hartree-Fock procedure to test this model by attempting to reproduce simultaneously the experimental ground-state binding energies, rms charge radii, and spin-orbit splittings of doubly-magic nuclei. Our potentials (scalar, vector, and Coulomb) are determined self-consistently using scalar and vector densities multiplied by coupling constants representing the effective interactions. Extensions to powers and derivatives of the densities are easily included. Imposing physical constraints on the coupling constants included, we have searched on grids of allowed values and have obtained initial results for ^{16}O and ^{40}Ca, using different forms of the potentials. Our progress on this topic was presented at the Spring 1990 APS Meeting in Washington DC.

K. Emission and Detection of Hadronic Axions from SN87A [A. Hayes, J. Engel and D. Seckel (Bartol Research Inst.)]

The potential importance of axions to particle physics, astrophysics, and cosmology has led to their continued study. Severe constraints are placed on axion properties by arguments concerning their potential emission from stars at various stages of evolution, particularly from type II supernovae. If axions exist, the SN87A neutrino data require axion-nucleon couplings to be either (a) $g_{\alpha N} \leq 10^{-11}$, or (b) $g_{\alpha N} \geq 10^{-7}$, provided the axion is "hadronic," *i.e.*, its coupling to ordinary non-nucleonic particles are all small. We calculated the flux of axions that may have emanated from SN87A and their detection rate at the Kamiokande proton-decay experiment for values of the axion-nucleon coupling $g_{\alpha N} \geq 10^{-7}$.

Axions can induce nuclear excitations in oxygen via the reaction $\alpha^{16}O \rightarrow {}^{16}O.^*$ We calculated the axion absorption cross section on ^{16}O using a set of nuclear wave functions that were derived from a large basis, non-spurious SU(3) shell model calculation, including up to 5 $\hbar\omega$ of excitation. The calculations showed that the subsequent deexcitation of ^{16}O often includes gamma-rays with energies of 5-10 MeV, which in turn would trigger the KII detector with an efficiency similar to that of electrons in the same energy range. For $6 \times 10^{-7} \leq g_{\alpha N} \leq 1.0 \times 10^{-3}$, the axion flux should have produced more than 5 (and up to 200) observable events at Kamiokande, and so this range of axion-nucleon coupling is ruled out. Because of uncertainties in our supernova model, we could not categorically rule out a small window around $g_{\alpha N} \simeq 7 \times 10^{-7}$.

* This work was carried out in collaboration with J. Engel and D. Seckel of the Bartol Research Institute, and has been accepted for publication in *Phys. Rev. Lett.*

L. The Soft Giant Dipole Mode of ^{11}Li (A. Hayes and D. Strottman)

Recent experiments have observed the electromagnetic dissociation cross section for ^{11}Li on ^{208}Pb at incident energies of 0.8 GeV/nucleon to be anomalously large. At relativistic energies, Coulomb excitation is dominated by electric dipole radiation, and the large enhancement of the cross section suggests that a soft giant dipole model exists in ^{11}Li in which about 20% of the total E1 strength lies at 1-2 MeV of excitation. We have examined in detail the electric dipole distribution for ^{11}Li in a large basis shell model that includes up to 3 $\hbar\omega$ of excitation.

The main contributions to the E1 matrix elements are the p $\rightarrow$ 1 s and p $\rightarrow$ d amplitudes, and for the low-lying states, these are of opposite sign and cancel strongly. However, when the weak binding energy of the last neutron is taken into account via the use of Woods-Saxon single particle wave functions, a very strong enhancement of the E1 strength between 1-4 MeV is predicted. This results from the large increase of the p $\rightarrow$ 1 s relative to the p $\rightarrow$ d single particle E1 matrix element, thus breaking the strong cancellation between these two large components. The predicted Coulomb excitation cross section is σ_C = .39b, which is about a factor of two smaller than experiment. However, this result does not necessarily mean that excitations omitted from standard shell model calculations are needed to explain the anomalous cross section. In particular, our analysis shows that the calculated E1 strengths are very sensitive to the $s_{1/2}$ *vs* $d_{5/2}$ amplitudes in the wave functions, so that a small adjustment of the ph interaction could lead to a significant increase in the predicted Coulomb cross section.

M. Nuclear Structure Corrections to Estimates of the Spin-Dependent Wimp-Nucleus Cross Section [D. Strottman and A. F. Pachecho (University of Zaragoza, Spain)]

The widely held belief that the bulk of matter in the universe has not been observed is currently based on the observation of gravitational fields stronger than can be explained by the known, visible baryonic matter. It is hypothesized that this dark matter consists of weakly interacting massive particles (WIMPs); several novel detector designs have been proposed for their detection. One of the stronger dark matter candidates is the lightest supersymmetric particle (LSP) which, in general, is a linear combination of a photino, higgsino and zino. Estimates within the extreme single-particle model of event rates, assuming elastic scattering from nuclei, have recently been made by Ellis and Flores[15] and Goodman and Witten.[16] We have investigated the accuracy of those estimates.

In common with earlier work, we assume the interaction of the photino with matter is basically realized by the exchange of scalar quarks with the quarks comprising ordinary nuclei resulting, at low energy, in a spin-dependent amplitude of the form

$$\mathcal{M} = \frac{4\, e^2\, Q_q^2}{m_{\tilde{q}}^2}\, \vec{s}_q \bullet \vec{s}_\gamma \qquad (1)$$

In Eq. (1) m_q is the mass of the exchanged squark, eQ_q is the electric charge of the struck quark, and s and s_q the spins of the photino and quark, respectively. Following Goodman and Witten and Ellis and Flores, $\mathcal{M}$ can be expressed as

$$< p / \mathcal{M} / p > = \frac{4\, e^2\, a_p}{m_q^2}\, \vec{s}_\gamma \bullet \vec{s}_p$$

$$< n / \mathcal{M} / n > = \frac{4\, e^2\, a_n}{m_q^2}\, \vec{s}_\gamma \bullet \vec{s}_n$$

with

$$a_p = \sum_q Q_q^2\, \Delta q_p$$

$$a_n = \sum_q Q_q^2\, \Delta q_n \ .$$

where the sum extends over all the flavors that comprise the nucleon and Δ_q is the mean fraction of the nucleon spin contributed by quarks (and antiquarks) of flavor q. The value of Δ_q may be obtained either from the naive quark model (NQM) or extracted from the recent results from the European Muon Collaboration (EMC).

The early estimates based upon the extreme single-particle model are suspect for two reasons. First, there is the obvious fact that in the shell model several single particle levels are simultaneously active within a given major shell. All must be normally included if an accurate calculation of spin observables is to be obtained. Because $j = l+s$, a brief consideration of the semi-classical model will convince one that the contributions from spin-orbit partners (*e.g.*, $0d_{5/2}$ and $0d_{3/2}$) will each contribute to <S> but with opposite signs.

Second, there is a great discrepancy in size between a_p and a_n in the photino case, especially in the Naive Quark Model. Thus, when Z is even, although the orbital angular momentum contribution, L_p, is very small, the relative smallness of a_n will make any contribution from the protons non-negligible. The finite value of L_p in these instances simply reflects the fact that not all the protons are paired to zero angular momentum. An excellent example of this is ^{9}Be. Although

L_p is 50 times smaller than L_n, it has a very appreciable effect on the expectation value of M. There is also a considerable sensitivity to the assumed values of the a_i. Our results for the photino interaction can be straightforwardly applied to the case of the higgsino by using the same values of L_i. The reduction for the higgsino is very similar to the case of the photino, except that the great sensitivity to small values of $\langle S_p \rangle$ is not present. This is a direct result from the near equality in magnitude in the a_i in the NQM case.

Because the final answers often result from a cancellation between the contributions from the protons and from the neutrons, there may be considerable sensitivity to the precise values calculated for the L_i. The greatest sensitivities naturally are for those cases of greatest cancellation. For example, in the case of ^{9}Be, the correction factor assuming the quark model values for the a_i produces a reduction factor from the extreme single-particle model of 12, yet a 10% change in L_p can increase this to a factor of 25! However, this sensitivity is also reflected in the large differences between the results obtained assuming the NQM or the EMC values.

We have performed a more accurate calculation of the figure of merit proposed by Ellis and Flores. Not surprisingly, near the beginning of major shells, the single-particle estimate employed by Ellis and Flores is reasonably reliable. However, near the middle and end of shells, as well as for even-Z nuclei, one must be extremely circumspect in the use of the single-particle model. Our more accurate calculation effectively excludes some nuclei from consideration as detectors. An extreme example is ^{35}Cl for which the single-particle estimate must be reduced by a factor of 20. However, the most favorable candidate remains ^{19}F as suggested by Ellis and Flores; since it is both near the beginning of the 1s-0d shell and is an odd proton nucleus, it is affected only by approximately 25% by more accurate shell model calculations.

A complete version of this work may be found in *Physical Review* D40, 2131 (1989).

N. Spin-Tensor Analysis of Realistic Shell Model Interactions [D. Strottmar and E. Osnes (University of Oslo, Norway)]

The evaluation of the shell model effective interaction from the underlying free nucleon-nucleon interaction is one of the outstanding problems of nuclear many-body theory. This is an exceedingly complicated problem, which, despite much progress made over the last 25 years, cannot be considered settled. One aspect of the problem is associated with the choice of the NN interaction that is taken to be either of a phenomenological nature, obtained by fitting phase shifts of NN scattering and the deuteron properties, or of a more fundamental nature, calculated by meson-exchange theory. Roughly speaking, typical phenomenological NN interactions, such as the Hamada-Johnston and Reid potentials differ from the more modern Paris and Bonn-Jülich meson-exchange potentials in the strength of the much debated tensor-force component. The former have rather strong tensor components, whereas the latter have somewhat weaker tensor components.

A second problem in obtaining the effective interaction is associated with its evaluation by many-body perturbation methods, once the initial NN interaction has been chosen. This procedure generally includes two steps. Because the NN interaction is strongly singular at short internucleon distances, it is usually regularized by evaluating the Bethe-Brueckner-Goldstone reaction matrix, G, which incorporates the two-nucleon short-range correlations by allowing the two nucleons to interact virtually any number of times. In a second step one uses the reaction matrix G as a starting point for a perturbation expansion of the effective interaction. One often either sums the diagrams order by order in G, or carries out infinite summations of subsets of diagrams.

To date, several reasonably effective interactions have been obtained. In order to understand their differences on a more fundamental level than just comparing energy spectra and related properties, it is instructive to analyze the various interactions in terms of their various spin-tensor components. In particular, it is of interest to see to what extent the presumed different tensor strengths in the original NN interactions show up in the corresponding G-matrices and renormalized effective interactions. Another reason for carrying out a spin-tensor decomposition of the effective interaction is to get an assessment of the salient features, which have to be incorporated into effective interactions for heavier nuclei that are not easily calculable from many-body theory because of the many single-particle degrees of freedom involved.

We have analyzed several realistic shell model effective interactions that have proven successful in reproducing nuclear properties. The effective forces examined were obtained from the phenomenological Hamada-Johnston potential as well as the meson-exchange Bonn-Jülich and Paris potentials and were calculated to various approximations. For the Hamada-Johnston potential, the effective interaction was calculated to first and second order in the reaction matrix G. In addition, we considered an interaction obtained by summing the core-polarization diagrams to all orders using particle-hole vertices screened to second order. For the Bonn-Jülich and Paris potentials, we considered the bare G and a renormalized interaction including essentially all long-range correlations self-consistently to arbitrary order. The latter interaction was also evaluated using a Hartree-Fock rather than a harmonic oscillator single-particle basis.

For all forces examined, the dominant contribution comes from the central part. The central part seems to be sufficient to produce the basic structure of the spectra for two nucleons outside closed shells. The effect of renormalization of the bare G-matrix can be substantial. The vector component is small for the bare G-matrix interaction, especially for T = 0, but is considerably modified by renormalization; however, it has little effect on the energy spectra for two-valence nucleons. The tensor component is somewhat larger than the vector component and is relatively larger for the Hamada-Johnston potential than for the Bonn-Jülich and Paris potentials. This is not surprising in view of the stronger tensor force component in the original Hamada-Johnston NN potential. The effect of the tensor component on the two-valence-nucleon spectra is fairly small,

particularly for T = 1 . It does, however, serve to compress the spectrum slightly. The effect on the T = 0 spectrum is somewhat larger, the main effect being to lift the 2^+ levels. Although the effect of the vector and tensor components on the spectra of two valence nucleons is small, it is likely to increase with the number of valence nucleons. A strong tensor force in the NN interactions will produce a strong central contribution to second order in the G-matrix. The strength of the tensor component in the NN interaction is reflected in the renormalized interactions. Thus, for the convergence of the effective interaction, it seems desirable to start from an NN interaction with a weak tensor force.

O. Two-Photon Decay of the First Excited 0^+ State in ^{16}O [A. C. Hayes, J. L. Friar (T-5), and D. Strottman].

Two-photon decay of excited states is one of the basic second-order electromagnetic processes seen in nuclei. The results of the recent measurements[17] of 2γ decay of $0^+ \rightarrow 0^+$ transitions in ^{16}O, ^{40}Ca, and ^{90}Zr, where the 2M1 matrix elements were observed to be of the same order of magnitude as the 2E1, were quite unexpected. Indeed, from Σ_{-2} cross-section measurements it is known[18] that $(\chi_{M1}/\alpha_{E1})^{g.s.} < 10^{-2}$, throughout the mass table. To understand the large difference between these diagonal matrix elements and the transition matrix elements measured in the $0^+ \rightarrow 0^+$ decays, we have examined in detail the 2γ decay of the 0^+ (6.05 MeV) state in ^{16}O.

^{16}O has the advantage of being well suited to an SU(3) shell-model description. Using the SU(3) scheme we could describe the wave functions, 2γ operators and the two-body effective interaction within a consistent framework, taking advange of their symmetry properties to simplify our results. The 2E1 operator involves both a $\Delta\hbar\omega = 0$ matrix and $\Delta\hbar\omega = 2$ term, which transform under SU(3) as $(\lambda,\mu) = (0,0)$ and $(\lambda,\mu) = (2,0)$, respectively. In calculating the 2M1 matrix element, we restricted ourselves to a one-body M1 operator (*i.e.*, to a $\Delta\hbar\omega = 0$ operator).

In evaluating the transition polarizability, it was necessary to include the full electric dipole strength built on both the ground state and the deformed state in order to reproduce the strong cancellation seen in the 2E1 matrix element. This meant using a large $(1 + 3 + 5)\hbar\omega$ 1^- basis to describe the intermediate T = 1 1^- states. Truncation of the basis and the elimination of spurious center-of-mass states were achieved by exploiting the SU(3) symmetry properties of the wave functions.

The suppression of the transition polarizability was found to arise from strong cancellation between the different $\Delta\hbar\omega = 0$ matrix elements, *i.e.*, contributions to α_{E1}^{fi} from the giant dipole resonance built on the closed shell added destructively with those from the resonance built on the 2p-2h and 4p-4h states. There was then a further cancellation between this total $\Delta\hbar\omega = 0$ and the $\Delta\hbar\omega = 2$ contributions to the 2E1 matrix element.

P. References-Section VI

1. A Gilbert and A. G. W. Cameron, Can. Journal of Physics 43, 1446 (1965).

2. W. Dilg, W. Schantl, H. Vonach, and M. Uhl, "Level Density Parameters for the Back-Shifted Fermi Gas Model in the Mass Range 40<A<250," Nucl. Phys. A217, 269 (1973).

3. A. V. Ignatyuk, Sov. J. Nucl. Phys. 21, 450 (1979).

4. E. D. Arthur, P. T. Guenther, A. B. Smith, and D. L. Smith, " Applied Uses of Level Density Models," Invited Presentation at the IAEA Specialists' Meeting on Nuclear Level Densities, Bologna, Italy, November, 1989.

5. M. Ivascu, Rev. Roum. Phys. 32, 697 (1987).

6. Zhuang Youxiang, Chinese Journal of Nuclear Physics 8, 199 (1986).

7. M. Bolsterli and J. A. Parmetola, "P-Wave Pion Scattering in the Los Alamos Soliton Model," Phys. Rev. D 39, 1304 (1989).

8. M. Bolsterli, "Maximum Quasiparticle Velocity in Nonrelativistic Quantum Field Theory," Phys. Rev. A 40, 5455 (1989).

9. M. Bolsterli, "Nucleon Kinematics in the Los Alamos Soliton Model," Proc. Int. Conf. Particles and Nuclei, Mass. Inst. of Technology (1990), VI-34.

10. M. Bolsterli, "Nuclear Kinematics in Semirelativistic Meson Field Theories," Proc. Symp. in Honor of Akito Arima, Santa Fe, N. M., May 1990, p. 98.

11. M. Bolsterli, "Canonical Transformation Method for Static-Source Meson Hamiltonians," (to be published in J. Math. Phys., 1990).

12. M. Bolsterli and J. A. Parmentola, "Shell Model of the Nucleon," Nucl. Phys. A 507, 245c (1990).

13. M. Bolsterli and J. A. Parmentola, "The Nucleon as a Few Body System," Proc. of Conference, TRIUMF, Vancouver, B.C., 1989, "Contributed Papers from Few Body XII," B. K. Jennings, Ed., H3.

14. P. Manakos and T. Mannel, "Short Note on Relativistic Hartree Fock Models for Nuclei with Skyrme Type Interactions," Z. Phys. A 330, 223 (1988).

15. J. Ellis and R. A. Flores, "Realistic Predictions for the Detection of Supersymmetric Dark Matter," Nucl. Phys. B307, 883 (1988).

16. M. W. Goodman and E. Witten, "Detectability of Certain Dark-Matter Candidates," Phys. Rev. D 31, 3059 (1985).

17. J. Kramp, D. Habs, R. Kroth, M. Music, J. Schirmer, D. Schwalm, and C. Broude, "Nuclear Two-Photon Decay in $O^+ \rightarrow O^+$ Transitions," Nucl. Phys. A474, 412 (1987).

18. J. Ahrens, H. Gimm, A. Zieger, and B. Ziegler, Nuovo Cm 32A, 364 (1976).

VII. OTHER THEORY

A. A Neural Model for Gamma-Ray Spectrum Recognition [L. C. Liu and B. Giraud (CEN-Saclay, France)]

One of the central issues in environmental restoration and monitoring of pollution is the identification and characterization of the toxic waste. It is desirable to devise a system that can accomplish these tasks with high speed and high accuracy even in the presence of high-level "noise" or poor spectral resolution. This is an excellent field for the application of the learning and retrieval abilities of neural networks (or neural nets).

We have started our investigation by implementing a neural model (on our Sun Workstation) that was developed by our collaborators at the University of Paris and has been successfully applied to the survey of water composition.[1] The model can be classified as a perceptron that uses the Widrow-Hoff least-mean-square error correction rule[2,3] for the learning. We have applied this model to the learning and recognition of gamma-ray spectra of nuclear fissions. Two typical spectra denoted, respectively, A and B are shown in Fig. VII-1.

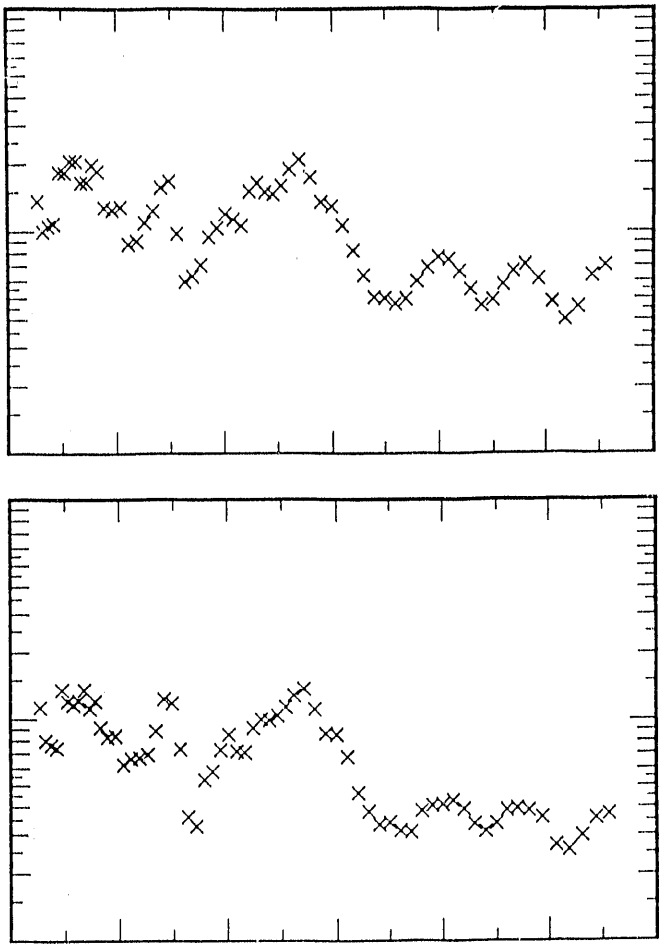

Fig. VII-1. Sample spectra of nuclear fission.

Our model recognizes and easily distinguishes individual samples. We then created a mixed spectrum, *e.g.*, $xA + yB$ with $x = 0.25$ and $y = 0.75$, and asked the neural net to examine it. The network has answered that the sample is neither *A* nor *B*; rather, it is a composition of *A* and *B*, with a one-to-three ratio.

Using the concept of a variational approach familiar to nuclear physics, we have developed a new learning rule. A comparison of the Widrow-Hoff rule and our new rule shows that the latter one gives equally good results. In addition, it has increased the learning speed by at least a factor of two to three for a database containing about 100 samples. Investigation of this new rule with larger databases is in progress. We are also improving the model's ability to recognize samples whose spectrum has been grossly mutilated.

B. Cold Fusion Topics [G. M. Hale, R. D. Smith (T-3), and T. L. Talley].

The strong interest in cold fusion phenomena during the spring of 1989 raised a raft of questions about the d+d reactions that we were uniquely positioned to answer because of the R-matrix work done in our group on the four-body system. Many of the questions centered on the branching ratio of the d+d reactions at very low energies. Our prediction for the branching ratio from a charge-independent R-matrix calculation (as shown in Fig. VII-2) is compared with the most recent measurements.[4,5] The calculated ratio is in good agreement with the data at energies above about 10 keV, and extrapolates to a value close to unity (1.044) at zero energy. This result certainly does not allow an explanation of the extraordinarily high ratios of heat and/or tritons to neutrons observed in some of the cold fusion experiments. The same R-matrix calculation, incidentally, also predicts quite accurately the low-energy branching ratio observed[6] for the P-wave part of the reaction in muon-catalyzed fusion experiments.

We derived an exact expression for the fusion rate in complex systems that undergo nuclear reactions at small distances describable by R-matrix theory. The conditions under which the exact expression reduced to the commonly used approximation given by Jackson[7] were investigated and found to be satisfied for simple screened-Coulomb potentials of the Hulthén form. Using these screened potentials, we did a parametric study of the dependence of fusion rates on the screening radius of the potential for several hydrogen-isotope reactions. The screening radii required to get rates comparable to those observed even in the experiments that detected low levels of neutrons corresponded to unreasonably high electron densities in the lattice. It appeared more likely that such rates could be obtained from the interactions of higher-energy ($E_{rel} > 100$ eV) particles. This work was reported[8] at the "Workshop on Cold Fusion Phenomena" at Santa Fe, N.M., in May 1989.

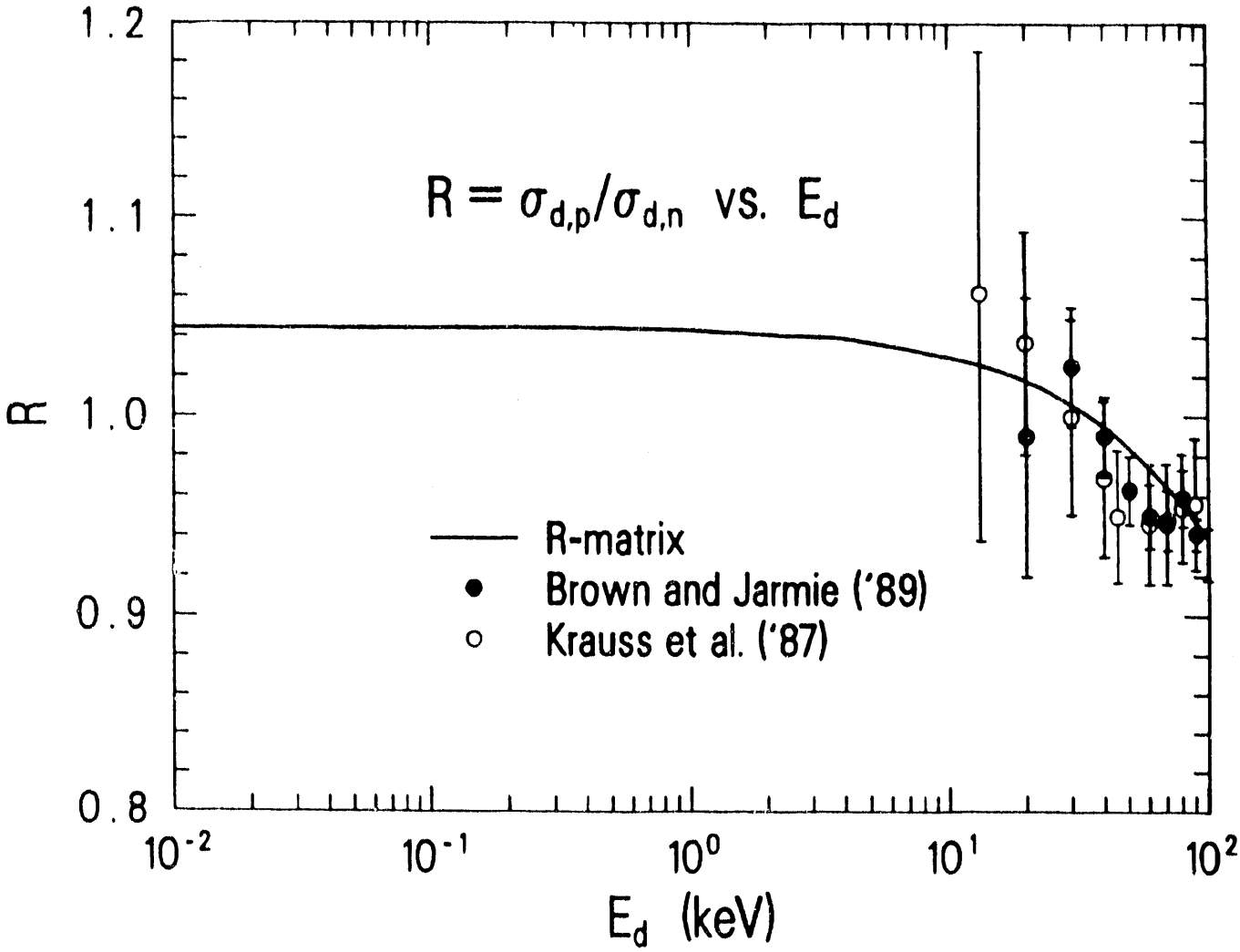

Fig. VII-2. Calculated branching ratio for the d+d reactions compared with the data of Brown and Jarmie[4] and Krauss *et al.*[5] at energies between 10 and 100 keV. The calculated curve extrapolates to a zero-energy value of 1.044.

C. Cold Fusion Theory (T. L. Talley)

On 23 March 1989 Martin Fleishmann and Stanley Pons announced by press conference that nuclear fusion had been achieved in an electrochemical cell! Attempts to understand their data and other related material occupied much of the remainder of 1989. Hale, Smith, and Talley presented a paper[8] at the Santa Fe Workshop in May. We also urged[9] experiments with deuterium-tritium mixtures to study reaction mechanisms. An updated version[10] was also presented at the Division of Nuclear Physics Fall meeting. In both meetings we pointed out that the ratio of dd to dt rates will give a good estimate of the average reacting pair energy.

A Cold Fusion review was given[11] at the Nuclear Explosives Design Physics Conference, 15-20 October 1989. Potential nuclear weapon implications were addressed.

On the theory front, the observations cannot yet be explained; however, Talley and Hale have pointed out[12] that the dominance of tritium over neutrons might be due to deuteron pairs populating the first excited state of ^{4}He, which will then preferentially decay via the p + T branch. We urged diagnostics that might infer conversion electrons. We continue to search for methods to populate that level.

D. Particle Filtration (M. Bolsterli)

A program developed at Los Alamos[13] has long been used in various applications having to do with sedimentation. Examples are the probable distribution of the fragments of the TMI reactor and the deposition of particles by a moving fluid. This year, in collaboration with Larry Schwartz of Schlumberger-Doll Research, the sedimentation code was reworked to eliminate a problem. The resulting improved code was used to simulate the filtration of particles into a consolidated granular network.[14] The code easily handles tens of thousands of particles of widely varying sizes. The simulation suggests that simple models can be used to describe the dependence of the final distributions on the invader sizes and on the pore and throat sizes in the host material.

E. Heisenberg Antiferromagnet (M. Bolsterli)

A new method for generating state vectors for Heisenberg antiferromagnets was developed and applied to the one-dimensional antiferromagnetic chain,[15] where it gave the best results ever obtained in a variational calculation. The method is based on a derived recursion relation that enables the Hamiltonian for 2N sites to be computed from the Hamiltonian for N sites if the basis set of state vectors is restricted so as to include any particular set of vectors. For example, the simplest basis set consists of just the lowest spin-0 state and the lowest spin-1 state. The computations showed that convergence of the energy per particle required the use of about 1000 sites; the method allowed the use of as many sites as were needed, with no difficulty involved in going to an arbitrary number of sites. Some interesting results for the low-lying spectrum of the open chain were also obtained. Operators responsible for certain of the observed degeneracies in this spectrum were constructed, while others of the degeneracies are as yet unexplained.

A useful feature of the method is that it is applicable to more than one dimension; it is hoped that it will be so applied.

F. Nuclear-Model Parameter Searches and Covariance Capability [D. W. Muir (on leave-of-absence from T-2, at IAEA, Vienna, Austria)]

In the past year we have developed a sensitivity-analysis version of the GNASH[16] preequilibrium-statistical nuclear theory code. This new code version makes it possible to do automated searches on the model parameters in order to improve consistency of code output with measured nuclear data and, at the same time, provide quantitative estimates of the uncertainties (covariances) of the computed results.

The strategy we chose in pursuing this objective was to implement GNASH on a VAX 8700 and then to utilize the VAX/VMS machine-dependent program GRESS[17] to operate on the resulting VAX-compatible GNASH source code to produce GNASH-S, the desired sensitivity-computing version.

The first step, to convert GNASH from CRAY to VAX compatible FORTRAN was successfully completed. Two separate test problems involving the reactions of 8-20 MeV neutrons with ^{93}Nb and with ^{184}W, respectively, gave results on the VAX that are essentially identical to results from analogous runs on a CRAY-1. There was a factor of 5 running time penalty on the VAX relative to the CRAY. The VAX version of GNASH, together with the results of the two test problems (both VAX and CRAY output) have been released to the National Energy Software Center at Argonne National Laboratory and to the Radiation Shielding Information Center at Oak Ridge.

The second phase of the work, the application of GRESS (Version 0.0) to develop a sensitivity version of GNASH, required some interaction with the authors of GRESS and some minor corrections to their code. It also required some minor rearrangements in GNASH, none of which changed the computed results. The derivatives of various results with respect to various code input parameters were obtained, and, in all cases examined to date, satisfactory agreement has been obtained with pseudo-derivatives obtained by direct recalculation with altered input.

This new capability in GNASH-S comes with a definite running time penalty--about a factor of 53 for a calculation of sensitivities to two input parameters, a factor of 90 for a 20-parameter problem, and a factor of 124 for a 37-parameter problem (in all cases, CPU time relative to a normal GNASH calculation on the VAX 8700). The incremental cost of adding an additional parameter is thus similar in magnitude to the cost of performing an additional recalculation to achieve somewhat the same result. Even though the GRESS path does not appear likely to save CPU charges, the real advantage of the approach is that it is suitable for the full automation of large-scale parameter optimization studies. The CPU costs of this approach, while not negligible, are certainly in the acceptable range.

The final phase of this work, namely the incorporation of GNASH-S into the framework of a conventional nonlinear least-squares analysis,[18] is now in progress. There appear to be no major

obstacles to prevent the achievement of the twin goals of optimum model parameter sets and defendable covariances of the computed quantities.

The present and future availability of computed covariances from the existing EDA[19] program and the new sensitivity version of GNASH have imparted new significance to the related development of a new ENDF/B covariance format to store the output covariances from such systems. An important aspect of the computed covariances is that they are made available explicitly as a triple matrix product. That is, for a given cross section vector σ,

$$D(\sigma) = R\, D(\alpha)\, R^T \ ,$$

where the sensitivity matrix R gives the change $\delta\sigma = R\ \delta\alpha$ due to a small change in the parameter vector $\delta\alpha$. Working with the members of the Cross Section Evaluation Working Group (CSEWG), we have devised a new data file, File 30 (having obtained CSEWG approval in April 1989), in which the evaluator supplies R and $D(\alpha)$, rather than $D(\sigma)$ itself, and this results in enormous reductions in the volume of data to be stored. We have constructed the MF = 30 format with an eye toward ease of later processing of the covariances into multigroup form, as is normally required in applications. This and other new ENDF/B-6 covariance formats are described in Ref. 20.

G. References-Section VII

1. C. Bernard *et. al.*, "Continuous Survey of Water Composition: Neural Network Identification of a Variety of Compounds from Their Individual Mass Spectrum in Different Samples," Univ. of Paris preprint, to be published in IEEE.

2. B. Widrow and M. E. Hoff, "Adaptive Switching Circuits," Proc., IRE WESCON Convention Record, Part 4, in Neurocomputing-Foundations of Research, J. A. Anderson and E. Rosenfeld, Eds. (MIT Press, Cambridge, Mass., 1989), p. 126.

3. B. Widrow and R. Winter, "Neural Nets for Adaptive Filtering and Adaptive Pattern Recognition," Computer 21, 25 (1988).

4. R. E. Brown and N. Jarmie, "Differential Cross Sections at Low Energies for ^{2}H(d,p)^{3}H and ^{2}H(d,n)^{3}He," Phys. Rev. C. 42, 1391 (1989).

5. A. Krauss, H. W. Becher, H. P. Trautvetter, and C. Rolfs, "Low-Energy Fusion Cross Sections of D+D and D + ^{3}He Reactions," Nucl. Phys. A465, 150 (1987).

6. D. V. Balin, E. M. Maev, V. I. Medvedev, G. G. Semenchuk, Yu. V. Smirenin, "Experimental Investigation of the Muon Catalyzed dd-Fusion," Phys. Lett. 141B, (1984); JETP Lett. 40, 112 (1984).

Page Range	NTIS Price Code	Page Range	NTIS Price Code	Page Range	NTIS Price Code	Page Range	NTIS Price Code
001–025	A02	151–175	A08	301–325	A14	451–475	A20
026–050	A03	176–200	A09	326–350	A15	476–500	A21
051–075	A04	201–225	A10	351–375	A16	501–525	A22
076–100	A05	226–250	A11	376–400	A17	526–550	A23
101–125	A06	251–275	A12	401–425	A18	551–575	A24
126–150	A07	276–300	A13	426–450	A19	576–600	A25
						601-up*	A99

*Contact NTIS for a price quote.

END

DATE FILMED

12/27/90